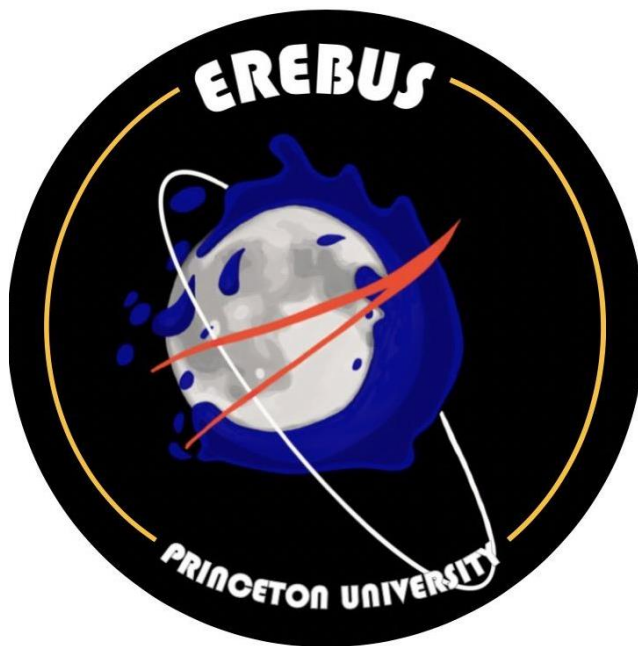


# Erebus Mission

## Critical Design Review



MAE342: Space Systems Design

Princeton University

05/12/2020

# Team Goddard

Adhitya Raghavan

Alex Rogers

Anthony Barnett

Bethwel Kiplimo

Beimnet Shitaye

Cassidy Crone

Douglas Chin

Divyanshu Pachisia

Emily McDonnell

Julian Castellon

Linus Wang

Marcus Jonas

Meredith Hooper

Michael Hauge

Milo Hughes

Nathan Spilker

Nathaniel Shields

Ofek Peres

Ricky Feig

Roger Hou

Sam van der Jagt

Samarie Wilson

Tristan LaCombe

For subteam assignments, please see Figures 8.4.1 and 8.4.2.

## Table of Contents

<b>List of Figures</b>	<b>4</b>
<b>List of Tables</b>	<b>6</b>
<b>Acknowledgments</b>	<b>7</b>
<b>List of Acronyms</b>	<b>8</b>
<b>Executive Summary</b>	<b>110</b>
Mission Description	110
<b>1. Introduction</b>	<b>111</b>
<b>2. Mission Overview</b>	<b>113</b>
2.1 Motivation and Mission Objectives	113
2.2 Lunar Lander Mission Overview	115
2.3 Lunar Orbiter Mission Overview	221
<b>3. Mission Analysis and Orbit Design</b>	<b>225</b>
3.1 Mission Phases	225
3.2 Delta-V Requirements	332
3.3 Space Environment	335
<b>4. OMV, Launch, and Separation System</b>	<b>337</b>
4.1 Orbital Maneuvering Vehicle (OMV)	337
4.2 Launch Vehicle	443
4.3 Separation System	444
4.4 LV and ESPA-driven Requirements for Lander and Orbiter	446
<b>5. Lunar Lander</b>	<b>447</b>
5.1 Structure	448
5.2 Mechanisms	554
5.3 Payload	663
5.4 Guidance, Navigation, and Control	669
5.5 Propulsion	889
5.6 Power	98
5.7 Thermal	101
5.8 Command & Data Handling	1528
5.9 Communications	11111
<b>6. Lunar Orbiter</b>	<b>1166</b>
6.1 Structure	1178
6.2 Mechanisms	12020
6.3 Guidance, Navigation, and Control	13031
6.4 Propulsion	1399
6.5 Power	1422
6.6 Thermal	1466
6.7 Command & Data Handling	1522
6.8 Communications	1565
<b>7. Systems Integration</b>	<b>159</b>
7.1 Reliability, Survivability and Safety	16059
7.2 Parts/Processes	16160

7.3 Ground Systems Integration	16261
7.4 Mass Properties Details	1632
7.5 Qualification	1643
7.6 Cost & Schedule	1655
<b>8. Project Management</b>	<b>167</b>
8.1 Guiding principles	1687
8.2 Communication channel	1687
8.3 Documentation	1687
8.4 Team Organization and flow of information	1698
8.5 Meetings and Discussions	169
<b>9. Conclusions</b>	<b>171</b>
9.1 Future Work	171
<b>References</b>	<b>173</b>
<b>Table of Appendices</b>	<b>18282</b>
Appendix A: Quad Chart	Error! Bookmark not defined.84
Appendix B: Requirements	1855
B.1 Lander Requirements	185
B.2 Orbiter Requirements	193
Appendix C: Detailed Mass Budgets	19999
Appendix D: Mission Planning	201
Appendix E: LV Integration	202
Appendix F: Structures	209
Appendix G: Mechanisms	213
Appendix H: Payload	228
Appendix I: Guidance, Navigation, and Control	229
Appendix J: Propulsion	24243
Appendix K: Power	24445
Appendix L: Thermal	24848
Appendix M: Command & Data Handling	25757
Appendix N: Communications	25858
Appendix O: Cost Estimation	26159
Appendix P: Technology Readiness Levels	259

# List of Figures

Figure i: CAD model of the OMV concept	10
Figure ii: CAD model of the lander	11
Figure iii: Orbiter CAD model	11
Figure 2.1: Packaging model of Erebus lunar lander	17
Figure 2.2: Top and bottom view of lander packaging model	18
Figure 2.3: Erebus lunar orbiter model and deployment scheme	22
Figure 3.1.2a: Visual of TLI to LLO	26
Figure 3.1.2b: Visual of orbiter in initial LLO	26
Figure 3.1.4: Transfer from LLO to frozen lunar orbit	28
Figure 3.1.5a: One year coverage with frozen lunar orbit	30
Figure 3.1.5b: 10 year coverage of frozen lunar orbit	30
Figure 3.1.5c: Visual of spacecraft orientation	31
Figure 4.1.1: CAD mockup of the OMV in GTO configuration	37
Figure 4.2.1: Volume available to primary and co-primary payloads atop the Erebus Mission	44
Figure 4.3.1: Secondary payload separation system	44
Figure 4.4.1: Volume and mass requirements driven by ESPA and the launch vehicle	46
Figure 5.1.1: Worst-case launch load factors	50
Figure 5.1.2: Lander assembly and octagonal frame	50
Figure 5.1.3: Static analysis of octagonal frame, scenario 1	51
Figure 5.1.4: Static analysis of octagonal frame, scenario 2	51
Figure 5.1.5: Results of modal analysis on octagonal frame	52
Figure 5.2.1: Landing system in deployed configuration	55
Figure 5.2.2: Primary damper cross-section	56
Figure 5.2.3: Landing system deployment sequence	57
Figure 5.2.4: Top view and full assembly view of stowed landing gear	57
Figure 5.2.5: Core type vs. powder type samples	58
Figure 5.2.6: TRIDENT drill with rotary brush attachment	60
Figure 5.3.1. Argus 2000 IR Spectrometer	64
Figure 5.3.2. Inficon Transpector Residual Gas Analyzer	65
Figure 5.4.1: Lander Body Axis Diagram	70
Figure 5.4.2: Thruster Misalignment Torque Generation, Top and Side View	72
Figure 5.4.3: RCS Torque Generation During Translation	72
Figure 5.4.4: Location of sun sensors from one side. Shows half the number of selected sensors	74
Figure 5.4.5: Plane Change Positional Error	76
Figure 5.4.6: Distance vs Error Plots	78
Figure 5.4.7: Lander GNC Block Diagram	80
Figure 5.4.8: Block Diagram for Velocity Targeting Mode	81

Figure 5.4.9: Phase Plane Targeting Diagram	82
Figure 5.4.10: Stabilized Hold Mode On the Phase Plane	83
Figure 5.4.11: Descent and Burn Mode Block Diagram	84
Figure 5.4.12: Powered Explicit Guidance Stages	85
Figure 5.4.13: 2D Trajectory Under PEG and Pitch vs Time	86
Figure 5.4.14: Spacecraft State History	86
Figure 5.5.1: 200N and 10N Thrusters for powering controlled descent and ADCS	92
Figure 5.5.2: Y-configuration of the 10N attitude control thrusters	93
Figure 5.5.3: Simplified schematic of the propulsion system	97
Figure 5.7.1: Watt density as provided by Minco	106
Figure 5.7.2: Minco Polyimide Thermofoil Patch Heater	106
Figure 5.8.1: Detailed Schematic of RAD750 Architecture	110
Figure 5.9.1: Endurosat S-band patch antenna	113
Figure 5.9.2: Radiation pattern for an Endurosat patch antenna	114
 Figure 6.1.1: The OMV with orbiter and lander modules	119
Figure 6.2.1: Deployment of HGA mast	123
Figure 6.2.2: Deployment of solar array	123
Figure 6.2.3: Hinge mechanisms	124
Figure 6.2.4: Release mechanism speed vs. time curves	124
Figure 6.2.5: Pyrotechnic cutter for shear tie cables	125
Figure 6.2.6: Moog Enhanced Gimbal Pointing Assembly	127
Figure 6.2.7: Honeybee ESPA Class Solar Array Drive Actuator	127
Figure 6.2.8: Basic dimensions of deployed solar array	128
Figure 6.3.1: Orbiter Body Axis Diagram	132
Figure 6.3.2: Cyclic vs Constant Torque Case	133
Figure 6.3.3: Block Diagram of Orbiter GNC	136
Figure 6.4.1: 1N monopropellant hydrazine thruster from the Ariane Group	140
Figure 6.4.2: Thruster Configuration from Spacecraft Reaction Thruster Configurations	141
Figure 6.5.1: Power-Voltage graph for the XTJ-Prime solar cell	144
Figure 6.5.2: Power layout for orbiter during sunlit period (a) and eclipse period (b)	145
Figure 6.6.1: Rosetta louvers and Cubesat louvers	149
Figure 6.8.1: Radiation pattern for a left hand circularized parabolic reflector antenna	158
 Figure 7.5.1: General Subsystem Integration and Testing Procedure	163
Figure 7.6.1: Preliminary Erebus Mission development timeline	166
 Figure 8.4.1: Lunar Lander Team Organization	168
Figure 8.4.2: Lunar Orbiter Team Organization	169

# List of Tables

Table 2.2.1: Lander mass budget by subsystem	19
Table 2.2.2: Lander propellant budget	20
Table 2.2.3: Lander power budget	20
Table 2.3.1: Orbiter mass budget by subsystem	23
Table 2.3.2: Orbiter propellant budget	24
Table 2.3.3: Orbiter power budget	24
Table 3.1.2: LLO Orbital Elements	26
Table 3.1.4: Orbital elements of frozen orbit upon entry	28
Table 3.1.5: Orbital elements of frozen lunar orbit after 10 years	29
Table 3.1.6: Phase Timeline	32
Table 3.2.1: Phase I Delta-V	33
Table 3.2.2: Phase III Delta-V	33
Table 3.2.3: Phase IV Delta-V	34
Table 4.1.1: Estimated launch mass of the Erebus Mission under two launch scenarios	40
Table 4.2.1: Summary of launch opportunities on current and near future EELV-class LVs	
43	
Table 5.4.1: GNC Fuel Budget	87
Table 5.5.1: Propellant mass budget	90
Table 5.5.3: Material Alloys and their Properties	94
Table 5.6.1: OXIS Energy Li-S cell specifications	99
Table 6.2.1: Deployment mechanism parameters	125
Table 6.5.1: XTJ-Prime Solar Cell Specifications	
144	
Table 7.1: Lunar lander center of mass	162
Table 7.6.1. Overview of Erebus Mission costs	166

*Note: Individual subsystem mass and power budgets have been omitted from this list for clarity. These budget tables can be found at the beginning of every subsystem chapter.*

# Acknowledgments

We are deeply grateful to Professor Edgar Choueiri for providing us the opportunity to challenge ourselves and for supplying us comprehensive background knowledge via lecture; to Madeline Vorenkamp and Andreas Giakas for their initial guidance in the design process and for their constant availability; to Mr. Michael Paluszek and Ms. Stephanie Thomas from Princeton Satellite Systems, who were extremely generous to share their practical knowledge and years of experience, for their detailed feedback in each design phase, and for their constant availability and feedback; to Mike Galvin, instrumental in every stage of the mission: providing direction, guiding individual members with technical expertise, encouraging ambition, and being available to the entire team practically continuously.

We are similarly grateful to Mr. Thomas Gryzmala of Lockheed Martin for supplying his expertise in spacecraft thermal analysis and providing guidance in our thermal design; to Mr. Joe Munder for his time and feedback on spacecraft mechanisms and ensuring a reliable design; to Dr. John Brophy and Dr. James Polk of NASA-JPL for sharing their experience, feedback, and encouragement; to Mr. Joe Troutman of EnerSys Advanced Systems for offering his industry experience to help select and size our batteries; and, finally, to our classmates in Team Oberth, who were extremely receptive to our presentation needs and actively shared ideas to improve our project.

# List of Acronyms

ACS	Attitude Control System
ADCS	Attitude Determination and Control System
AIAA	American Institute of Aeronautics and Astronautics
BOL	Beginning Of Life
C&DH	Command and Data Handling
CAD	Computer Aided Design
CHEOPS	Characterizing ExOPlanet Satellite
COM	Center of Mass
COTS	Commercial Off-the-Shelf
DoD	Depth of Discharge
EELV	Evolved Expendable Launch Vehicle
EM	Electromagnetic
EOL	End Of Life
EPGA	Enhanced Pointing Gimbal Assembly
EPS	Electric Power System
ESA	European Space Agency
ESPA	EELV Secondary Payload Adapter
FCV	Flow Control Valves
GCR	Galactic Cosmic Ray
GNC	Guidance, Navigation & Control
GPR	Ground Penetrating Radar
GEO	Geostationary Orbit
GTO	GEO Transfer Orbit
HGA	High-Gain Antenna
IFD	In-Flight Disconnect
IMU	Inertial Measurement Unit
IR	Infra-Red
ITO	Indium Tin Oxide
LCROSS	Lunar CRater Observation and Sensing Satellite
LEO	Low Earth Orbit
LLO	Low Lunar Orbit
LRO	Lunar Reconnaissance Orbiter
LRPR	Lunar Regolith Penetrating Radar
LV	Launch Vehicle
MGA	Mass Growth Allowance
MLI	Multi-Layer Insulation
MMH	Monomethylhydrazine
MON	Mixed Oxides of Nitrogen
NASA	National Aeronautics and Space Administration
NIR	Near Infra-Red
O/F	Oxidizer to Fuel
OMV	Orbital Maneuvering Vehicle

RCS	Reaction Control System
RF	Radio Frequency
RGA	Residual Gas Analyzer
RIMFAX	Radar Imager for Mars' Subsurface eXploration
SADA	Solar Array Drive Actuator
SBC	Single Board Computer
SMAD3	Space Mission Analysis and Design, 3rd ed.
SPE	Solar Particle Events
SRP	Solar Radiation Pressure
TLI	Trans-Lunar Injection
TRL	Technology Readiness Level
TVC	Thrust Vector Control
TDRS	Tracking and Data Relay Satellites
VDA	Vacuum Deposited Aluminum
VNC	Velocity, Normal, Co-Normal Frame

# Executive Summary

With the Artemis program, NASA has placed the moon at the core of its space exploration ambitions, eventually aiming to use the moon as a base for further space exploration, with Mars being the first and foremost target. To achieve this, the Artemis program includes plans for various lunar landers and an orbiting spacecraft called the Lunar Gateway. Following results from the NASA LRO and LCROSS missions, lunar surface ice was identified in some regions of the moon that are permanently shaded, such as in Shackleton Crater on the lunar South Pole. While the ice's presence is confirmed, its volume is unknown, and on-surface measurements of depth and density are crucial to providing the next level of detail.

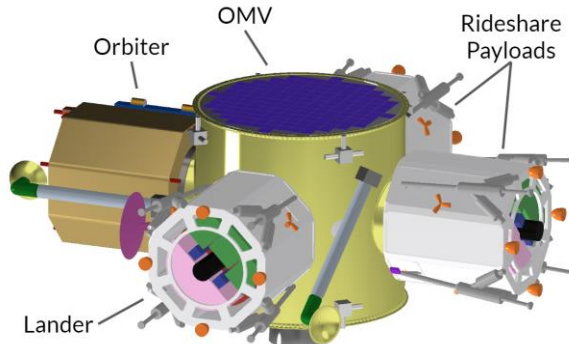
This context has been the ultimate motivation for the development of the Erebus mission, which derives its name from the Greek deity of darkness and shadows. The mission consists of two main components: a lunar lander and a lunar orbiter module. Together, these modules will serve to advance scientific understanding of lunar surface ice and its composition, providing the opportunity to further the understanding of the moon's origins and to help inform and guide the mission planning of future steps in the Artemis program. Moreover, the orbiter will signify the start of the development of a lunar communications network, providing stable communications services for lunar missions with Earth. The Erebus mission relies heavily on heritage architecture, standardized ESPA interface requirements, and broad freedom in launch opportunities. The spacecraft of the Erebus mission, the lunar lander and an accompanying lunar orbiter, are designed to be replicable and allow for low-cost development of future science missions to the lunar surface.

## Mission Description

Following launch as a co-primary payload on the Falcon 9 (or rideshare payload on the Falcon Heavy), with a dropoff at either GEO Transfer Orbit (GTO) or Trans-Lunar Injection (TLI), an Orbital Maneuvering Vehicle (OMV), as visualized in Figure i, will transfer both the lander and orbiter module towards a Low Lunar Orbit (LLO). The OMV will be an adaptation of *Figure i. CAD Model of the OMV concept.*

an off-the-shelf solution produced by Moog, based on Moog's standard bus Comet/Astro concept, which comes with a power, ADCS, thermal and avionics systems. The current design concept offers room for 4 ESPA-class spacecraft, of which two will be occupied by the Erebus mission. The remaining two slots can be used for rideshare vehicles.

Once arrived in lunar orbit, the 433.7 kg wet mass lander (Figure ii) will separate from the OMV and commence its four-hour-long, fully-automated landing procedure towards Shackleton Crater, on the South Pole of the moon. Using four main thrusters for the main entry burn, the lander will slow down and land within a 5km landing ellipse, using its four deployable landing gear legs. The reason for the presence of surface ice in that crater is that it largely lies in permanent shade. Therefore, the lander will operate without any solar power, relying solely on batteries to power its components. The main power draw comes from the drill, which is located along the main axis of the lander. The lander will drill into the



lunar surface to a depth of at least 50 centimeters, retrieving powdered samples that will be analyzed by the on-board science payload.

The lander's payload houses a near infrared spectrometer, a residual gas analyzer, and a ground penetrating radar. These components will provide a compositional analysis at various depths of lunar regolith at the landing site, as well as a depth analysis of water-ice deposits through ground penetrating radar. This will provide significantly detailed knowledge on lunar surface ice composition and volume, which will help inform crucial future lunar missions and provide a basis for scientific research on the moon's origins and human-lunar habitation.

All scientific data will be relayed to the lunar orbiter module using an

*Figure ii. CAD model of the lander.*

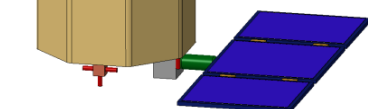
S-band patch antenna before the end of the 20-hour on-surface lifetime.

Following lander separation, the OMV, with the orbiter module still attached, will commence its transfer towards a frozen, near-polar lunar orbit with an orbital period of roughly 2.4 hours. Upon completion of this transfer, the 243.2 kg wet mass lunar orbiter module (Figure iii) will separate from the OMV, after which the latter will de-orbit into the lunar surface. After successful separation, the orbiter will deploy its High-Gain Antenna (HGA) mast, which houses a Ka-band dish antenna for communications with Earth. Additionally, the orbiter will deploy its 2.26 square meter solar array, which will power the orbiter's systems.

Throughout its 10 year lifetime, the spacecraft's central axis will always be aligned with the nadir (with the possibility of 15-degree off-axis pointing). This means that the S-band patch antenna on the bottom of the spacecraft will always be pointed towards the lunar surface, always allowing for a connection with the lunar surface, the Erebus lunar lander, and many lunar missions to come. However, since the orbit is neither sun- nor earth-synchronous, the HGA and solar arrays have been fitted with gimbals to allow for active Earth- and Sun-pointing, respectively.

The orbiter will neglect stationkeeping, resulting in only a slight change in orbit over its lifetime (slightly more eccentric and a shifting RAAN). This allows for significant mass savings, while providing optimal coverage to the lunar poles, as well as good coverage for the rest of the lunar surface: The longest average revisit time of a location on the lunar surface is 6.6 hours.

One of the main challenges for the orbiter is the survival of eclipses, putting a high strain on the thermal management system and consequently the power requirements. Through active thermal systems and a significant battery, the orbiter will be able to survive regular eclipses in full-power mode and the longest (lunar) eclipse in a low-power mode.



## 1. Introduction

This report was written within the context of an undergraduate course at Princeton University, titled MAE342: Space Systems Design. In this course, the principles and design aspects of the structure,

propulsion, power, thermal, communication, and control subsystems are studied. The course also introduces elements of systems engineering, mission operations, mission design, and space policy. The purpose of this project was to familiarize students with the complexity and challenges associated with all aspects of space systems design through the development of a space mission of our own choice, from conception to critical design review. Team Goddard, consisting of the group of twenty-three students listed on the title page, is delighted to present the critical design review report of the Erebus lunar mission.

The initial focus of the mission was the design of a small-scale lunar lander, which has been developed to a CDR level of design. Later in the project, this work expanded into the design of a lunar orbiter, which in this report is presented at a PDR level. In addition to those spacecraft, this report provides some work on an Orbital Maneuvering Vehicle (OMV), which will be a commercial craft especially adapted for the Erebus mission purposes. This spacecraft is only covered at the highest level.

We're delighted to present the Erebus mission and all of its components to you. Through a challenging time in the context of a global pandemic, conducting work from all around the world, we are proud of the work shown in this report, and we hope you enjoy reading it.

- Team Goddard

## 2. Mission Overview

### 2.1 Motivation and Mission Objectives

With the Artemis program, NASA has put the moon at the core of its space exploration ambitions. With the goal of putting the first woman and next man on the lunar surface in 2024, NASA eventually aims to use the moon as a base for further space exploration, with Mars being the first and foremost target. To achieve this, the Artemis program includes plans for various lunar landers and an orbiting spacecraft called the Lunar Gateway.<sup>1</sup> The Gateway will be a small spaceship in orbit around the Moon that will provide access to a large part of the lunar surface with living quarters for astronauts, a lab for science and research, ports for visiting spacecraft, and more. It will be placed into a polar halo orbit with a period of roughly seven days, the orbital parameters of which will roughly be held constant over its lifetime.<sup>2</sup>

This context provides the background and main motivation for the Erebus mission. For the development of on-surface lunar resources, such as production of rocket fuel, and providing resources for human lunar habitation, it is essential to research lunar surface ice. Lunar surface ice has been identified in some regions of the moon that are in permanent shade. An example of this is Shackleton Crater, which is located near the south pole.<sup>3</sup> While the presence of ice is confirmed, its volume is unknown, and on-surface measurements of depth and density are crucial to providing the next level of detail.

Through analysis of the ice and its composition, the Erebus lunar lander, which derives its name from the Greek deity of darkness and shadows, will provide the opportunity to further the understanding of the moon's origins. It will also help guide the mission planning of future steps in the Artemis program. Traditionally, science missions to the lunar surface are expensive and require a lot of development. To mitigate this challenge, the Erebus mission relies heavily on heritage architecture, standardized ESPA interface requirements, and small-scale spacecraft to allow for freedom in launch opportunities. The spacecraft of the Erebus mission, the lunar lander and an accompanying lunar orbiter, are designed to be replicable and allow for low-cost development of future science missions to the lunar surface.

In addition to gaining knowledge on lunar surface ice, the second primary objective of the Erebus mission is to provide a communication link between the moon and Earth. While the Lunar Gateway will eventually provide this service as well, its constant polar orbit limits its ground coverage. Additionally, its relatively long orbital period of seven Earth days results in a long intermittency between contact with the lunar surface, which the Erebus mission will mitigate. Through an ESPA class communications satellite the Erebus mission can provide an alternative communication link with Earth with coverage of most of the lunar surface, providing a faster relay of data to and from on-surface missions. While the Erebus mission will only launch one such communications spacecraft, its replicability allows for the possible development of a reliable lunar communications network, further advancing the possibility of lunar habitation and reducing the need for orbiting vehicles in future science missions to provide the crucial communication link for scientific data.

---

<sup>1</sup> NASA (2020). Artemis Program. Retrieved from <https://www.nasa.gov/specials/artemis/>. Accessed on May 7th, 2020.

<sup>2</sup> ESA (2019). Angelic halo orbit chosen for humankind's first lunar outpost. Retrieved from [https://www.esa.int/Enabling\\_Support/Operations/Angelic\\_halo\\_orbit\\_chosen\\_for\\_humankind\\_s\\_first\\_lunar\\_outpost](https://www.esa.int/Enabling_Support/Operations/Angelic_halo_orbit_chosen_for_humankind_s_first_lunar_outpost). Accessed on May 7th, 2020.

<sup>3</sup> NASA (2012). Researchers Estimate Ice Content of Crater at Moon's South Pole. Retrieved from [https://www.nasa.gov/mission\\_pages/LRO/news/crater-ice.html](https://www.nasa.gov/mission_pages/LRO/news/crater-ice.html). Accessed on May 7th, 2020.

### 2.1.1 Lunar Lander Mission Objectives

The Erebus Lunar Lander's main objective is to gather data on the lunar ice composition in the Shackleton Crater. Since it will operate in total darkness, the lander will rely solely on battery power and have a relatively short on-surface lifetime of twenty hours. Once landed, it will drill into the lunar surface, and transport samples into a science laboratory that will carry out a thorough analysis. This analysis, coupled with data acquired from Erebus' ground penetrating radar, will:

- Provide a compositional analysis vs. depth of lunar regolith at the landing site, with an interest specifically on water-ice.
- Provide a depth analysis of water-ice deposits through ground penetrating radar, as the deposits potentially extend much lower than our drill bit can reach.
- Estimate the total volume of water-ice in the vicinity of the landing site.

This data will be processed to determine:

- Availability of on-surface lunar resources.

Ultimately, because surface ice may exist due to both asteroid and comet impact or additionally due to other factors present during the moon's formation, these composition and depth data will also be used to:<sup>4</sup>

- Gain insights into the formation and history of the moon.

Following the data acquisition, the lander will communicate its findings back to Earth through the Erebus Lunar Orbiter and after completion of its mission, it will eventually run out of battery power and go dormant on the surface. If successful, the lander will offer a primer for landers powered solely by batteries on a smaller scale than ever before, in a well-established ESPA format. This would allow for many future science missions using the same format with their own respective science payloads, drastically reducing those missions' costs.

### 2.1.2 Lunar Orbiter Mission Objectives

The Erebus Lunar Orbiter's main objective, in its most general terms, is to provide a data link between the lunar surface and Earth. More specifically, the orbiter will provide communications services to the lander and communicate all telemetry and scientific data back to Earth through a connection with the TDRS network. Beyond the lander mission lifetime, the orbiter's purpose shifts to become a more general purpose lunar surface communications satellite, providing a data link opportunity for future science or human missions to the Moon. This translates to the following main mission objectives:

- Maintain a lunar orbit for a lifetime of 10 years, providing communication coverage to a majority of the lunar surface

---

<sup>4</sup> Deutsch, Head III, Neumann, (2019), "Analyzing the ages of south polar craters on the Moon: Implications for the sources and evolution of surface water ice," retrieved from: <https://doi.org/10.1016/j.icarus.2019.113455>

- Relay all lander scientific data and telemetry back to Earth
- Provide sufficient data rates to support lunar missions at a larger scale than the Erebus lander in the future

Following successful orbiter deployment, the Erebus orbiter can serve as a primer for future lunar communications satellite missions, and even the start of a dedicated lunar communications network. Its small scale, high replicability, relatively low development cost and a wide variety of launch opportunities (all to be covered later in this report) offer the perfect base for the development of such a network, which can serve the greater advancement of science, space exploration, and NASA's Artemis program.

## 2.2 Lunar Lander Mission Overview

### 2.2.1 System-Level Requirements

The lander's mission main objectives as they are outlined in section 2.1.1 guided the development of a set of system-level performance requirements that guided the overall design of the spacecraft. These requirements, as they are outlined below, have been refined throughout the iterative design process and are presented here in their final form. While they are formulated at a system level, the requirements are categorized by subteam to indicate their ownership. All detailed subsystem requirements are numbered and can be found in Appendix B.1. Throughout the report, sections will mention these requirement numbers.

#### *Mission planning*

- The lander shall complete a fully automated landing sequence, landing within a 6 km landing ellipse in Shackleton Crater (more information and justification in Sections 3.1.3 and 5.4.1).

#### *Launch Vehicle and ESPA class requirements*

- The lander shall comply with all mass, volume and resonant frequency constraints put forth by LV integration requirements and ESPA class design guidelines (see Section 4.4).

#### *Landing System*

- The landing system shall absorb energy of impact on the lunar surface, minimizing the risk of damage to spacecraft components.
- The landing system shall provide a stable, non-rotating, leveled stance throughout all on-surface operations.

#### *Payload*

- The lander's science payload shall provide a compositional analysis vs. depth of lunar regolith at the landing site, with an interest specifically on water-ice.
- The lander's science payload shall provide a depth analysis of water-ice deposits through ground penetrating radar.

#### *Drill Mechanism*

- The lander's drill mechanism shall drill to a depth of at least 50 centimeters into the lunar surface, delivering samples in a powdered form.
- The lander's drill mechanism shall retain more than 75% of the volatiles in the sample.

*Propulsion*

- The lander's propulsion system shall provide a delta-V capacity of at least 1700 m/s, required to slow the lander down sufficiently on its descent towards the lunar surface.

*GNC*

- The lander's GNC system shall guide, navigate, and control the spacecraft using both the reaction control and main thrusters to a landing within the accuracy requirements of the mission planning team (6 km) and with touchdown characteristics within mechanically survivable limits.

*Power*

- The lander's power system shall provide all lander components with sufficient power to survive and operate during the ~4 hour landing procedure and ~20 hour on-surface lifetime.
- The lander's power system shall provide all electric power using solely batteries, as the lander will operate in complete darkness.

*Communications*

- The lander's communication system shall communicate telemetry data to the Erebus lunar orbiter during lander descent and on-surface operations.
- The lander's communication system shall communicate all scientific data to the Erebus lunar orbiter during on-surface operations.

*Thermal*

- The lander's thermal system shall ensure that all components will remain within their respective allowable temperature limits for the entire mission duration.

## 2.2.2 Spacecraft Architecture

The Erebus lunar lander is designed to fit all of the subsystem components of a planetary lander within the ESPA Grande volume envelope, and the final design packages all components within a structure that is less than one cubic meter in volume. The main structure of the spacecraft is an octagonal prism; this allows for symmetrical placement of the four main thrusters and the four deployable legs, the latter of which fold up into the ‘corners’ of the ESPA volume envelope. An octagonal structure was chosen over a hexagon because it allows for greater internal volume, given the same limits on the outer dimensions.

The most important feature of the lander’s architecture is the axial placement of the drill. In order to maximize drilling depth without requiring significant complex robotic drilling assemblies, the drill must take up as much vertical space within the body of the lander as possible.<sup>5</sup>

---

<sup>5</sup> A drill mounted on a robotic arm was considered, but the following considerations made the axially-mounted drill more attractive: a fully articulated robotic arm would be a completely new component, and introduce huge complexity and development cost to the spacecraft; the depth of an arm-mounted drill would be limited; and the necessary counter-torque to resist the motion of an arm-mounted drill would be difficult to ensure.

Figure 2.1 shows two views of the lander in its deployed configuration, with important components labeled. The image on the left shows the lander without the aluminum honeycomb panels that cover the sides; in the image on the right, the panels are shown. These will provide mounting points for interior hardware, as well as a surface to attach the insulation and low-emissivity coating.

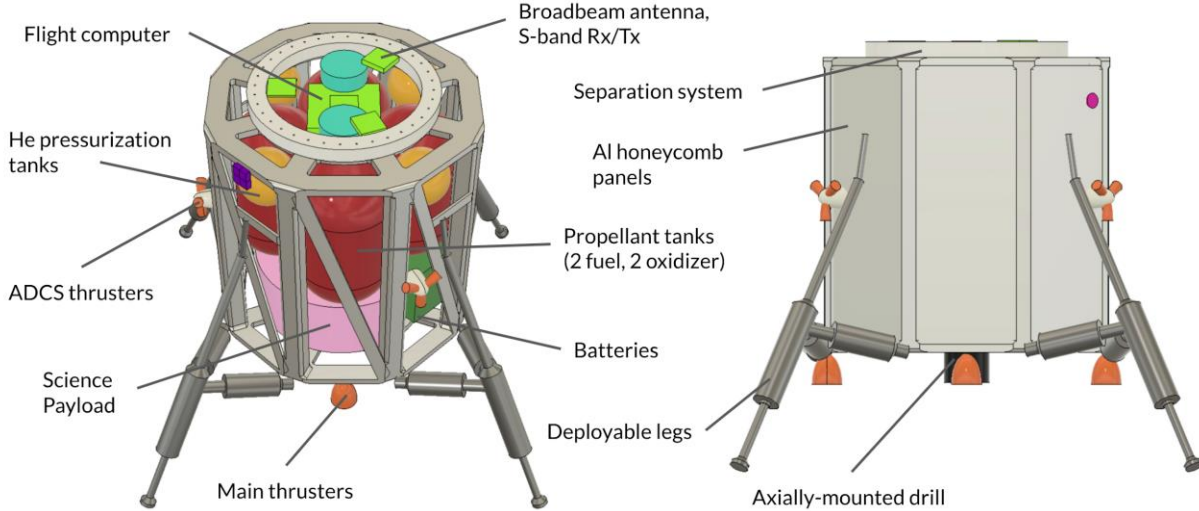


Figure 2.1: Packaging model of Erebus lunar lander.

The internal placement of components was driven by the placement of the axial drill and center of mass considerations. The top surface of the lander serves as the attachment point to the ESPA ring; as a result, it is desirable to keep the center of mass close to this surface at launch. However, when landing, having the center of mass towards the bottom of the lander is better for stability. To achieve this, the propellant tanks (which dominate the internal volume, and are shown in red) are placed towards the top of the lander so that, as the propellant is consumed, the center of mass moves towards the bottom of the lander.

The lower part of the lander is occupied by the science payload (pink) and the batteries (dark green), visible on the right in Figure 2.2. The science payload is placed at the bottom of the lander to ensure easy access to regolith retrieved by the drill. Four main thrusters are mounted to the bottom of the lander, while the smaller ADCS thrusters are grouped in three groups of three and mounted to the sides.

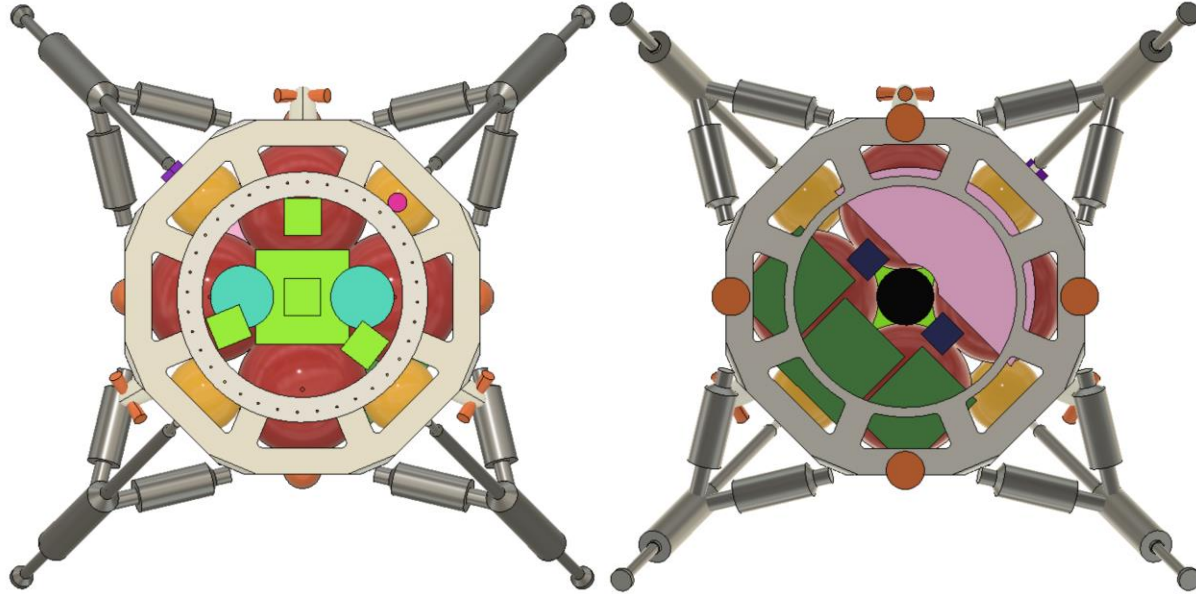


Figure 2.2: Top (left) and bottom (right) views of the lander packaging model.

Also visible on the bottom of the lander are the downward-facing radar sensors, in dark blue. The broadband antenna, as well as the S-band transmitter and receiver, are placed on the top surface of the lander to ensure maximum communication time with the orbiter; these are shown as the smaller bright green squares in Figure 2.2. The larger bright green square is the flight computer, and the teal discs are the IMUs. Furthermore, the packaging model includes the six sun sensors and two star trackers on the exterior of the lander.

Not included in the lander packaging model are the eight-inch-diameter landing pads, which will be affixed to the ends of the legs; the anti-torque spikes which will protrude from the center of the landing pads and stick into the regolith upon impact; and the ground proximity sensors, which will hang off of the legs and indicate when the lander is just above the lunar surface.

### 2.2.3 Mass Budget

Various subsystems of the lunar lander had varying levels of specificity in their designs for the CDR; as a result, the mass budget is presented by giving each subsystem an individual mass growth allowance (MGA) depending on the design. Then, an overall system-level margin of 10% is applied to the sum of the subsystem masses in order to arrive at the total dry mass. The dry mass of the lander is 213.7 kg, and the wet mass is 433.7 kg. Detailed mass budgets for each subsystem may be found in each of the following chapters.

### Subsystem Mass Budget

Subsystem	Component Mass (kg)	MGA (%)	Total Mass (kg)
Structure/LV Integration	41.5	15	47.7
Mechanisms	25.8	25	32.2
Payload	20.0	25	25.0
Power/C&DH	28.6	25	35.8
Propulsion	36.4	15	41.8
GNC	3.6	15	4.2
Communications	2.9	15	3.3
Thermal	1.1	300	4.2
<b>Total:</b>			<b>194.2</b>
<b>10% System-Level Margin:</b>			<b>19.5</b>
<b>Total Dry Mass:</b>			<b>213.7</b>
<b>Propellant Mass:</b>			<b>220.0</b>
<b>Total Wet Mass:</b>			<b>433.7</b>

Table 2.2.1: Lander mass budget by subsystem.

The structure of the lander has a detailed CAD model, and a specific COTS ESPA separation system has been selected, so the structure/LV integration mass is fairly well-defined, and therefore gets an intermediate 15% MGA; this is to account for mounting hardware, the detailed design of which was outside the scope of this report. The mechanisms and payload, which will require additional robotic components in addition to the components and instruments already selected, get a large 25% MGA. The power and C&DH subsystems are also allowed a mass growth of 25%, with this extra mass allotted for battery mounting/packaging and overall harnessing. The propulsion system is well-characterized, and the component mass includes a SMAD3-based estimate for plumbing line and valve mass (1.2x the total mass of all thrusters), so an intermediate 15% mass growth is allowed.<sup>6</sup> The GNC and communications subsystems have selected their components, but some may require modification or customization; as a result, their MGA is the intermediate value of 15%. The thermal subsystem is a special case; only single-node thermal analysis has been carried out to this point, so the thermal subsystem mass only covers heating elements and coatings. The 300% MGA is to anticipate the eventual inclusion of additional components, such as heat pipes and MLI blankets. As is customary for spacecraft reaching CDR, a 10% system-level margin is applied to the subsystem totals to arrive at a total dry mass of 213.6 kg.

---

<sup>6</sup> *Space Mission Analysis and Design*, 3rd ed., ed. by James R. Wertz and Wiley J. Larson (Hawthorne, CA: Microcosm Press, 1999), 346.

### *Propellant Budget*

The propellant budget is broken down into four categories: delta-V propellant, ADCS propellant, propellant margin, and residual; the lander uses MMH and MON as its propellants. The delta-V propellant is 90% of the total dry mass, and the total propellant mass is 220 kg.

Purpose	Mass (kg)
Delta-V	192.3
ADCS	5.0
10% Margin	19.2
2% Residual	3.5
<b>Total:</b>	<b>220.0</b>

Table 2.2.2: Lander propellant budget.

### 2.2.4 Power Budget

Component	Power (W)	Energy (Wh)
Comms/C&DH	20.4	510
Mechanisms	250	5500
Payload	55	110
Propulsion	25	0.25
GNC	31.6	52
Thermal	50	1250
<b>Subsystem total</b>	<b>432</b>	<b>7422.2</b>
<b>Allocated</b>	<b>546.25</b>	<b>9280.1</b>
<b>Margin</b>	<b>114.25 (26%)</b>	<b>1857.8 (25%)</b>

Table 2.2.3: Lander power budget.

All components have the 25% power margin standard to components only moderately defined (SMAD3), with the exception of the propulsion system, which has a 50% margin. Propulsion power consumption is a result of valve actuation (an impulse each time a thruster is fired), the particular sequence of which is highly dependent on the particular trajectory and unforeseen disturbances: almost random.

## 2.3 Lunar Orbiter Mission Overview

### 2.3.1 System-Level Requirements

The lunar orbiter's mission main objectives as they are outlined in section 2.1.2 guided the development of a set of system-level performance requirements that guided the overall design of the spacecraft. These requirements, as they are outlined below, have been refined throughout the iterative design process and are presented here in their final form. While they are formulated at a system level, the requirements are categorized by subteam to indicate their ownership. All detailed subsystem requirements are numbered and can be found in Appendix B.2. Throughout the report, sections will mention these requirement numbers.

#### *Mission planning*

- The orbiter shall be placed in a stable orbit with minimal stationkeeping requirements.
- The orbiter shall be placed in an orbit that minimizes revisit time to locations on the lunar surface, while providing coverage to as much of the lunar surface as possible.

#### *Launch Vehicle and ESPA class requirements*

- The orbiter shall comply with all mass, volume and resonant frequency constraints put forth by LV integration requirements and ESPA class design guidelines (see section 4.4).

#### *Mechanisms*

- The orbiter shall deploy a high-gain antenna (HGA) mast and solar array.
- The orbiter shall operate a HGA gimbal to provide maximum communications time with Earth.
- The orbiter shall operate a solar array gimbal to maximize solar power capture.

#### *Propulsion*

- The orbiter's propulsion system shall provide a delta-V of 30 m/s, required to de-orbit the orbiter at the end of its lifetime.
- The orbiter shall provide necessary total impulse for ACS pointing requirements.

#### *GNC*

- The orbiter's GNC system shall determine the spacecraft's attitude for accurate Earth communications antenna gimbaling, point at the lunar surface to communicate with other missions, with 15 degree off-nadir pointing capability, and reject external disturbance torques. It will also perform control and guidance for the final deorbit burn.

#### *Power*

- The orbiter's power system shall provide all orbiter components with sufficient power to operate in full-power mode when the orbiter is in direct sunlight.
- The orbiter's power system shall ensure sufficient power to survive regular (48.3 min) eclipses in full-power mode and rare (3h15 min) eclipses.

### *Communications*

- The orbiter's communication system shall communicate telemetry and scientific data received from the Erebus lunar lander to Earth.
- The orbiter's communication system shall have sufficient capacity to provide communication services to future lunar missions with higher data link requirements than the Erebus lunar lander.

### *Thermal*

- The lander's thermal system shall ensure that all components will remain within their respective allowable temperature limits for the entire mission duration.

## 2.3.2 Spacecraft Architecture

In order to take advantage of the work done on the lunar lander in terms of compliance with ESPA requirements, in terms of both volume and structural integrity, the Erebus lunar orbiter uses the same octagonal paneled structure as the lander; as the design process moves forward, the internal structure of the orbiter is subject to change, as it no longer needs to support large internal propellant tanks and an axially-mounted drill, but instead has to support two significant deployable structures: the high-gain antenna (HGA) mast, and the deployable solar array. During operation, the side opposite the ESPA attachment points towards the Moon.

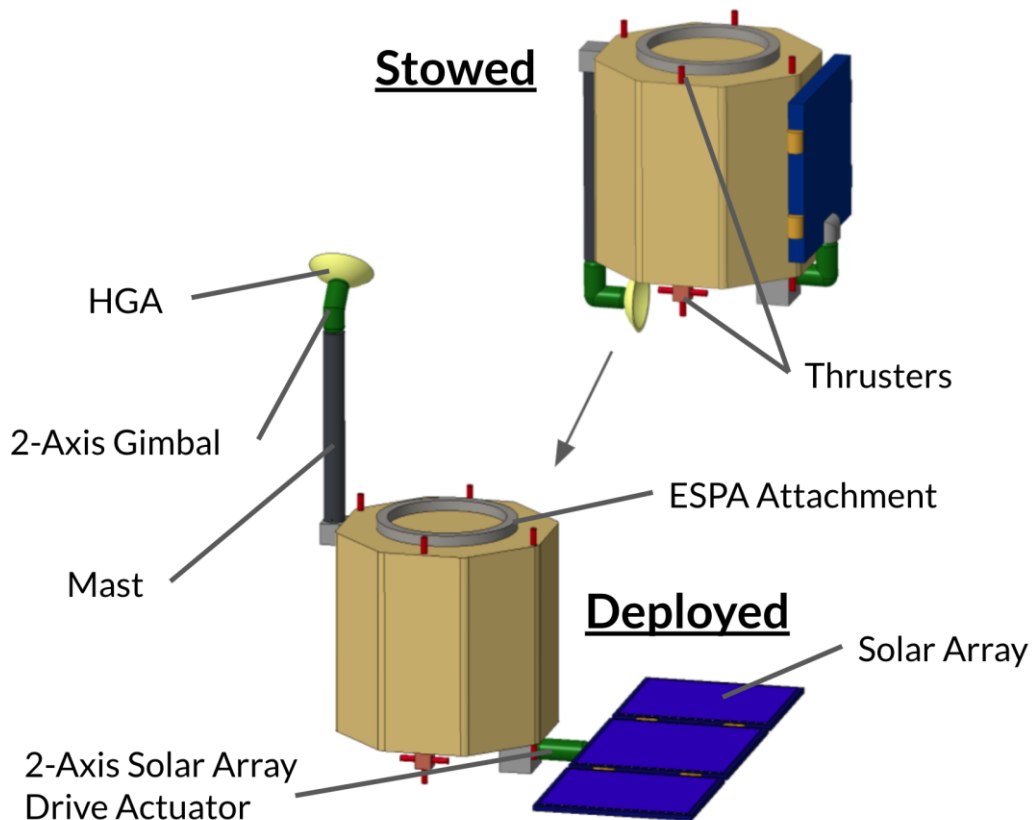


Figure 2.3: Erebus lunar orbiter model and deployment scheme.

As shown in Figure 2.3, in the stowed configuration, the mast and solar array lie flat against the spacecraft body, within the ESPA volume envelope. After separating from the OMV, the orbiter deploys

the mast and gimbals to communicate with Earth and meet its power requirements. The HGA is mounted on a mast, far away from the body of the orbiter, mainly to limit the area of sky blocked by the spacecraft, maximizing the HGA's field of view and maximizing line of sight with Earth. A 2-axis gimbal allows the HGA to point at Earth, and establish a link, whenever there is line of sight from Earth to the orbiter, thereby maximizing communication time. The solar array can also rotate about two axes, facilitated by two solar array drive actuators with slip rings, in order to orient itself towards the sun. The solar arrays will be slightly larger than portrayed in Figure 2.3, but they will be stowed and deployed in the same triptych configuration. Not shown in the visualization is the Moon-pointing antenna, on the bottom surface of the orbiter; the orbiter's low-gain antennas; and the thermal louvers.

### 2.3.3 Mass Budget

The following table shows the orbiter subsystem masses; detailed mass budgets can be found in each subsystem chapter. Because the design of the orbiter has not yet reached the level of maturity of the lander, all subsystem mass growth allowances are treated as 25%. In addition, as is customary for a spacecraft approaching its preliminary design review, a 20% system-level mass margin is added after the mass growth allowance. These two margins together create a 50% total mass margin. The dry mass of the orbiter is 230.5 kg, and the wet mass is 243.2 kg.

*Subsystem Mass Budget*

Subsystem	Component Mass (kg)
Structure/LV Integration	41.5
Mechanisms	14.9
Power/C&DH	47.1
Communications	7.5
Propulsion	8.9
GNC	17.7
Thermal	16.0
<b>Subsystem Total:</b>	<b>153.7</b>
<b>25% Mass Growth Allowance:</b>	<b>38.4</b>
<b>Subtotal:</b>	<b>192.1</b>
<b>20% System-Level Margin:</b>	<b>38.4</b>
<b>Total 50% Mass Margin:</b>	<b>76.8</b>
<b>Dry Mass:</b>	<b>230.5</b>
<b>Propellant Mass:</b>	<b>12.7</b>
<b>Wet Mass:</b>	<b>243.2</b>

Table 2.3.1: Orbiter mass budget by subsystem.

### *Propellant Budget*

The propellant budget consists of propellant needed for ADCS, propellant needed for the EOL delta-V maneuver, and a margin. The orbiter uses a total of 12.7 kg of hydrazine.

Purpose	Mass (kg)
ADCS	5.7
EOL delta-V	3.0
Margin (31.5%)	4.0
<b>Total:</b>	<b>12.7</b>

Table 2.3.2: Orbiter propellant budget.

### 2.3.4 Power Budget

Component	Power (W)	Energy (Wh)	Notes
Comms/C&DH	64	103.4	
Mechanisms	56	132	
Propulsion	60	0.12	5 min every 95 hrs
GNC	57.18	130.8	
Thermal	300	1500	
<b>Subsystem total (shade)</b>	<b>477.18</b>	<b>516.46</b>	Not including propulsion
<b>Subsystem total (sun)</b>	<b>177.18</b>	<b>366.46</b>	Not including thermal or propulsion
<b>Allocated (shade)</b>	<b>620.33</b>	<b>671.39</b>	Not including propulsion
<b>Allocated (sun)</b>	<b>230.33</b>	<b>476.39</b>	Not including thermal or propulsion
<b>Margin (shade)</b>	<b>143.15 (30%)</b>	<b>154.93 (30%)</b>	
<b>Margin (sun)</b>	<b>53.15 (30%)</b>	<b>109.93 (30%)</b>	

Table 2.3.3: Orbiter power budget.

All systems are supplied the 30% margin standard where hardware choices are only loosely defined (SMAD3).

## 3. Mission Analysis and Orbit Design

### 3.1 Mission Phases

#### 3.1.1 Phase I: Launch to Trans-Lunar Injection

The resultant plan for the mission followed careful consideration of four different launch opportunities. Delta-V analysis of launch opportunities from LEO, GTO, GEO, and a dedicated launch proved the lowest requirements belonged to a launch from GTO, as shown in Table 3.2.1. These values were calculated using STK with the assumption that all maneuvers are impulsive. This assumption aligns with Team Goddard's use of chemical thrusters and resulting short maneuvers.

Completing a launch from LEO would require the greatest delta-V. Therefore, launch from LEO is the least efficient option. Though a dedicated launch would permit independence, it is also demanding in its delta-V requirements.

In addition to requiring the lowest delta-V, a geostationary transfer orbit for reaching a lower lunar orbit allows for greater launch opportunities, as it is commonly utilized and previously explored. Because GTO has this advantage associated with launch opportunities, it is chosen over a rideshare option allowing for launch from TLI. Following a launch from GTO, the space vehicle will complete a trans-lunar injection.

#### 3.1.2 Phase II: Transfer to LLO

The TLI phase of the mission will take the OMV with lander and orbiter to the southern pole of the moon, at which point the OMV will execute an impulsive maneuver with thrust in the anti-velocity direction to ensure that it is caught by the lunar gravity in a circular orbit. The launch to TLI phase is extremely important, as this will ensure entry to the lunar region at the proper inclination and altitude, making it necessary to only perform a maneuver in one direction in order to obtain the desired lunar orbit. Though the eccentricity of the orbit is meant to be 0, the LLO entry point over the lunar south pole will serve as the periapsis of the orbit. Once in LLO, the OMV will complete two full orbits in order to confirm with ground control that the proper lunar orbit for lander departure has been obtained. The OMV will experience sunlight for the entirety of its time in LLO. In the LLO the OMV will have communications access with the Earth for approximately 58 minutes at a time, and during the entirety of the GNC part of the landing sequence (described in Section 3.1.3). The orbital elements for this initial LLO are described in Table 3.1.2.

LLO Element Upon Entry	Value
------------------------	-------

Inclination	$90^\circ$
Eccentricity	0
Altitude of Periapsis	50 km
Argument of Periapsis	$0^\circ$
RAAN	$0^\circ$
True Anomaly	$180^\circ$

Table 3.1.2: Orbital elements of LLO.

Entering at an altitude of 50 km is a suitable compromise between obtaining an altitude that is as close as possible to the braking altitude (Section 3.1.3) and also providing adequate communications time with the Earth and lander during the landing sequence.

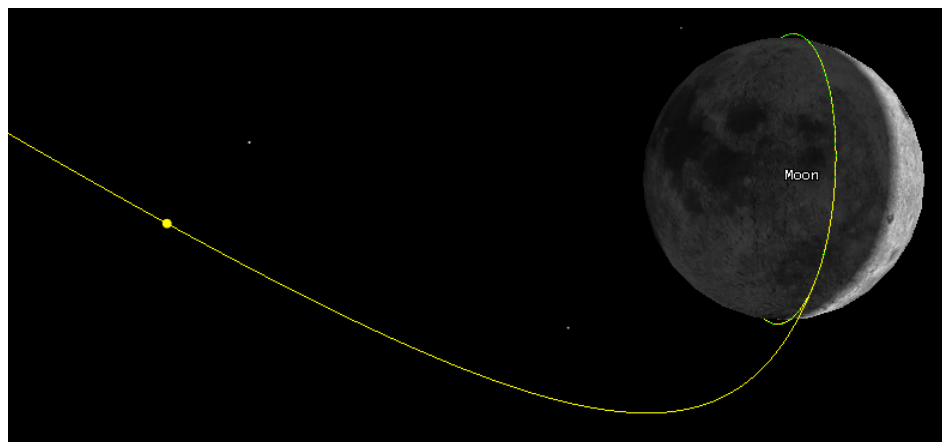


Figure 3.1.2a. Depiction of orbit going from TLI (yellow) to LLO (green).

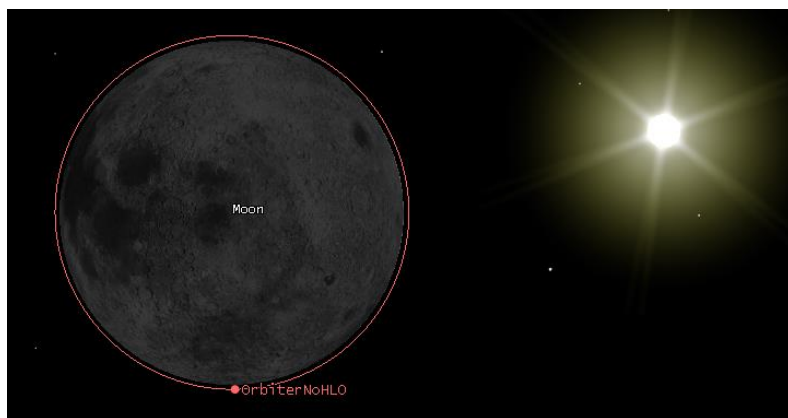


Figure 3.1.2b. Visual of orbiter in initial LLO.

### 3.1.3 Phase III: Lander Descent to Surface

The burn time, burn distance and resulting velocity from this section were obtained using STK reporting functionality. Mike Paluszek's lunar lander control document was used to target specific velocities and altitudes for this trajectory.

After the OMV orbits twice around the moon in order to verify its orbit with ground control, the lander will detach from the OMV 1 minute before reaching the apoapsis of the orbit. The first burn will occur at apoapsis. The choice for detaching at apoapsis is reliant on the fact that the periapsis of the LLO is at the entry point over the south pole. Additionally, detaching 1 minute before a burn is done to meet the GNC requirement for control. This fact leads to orbital apoapsis occurring over the north pole of the moon, which has been determined to be the departure location that provides the best mid-transfer communications opportunities and simplest maneuver sequence for the lunar lander.

After detaching from the lunar north pole apoapsis location, the lander performs an impulsive periapsis-lowering maneuver by firing in the direction opposite of its velocity, entering an elliptical transfer orbit with a periapsis of 0.3 km. Upon reaching a periapsis of the elliptical transfer orbit, the orbiter will impulsively circularize at this altitude, proceeding to orbit once before completing a finite burn for 1653 s after reaching the point in orbit that is 2100 km before the center of Shackleton Crater. This will yield an in-track velocity of 0.3 m/s and radial velocity of -50 m/s. The lander height at the end of this burn is 0.1 km and the downrange length from the ideal landing site is 0.1 km. This burn will be monitored by GNC, and the end of the finite burn will be completely controlled by GNC, which will ensure the lander will touch down safely in Shackleton Crater. This final landing sequence is expected to take 15 minutes. The location of the lander within Shackleton Crater is meant to be exactly in the center. However, potential error in this location is acceptable, as the entire interior of the crater does not receive sunlight and is covered in lunar surface ice. Since the crater is 20 km in diameter, inaccuracies in tracking during the landing procedure or slight differences in orbital elements of the lander orbit should not be of concern. The lander will have a direct line of sight to the OMV and orbiter during the entire landing procedure, allowing for communication with ground control during the entire phase.

The lander will collect lunar surface ice and analyze it, proceeding to then send the results to the lunar orbiter for transfer to the moon. The lifetime of the lander is approximately 20 hours after landing. This will provide 8 opportunities to transfer the science payload data to the orbiter, each 152 seconds long. The limited communications time is due to the confines of the crater, which for calculation was assumed to have a line of sight capabilities only over an elevation of 70° at any given azimuth. This is an extremely strict limitation that will hold true even if the lander arrives at the edges of its potential landing ellipse.

### 3.1.4 Phase IV: OMV Transfer to Frozen Orbit

Directly following the departure of the lander from the OMV, the OMV will orbit twice around the moon to ensure constant communications with the lander, then will perform an impulsive apoapsis-raising maneuver, resulting in a transfer orbit with an apoapsis of 400 km. When apoapsis is reached, the OMV will circularize with another in-track impulsive burn. The OMV will travel to the ascending node of the orbit, and then perform an impulsive plane change to an inclination of 86°. The plane change takes place after the raising of the altitude of the orbit in order to limit the delta-V required, as the velocity of the spacecraft will be lower at the higher altitude.

This  $86^\circ$  orbit was chosen for the purpose of long-term stability. Maintaining an inclination of  $90^\circ$  would require unattainable levels of station-keeping to avoid unintentional deorbiting. Additionally, other known stable lunar orbits required a great deal of delta-V to obtain. At an inclination of  $86^\circ$ , a lunar orbit will not be affected by lunar mascons, which are regions of particularly dense mass due to high-density material that resides in craters on the lunar surface. These regions cause regions of increased lunar gravitational pull. By choosing this  $86^\circ$  frozen orbit, the satellite will not be affected by these regions of increased gravity, and the altitude of the orbit will provide adequate communication time with the lunar lander during its mission lifetime. The orbital elements of this orbit can be seen in Table 3.1.4.

Frozen Orbit Elements Upon Entry	Value
Inclination	$86^\circ$
Eccentricity	0
Altitude of Periapsis	400 km
Argument of Periapsis	$0^\circ$
RAAN	$0^\circ$
True Anomaly	$0^\circ$

Table 3.1.4: Orbital elements of frozen orbit upon entry.

Five minutes after taking the orbiter to the frozen orbit chosen for the rest of the orbiter's lifetime, the OMV will deorbit itself into the surface of the moon. This will take place by firing in the radial direction at the periapsis of orbit. The thrust will not interfere with orbiter trajectory due to separation happening far before the deorbit maneuver. With this maneuver the OMV will deorbit into the surface of the moon near the equator and at  $0^\circ$  longitude, avoiding any previous or planned mission sites.

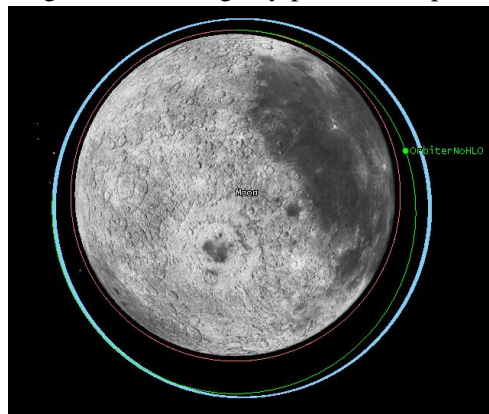


Figure 3.1.4. Initial LLO represented in red, frozen lunar orbit shown in blue, and the transfer used to travel from initial LLO to frozen lunar orbit is depicted in green.

### 3.1.5 Phase V: Orbiter Operations in Frozen Orbit

The orbiter will serve as a communications relay from the lunar surface to the Earth after it is released in the frozen orbit. The primary orbit perturbation in the chosen frozen orbit is due to the third-body effect of the Earth. This causes the eccentricity to increase and the RAAN to decrease. In the event that it would be advantageous to maintain these orbital elements, station-keeping would require 60 m/s every year at a maneuver frequency of 18 days. This station-keeping requirement would limit the lifetime of the orbiter, especially if space is meant to be saved for the potential of other instruments to be added to the orbiter, as 60 m/s worth of fuel adds up very quickly and significantly reduces the internal volume available on the orbiter. With the thrusters selected for the orbiter, an extra 72 kg of fuel would have to be added to the orbiter to meet this requirement, which would take up over 10% of the internal volume.

For this reason, station-keeping for the orbiter will be neglected. This decision allows for a satellite lifetime determined by mechanical failure instead of fuel limitation and does not significantly alter the communications benefits of the orbit chosen. The orbital elements for the lunar orbiter 10 years after entry to the frozen orbit are listed in Table 3.1.5. It is evident from these elements that the nominal lifetime of 10 years could potentially even be extended should the mechanical parts on the satellite outlive their estimated lifetimes.

Frozen Orbit Elements Upon Entry	Value
Inclination	86°
Eccentricity	0.100
Altitude of Periapsis	300 km
Argument of Periapsis	210.623°
RAAN	268.703°
True Anomaly	18.859°

Table 3.1.5: Orbital elements of frozen lunar orbit after 10 years.

The frozen orbit will be effective for communicating from the lunar surface to the Earth, as the longest average revisit time for a location on the lunar surface is 6.6 hours. The longest revisit times are located in a 36° latitude band around the lunar equator. The revisit time at locations around the poles of the moon is much lower; the area around the lunar poles benefits from an average revisit time of under an hour. As this satellite is meant to support future lunar missions and the lunar poles are a specific region of interests for many NASA projects, this orbit provides a very adequate and extremely useful communications service.

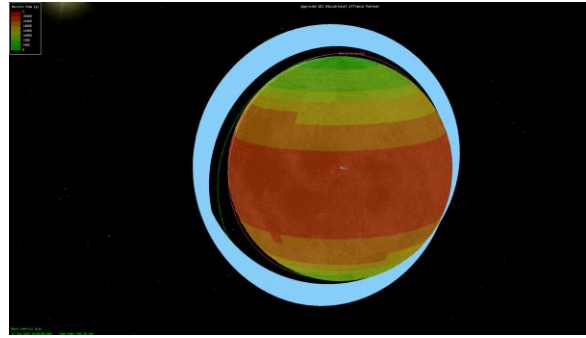


Figure 3.1.5a. Coverage over the course of a year with the frozen lunar orbit (blue). Areas of greater coverage are green and areas with less coverage are shown to be red.

Over the estimated 10 year lifetime, the orbiter will never be eclipsed for more than 3 hours and 25 minutes. This happens twice due to full lunar eclipses. Otherwise, the orbiter will never be shadowed for more than 0.805 hrs. This is due to the orbiter falling into the moon's umbra during its orbit and happens once every orbit but never for longer than 0.805 hrs at a time. The orbiter is never without line of sight to the Earth for longer than 0.877 hrs, which yields plenty of time for data transmission to Earth.

Over its lifetime, the lander will maintain a nadir-pointing attitude to allow for the easiest possible communications with the lunar surface.

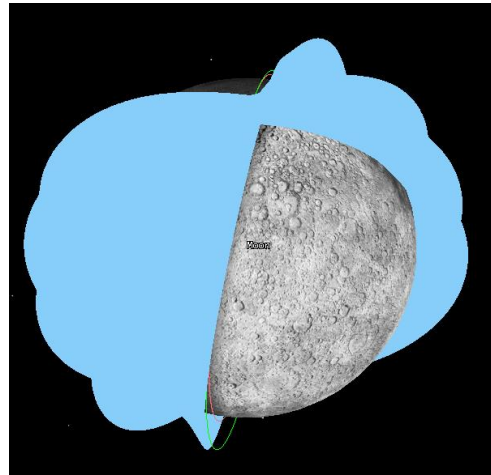


Figure 3.1.5b. Coverage with frozen lunar orbit over 10 years.

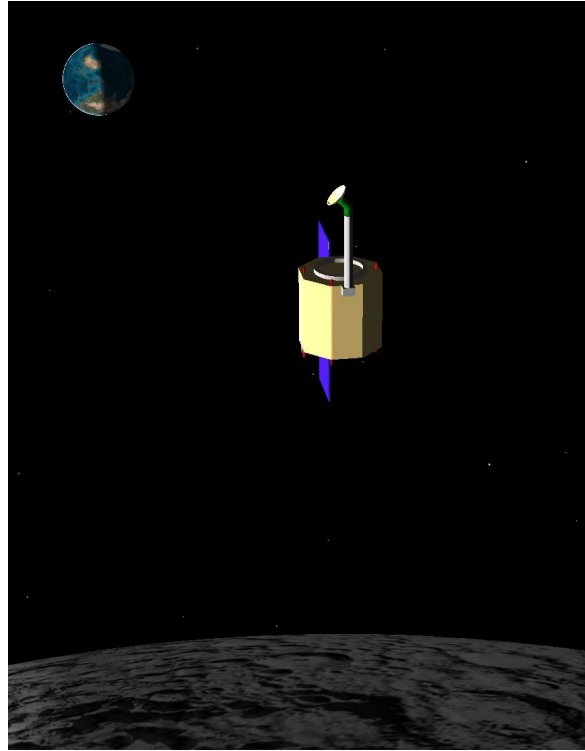


Figure 3.1.5c. Visual of spacecraft and its orientation while orbiting the Moon.

### 3.1.6 Phase VI: End Of Life

At the end of life, the orbiter will fire thrusters retrograde while at perilune. Deorbit will take a deltaV of 30 m/s. The orbiter will crash into the south pole region of the moon. The exact crash location has not yet been determined. NASA recommends avoiding historical sites on the moon by at least 2 km. As humans and probes return to the moon over the next decade, these guidelines will likely be extended to all active missions as well. Since the orbiter will not be crashing into the moon for another 10 years from launch, it is necessary to maintain some degree of flexibility with EOL plans. As the mission nears termination, the team will determine an exact crash location that prioritizes the safety of active missions and historical sites.

### 3.1.7 Phase Timeline

Phase	Maneuver	T+ (Hours)
I	TLI from GTO	0.00
II	Enter LLO	120.283
III	Lander Separation	123.998
III	Lander Periapsis Lowering	124.015
III	Lander Circularization	124.948
III	Lander Braking Start	125.248
III	Lander Braking End	125.698
III	Lander Begins Surface Operations	125.948
IV	OMV Apoapsis Raise	127.780
IV	OMV Circularization	128.865
IV	OMV Plane Change	129.465
V	Orbiter Separation	129.548
V	OMV De-orbit	129.565
III	Lander Surface Operations End	145.948
VI	Theoretical Orbiter Deorbit	87729.6

Table 3.1.6: Phase Timeline

## 3.2 Delta-V Requirements

All maneuvers except for the braking maneuver are assumed to be impulsive using chemical thrusters. Given the period of the orbits used and the short time required to achieve the delta-V values listed using the selected chemical thrusters, this is an acceptable assumption. The calculations for delta-V values per maneuver are from STK.

### 3.2.1 Phase I Delta-V

Consideration of multiple launch options and their associated delta-V requirements led to the realization that a geostationary transfer orbit would be the most logical.

Launch	$\Delta V$ (m/s)
From LEO	4400
From GTO	670
From GEO	1060
Dedicated Launch	3107

Table 3.2.1: Phase I Delta-V.

### 3.2.2 Phase II Delta-V

In order to obtain the desired LLO from the TLI orbit, the spacecraft will perform an anti-velocity impulsive maneuver to achieve circularization around the moon. The delta-V required for this maneuver is **828.9 m/s**.

### 3.2.3 Phase III Delta-V

The lander will perform 3 separate maneuvers in order to land at the desired location at Shackleton Crater. These maneuvers are all anti-velocity and are outlined in the table below.

Maneuver	$\Delta V$ (m/s)
Lower Periapsis	8.03
Circularization	7.9
Braking Burn	1671.7

Table 3.2.2: Phase III Delta-V.

Beginning the landing sequence at an LLO with a very low altitude (50 km) and with a ground track that falls directly over the desired landing site provides the opportunity to reach the braking orbital altitude with very little delta-V. Unfortunately there is no way to lower delta-V of the braking maneuver

due to the inherent high velocity of the lander at low altitudes. The braking burn will take 1653 s. The fuel required for the final portion of the landing sequence is contained within Propulsion, Section 5.5.2.

### 3.2.4 Phase IV Delta-V

The OMV will perform three maneuvers in order to place the satellite into the desired frozen orbit. The first two of these maneuvers are completed by thrusts in the direction opposite the velocity vector. The plane change maneuver is defined by thrust in both the velocity and normal directions (in a Lunar VNC frame with normal defined by the radius vector from a lunar point mass to the satellite).

Maneuver	$\Delta V$ (m/s)
Raise Apoapsis	72.36
Circularization	16.6
Plane Change (Velocity direction)	15.3505
Plane Change (Normal direction)	110.7
Plane Change (Total)	11.78

Table 3.2.3: Phase IV Delta-V.

### 3.3 Space Environment

#### 3.2.1 Thermosphere

The spacecraft only spends a couple hours in the thermosphere, which has relatively low radiation compared to Van Allen Belts and outside of the Earth's magnetosphere. Radiation here is negligible, but there is possibility of collision with small space junk.

#### 3.2.2 Van Allen Belts

After crossing the thermosphere, the spacecraft passes through the VAB. Hence, appropriate precaution is taken to protect the electronics in the spacecraft from the electromagnetic radiation. The use of chemical propulsion will allow the craft to transit through the VAB rapidly. The ship will only spend 2.5 hours in the heavy radiation of the VAB. Data amassed from the Apollo mission provides an estimate of radiation from rapid transit of the Van Allen Belts. For 2.5 hours in the VAB, with 0.05 mm Al shielding, Märki<sup>7</sup> finds a maximum VAB exposure of 0.9 Krad. That exposure drops to 4.0 rad if shielding is increased to 4 mm Al.

#### 3.2.3 Lunar Transit and Orbit

Märki provides estimates of radiation in lunar orbits at solar minimum and maximum. The lander will be in lunar orbit for less than a week . Over three days in orbit, with 0.05mm Al shielding, the 95% and 50% confidence intervals of maximum radiation are 2.9 Krad and 0.8 Krad, respectively. Using 4 mm Al shielding, drops those doses to 30 rad and 1.5 rad respectively.

The ten year lifetime of the orbiter will encompass a full solar cycle. With 0.05 mm Al shielding, the orbiter will have a dose of 22 Mrad of radiation. With 4 mm of Al shielding this drops to 1.9 Mrad and with 10 mm of Al shielding, this drops to 550 Krad.

#### 3.2.4 Lunar Surface

As the moon has no atmosphere, the radiation environment on the lunar surface should be identical to that of a very low lunar orbit. We again turn to Märki for radiation estimates, verified by Tripathi et al.<sup>8</sup> With 0.05 mm Al shielding, the 95% and 50% confidence intervals of maximum radiation are 7.3 Krad and 2.0 Krad, respectively. With 4 mm Al shielding, those doses drop to 76 rad and 3.8 rad.

---

<sup>7</sup> Märki, A. (2018). Radiation Analysis for Moon and Mars Missions. *arXiv*. Retreived from <https://arxiv.org/ftp/arxiv/papers/1805/1805.01643.pdf>

<sup>8</sup>Tripathi, R. K., Wilson, J. W., Badavi, F. F., & De Angelis, G. (2006). *A characterization of the moon radiation environment for radiation analysis*. Retrieved from doi:<https://doi-org.ezproxy.princeton.edu/10.1016/j.asr.2006.03.016>

### 3.2.5 Shielding

The acceptable radiation limit on the orbiter's computer is 1 Mrad, so the orbiter will need 10 mm AL shielding between critical electronics and the sun. This will reduce the total radiation dose for the orbiter to 551 Krad.

All of the electronics on the lander are rated for longer missions, so 0.05 mm Al shielding is sufficient. With 0.05 mm of shielding the lander will still only get a dose of 11 Krad which is well below the maximums of any of the components.

## 4. OMV, Launch, and Separation System

### 4.1 Orbital Maneuvering Vehicle (OMV)

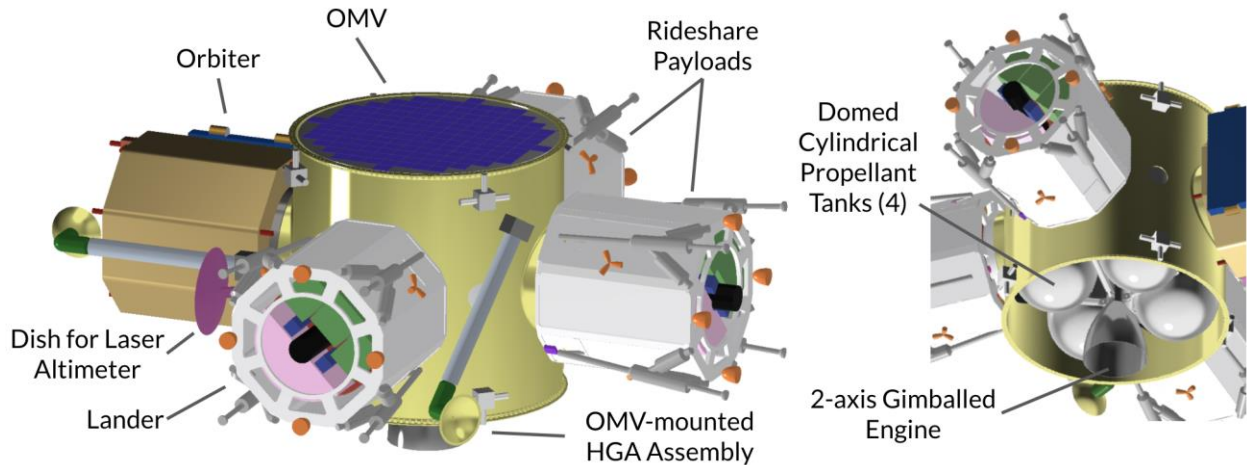


Figure 4.1.1 CAD mockup of the OMV in GTO configuration, using a 59"-tall “stretched” ESPA Grande as its main structural frame.<sup>9</sup>

#### 4.1.1 OMV Requirements, Specifications, and Baseline

##### *Requirements*

- The OMV shall be responsible for transporting the lander and the orbiter from the launch vehicle drop-off orbit (either GTO or TLI) to LLO. A secondary objective would be to transport ESPA-class rideshare payloads from launch to LLO, making use of excess propellant capacity and slot vacancies in the ESPA ring.
- The thermal system shall keep the interior of the OMV and all the ESPA ring payloads between 2 and 30°C during the trans-lunar injection. This ensures that all the components remain within the minimum and maximum operable temperatures of all the subsystems in both the lander and orbiter.
- During transit, the OMV shall replenish any losses that the lander, orbiter, and rideshare payloads’ batteries experience due to self discharge.
- Once the OMV arrives at LLO, the OMV shall deploy the lander and other rideshare payloads through a COTS separation system installed on each ESPA port. The OMV shall stay briefly in LLO to aid the orbiter (a module attached to the OMV at this point) in guiding the lander’s descent. (Refer to Appendix E.5 for a sketch of the OMV operating in LLO.)
- After lander touchdown confirmation, the OMV will maneuver to the frozen communications orbit as described in Section 3.1.4, where it shall deploy the orbiter.

<sup>9</sup> Please note that all OMV-related components *aside from the ESPA ring and propellant tanks* are for visualization purposes only. They are assumed to be part of a standard bus from Moog and have not been rigorously selected or sized, tasks which are outside the scope of this project. A white enamel coating will cover the OMV, but it is not shown.

- The OMV shall deorbit itself into the Moon after deploying the orbiter.

### *Assumptions*

- A standard bus developed, manufactured, and integrated by Moog based on existing concepts will handle the avionics, power, CD&H, ADCS, and GNC needs of the OMV.
- All maneuvers performed by the OMV can be approximated as being impulsive.
- Earth albedo, Earth IR, lunar albedo, and lunar IR effects are assumed to be negligible for most of the trans-lunar injection maneuver, due to the spacecraft's large distance from both the Earth and Moon, which results in a very small shape factor.
- During the majority of the TLI maneuver, the only heat gains and losses are assumed to be from solar and deep space radiation.

### *Specifications*

The Erebus OMV is based on features of the Astro and Comet OMV concepts by Moog.<sup>10</sup> As such, it will use an ESPA Grande ring as its structural frame. The standard ESPA Grande ring is 42" tall, made out of a series 7000 aluminum alloy, and weighs 211 kg. It interfaces with both the forward adapter of the launch vehicle and the base of the primary payload through 62"-diameter bolt circles at the top and bottom. Additionally, the OMV will have four ports with 24"-diameter bolt circles on the lateral face to which secondary payloads can be attached.<sup>11</sup> It was decided that the Erebus OMV would retain the launch vehicle, primary payload, and secondary payload interfaces of the standard ESPA Grande in order to preserve the volume requirements on the much-further-progressed lander, to fit standard LV adapters<sup>12,13</sup>, and to keep in line with expectations of potential rideshare clients. Thus, when tailoring OMV dimensions to propellant volume needs as described in Section 4.1.2, the diameter of the ESPA ring is kept constant.

### *Baseline Vehicle*

Moog has put out a diverse array of OMV concepts, of which Comet and Astro have elements that are suitable for the Erebus mission. Comet is an ESPA-Grande-based OMV that is meant to disperse small satellite constellations or serve as a host platform in Earth orbit for up to 1500 kg of combined payload. It comes with a standard bus for avionics, power, propulsion, and communications.<sup>14</sup> ADCS and GNC can be addressed by Moog, but will have to be tailored to the specific mission and thus is not part of the standard bus.<sup>15</sup> The Astro concept retains most of this standard bus but has an upgraded propulsion system that enables fast high-delta-V transfers, such as from GTO to GEO.<sup>16</sup> Moog's Jupiter concept, an electrically-propelled high-delta-V OMV, was also considered but was ruled out due to its low-TRL roll-

---

<sup>10</sup> "The Orbital Maneuvering Vehicle." Moog Inc. Accessed April 25, 2020.

<https://www.moog.com/markets/space/omv.html>

<sup>11</sup> Moog Space and Defense Group. *ESPA User's Guide*. November 2018. Accessed March 30, 2020.

<sup>12</sup> United Launch Alliance, *Atlas V Launch Services User's Guide - March 2010*. Accessed May 01, 2020. p9-4.

<sup>13</sup> Space Exploration Technologies Corp., *Falcon User's Guide - January 2019*. Accessed May 01, 2020. p36.

<sup>14</sup> "Orbital Maneuvering Vehicle | Comet" Moog Inc. Accessed April 25, 2020.

<sup>15</sup> Pearson, C. et al. "Extending Rideshare: Mission Case Studies Using Propulsive ESPA." *31st Space Symposium*. April 13, 2015.

<sup>16</sup> "The Orbital Maneuvering Vehicle." Moog Inc. Accessed April 25, 2020.

out solar arrays, long transfer duration, and a large volume that would eliminate economical rideshare and coprimary launch opportunities.<sup>17</sup>

A few studies have explored the idea of using a chemically-propelled ESPA-based OMV to deliver spacecraft beyond Earth orbit, such as to lunar orbit<sup>18</sup> and the Earth-Sun L1 point<sup>19</sup>. These studies demonstrate that Erebus-scaled missions are possible under the ESPA architecture using internal propellant tanks. For the purposes of sizing the OMV, it will be assumed that all but the thermal, separation, propulsion, and communications subsystems of the OMV will be handled by a standard bus adapted by Moog from the Astro/Comet concepts, and that this bus can fit either externally in between payload modules or internally in the voids left by the propellant tanks of maximal volume described later in this section.

For the purpose of guiding lander descent, the OMV will be equipped with a laser altimeter for orbit determination (described in more detail in Section 5.4.3, Subsection *Navigation Scheme*) and a copy of the orbiter's high gain antenna, gimbal, and mast assembly (described in Section 6.2.3).

Considerations involving two key subsystems that would need to be modified from previous concepts for the Erebus Mission are discussed in the next few subsections. Please note that the OMV subsystems are not as fully or evenly developed as those on the lander and orbiter, as is not the central focus of the project. Rather, they are explored primarily to provide mass and volume estimates for the mission as a whole, which is vital for the characterization of launch opportunities in Section 4.2.

#### 4.1.2 OMV Propulsion Subsystem

To size the propellant tanks, the dry mass of the OMV was first estimated using an average of historical planetary spacecraft mass distributions compiled in the New SMAD. The ESPA ring, HGA assembly, laser altimeter, and an additional propulsion allotment are billed as the “payload” of the OMV, as components are mission-specific. 80% of the structural mass and ~15% of all other subsystem allotments were redistributed to the “payload” subsystem to offset the ESPA ring, which is dramatically overbuilt as the structural frame of the spacecraft. A 25% system-level margin was included in this step. Afterwards, the mass at launch and propellant mass were computed using the Tsiolkovsky rocket equation, hand-calculated delta-V values of some maneuvers, STK-calculated delta-V values of the other maneuvers, and an  $I_{sp}$  of 270s for the MON-MMH bipropellant (taken to be the same as the lander as a simplifying assumption - see Section 5.5.2). A 20% propellant mass margin was included.

Concurrently, propellant capacity was estimated by filling the ESPA interior with four spherically-domed cylindrical tanks that have the same height as the ESPA ring and are tangent to each other and the inside of the ESPA wall. Two of these would be filled by the fuel and two others by the oxidizer, which incidentally have a volume ratio of nearly unity for the O/F ratio chosen. The height of the ESPA ring can be adjusted to tune the propellant capacity to the demand, and this is allowed by Moog up to a maximum height of 60”.<sup>20</sup> Doing so, however, increases the dry mass of the OMV, which in turn increases the propellant demand, necessitating an iterative approach.

---

<sup>17</sup> Ibid.

<sup>18</sup> Derewa, C. et al. “LOTUS: Standardized ESPA Propulsion System.” *AIAA Propulsion and Energy Forum*. July 2015.

<sup>19</sup> Pearson, C. et al. “Rideshare and the Orbital Maneuvering Vehicle: the Key to Low-cost Lagrange-point Missions.” *29th Annual AIAA/USU Conference on Small Satellites*. August 2015.

<sup>20</sup> Moog Space and Defense Group. *ESPA User’s Guide*. November 2018. Accessed March 30, 2020.

Such a process was carried out for three different LV drop-off scenarios: TLI, GTO, and LEO. The TLI case was found to be achievable using the standard 42" tall ESPA Grande, and the GTO case possible through a “stretched” 59"-tall custom ring. The LEO case did not converge within reasonable volume limits, even with the addition of multiple layers of external fuel modules, and it was determined to be infeasible under the chemically-propelled ESPA architecture. Electrical propulsion may still be an option for the LEO case, but it would drastically lengthen the mission time and heighten payload survivability requirements. It is therefore outside the scope of the project. The results of the TLI and GTO analyses is summarized in the table below. Please refer to Appendix E.2 and E.3 for intermediate results.

	<b>Scenario I: Drop off at Trans-Lunar Injection (TLI)</b>	<b>Scenario II: Drop off at GEO Transfer Orbit (GTO)</b>
<b>Dimensions</b>	Standard ESPA Grande: 62"Dia x 42"H	“Stretched” ESPA Grande: 62"Dia x 59"H
<b>Slot Occupancy</b>	<b>1</b> orbiter + <b>1</b> lander + <b>2</b> x 400 kg* rideshares (to LLO)	<b>1</b> orbiter + <b>1</b> lander + <b>2</b> x 340 kg* rideshares (to LLO or GTO)
<b>Mass</b>	732 kg + 1483 kg + 1117 kg = <b>3332 kg</b> Dry OMV Payload Propellant <b>Total at Launch</b>	942 kg + 1363 kg + 1717 kg = <b>4020 kg</b> Dry OMV Payload Propellant <b>Total at Launch</b>

Table 4.1.1: Estimated launch mass of the Erebus Mission under the two launch scenarios

*\*Note: It was stated during the CDR presentation that the OMV would transport two additional lander-sized rideshare payloads to LLO. Since then, the masses of both the lander and orbiter have grown, necessitating a reduction in the rideshare capacity to meet propellant volume constraints.*

A single, gimballed delta-V engine is the preferred thruster configuration for the OMV. This would be necessary to efficiently account for the changing center-of-mass location throughout the mission as payloads are dropped off. Future work would include selecting the thruster and designing for it a two-axis TVC actuation system.

#### 4.1.3 OMV Thermal Subsystem

As mentioned in the requirements section, the temperature of the spacecraft had to be kept between 2 and 30°C during the trans-lunar injection maneuver due to the thermal requirements of the lander and the orbiter. During TLI, the spacecraft is modeled as the ESPA-Grande-based OMV with four payloads: three landers and the orbiter. Thus, the previously chosen coatings of the landers and orbiter must be taken into account in this section. There are two main cases considered in this analysis. First, is the majority of TLI (or 193.6 hours, as calculated by STK from the orbital maneuvers), which occurs with a full viewfactor of the sun. The heat gained by this solar radiation is calculated using the below equation, where the average solar constant is  $H_{su} = 1353 \text{ W/m}^2$  when within 1 AU of the sun, and PAS is the projected area of the spacecraft to the sun.<sup>21</sup>

$$Q_{su} = PAS * H_{su} \quad (4.1)$$

---

<sup>21</sup> Choueiri, Edgar. “Spacecraft Thermal Control.” MAE 342 Lecture Notes. February 2020, 13.

During this case, the only other source of radiation considered is the heat loss from deep space radiation. The area that radiates to deep space is calculated as the areas of the OMV, landers, and orbiters, which do not face other parts of the spacecraft. A complete calculation of this value can be found in Appendix L.6. The equation for heat loss from deep space radiation is shown below<sup>22</sup>.

$$Q_{\text{deep space}} = \sigma * A_{\text{deep space}} * T_{\text{sc}}^4 \quad (4.2)$$

The second case considered is the very brief 27-minute portion the spacecraft spends in umbra. Because this case is during the very initial portion of TLI, the distance of the spacecraft from Earth is small enough such that Earth lunar and albedo effects still matter. These effects are calculated using the equations found in Professor Choueiri's lecture notes about Earth-centered thermal calculations<sup>23</sup>. The equations for Earth albedo effect  $Q_{er}$  and Earth IR flux effect  $Q_{et}$  are found below, where the albedo factor for Earth is  $a = 0.36$ , and the Earth-emitted IR energy flux constant is  $H_{et} = 0.16 * H_{su}$ .

$$Q_{er} = a * F_{er} * A_{sc} * H_{su} \quad (4.3)$$

$$Q_{et} = F_{et} * A_{sc} * H_{et} \quad (4.4)$$

From all these calculations, white enamel coating with an emissivity of 0.91 and an absorptivity of 0.09 was chosen<sup>24</sup> mostly for the warm sunlit conditions of TLI, since it makes up the majority of the maneuver. During the brief 27-minute section of umbra, 250 W of heating is necessary, that can be provided from heaters in the landers and orbiter, with power from the battery in the OMV. This would keep the spacecraft at 3.3°C during the brief umbra portion, and between 20.3 and 27.5 °C during the sunlit portion.

---

<sup>22</sup> Choueiri, Edgar. "Spacecraft Thermal Control." MAE 432 Lecture Notes. February 2020, 12-13.

<sup>23</sup> Choueiri, Edgar. "Spacecraft Thermal Control." MAE 432 Lecture Notes. February 2020, 13-14.

<sup>24</sup> AZ Technology. "Spacecraft Thermal Control and Conductive Paints/Coatings and Services Catalog." January 2008, iv.

#### 4.1.4 Components

Specific product selection for the OMV had been forgone in favor of focusing on the orbiter. Instead, a general description of the types of components needed is provided below.

- ESPA Grande Ring (TRL 8)
- Standard Bus adapted from Astro/Comet (TRL 6; all components within are TRL 8-9)  
The bus will be developed by Moog and will comprise the avionics, power, CD&H, ADCS, and GNC subsystems.
- Propulsion subsystem (TRL 8)
  - Conventional bipropellant thruster (TRL 9)
  - Propellant tanks (TRL 9)
  - TVC actuators (TRL 8)
  - Valves and plumbing (TRL 9)
- Separation systems (x4) (TRL 9)  
See Section 4.3.
- White enamel coating<sup>25</sup> (TRL 9)  
This white enamel coating is from the manufacturer AZ Technology. It was chosen for its emissivity and absorptivity values. White enamel coatings have been used on spacecraft for decades now, hence its high TRL value.
- Laser altimeter (TRL 7)  
The altimeter consists of a moon nadir-pointing laser emitter and parabolic dish based on that of the Mars Orbiter.<sup>26</sup> It will help determine the orbit of the OMV prior to lander descent and serves to narrow the landing ellipse.
- High gain antenna assembly (TRL 7)  
This is a copy of the HGA assembly on the orbiter (see Section 6.2). It will deploy prior to lander descent and gimbal to cover the hemisphere complementary to the orbiter HGA's range, ensuring a communications link between the lander and Earth during descent as long as line of sight is maintained.

---

<sup>25</sup> AZ Technology. "Spacecraft Thermal Control and Conductive Paints/Coatings and Services Catalog." January 2008, iv.

<sup>26</sup> Smith, D. et al. "Mars Orbiter Laser Altimeter: Experiment summary after the first year of global mapping of Mars." Journal of Geophysical Research. Vol. 106, No. E10, p23689-722. October 25, 2001.

## 4.2 Launch Vehicle

Using the OMV mass estimates from the previous section, launch opportunities can be characterized. Having the propulsive OMV enables our mission to fly on most EELV-class vehicles that go to TLI and GTO (see Table. 4.2.1). The table includes a color spectrum ranging from “not possible” to “rideshare opportunity” based on the share of total lift capacity available to other payloads and is explained in the legend. The delineation between categories is not well defined in industry and was thus arbitrarily chosen. In general, primary and co-primary payload opportunities (in orange and yellow) are available on the smaller launch vehicles, while the more economical rideshare opportunities (in green) open up on the larger ones. Falcon 9 and Falcon Heavy are chosen as our ideal co-primary and rideshare opportunities, respectively, due to their low cost and comparatively frequent launches. The Vulcan Centaur class may become a reliable yet economical alternative by the time Erebus is ready to launch. Figure 4.2.1 illustrates that there is plenty of space remaining for a primary or co-primary payload atop the Erebus OMV, even with the 59” tall stretched ESPA ring and the *shortest* fairings available.

Current and Near-Future EELV-Class Launch Vehicles (# of Flights to date)	Lift Capacity (kg)			Lift capacity in excess of Erebus Mission (kg)		Share of total lift capacity available to other payloads (%)	
	to TLI	to GTO	to LEO	drop off at TLI		drop off at GTO	
				Mission Mass: 3332 kg	Mission Mass: 4020 kg		Scaled Mass: ~20000 kg
Atlas V 501* (6)	2210	3780	8210	-1122	-51%	-240	-6%
Atlas V 511* (0)	3400	5250	11000	68	2%	1230	23%
Atlas V 521* (2)	4360	6480	13500	1028	24%	2460	38%
Atlas V 531* (3)	5120	7450	15530	1788	35%	3430	46%
Atlas V 541* (6)	5800	8290	17410	2468	43%	4270	52%
Atlas V 551* (10)	6330	8900	18850	2998	47%	4880	55%
Delta IV M+(5,2) <sup>†</sup> (3)	4000	5080	11060	668	17%	1060	21%
Delta IV M+(5,4) <sup>†</sup> (8)	5000	6890	13730	1668	33%	2870	42%
Delta IV Heavy* (11)	11290	14210	28370	7958	70%	10190	72%
Vulcan Centaur (0 Solids)* (0)	2300	2900	10600	-1032	-45%	-1120	-39%
Vulcan Centaur (2 Solids)* (0)	6300	7600	18500	2968	47%	3580	47%
Vulcan Centaur (4 Solids)* (0)	9000	10800	23900	5668	63%	6780	63%
Vulcan Centaur (6 Solids)* (0)	11300	13600	27200	7968	71%	9580	70%
Vulcan Centaur Heavy* (0)	12100	14400	27200	8768	72%	10380	72%
Falcon 9 (Block 5, Expendable) <sup>§‡</sup> (27)	6000	8300	22800	2668	44%	4280	52%
Falcon Heavy (Expendable) <sup>§‡</sup> (3)	20000	26700	63800	16668	83%	22680	85%

Lift capacity sources: \*ULA Rocket Rundown Graphic<sup>27</sup>, †ULA Delta IV Webpage<sup>28</sup>, ‡Extrapolated to TLI, §SpaceX Website<sup>29</sup>

Legend, based on share of total lift capacity available to other payloads:

100-70% Rideshare Opportunity, 69-30% Co-primary Opportunity, 29-0% Primary Only, <0% Not Possible

Table 4.2.1: Summary of launch opportunities on current and near future EELV-class launch vehicles.

<sup>27</sup> “ULA Rocket Rundown.” United Launch Alliance. <https://www.ulalaunch.com/docs/default-source/rockets/atlas-v-and-delta-iv-technical-summary.pdf>, Accessed April 10, 2020. Source has since been stripped of all technical details. Refer to archived version here: <https://web.archive.org/web/20200404202142/https://www.ulalaunch.com/docs/default-source/rockets/atlas-v-and-delta-iv-technical-summary.pdf>

<sup>28</sup> “Delta IV.” United Launch Alliance. <https://www.ulalaunch.com/rockets/delta-iv>. Accessed April 10, 2020

<sup>29</sup> “Falcon 9.” Space Exploration Technologies Corp. <https://www.spacex.com/falcon9>. Accessed April 10, 2020

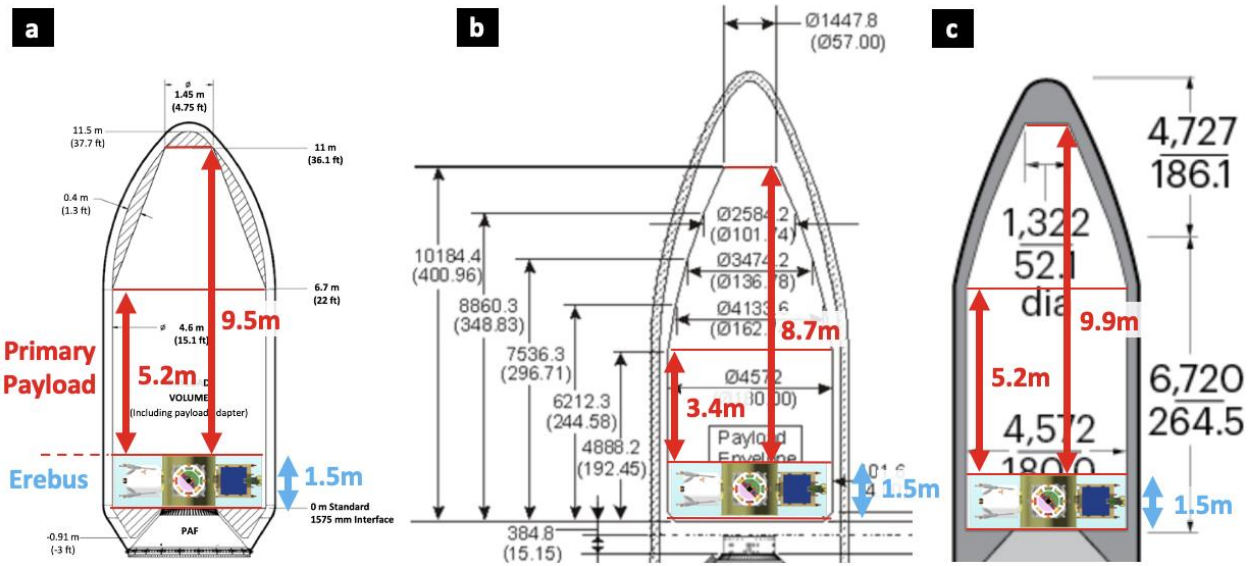


Figure 4.2.1: Volume available to primary and co-primary payloads atop the Erebus Mission within the fairings of a) Falcon 9/Heavy;<sup>30</sup> b) Atlas V (5m Dia. “Short”);<sup>31</sup> and c) Delta IV (5m Dia. 14.3m).<sup>32</sup>

### 4.3 Separation System

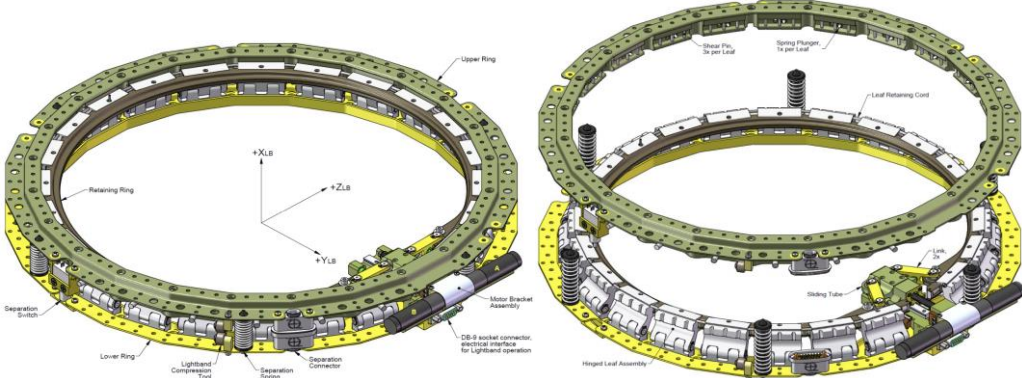


Figure 4.3.1: Secondary payload separation system from Planetary Systems Corp. in undeployed (left) and separated (right) states.<sup>33</sup>

The main factor to consider while choosing a separation system is whether it is triggered pyrotechnically or via a motor. Pyro systems are seen as more reliable since they have been in use since before Apollo, whereas newer non-pyro systems produce much less shock. Considering that motorized systems have seen a near perfect record in recent ground testing and flights,<sup>34,35,36</sup> there was little added risk in choosing

<sup>30</sup> Space Exploration Technologies Corp., *Falcon User’s Guide* - January 2019. Accessed May 01, 2020. p37.

<sup>31</sup> United Launch Alliance, *Atlas V Launch Services User’s Guide* - March 2010. Accessed May 01, 2020. p6-4.

<sup>32</sup> “Delta IV.” United Launch Alliance. <https://www.ulalaunch.com/rockets/delta-iv>. Accessed April 10, 2020

<sup>33</sup> 2000785G MkII MLB User Manual. Planetary Systems Corporation. Accessed April 10, 2020.

<sup>34</sup> Space Technologies Product Catalog - 2015. Sierra Nevada Corporation. Accessed April 10, 2020. p35-36.

<sup>35</sup> “PAS 610S (24”) Separation System.” RUAG Space. Accessed April 10, 2020.

<sup>36</sup> 2000785G MkII MLB User Manual. Planetary Systems Corporation. Accessed April 10, 2020.

one such system to reduce the lander deployment shock, which occurs inches away from some of our key components. Separation systems triggered by frangible bolts were briefly considered for their high reliability and low shock, but they were ruled out due to the large uncertainty in separation duration,<sup>37</sup> which would complicate mission planning and GNC. The Mark II Lightband from Planetary Systems Corporation was ultimately chosen, and is shown in Figure 4.3.1.<sup>38</sup> Its merits include its low profile, extremely low shock, and actuator redundancy. Additionally, its two motors operate on the same separation pulse as pyro systems, so it does not place any special demands on the OMV. It also comes with an option for built-in in-flight disconnect (IFD) connectors, which frees up some of the prime real estate at the top of the lander. Lastly, the Mark II lightband is extremely well-documented. Although it is slightly heavier than the other designs, its many merits make up for the added weight. The full product study is included in Appendix E.4.

A conservation of energy approach provided by the manufacturers of the Mark II Lightband was used to select the number of springs needed per separation event, which is driven by the desired velocity and tolerable rotation rate at separation.<sup>39</sup> From the desired separation velocity  $V$ , the increase in kinetic energy associated with the separation,  $E$ , can be expressed as

$$E = \frac{mMV^2}{2(m+M)}, \quad (4.5)$$

where  $m$  and  $M$  are the masses of the deployed spacecraft and the OMV, respectively. Given that the portion of elastic potential energy released by each spring is  $E_s = 0.85$  J, the number of springs  $n$  can be calculated:

$$n = \left\lceil \frac{E}{E_s} \right\rceil. \quad (4.6)$$

The actual separation velocity can then be calculated using Eq. 4.5, setting  $E = n * E_s$ . Rotation rate is calculated via the equation

$$\omega = \frac{mVd}{I}, \quad (4.7)$$

where  $\omega$  is the rotation rate (in radians),  $I$  is the moment of inertia of the separating spacecraft, and  $d$  is the distance by which the center of mass is offset from the central axis of the ESPA port. The maximum tolerable value of  $d$  is lowered until  $\omega$  is small enough to meet orbiter requirement 5.5.2 and lander requirement 6.3.3, and this in turn drives orbiter requirement 3.1.2 and lander requirement 4.1.2 for CoM offset. 19, 15, 15, and 6 separation springs were found to be needed in the separation systems of the lander, 2nd payload (rideshare), 3rd payload (rideshare), and orbiter, respectively. Inputs to these equations and intermediate results are documented in Appendix E.4.

Deployment of anything above the OMV in the payload stack from the top of the ESPA ring, as well as the OMV from the LV, will be handled by the launch provider using their provided separation systems. The OMV may be equipped with harnessing and IFD connectors on both the top and bottom separation planes as necessary to facilitate primary payload charging, telemetry, and separation.

---

<sup>37</sup> Joe Munder, Spacecraft Design Course - Mechanisms Overview. Class lecture, given April 16 2020.

<sup>38</sup> 2000785G MkII MLB User Manual. Planetary Systems Corporation. Accessed April 10, 2020.

<sup>39</sup> Ibid. p38.

## 4.4 LV and ESPA-driven Requirements for Lander and Orbiter

The launch vehicle and the ESPA ring are the primary drivers of lander and orbiter physical requirements. Key requirements that have significantly influenced design decisions for the Erebus mission are explained here. Appendix B lists many other requirements that are specified at a level of detail beyond the scope of this project and would need to be addressed in future work.

The stowed lander/orbiter shall...<sup>40</sup>

- ...not interfere with the ESPA Grande ring, primary payload, vehicle fairing, or neighboring secondary payloads. To guarantee this, the lander/orbiter should fit in a rectangular envelope less than 56" in length, 46" in width, and 42" in height to avoid interference with the vehicle fairing (5m-diameter), neighboring payloads, and the LV forward adapter & primary payload, respectively. (All dimensions expressed from the LV's point of view - see Figure 4.4.1a.) (lander req. 3.1.1; orbiter req. 2.1.1)
- ...be mounted to the ESPA Grande ring via a 24"-diameter bolt circle. No component of the lander/orbiter shall stick through this interface into the ESPA interior, to avoid interference with OMV components. (lander req. 3.1.2; orbiter req. 2.1.2)
- ...have a mass and center-of-mass location (measured from the ESPA interface plane) that fits within the region bounded from above by the purple curve in Figure 4.4.1b. Otherwise, the structural integrity of the ESPA ring and separation system may not be guaranteed. For example, the Erebus lander, whose center-of-mass is 22" from the interface plane, shall not exceed a mass of 620 kg. (lander req. 3.1.6-7; orbiter req. 2.1.6-7)
- ...have all of its resonant modes above 35 Hz. Otherwise, the excitations may couple between the LV and the lander/orbiter, pushing worst case load factors beyond those reported in LV payload user's guides. This particular frequency requirement comes from Falcon 9/Heavy, the most stringent of all EELV-class vehicles in this respect.<sup>41</sup> Refer to Section 5.1.3 for a discussion of load factors. (lander req. 3.1.4; orbiter req. 2.1.4)

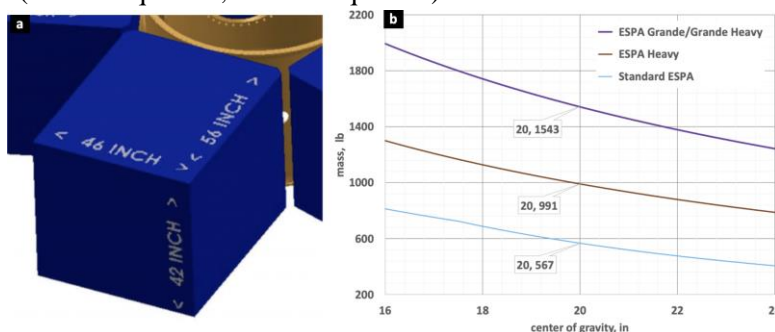


Figure 4.4.1: Volume and mass requirements driven by ESPA and the launch vehicle:<sup>42</sup> a) Maximum allowable rectangular-prism volume envelope. b) Mass vs. CoM Location upper boundary (purple).

<sup>40</sup> Moog Space and Defense Group. *ESPA User's Guide*. November 2018. Accessed March 30, 2020.

<sup>41</sup> Space Exploration Technologies Corp., *Falcon User's Guide* - January 2019. Accessed May 01, 2020. p15.

<sup>42</sup> Moog Space and Defense Group. *ESPA User's Guide*. November 2018. Accessed March 30, 2020.

## 5. Lunar Lander



## 5.1 Structure

The structure of the lander must serve the needs of the other subsystems (by providing attachment points, protection, and support) while withstanding the various loads that the lander will encounter at different points in the mission. The design of the main structure, which is a beam-and-panel structure, will be dominated by the launch loads, in terms of strength and deflection (to stay within the required volume envelope and avoid putting unnecessary loads on other subsystems' components) and also stiffness (to meet resonant frequency requirements). Packaging of components will be a primary concern for overall dimensions, as the design of the lander structure will be limited as much by volume as by weight. In addition, the structure should allow for efficient electrical harnessing and propulsion flow line pathways. For the purposes of this project, calculation and communication of mass properties also fall under the purview of Structures.

### 5.1.1 Key Requirements and Assumptions

#### *Requirements*

The structure shall...

- ...fit all other subsystems internally or externally as required.
- ...support all masses with a safety factor greater than 3.
- ...have no resonant modes below 35 Hz, per requirement 4.2.1.
- ...have a total weight approximately 10% of wet mass.

Requirements are largely defined by other subteams to ensure that the lander is functional. All subsystems must be integrated safely and efficiently. LV integration and loading conditions can provide many of the operational worst case scenarios at which design can be evaluated. A large safety factor is desired to increase security so long as weight is not significantly negatively impacted.

#### *Assumptions*

- All component masses less than 2 kg were ignored for modeling the structure's safety factor and resonant modes.
- All masses other than the structure were modeled as point loads.
- LV launch load case condition is 8.5 g LV axial and 3 g LV lateral.
- LV launch volume envelope is 42”x46”x56” (ESPA volume envelope).
- Aluminum honeycomb paneling will not have significant structural impact.
- Landing sequence will adequately brake such that LV launch loads are the worst case scenario.

### 5.1.2 Mass Budget

Component	Mass (kg)	Notes
Frame	30.4	
Bracing	7.6	
Honeycomb Panels	1.1	Based on 3.62 kg/m <sup>2</sup> (see Appendix F.1)
Separation System	2.42	
<b>Subsystem Total</b>	<b>41.5</b>	
<b>Allocated Mass</b>	<b>47.7</b>	
<b>MGA</b>	<b>6.2 (15%)</b>	

#### *Margins and Contingency*

The frame and bracing dominates the total mass of the structure. The honeycomb panel mass is an estimate based on  $\frac{1}{2}$ " thick panels; see Appendix F.1 for calculations of the panel mass. All materials making up the structure are readily available from commercial suppliers, so large deviation from total mass is not expected. However, the mounting systems could add some significant amount of material, and so the mass growth allowance was given to be 15%.

### 5.1.3 Design

The overall shape of the structure was decided to be an octagonal prism for flat paneling and maximization of internal volume. A shell design was decided on for ease of wiring and strength to mass ratio. The volumetric constraints are defined by the LV envelope and the capacity of an ESPA Grande port. The volume envelope is then 42"x46"x56". Additionally aluminum was then selected for its lightweight properties and large commercial availability. A welded frame is desired, and so aluminum 6061 was selected for its relative ease of weldability. Consult Appendix F.2 for information on aluminum alloy weldability.

The largest volumetric constraint was the fuel tanks, for which a larger diameter size is preferred to minimize fuel tank mass, and so a larger diameter is better designed towards a wider and shorter design. The ultimate height of the chassis came out to 38" at a maximum width and length to still fit in the volume envelope (42"x46").

The largest loads that can be experienced by the structure are dependent on the acceleration experienced by the lander during launch. This will be evaluated at the worst case scenario of all the launch vehicles considered, a Falcon 9 with payload less than 4,000 kg. For the ESPA Grande, this is defined as 8.5 g to LV central axis and 3 g to LV lateral.

The lander is constructed of  $\frac{1}{8}$ " thick rectangular tubes that make up plates and struts with 2" wide by 0.3" thick bracing them (consult Appendix F.3 for a drawing of the frame). When modeled with point loads, this results in a stress safety factor of 11.97 under the worst case load scenario. There is also the first resonant mode of 50.56Hz above the required 35 Hz, as defined by LV conditions, of the lander. This is accomplished with a total mass of only 38.1 kg. This overall design can then easily be resized solely along its height to create modules to enter into the available ESPA ports for systems such as an orbiter, with a significant margin in both resonant mode and stress safety factor.

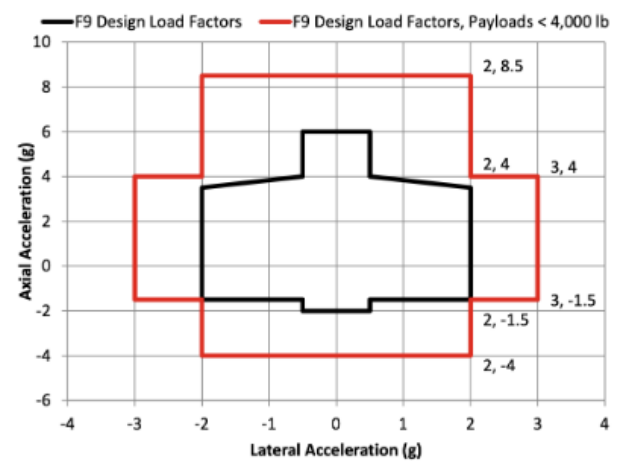
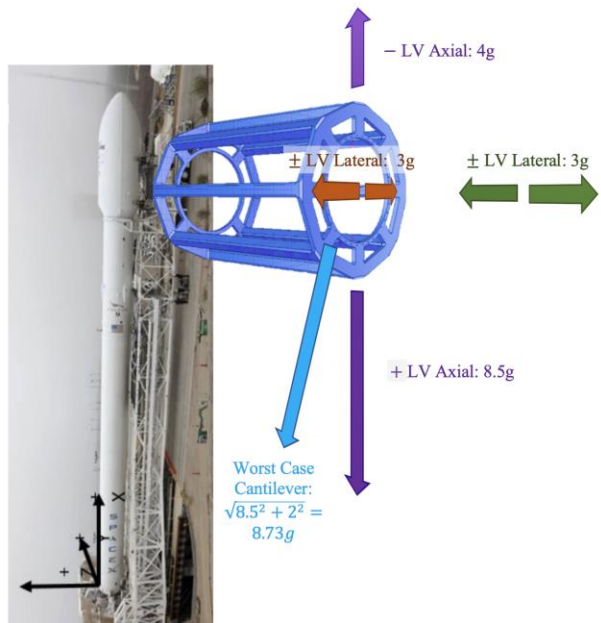


Figure 4-2: Falcon 9 payload design load factors, light mass (under 4,000 lb)

Figure 5.1.1: Worst-case launch load factors, based on a Falcon 9 with payload < 4000 kg.<sup>43</sup>

#### 5.1.4 Layouts and Finite Element Analysis

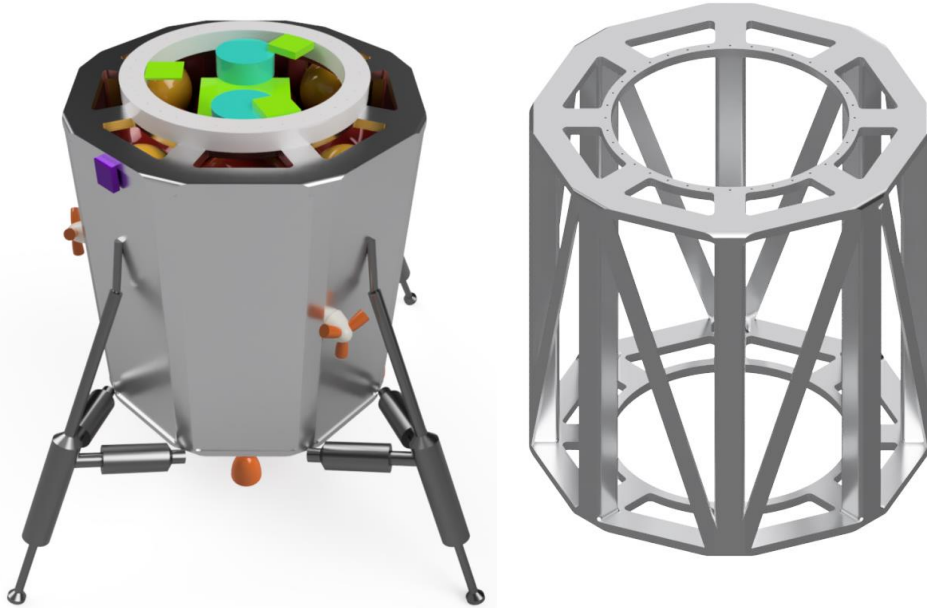


Figure 5.1.2: Lander assembly (left) and octagonal frame (right).

Finite element analysis was performed on the octagonal structure, with point masses ‘hung’ on the structure to represent all internal components with a mass greater than 2 kg. For all of the analyses, the frame was constrained along the 24” diameter bolt circle that serves as the attachment to the ESPA Grande ring. The following three figures show the results of that analysis. (There are two scenarios for worst-case launch loads to represent the two possible directions of lateral loading.)

---

<sup>43</sup> Space Exploration Technologies Corp., “Falcon User’s Guide.” Accessed May 1, 2020.

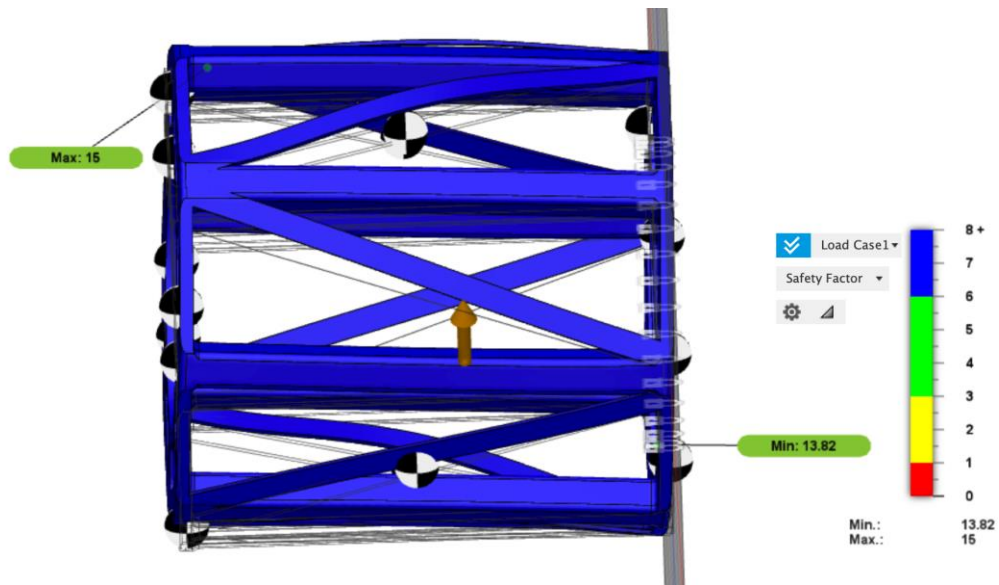


Figure 5.1.3: Static analysis of octagonal frame with point masses under worst-case launch loads scenario 1.

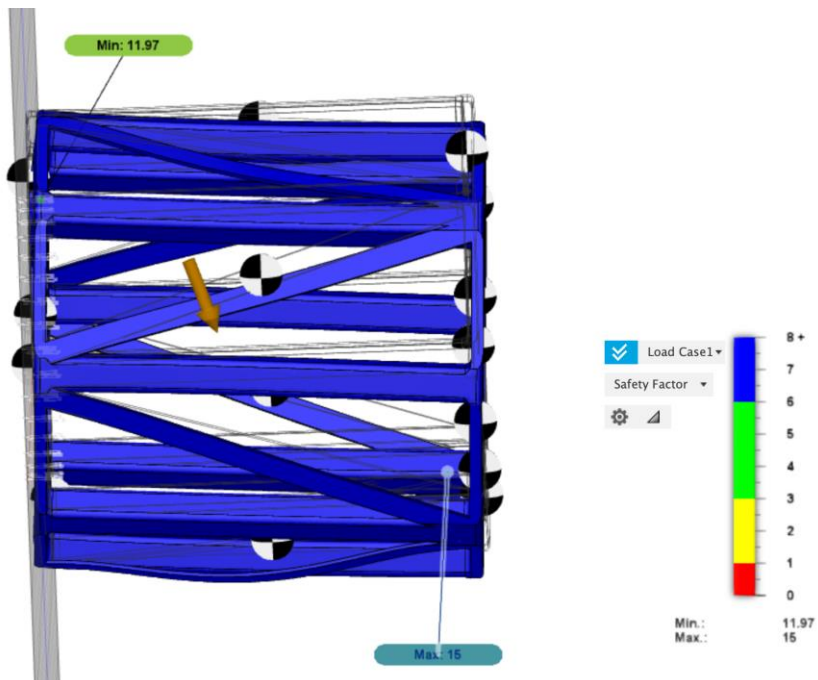


Figure 5.1.4: Static analysis of octagonal frame with point masses under worst-case launch loads scenario 2, showing a minimum safety factor of 11.97.

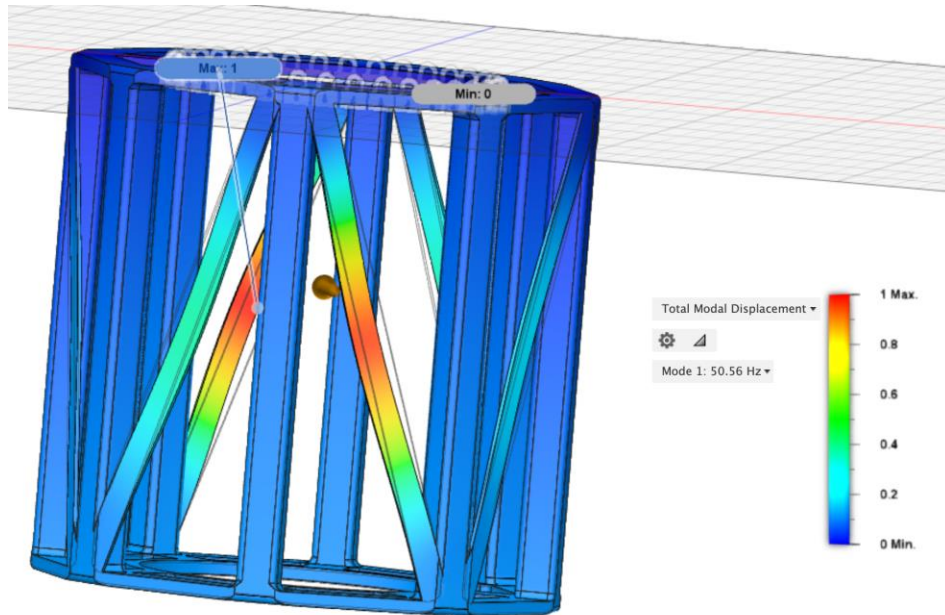


Figure 5.1.5: Results of modal analysis on the frame, showing the lowest resonant mode as 50.56 Hz.

### 5.1.5 Components

- Aluminum 6061 Welded Hollow Frame (TRL 9)  
These are standard aluminum 6061 tubes made of a standard thickness and size, and should be readily available from mass manufacturers.
- Aluminum 6061 Welded Solid Bracing (TRL 9)  
These are standard aluminum 6061 bars made of a standard thickness and size, and should be readily available from mass manufacturers.
- Aluminum Honeycomb Panels (TRL 9)  
These are standard aluminum honeycomb panels of a standard thickness and size, and should be readily available from a variety of specialty manufacturers, including APCO Technologies and Collins Aerospace.

## 5.2 Mechanisms

The primary responsibilities of the lander mechanisms subsystem are to deploy the landing system, which will ensure a safe, soft landing on the lunar surface; and operate the drill and its related components. The landing system legs, which must start in a stowed position to fit within the ESPA volume envelope, deploy during the landing sequence; they are designed with aluminum crush core dampers to absorb the energy of impact, leveling springs to ensure the lander returns to and remains vertical, and landing pads so that the spacecraft does not sink into the regolith. The drill is the primary focus of the science mission, and will extract lunar regolith samples and transport them to the scientific instruments within the lander, down to a depth of 60 cm.

### 5.2.1 Key Requirements and Assumptions

#### *Requirements*

##### Landing System

The landing system shall...

- ...withstand a landing with vertical velocity of 1.6 m/s and horizontal velocity of 1 m/s, per requirements 4.3.1 and 4.3.2.
- ...have a leg base of at least 1.15 m, per requirement 4.3.3, in order to avoid rollover or other instabilities when landing.

##### Drill Mechanism

The drill mechanism shall...

- ...drill through material with a density of 1.5 g/cc, per requirement 4.4.1, the density of lunar regolith mixed with ice.<sup>44</sup>
- ...penetrate the lunar regolith to as great a depth as allowed by the packaging of the spacecraft, in order to maximize science return.
- ...retrieve samples by depth that can be analyzed using the science payload for depth vs. composition analyses.
- ...complete its drilling operation in a given time period, and at a given temperature, such that at least 75% of the volatiles in the sample are preserved, per requirement 4.4.8.

#### *Assumptions*

##### Landing System

- Lander mass is less than 251 kg at touchdown (at most,  $\frac{1}{4}$  the fuel remains).
- Maximum vertical velocity on landing is 5 m/s (three times the worst-case scenario impact velocity as given in requirement 4.2.2).
- Maximum horizontal velocity on landing is 1 m/s.
- Aluminum honeycomb crush strength does not depend on the length of the core.

---

<sup>44</sup> *Lunar Sourcebook*, ed. by Grant H. Heiken, David T. Vaniman, and Bevan M. French (Cambridge: Cambridge University Press, 1991).

- Primary struts are approximately vertical.

#### Drill Mechanism

- The hardness of a granular material may be approximated by its density.

### 5.2.2 Mass and Power Budgets

#### *Mass Budget*

Component	Mass (kg)	Notes
TRIDENT drill	16	
Landing system legs	5.33	See Appendix G.5 for calculation
Crush cores	0.2	
Dampers	2	
Landing pads	2.23	See Appendix G.5 for calculation
<b>Subsystem total</b>	<b>25.8</b>	
<b>Allocated Mass</b>	<b>32.2</b>	
<b>MGA</b>	<b>6.4 (25%)</b>	

#### *Power Budget*

Component	Power (W)	Energy (Wh)
TRIDENT drill	250	5500
<b>Subsystem total</b>	<b>250</b>	<b>5500</b>
<b>Allocated</b>	<b>312.5</b>	<b>6875</b>
<b>Margin</b>	<b>62.5 (25%)</b>	<b>1375 (25%)</b>

#### *Margins and Contingency*

Margins of 25% are applied to both mass and power due to the possible need for additional mechanism components, particularly in the case of the landing system deployment mechanism and the robotic assembly that will transport regolith from the drill to the science payload.

### 5.2.3 Design

#### *Landing System*

The landing system is designed to support the lander securely after absorbing touchdown kinetic energy. Figure 5.2.1 shows the landing system in its deployed configuration; the main strut is shown in yellow, the upper link is shown in green, and the secondary struts are shown in red.

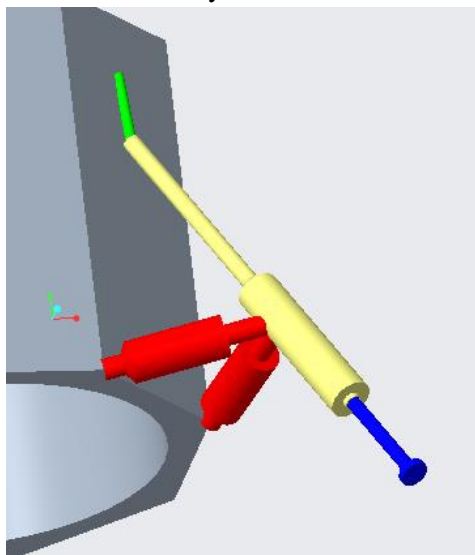


Figure 5.2.1: Landing system in deployed configuration.

The primary dampers, shown in Figure 5.2.2, use aluminum honeycomb crush cores from Hexcel that take 7.9 kN to crush.<sup>45</sup> They will be pre-crushed approximately 20% to surpass the buckling region, and 0.2 m (8") of stroke will be available, which is more than enough to absorb the energy of landing (see Appendix G.1 for details). Even if the crush cores compress entirely, the landing system ensures that there will be at least 6 inches of ground clearance, which is enough room for both the main thrusters and the drill, which protrude from the bottom of the structure. Leveling springs support the static lander mass and allow each leg to conform to rough terrain in a manner similar to a car's suspension. There is 4" of travel available at each leg (even if none of the cores crush, e.g. a zero-velocity landing), so the spring constant is chosen so that  $\frac{1}{4}$  of the lander's weight (as supported by each leg) compresses the springs 2". No matter how far each of the crush cores compresses, the leveling springs will return each leg to the same relative position. Sliding friction dampers dissipate rebound energy coming from the leveling springs after touchdown.

---

<sup>45</sup> "HexWeb CR III Corrosion Resistant Specification Grade Aluminum Honeycomb," Hexcel Corporation, 2017. Accessed May 9, 2020. [https://www.hexcel.com/user\\_area/content\\_media/raw/HexWeb\\_CRIII\\_DataSheet.pdf](https://www.hexcel.com/user_area/content_media/raw/HexWeb_CRIII_DataSheet.pdf).

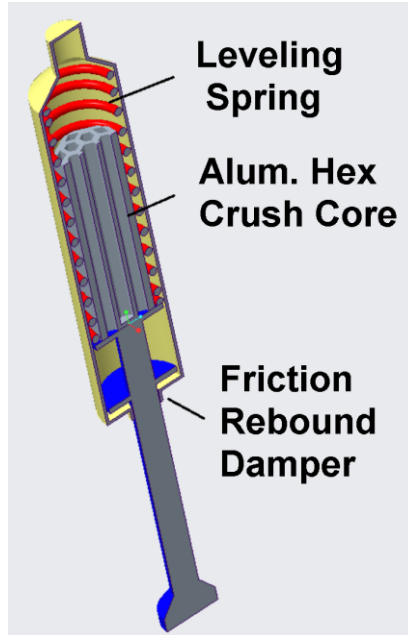


Figure 5.2.2: Primary damper cross-section.

Secondary dampers, mounted on the secondary struts, provide friction and restoration forces in both compression and tension directions, allowing the main struts some play to prevent damaging the lander in the case of a translational landing.

The main landing pads are 0.2m in diameter, capturing 9.4 kN of bearing capacity from the lunar regolith, which has a bearing strength of 300 kPa at that footing width.<sup>46</sup> It is estimated that the lander would only settle 1.6 cm into the lunar regolith. On impact, spikes fixed to the bottom of the landing pads penetrate the moon's surface and provide assistance in reacting the drill counter-torque. Ground proximity sensors mounted to the pads indicate a touchdown, allowing thrusters to stop and allowing other systems to proceed ground operations. Each leg has a ground proximity sensor, which is essentially a thin aluminum bar that hangs off the edge of the pad; when the end of the bar makes contact with the lunar surface, it is pushed up slightly, which closes a circuit and indicates to the spacecraft that it is within a given distance from the surface.

A schematic of the landing system deployment is shown in Figure 5.2.3. The deployment is based on a 4-bar linkage: the lander frame, the upper link, the main strut, and the secondary struts. Initially, the upper link is held in place at the top with a pin and the entire system is stowed compactly. Upon activating the release mechanism, a pyrotechnic pin-puller removes the pin from its housing and a torsion spring drives the upper link to latch into the 'down' position. During this time, the other components are moved into place.

---

<sup>46</sup> *Lunar Sourcebook*, ed. by Grant H. Heiken, David T. Vaniman, and Bevan M. French (Cambridge: Cambridge University Press, 1991).

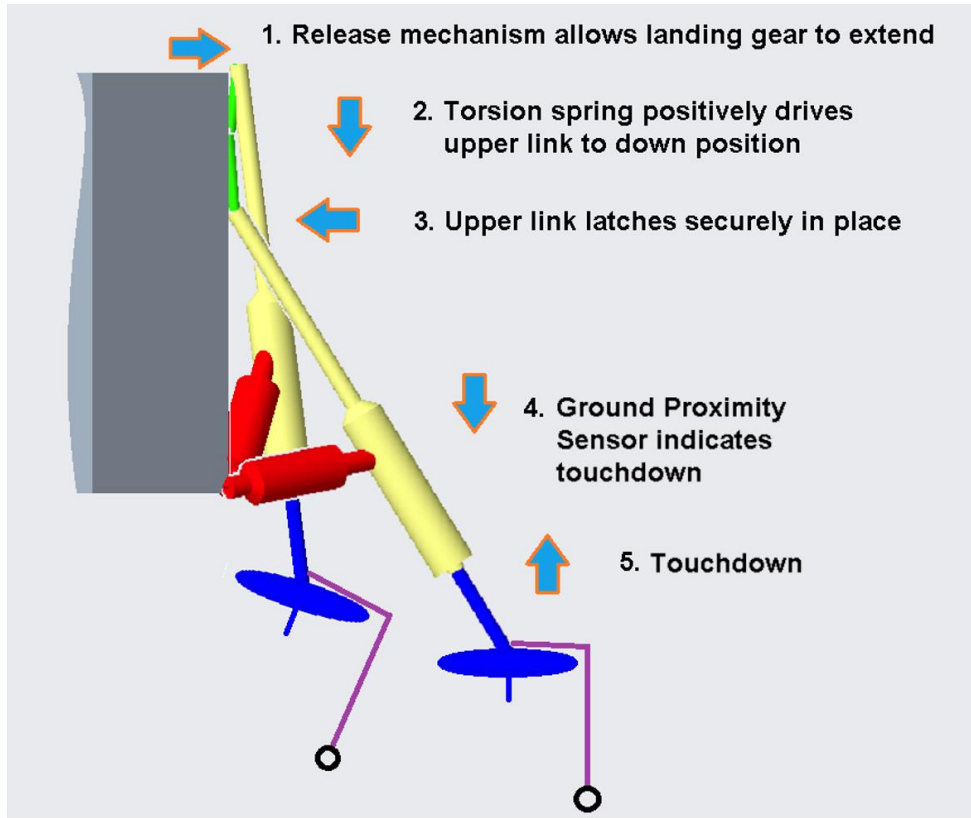


Figure 5.2.3: Landing system deployment sequence (note: ground proximity sensor not shown to scale).

When stowed, the legs fold into the corners of the ESPA volume envelope, as shown in Figure 5.2.4 below. In the deployed configuration, the legs provide a 45" (1.15 m) base such that, even given the worst-case combination of horizontal velocity, the lander would not tip over on impact (see Appendix G.1 for details).

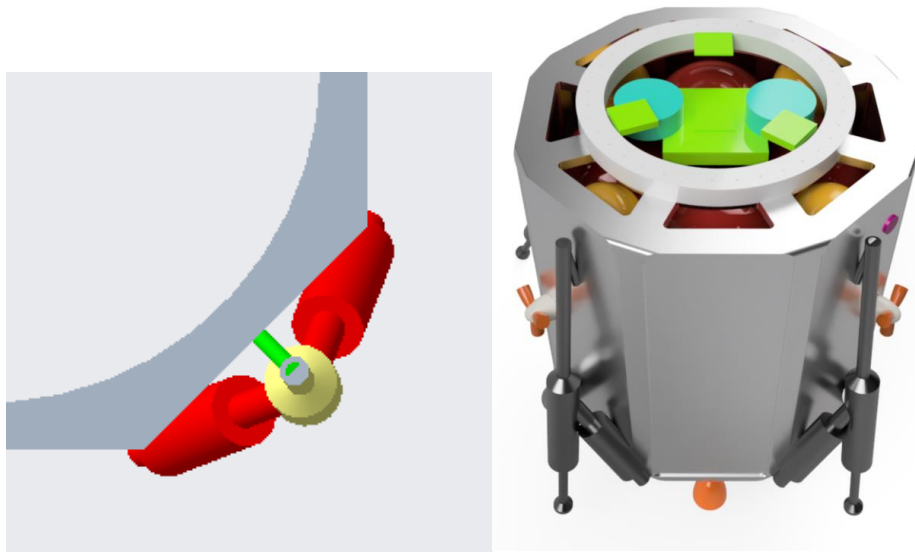


Figure 5.2.4: Top view (left) and full assembly view (right) of stowed landing gear.

## *Drill Mechanism*

The drill mechanism is responsible for collecting the lunar regolith samples that will be analyzed to determine its composition, including water content. Therefore, it must be able to penetrate the lunar surface and actuate the drill or secondary components such that the samples can be returned to the lander. Additionally, the method of extracting these samples must not damage or modify the samples. In particular, the volatiles in the sample should be preserved as much as possible. Next, since the mission aims to characterize the composition of the regolith by depth, the drill had to retrieve samples in a way that can sort them by depth. Finally, the drill mechanism must adhere to the mass and volume constraints of the lander and minimize complexity as it needs to be operated autonomously. Based on these requirements, the choice of the drilling mechanism was determined using the decision criteria listed below:

(1) Target Material Density:

This measures the ability of the drill to penetrate a surface. In particular, this is quantified by examining the density of a surface that it has successfully penetrated.

(2) Drilling Depth:

Ideally, the lander would drill as deep as possible as this yields the greatest scientific value in terms of characterizing the lunar regolith.

(3) Preservation of Volatiles:

This criteria is to minimize the sublimation of volatiles that result from the drilling process. This is primarily determined by the type of sample that the drill collects. There are two options for the type of sample collected: a core type sample and a powder type sample (Figure 5.2.5). A core type sample is a cylindrical chunk of regolith, where only the outside surface comes in contact with the drill. Therefore, this sample provides the greatest preservation of regolith, leading to the greatest scientific value. The powder type sample, however, splits and crushes the regolith into multiple smaller fragments, exposing more of the volatiles to the drill. Therefore, with this approach the volatiles are in greater danger of being sublimated.



Core Type Sample<sup>47</sup>

Lunar Regolith Simulant<sup>48</sup>

Figure 5.2.5: Core Type versus Powder Type Sample.

(4) Sample Localization

<sup>47</sup> De Almeida, Bruno, “Testemunho,” Projecto Situ, 2015. <https://projetositu.wordpress.com/2015/08/07/situ-2-daniel-de-paula-2/>.

<sup>48</sup> “Lunar regolith simulant,” Wikipedia. Accessed May 8, 2020. [https://en.wikipedia.org/wiki/Lunar\\_regolith\\_simulant](https://en.wikipedia.org/wiki/Lunar_regolith_simulant)

This measures the ability of the drill to return the samples in a way that can be sorted by depth. In other words, regolith from different depths must not be mixed together. This is crucial to achieve the desired scientific value of our mission.

(5) Power

The power consumption of the drill must be as low as possible given that the lander is operating in Shackleton Crater which has no sunlight. Therefore, the lander is completely battery powered which would mean that the drilling process must have power requirements that allow for sufficient lifespan with the battery sizes.

(6) Mass

The lander also has limited space for propellant and minimizing mass of the drill, as with every component was a key criteria.

(7) Complexity

This lander must operate autonomously. Therefore, to simplify the operations, the complexity of the drill must be minimal to ensure that there are as few points of failure as possible.

(8) Level of Autonomy

This criteria ensures that the drill can not only operate but also troubleshoot autonomously. For example, it was considered whether the drill has sensors integrated into it that can, for instance, sense temperature and drill to ensure that the temperature is maintained to a level that is acceptable as to not sublime the volatiles in the regolith.

(9) Published Specifications

Finally, using drills with heritage and available specifications that could be drawn upon was prioritized. Given the timeframe of this project, this was critical to ensure that the rest of the mission could proceed as the drill was one of the first few things in the critical path of the lander design. It was determined that it was out of the scope of this project to design a new drill or robotics platform given time constraints.

With these decision criteria established, four drills were evaluated to arrive at a trade study, which is summarized in Appendix G.3. The drill selected for the mission was the Honeybee TRIDENT, described below.

### Honeybee TRIDENT

The drill chosen for the Erebus lunar lander was the Honeybee Robotics TRIDENT Drill, which will be used on the VIPER rover in 2024 with the objective of collecting lunar regolith samples to characterise water.

The TRIDENT drill is an auger type drill and has a powder type sample. It was tested by Honeybee Robotics on artificial lunar regolith mixed with ice compressed to 1.5 g/cc. It has a maximum drilling depth of 1 meter, requires 250 W of power and weighs 16 kg. The TRIDENT drill is able to integrate a temperature sensor on the drill bit as well as synchronize drilling between a hammer and a rotating drill bit. The TRIDENT drill also has readily available published specifications.

The TRIDENT drill has a number of positive features that were key factors in selecting it for our mission. The drill is able to be modified; a decrease in drilling depth of 10 centimeters results in 0.5 kg of mass being shed. The TRIDENT allows for easy handling of the powder type sample as it comes with a rotary attachment to help bring the lunar regolith into the onboard science lab. Additionally, it drills in 10cm “bites,” allowing for depth versus sample characterization, since after every 10 centimeters a sample is collected. Its light mass, modest power requirements, adaptable dimensions, and ease of

handling of the sample all support the decision to pick the TRIDENT drill as the drill for the lander's mission.<sup>49</sup>

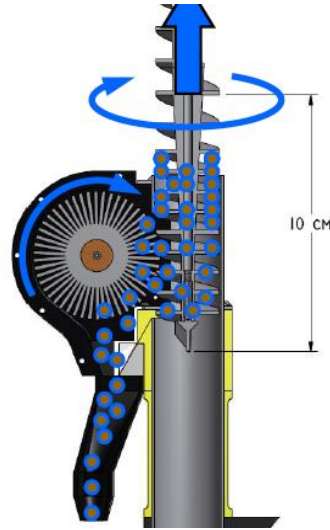


Figure 5.2.6: TRIDENT drill with rotary brush attachment.

The only drawback with the TRIDENT drill was that it has a powder-type sample, which, as explained previously, risks the sublimation of volatiles. However, the further characterization of this risk, as explained below, shows that at least 82.3% of the ice will remain in the regolith given the operating temperatures of the TRIDENT. The calculations for this drill are shown in the Appendix G.4. Therefore, the benefits of the TRIDENT drill outweighed the risks.

For this particular application, given size constraints the drilling depth is 60 cm. While this does reduce the mass of the drill by 2 kg (0.5 kg/10cm reduction in depth), a 2kg margin was added for the mounting architecture needed for the drill in the lander. Therefore, despite the shortening of the length, the mass of the drilling mechanism remains 16kg. Additionally, the drill was mounted in the center of the lander to ensure that the pegs in our landing mechanism provide counter torque in a symmetric fashion. This also allowed the science payload to be located around the sample collection minimizing the travel distance (and therefore the robotics) associated with processing the samples.

---

<sup>49</sup> Indyk, Stephen. "TRIDENT: The Regolith and Ice Drill for Exploration of New Terrains." Honeybee Robotics Spacecraft Mechanisms Corporation, [www.hou.usra.edu/meetings/leag2017/presentations/wednesday/zacny2.pdf](http://www.hou.usra.edu/meetings/leag2017/presentations/wednesday/zacny2.pdf).

## 5.2.4 Components

### *Landing System*

- Al 7075 linkages (TRL 9)  
Circular cylindrical beams that make up the primary structure of the landing system, 1 ½" in diameter and 3/32" thick (see Appendix G.5), fabricated in-house.
- Landing pads with fixed anti-torque spikes (TRL 9)  
Aluminum discs, slightly concave, 8" in diameter and ¼" thick (see Appendix G.5), fabricated in-house.
- Aluminum crush core primary dampers (TRL 9)  
In use since the Apollo missions, aluminum crush cores may be ordered from a variety of vendors, including Hexcel, as mentioned previously in this chapter.
- Friction rebound damper (TRL 9)  
Standard spacecraft mechanism component, available from many vendors.
- Leveling spring (TRL 9)  
Standard spacecraft mechanism component, available from many vendors.
- Pyrotechnic pin-puller release mechanism (TRL 9)  
Standard spacecraft mechanism component, available from many vendors.
- Hinge with torsion spring and latch (TRL 9)  
Standard spacecraft mechanism component, available from many vendors.
- Ground proximity sensor (TRL 7)  
An adaptation of the Apollo Lunar Surface Sensing Probe for the smaller-scale Erebus lunar lander, this device would be developed and tested in-house.

### *Drill Mechanism*

- TRIDENT Drill with rotary brush attachment (TRL 6)  
Honeybee has tested their TRIDENT drill in a cryogenic/vacuum environment on Earth with lunar regolith simulant. Honeybee would be contracted to adapt a version of the TRIDENT drill, which will go to the Moon aboard the VIPER rover in 2024, for the Erebus lunar lander.<sup>50</sup>

---

<sup>50</sup> “New VIPER Lunar Rover to Map Water Ice on the Moon,” NASA, 2020. Accessed May 10, 2020. <https://www.nasa.gov/feature/new-viper-lunar-rover-to-map-water-ice-on-the-moon>.

## 5.3 Payload

The Erebus mission is, primarily, a science mission with an objective of characterizing water concentrations at varying depths in Shackleton crater. In order to meet this objective, the successful function of the science payload is imperative. In order to accomplish this, the science payload team has designed a suite of machinery and instrumentation referred to as the “laboratory” with a purpose of analyzing and retrieving data about the lunar water-ice. Based on research into previous attempts at lunar soil analyzation, three primary analyses must take place within the laboratory: an infrared spectrometer analysis for general composition data, a residual gas analysis for volatile composition data, and a ground penetrating radar analysis for composition versus depth data. Components were chosen to accomplish these tasks based on their robustness and space heritage, and this process is detailed here as well as their ability to accomplish the necessary analyses.

### 5.3.1 Key Requirements and Assumptions

#### *Requirements*

The payload shall...

- ...fulfill the scientific objectives of the mission as laid out in section 2.1.1.
- ...contain scientific equipment that will identify the composition of water-ice on the lunar surface.
- ...contain necessary scientific equipment within the allotted payload volume and mass allocation, in accordance to the ESPA requirements.
- ...be developed with proper risk mitigation procedures to prevent a total mission failure.
- ...not contaminate the lunar surface with microbes.

#### *Assumptions*

- The payload laboratory’s internal systems (specifically, robotics for sample transfer) are outside the scope of this report and are classified as future work.

### 5.3.2 Mass and Power Budgets

#### *Mass Budget*

Component	Mass (kg)	Notes
Laboratory	14	Includes shielding, micropump, scale, heating element, robotic regolith transportation unit
ARGUS 2000 IR Spectrometer <sup>51</sup>	1	
NASA RIMFAX <sup>52</sup>	3	Ground-Penetrating Radar
Inficon Transpector Residual Gas Analyzer <sup>53</sup>	2	
<b>Subsystem total</b>	20	
<b>Allocated Mass</b>	25	
<b>MGA</b>	5 (25%)	Margin accounts for harnessing and sensors, as well as secondary components listed in “laboratory”

#### *Power Budget*

Component	Power (W)	Energy (Wh)	Notes
ARGUS 2000 IR Spectrometer	5	5	6 min/sample
Inficon Transpector Residual Gas Analyzer	20	15	0.75 min/sample
NASA RIMFAX	10	13	1.3 min/sample
<b>Subsystem total</b>	45	33	
<b>Allocated</b>	60	44	
<b>Margin</b>	15 (33%)	11 (33%)	Margin accounts for lab robotic processing

#### *Margins and Contingency*

The mass margin for the science payload (25%) is quite high due to uncertainty of the design of the robotic suite for sample processing. Although the general function required of the suite is known, due to the scope and time constraints of this project, the detailed design of a robotic suite is considered future work. A larger mass margin provides more flexibility for the design of robotics in the sample processing lab. For similar reasons the power margin is high because the exact power requirements of the lab’s robotic systems are unknown, as well as the power requirements of secondary components (scale, heating element, micropump).

<sup>51</sup> “ARGUS IR Spectrometers,” retrieved from from <http://thothx.com/products/argus-ir-spectrometers>

<sup>52</sup> “RIMFAX,” retrieved from <https://mars.nasa.gov/mars2020/spaceship/instruments/rimfax/>

<sup>53</sup> “Transpector MPH High Performance Residual Gas Analyzer For Semiconductor Manufacturing,” retrieved from <https://products.inficon.com/getattachment.axd?attaName=118b3bc1-dacb-49c4-b563-ef752c7f5799>

### 5.3.3 Design

#### *Research*

To meet the requirement of fulfilling the scientific objectives of the Erebus mission, the science payload must be able to characterize the composition of water-ice in Shackleton crater. In order to best accomplish this, payloads from previous or developing missions to examine lunar and Martian soil were researched. The payload that most heavily influenced Erebus' laboratory is the NASA RESOLVE lunar rover for "Regolith & Environment Science and Oxygen & Lunar Volatile Extraction."<sup>54</sup> The RESOLVE rover is a future NASA mission to the sunlit surface of the moon to drill and analyze volatile concentrations in the soil, which are substances that evaporate easily.

Due to the extremely low pressure at the lunar surface ( $\sim 3 \times 10^{-15}$  atm) being less than the vapor pressure of water at nominal surface temperatures, water is considered a volatile in the lunar soil. The first method RESOLVE plans to use to analyze regolith is infrared spectrometry. This will provide a compositional analysis of the minerals in the regolith, while also identifying the presence of water. This method was also used by the NASA LCROSS orbiter to determine a rough compositional analysis of the surface regolith in lunar craters.<sup>55</sup> The next method RESOLVE uses is a volatile analysis using a residual gas analyzer. In order to change the state of the volatiles in the lunar regolith to gas, the regolith must be heated. After the volatiles are in the gaseous state, the gases may be pumped from their initial analysis chamber into the residual gas analyzer chamber for testing. These methods were tailored to our use within our constrained payload.



Figure 5.3.1. Argus 2000 IR Spectrometer<sup>56</sup>

#### *Erebus Laboratory*

The smallest commercially available space-grade infrared spectrometer is the ARGUS 2000. Weighing in at only 220g, this solution will provide a robust analysis of regolith composition while fitting within our mass allowance. As for volatile analysis, we chose to employ the Inficon Transpector RGA, like the NASA RESOLVE solution. These choices will provide robust analyses necessary to the realization of Erebus' scientific objectives while also having the added benefits of space heritage or future high-profile usage in space. Concerning how these components and other secondary components will be used in our laboratory, the regolith will first enter the payload from the drill bit assembly. The sample will be

<sup>54</sup> Sanders, G.B. et al., (2011), "RESOLVE for Lunara Polar Ice/Volatile Characterization Mission," retrieved from <https://ntrs.nasa.gov/archive/nasa/casi.ntrs.nasa.gov/20110014548.pdf>

<sup>55</sup> "LCROSS Impact Data Indicates Water on Moon," (2009), retrieved from <https://ntrs.nasa.gov/archive/nasa/casi.ntrs.nasa.gov/20110014548.pdf>

<sup>56</sup> "ARGUS IR Spectrometers," retrieved from <http://thothx.com/products/argus-ir-spectrometers>

weighed (we have set the sample size at 30 grams, in accordance to RESOLVE sample size). Next, the infrared spectrometer test will occur, taking approx. 6 min. The chamber will then be sealed and the sample will be heated to a value where models predict the volatiles will have evaporated. The gases will be pumped into the RGA for the volatile analysis, taking approx. 0.75 min. The results of this test will give us parts per million data of all of the gases evaporated and pumped into the RGA. This, coupled with the weight data, temperature and pressure of gas data (from internal sensors) will give us extremely accurate regolith volatile compositional data, namely water-ice concentration. Finally, the gases will be pumped out to the lunar atmosphere, the remaining sample dumped, and the next depth's regolith sample will be channeled into the laboratory. An important problem to note with the compositional results is that some volatiles will be lost through the powder drilling process. These losses will need to be accounted for with modeling.



Figure 5.3.2. Inficon Transpector Residual Gas Analyzer<sup>57</sup>

#### *Ground Penetrating Radar*

The next important component in the science payload is ground-penetrating radar (GPR) to return data on the geologic features and composition of lunar ice and regolith at the landing site. Radar can collect data on rock far below the distance the drill on the lander will reach, which allows for data collection over a wider area. When choosing a GPR, the first option was the Lunar Regolith Penetrating Radar (LRPR) used on the Chang'e 5 Lunar Mission set to launch in 2020. The LRPR can return high-resolution images of regolith up to 2 meters below the surface, has a power consumption of 15W, and weighs 3.84 kilograms. Because the LRPR uses a system of 12 antennae, it requires only one receiver and one transmitter to collect and send data, which reduces the weight and power consumption compared to traditional radar systems.<sup>58</sup> However, the imaging method used to interpret data from the LRPR can have difficulty identifying small (less than 19 cm) rocks and image quality can be negatively affected by clutter and ground reflections at shallow depths.<sup>59</sup>

The second option for the GPR was the RIMFAX system used on the Mars Perseverance Rover scheduled for launch in 2020. The RIMFAX can emit a broad range of wavelengths to collect detailed images at all depths, including up to 30 feet below the surface. The RIMFAX system weighs 3 kilograms,

<sup>57</sup> "Transpector MPH High Performance Residual Gas Analyzer For Semiconductor Manufacturing," retrieved from <https://products.inficon.com/getattachment.axd/?attName=118b3bc1-dacb-49c4-b563-ef752c7f5799>

<sup>58</sup> S. X. Shen et al., (2018). "Lunar Regolith Penetrating Radar on the Lander for Chang'E-5 Mission," 2018 17th International Conference on Ground Penetrating Radar (GPR), Rapperswil, 2018, pp. 1-4, doi: 10.1109/ICGPR.2018.8441614

<sup>59</sup> Feng, J. et. al., (2019), "An imaging method for Chang'e-5 Lunar Regolith Penetrating Radar," doi: <https://doi.org/10.1016/j.pss.2019.01.008>

has a power consumption of 5-10 W, and is quite small at 7 by 4.7 by 2.4 inches. Because of the high image resolution, compact size, lower power consumption, and greater availability of information compared to the LRPR on the Chang'e 5 mission, the RIMFAX system was chosen for this mission over the LRPR.

#### *Adapting COTS Payload Components*

An issue with using COTS solutions for the science payload is making certain that they are upgraded enough to be used in the space environment. Specific to our RGA (our only non-space-grade COTS component), vibration and particle radiation must be addressed. Particle radiation fluxes can be mitigated by high-hydrogen plastic shielding.<sup>60</sup> With regards to vibration, testing has been performed on the RGA by NASA. They found that internal fasteners would need to be bolstered to prevent system damage.<sup>61</sup>

#### *Contamination*

Another important problem to address is lunar surface microbial contamination. Although microbes cannot live on the sunlit surface of the moon due to the high UV flux, it is theorized that some could survive on the low UV regions of the moon, such as Shackleton crater.<sup>62</sup> Therefore, the payload will utilize the NASA protocol of dry heat microbial reduction on all surfaces that directly interface with lunar regolith. This process involves first cleaning the surfaces then heating them up to 111.7 deg C for 30 hours.<sup>63</sup> This will eliminate almost any possibility of microbes contaminating the lunar surface.

#### *Future Work*

Future work regarding the GPR on this mission is to investigate mounting the RIMFAX to a gimbal to increase the range of motion. While this isn't as much of a concern on the moving Perseverance Rover, because the lander is stationary, the area that the RIMFAX can scan is limited to the landing site where the RIMFAX is pointed. By mounting the RIMFAX to a gimbal, the orientation can be moved to scan more of the landing site and collect more data on lunar ice and regolith composition in multiple areas instead of only directly where drilling is occurring. Regarding the laboratory, although we have selected specific components, there is an opportunity for future work in detailed design of internal sensors, secondary components, and a regolith transportation unit. More future work could be found through research into the method of seal for the gas evaporation chamber.

### 5.3.4 Components

- ARGUS 2000 IR Spectrometer (TRL 8)  
COTS solution with some space heritage.

---

<sup>60</sup> Arevalo, R., Ni, Z., & Danell, R., (2019), "Mass spectrometry and planetary exploration: A brief review and future projection," retrieved from <https://onlinelibrary.wiley.com/doi/full/10.1002/jms.4454>

<sup>61</sup> Santiago-Bond, Jo., (2015), "INFICON Transpector MPH Mass SPectrometer Random Vibration Test Report," retrieved from <https://ntrs.nasa.gov/archive/nasa/casi.ntrs.nasa.gov/20160012024.pdf>

<sup>62</sup> Glavin D. et al., (2010), "In Situ Biological Contamination studies of the Moon: Implications for Future Planetary Protection and Life Detection Missions," retrieved from <https://ntrs.nasa.gov/archive/nasa/casi.ntrs.nasa.gov/20100036597.pdf>

<sup>63</sup> Hereath, Anuradha, (2009), "How to Protect Other Planets from Earth Microbes," retrieved from <https://www.space.com/7410-protect-planets-earth-microbes.html>

- Inficon Transpector residual gas analyzer (TRL 7)  
COTS solution slated to be used on RESOLVE, must be adapted for the space environment.
- NASA RIMFAX (TRL 9)  
NASA technology for PERSEVERANCE Mars rover.
- Micropump (TRL 9)  
COTS component for laboratory
- Scale (TRL 9)  
COTS component for laboratory
- Regolith heater (TRL 9)  
COTS component for laboratory
- Internal robotic regolith transportation unit (Unknown)  
More research and design will be done in this area.

## 5.4 Guidance, Navigation, and Control

The GNC subsystem is crucial to the fulfillment of the lander's mission. The subsystem is in charge of ensuring the spacecraft approaches and lands in the desired location without crashing. It achieves this by performing orbit determination and control of the spacecraft. The data from these functions are sent to the earth for analysis purposes.

### 5.4.1 Key Requirements and Assumptions

#### *Requirements*

The GNC system shall...

- ... ensure that the lander will land within a 6 km diameter landing circle. (6.2.1)
- ... shall ensure that the impact is survivable by the mechanical structure of the lander, finalized at 1.6 m/s vertical velocity, 1 m/s horizontal velocity, 0.5 deg/s angular rate. (6.3.1, 6.3.4, 6.3.5)
- ... shall not excite the vehicle at frequencies greater than 35 Hz to prevent resonance in the vehicle structure. (6.3.2)
- ... shall roll the lander at a rate of 0.6 deg/s during long idle times throughout the descent for thermal management. (6.7.3)

While the landing ellipse might seem big, it's extremely difficult to accurately pinpoint a landing site. This is due to the navigational challenges in lunar orbit rather than a guidance or control problem and the difficulty of accurately propagating these errors within the time period of this project. For reference, the Beresheet lander had a 7.5 km radius landing ellipse for a similar class of mission<sup>64</sup>. However, the landing ellipse radius does not need to be very precise, as the surface is mostly flat (as communicated to the GNC team by the mission planning team) and almost all of Shackleton crater, which has a 10.5 km radius, contains lunar surface ice therefore a precise landing was not a tight requirement.

The vehicle impact characteristics were an ever-changing trade between the mechanical team and the GNC team, with the final characteristics at ranges that both teams were able to achieve with available analysis tools.

The maximum excitement frequency is determined by the mechanical structure. The requirement originates with launch vehicle integration.

The roll rate during the rotisserie mode is the thermal team's approximation based on the Apollo command module's roll rate<sup>65</sup> during transit to the moon and is expected to change as further analysis is conducted. However, as long as the roll rate remains under 2 deg/sec, the maximum operable slew rate of the star trackers, it presents no additional challenge to the system.

---

<sup>64</sup> Grossman, Y. et al., Landing Site Selection for the SpaceIL Mission to the Moon. *Lunar and Planetary Science XLVIII*. Accessed on May 5, 2020. Retrieved from [https://www.researchgate.net/publication/313314811\\_Landing\\_site\\_selection\\_for\\_the\\_SpaceIL\\_mission\\_to\\_the\\_Moon](https://www.researchgate.net/publication/313314811_Landing_site_selection_for_the_SpaceIL_mission_to_the_Moon)

<sup>65</sup> Widnall, William S. Some Dynamics and Control Challenges That Occurred During the Apollo Project. MIT. 16.07 Dynamics, 2009.

### *Assumptions*

- Numerical simulation of the control system is beyond the scope of this project and classified as future work.
- Communications subsystem does not impose an attitude requirement.
- The entire landing ellipse contains lunar surface ice, based on the following analysis<sup>66</sup>.
- The entire landing ellipse is flat and free of debris, as communicated by the mission planning team.
- Detailed (algorithm-level) design of the attitude determination algorithm, orbit determination algorithm, guidance algorithm and orbit propagation algorithm are beyond the scope of this project

### 5.4.2 Mass and Power Budgets

#### *Mass Budget*

Component	Mass (kg)	Notes
Radar (2)	1.72	Includes radar altimeter and velocimeter
Star Tracker (2)	0.70	Does not include mounting
Sun Sensor (6)	0.21	Does not include mounting
IMU (2)	1.00	Does not include mounting
<b>Subsystem total</b>	<b>3.63</b>	
<b>Allocated Mass</b>	<b>4.2</b>	
<b>MGA</b>	<b>0.54 (15%)</b>	Margin accounts mostly for radar mass growth

#### *Power Budget*

Component	Power (W)	Energy (Wh)	Notes
Radar (2)	22.4	36.8	Only used in the last 800 m (altitude) of descent
Star Tracker	3	4.9	Used the entire mission
Sun Sensor	0.2	0.3	Used for the first 0.3333 hrs of descent
IMU	6	9.87	Used for the entirety of the orbit
<b>Subsystem total</b>	<b>31.6</b>	<b>52.0</b>	
<b>Allocated</b>	<b>39.5</b>	<b>65.0</b>	
<b>Margin</b>	<b>7.9 (25%)</b>	<b>13 (25%)</b>	Moderate margin for well-characterized reqs

<sup>66</sup> Spudis, Paul D. Geology of Shackleton Crater and the south pole of the Moon. Accessed 7 May 2020. <https://agupubs.onlinelibrary.wiley.com/doi/full/10.1029/2008GL034468>

### *Margins and Contingency*

The mass margins mostly consist of margins for the radar system, which is not space qualified and intended to be a stand-in for a space qualified system custom made. In addition, the second radar system is a stand-in for a space qualified radar velocimeter, which is expected to be very similar in mass but may be slightly heavier. The other sensors, IMU, sun sensor, star trackers, all have a flight heritage and little mass growth is expected from them.

The landing radar and velocimeter are only expected to be used for the final kilometer in altitude of the descent. Assuming approximately a quarter of the orbital period is under a kilometer in altitude (a very large overestimate) gives the required energy usage. The power team, however, calculated as if every sensor was used for the half the descent for a significant margin overall. This is why the energy numbers in the above table do not seem to correspond with the notes. The IMU, the sun and the star sensors are expected to be powered during the entirety of the descent. However, their power draws are well known and do not deviate far from the average power draw. This reduces the margin needed for these components.

#### 5.4.3 Design and Analysis

##### *Spacecraft Body-Centered Coordinate Frame Convention*

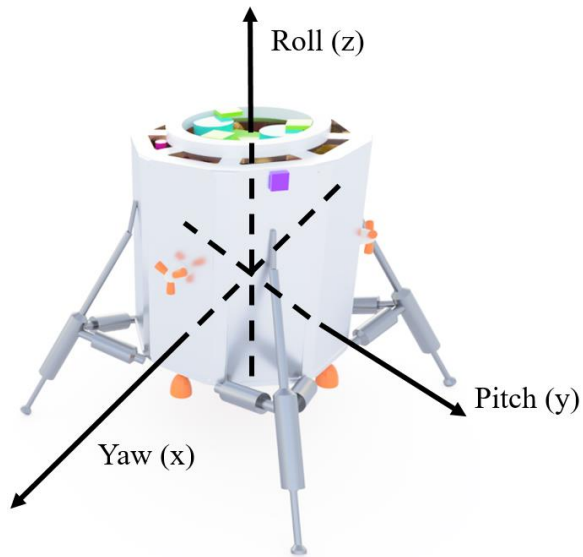


Figure 5.4.1. Lander Body Axis Diagram

As a convention for discussion of the spacecraft within this chapter, a body-centered reference frame is defined as shown in Figure 5.4.1. The axes are centered on the wet center of mass of the spacecraft. The z axis is defined as being normal to the plane of the separation ring. The x-axis passes directly above one of the main descent thrusters, and the y-axis passes directly above the main descent thruster located 90 degrees counterclockwise of the x-axis's main descent thruster. This convention was chosen to simplify main thruster control for pure pitch and yaw rotation.

### *Lander Disturbance Environment*

The first step in determining the necessary actuators is characterization of the disturbance environment of the vehicle. A typical lander features thrusters as the primary attitude control system, but it was still important to characterize the expected disturbances. To characterize small disturbances, which typically include solar radiation pressure, gravity gradient, and magnetic field, the gravity gradient was selected for analysis to determine the overall order of magnitude of these small disturbances. The equation for the gravity gradient torque is as represented in equation 5.4.1, where  $\mu$  is the gravitational parameter,  $R$  is the orbital radius,  $I_z$  and  $I_y$  are the moment of inertias of the spacecraft around its z and y axis respectively (it is assumed that  $I_y$  is approximately equal to  $I_x$ ), and  $\theta$  is the angle between the local vertical and spacecraft's z-axis<sup>67</sup>.

$$T_g = \frac{3\mu}{2R^3} |I_z - I_y| \sin(2\theta) \quad (5.4.1)$$

Under the simplifying assumptions of a cylindrical spacecraft with evenly distributed mass, this results in a  $1.4 \times 10^{-5}$  Nm torque due to gravity gradient in the worst case, in which the spacecraft's z axis is 45 degrees rotated from the local vertical. All other small disturbance torques will be approximately this order of magnitude.

The main disturbance torque on the vehicle that must be corrected by the attitude control system is main thruster misalignment. The main thrusters are the 4 large 200 N descent thrusters on the bottom of the spacecraft, which are to be used for pitch and yaw control during descent. However, because these thrusters cannot gimbal, they cannot provide roll control. Uncertainty in the center of mass of the spacecraft and main thruster output mismatches will nominally result only in pitch and yaw disturbances during main thruster burns, as both of these disturbances create a net force vector that is parallel to the z axis of the spacecraft, and thus cannot create a torque in that axis. However, thruster misalignment can indeed create a torque in the z-axis. As shown in figure 5.4.2, the worst case of torque generation is when all 4 main thrusters are misaligned such that all of their off-axis thrust creates a torque in the z-direction and none of the torques cancel out. Using the SMAD estimate of 0.5 degrees maximum thruster misalignment<sup>4</sup>, a torque of 3.5 Nm is expected from equation 5.4.2, where  $N$  is the number of thrusters,  $F$  is the nominal thruster force,  $l$  is the moment arm of the force, and  $\theta$  is the thruster misalignment. Since the finite burn is expected to be 1701 seconds long, this results in a total angular momentum change of 5954 Nms.

$$T_{misalignment} = NF l \sin(\theta) \quad (5.4.2)$$

Clearly, this is far larger than the external disturbances, which can be neglected.

---

<sup>67</sup> Wertz, James R., et al. Space Mission Analysis and Design, Third Edition. Microcosm Press, El Segundo, CA, 1999.

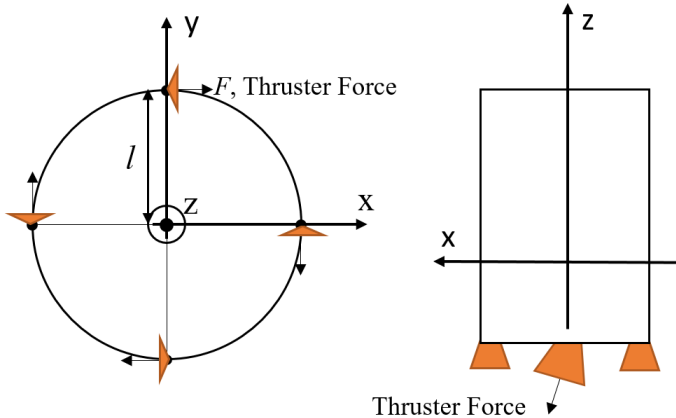


Figure 5.4.2. Thruster Misalignment Torque Generation, Top and Side View

Another source of spacecraft-induced disturbance is the changing center-of-mass. Again, it is assumed that if the center of mass is offset in the xy plane, a combination of main thruster placement to ensure thrust through the center of mass and main thruster off-pulsing will correct for torques created by the main thrusters. However, such a scheme is not possible for the RCS (reaction control system) thrusters. During translational maneuvers, these thrusters may exert a torque on the vehicle, as in figure 5.4.2. Initially, the thrusters will be placed midway in the z-axis between the wet and dry center of mass. These differ by approximately 15 cm (refer to the orbiter mass properties documentation). Thus, the maximum moment arm is 7.5 cm. Assuming a thrust of 20 N (2 10 N thrusters), this results in 1.5 Nm of torque. The RCS thrusters will not be used for significant translation during descent, so a thruster on-time of 30 seconds is reasonable and likely a very large overestimate. This totals to 45 Nms of angular momentum generation.

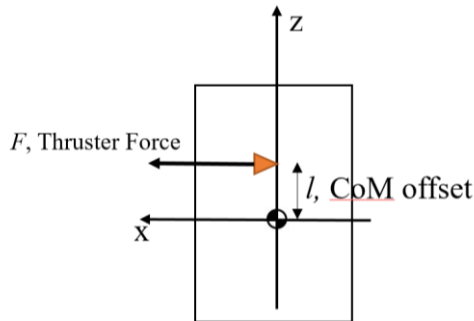


Figure 5.4.3. RCS Torque Generation During Translation

### *Actuator Selection Trade Study*

Three different actuation schemes were considered for the ACS (attitude control system) of the lander. These were thruster-only, thruster + control moment gyro, and thruster + reaction wheel. Magnetic torquers were not considered as the Moon's magnetic field is not dipolar, making it difficult to predict the

functionality of magnetic torquers in lunar orbit<sup>68</sup>. Thrusters were deemed necessary for translational control for course correction during descent. The trade study, detailed in Appendix I.1.4, resulted in the conclusion that both control moment gyros and reaction wheels had insufficient angular momentum storage and torque generation for the purposes of controlling the disturbances created by the translational thruster torque generation and main thruster offset, and that the added mass of these systems was large compared to the additional fuel needed to allow the thruster-only system to perform any task that the reaction wheels or control moment gyros would have been able to fulfill. The sizing of these thrusters was left as a task to the propulsion subteam, and the requirements of 5 Nm of torque generation were passed on, derived from the 3.5 Nm torque generation from the main thrusters with a 1.5 Nm (approximately 50%) safety margin due to the lack of detail on the method and precision of the mounting the main thrusters.

### *Sensor Selection Trade Study*

The first step of the sensor selection (detailed in Appendix I.1) was to determine which combination would fit the mission requirements. The sensors available were sun sensors, star trackers, horizon sensors, gyros and inertial measurement units (IMU), and the final selection would be a combination of at least three of the sensors to provide three -axis orbit determination. The guiding constraints would be the accuracy required during descent (6.2.1), the power and the mass. Sun sensors were deemed necessary to provide two-axis attitude data during the early stages of descent, and to provide fail-safe mode capabilities during that time. Horizon sensors were not considered since the spacecraft would not be spinning, and they are also generally less accurate compared to the sun and star sensors. Four sun sensors are enough to achieve full sky coverage, however, two redundant sensors were included to ensure the lander can withstand the loss of some of its sensors.

Star trackers were deemed necessary during descent. The lander landed in the Shackleton crater on the farside of the moon, therefore, a sensor that could provide three axis data in the absence of the horizon and sun sensors was needed. Star trackers also provided much greater accuracy, at a cost, compared to the preceding sensors. One star tracker is enough for the lander however, an extra one is also included for redundancy.

An IMU was chosen over gyros. It included gyros in it's configuration to provide more data both acceleration and ang drift unlike the gyros which could only provide the angular rates. One sensor is needed for the lander but two were chosen with one being redundant.

The final selection was thus a combination of star trackers, IMU and sun sensors. The NFSS 411 sun sensor and the NST-3 Nano Star Tracker were finally chosen as the preferred sun and star sensors based on their accuracy, 0.1 deg and 5 arcseconds 3-sigma respectively, which is a critical requirement for the lander (6.1.3).

The star trackers would be located on the surface, pointing normal to the sun sensors and 180 degrees apart. The sun sensors would be placed normal to the star trackers, there would be 2 sun sensors on the top surface, 2 on the bottom surface and 2 on the cylindrical surface, 180 degrees apart and normal to the sun sensors. The IMU could be anywhere inside the lander provided it was closest to the center of mass of the lander. However, additional calculations will be required to convert IMU measurements into spacecraft dynamics. Below is a simple schematic showing the sensor locations in one plane.

---

<sup>68</sup> Choi, Charles Q. A Real Dynamo: Moon's Magnetic Field Lasted Far Longer Than Thought. Accessed 5 May 2020. <https://www.space.com/37756-moon-magnetic-field lasted-billion-years-longer.html>

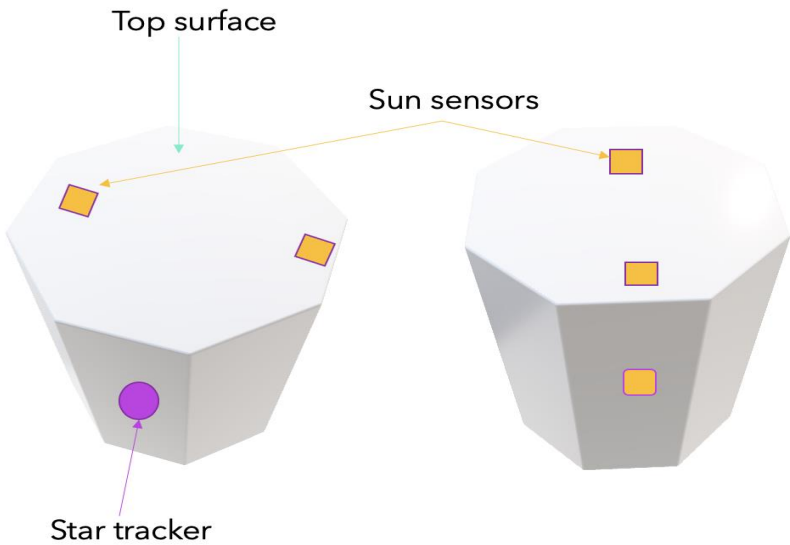


Figure 5.4.4. Location of sun sensors from one side. Shows half the number of selected sensors.

#### *Telemetry Rate Requirements*

The GNC team was required by the communications team to find the required upload rate upon descent (which is completely autonomous). Since algorithm-level design is out of the scope of this project, a minimum approximation was found with the telemetry rate of the Surveyor spacecraft, the first US lunar landers. These required a telemetry rate of 1.1 kb/s during descent<sup>69</sup>, which was communicated to the communications team. Such data would include lander position, attitude, velocity, sensor and actuator status, etc. to ensure that in the event of a failed landing the cause of failure would be able to be reconstructed, and in the event of a success the data could be analyzed to improve future missions.

#### *Navigation Scheme*

In order to track the vehicle and determine its orbit, it was originally planned to use only ground tracking for orbit determination. Note that only the OMV will be tracked, not the lander, as a direct Earth-to-lander link is not a capability of the lander because of the communications team's scheme. Thus orbit determination will only be done while the lander is docked to the OMV. After separation, the lander will rely on inertial navigation only until the radar altimeter and velocimeter become available. The IMU's velocity random walk is expected to be very small, such that the inertial velocity error due to the IMU error will only be 0.03 m/s after the entire descent<sup>70</sup>. However, it was found very difficult to quantify the propagation from initial navigational accuracy to final landing ellipse size. In order to land within a landing ellipse smaller than that of the Beresheet, after initial analysis it was determined that navigation to the accuracy of standard ground tracking (approximately 100 m accuracy) was insufficient to confidently

---

<sup>69</sup> Surveyor III Mission Report. Accessed 8 May 2020. <https://www.hq.nasa.gov/alsj/a12/Surveyor-III-MissionRpt1967028267.pdf>

<sup>70</sup> HG1900 Inertial Measurement Unit. Accessed 7 May 2020. <https://aerospace.honeywell.com/content/dam/aero/en-us/documents/learn/products/sensors/brochures/N61-1468-000-001-HG1900-InertialMeasurementUnit-bro.pdf?download=true>

achieve the 10 km accuracy requested by the mission planning team. Thus, a laser altimeter similar to that placed on the Mars Global Surveyor spacecraft will be placed on the orbital maneuvering vehicle, which should bring orbital position accuracy to approximately 30 m, and 1 m radially<sup>71</sup>. In addition, the orbital maneuvering vehicle will be planned to carry an experimental GNSS (Global Navigation Satellite System) receiver, as an experiment as to whether GNSS signals can be used in lunar orbit for navigation, potentially to accuracies less than 10 m<sup>72</sup>. However, this will not be the primary system of navigation as it is unproven (approximately TRL 4). Extensive research into this receiver was not conducted.

For final descent altitude and velocity determination, a greater precision is required than during the orbit and initial descent phase. A trade study was conducted on radar and lidar systems, detailed in Appendix I.1.5. In the end, it was decided that a radar system would offer significantly more range than lidar systems, and that system was chosen. Since radar systems for planetary descent are quite specialized devices, a helicopter radar system was chosen as an analogue for easier access to datasheets on the device. It was assumed that a space-qualified version of the system would be easily obtainable from Honeywell, who has traditionally produced space-qualified radar systems for NASA. For horizontal velocity determination, a duplicate of the same radar system is used. There is no analogue for this system commercially, so it was simply assumed that the same mass and volume as the original radar system would be sufficient for a multi-beam radar system similar to that used on various Mars landers, with an approximately 2x reduction in velocity accuracy to about 0.4 m/s<sup>73</sup>.

### *Main Thruster Torque*

Assume 4 200 N thrusters, 0.5 m from the centerline in a square. If one of these thrusters is deactivated, the center of thrust becomes 0.17 m from the centerline. The thrust is 600 N, with a 0.17 m moment arm this results in 102 Nm of torque. With an approximate moment of inertia of about 64.5 kg m<sup>2</sup> (assuming a 400 kg evenly distributed mass sphere with a 1.27 m diameter), this results in an angular acceleration of 1.6 rad/s<sup>2</sup> or 90.6 deg/s<sup>2</sup>. The minimum off-time of the main thrusters is 28 ms, resulting in a 2.5 deg/sec change in angular velocity. This can be used for large corrections in angular velocity during the descent burn.

For finer course correction, an individual thruster can be reduced to a minimum thrust of 165 N. This results in a moment arm of 0.02 m, a torque level of 15.3 Nm, and an angular acceleration of 13.6 deg/s<sup>2</sup>. Assuming the minimum off-time is the same as the minimum time for which the thruster can be throttled down to its minimum thrust and then throttled back to maximum thrust, this results in a 0.38 deg/s change in angular velocity. In the case of a burn, the mechanical excitation frequency of 35 hz is the limiting factor of command frequency, not the 28 ms minimum pulse or time between pulses. This is equivalent to 29 ms is taken as the time between these full throttle - minimum throttle - full throttle cycles. It is reasonable that during a burn while maintaining as tight of a deadband as possible the spacecraft will rotate at 0.19 deg/s angular velocity (so that after each pulse the spacecraft rotates in the opposite direction at the same angular velocity) for 29 ms before the spacecraft can perform a full throttle - minimum throttle - full throttle cycle, which would result in a 0.006 deg angular travel, thus maintaining

---

<sup>71</sup> Mazarico, Erwan, et al. Orbit Determination of the Lunar Reconnaissance Orbiter. Accessed 5 May 2020.  
[http://www-geodyn.mit.edu/mazarico\\_LROPOD\\_jgeod11.pdf](http://www-geodyn.mit.edu/mazarico_LROPOD_jgeod11.pdf)

<sup>72</sup> Capuano, Vincenzo. GNSS/INS/Star Tracker Integration for Real-Time On-Board Autonomous Orbit and Attitude Determination in LEO, MEO, GEO and Beyond. Accessed 5 May 2020.  
[https://www.researchgate.net/publication/320358049\\_GNSSINSStar\\_Tracker\\_Integration\\_for\\_Real-Time\\_On-Board\\_Autonomous\\_Orbit\\_and\\_Attitude\\_Determination\\_in\\_LEO\\_MEO\\_GEO\\_and\\_Beyond](https://www.researchgate.net/publication/320358049_GNSSINSStar_Tracker_Integration_for_Real-Time_On-Board_Autonomous_Orbit_and_Attitude_Determination_in_LEO_MEO_GEO_and_Beyond)

<sup>73</sup> Foessel-Bunting, Alex, et al. MMW-Scanning Radar for Descent Guidance and Landing Safeguard. Carnegie Mellon, Pittsburgh. Accessed 5 May 2020.  
[https://ri.cmu.edu/pub\\_files/pub2/foessel\\_alex\\_2001\\_1/foessel\\_alex\\_2001\\_1.pdf](https://ri.cmu.edu/pub_files/pub2/foessel_alex_2001_1/foessel_alex_2001_1.pdf)

the spacecraft within 0.003 deg of its intended attitude. This more than meets the 0.1 deg pointing error expected in the rest of this analysis.

### *Pointing Error Analysis*

It is now desirable to approximate the effect of pointing errors on the vehicle's trajectory. Assume that pointing error only matters for the approximately impulsive burns, for which the burn time is too short for active guidance to occur. This limits the pointing error to only the initial orbital lowering burn and the following circularization burn – the landing burn is minutes long, and the guidance algorithm will be able to correct for the majority of pointing errors.

Assuming the attitude error is 1/10 of a degree off of the ideal thrust axis, with the off-axis burn being in the orbit normal direction results in a positional error of approximately 1.98 km at the worst point (90 and 270 degrees ahead of the plane change), as seen in figure 5.4.5, which shows how the orbital radius, inclination difference, and total position difference are related. See Appendix I.1.7 for this full calculation.

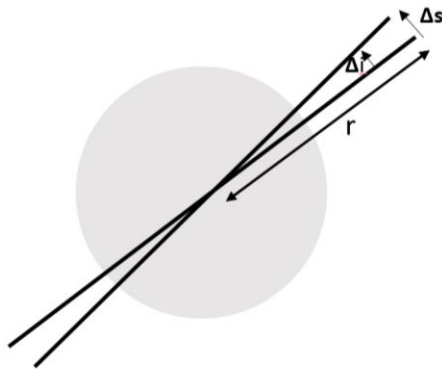


Figure 5.4.5. Plane Change Positional Error

This position error is too much to leave unaccounted for. The onboard IMU will be able to detect this improper thrust with the accelerometer and attempt to correct for it before the final descent in a 0.0038 m/s course correction maneuver, which is easily achieved by the translational thrusters in a less than 1 second pulse. See Appendix I.1.8 for the full calculation. Thus, off-nominal thrust during the approximately impulsive maneuvers will present a large translational error, but with course-correction maneuvers this error is easily nullified.

### *Navigational Accuracy Analysis*

To approximate how tracking errors will affect the endpoint landing site, position errors were mostly considered. In making these considerations, an assumption that both acceleration and velocity errors will be corrected by the control algorithms and therefore will not propagate over the entire orbit was made.

One way to accurately model the landing ellipse, and therefore the tracking error, demands the derivation of the lander's initial covariance matrix, and then followed by the development of a Monte Carlo simulation of the problem. However, this was deemed too demanding in terms of the time and expertise required. Therefore, it was assumed that developing the simulation was beyond the scope of this project.

To approximate the tracking error, therefore, the landing trajectory was modeled as a 2d problem closely approximated by the first quarter of an ellipse. This allowed for a simplified but relatively accurate approximation of the landing ellipse. The full program can be found in Appendix I.1.7.

The Lunar Reconnaissance Orbiter (LRO) was able to get position estimates in the radial direction up to around 1m<sup>8</sup>, or  $\pm 0.5$  m, and adding some margin, a  $\pm 1.5$  m accuracy was assumed as the achievable tracking accuracy for the purposes of this analysis. Three possible position errors are bound to occur during descent:

- Vertical (orbit radial) position error of  $\pm 0.0015$  km
- Horizontal (orbit tangent) position error of  $\pm 0.045$  km
- Lateral (orbit normal) displacement error of  $\pm 0.045$  km

Since the model is modeled as a 2D problem, the third scenario is not considered. This is due to the fact that the lateral displacement is similar in effect to the horizontal one.

Starting at 10km altitude and assuming a horizontal distance of 350km, The maximum possible horizontal error is summed up assuming the maximum vertical error of  $\pm 0.0015$  km occurs at every kilometer of the way. This method is then repeated to find the maximum horizontal error that can be made if a horizontal error of  $\pm 0.045$ km is made every kilometer of the way. This then gives the approximated maximum landing error if errors are made in both directions as shown in the plots below.

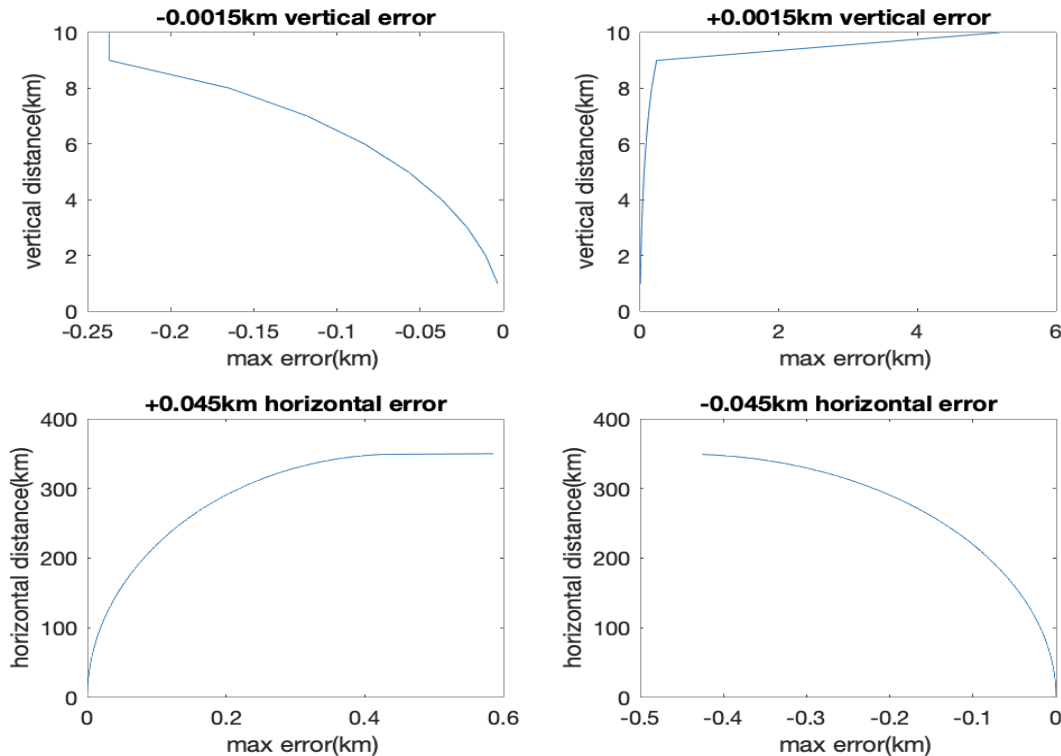


Figure 5.4.6. Distance vs Error Plots

The results show that, when approximated, the extreme possible landing errors are [-0.426km, 0.585km], [-0.237km, 5.186km] due to the horizontal and vertical errors respectively. This is well within the crater.

### *Final Descent Scheme and Analysis*

Due to the lunar dust cloud generated by the plume by the main thrusters, it is expected that the radar and doppler velocimeter sensors will be inoperable below an altitude of 20 m<sup>74</sup>. Due to the initial velocity error in the doppler velocimeter, approximately 0.2 m/s, plus the error in the position radar of 0.4 m, the vehicle will have a vertical position error of approximately 1.6 m near touchdown. Since the mechanical system cannot withstand a “bounce,” where the spacecraft lifts off of the lunar surface and then falls back onto it after impact, which would occur if the vehicle is still thrusting after the impact, the choices were either to completely cut off the main engines at an altitude of 1.6 m ( $\pm 1.6$  m) or use a mechanical sensor to detect touchdown. In order to reduce strain on the mechanical system, the latter option was chosen. For the last 3.2 m of the descent, the lander will pulse its thrusters for approximately 117 ms every 250 ms, which is longer than the 28 ms minimum pulse length and exceeds the 28 ms minimum time between pulses while having a frequency of approximately 4 Hz, which is far below the minimum lander mechanical excitation frequency of 35 Hz. This results in an approximately constant velocity. By targeting 1 m/s nominal descent velocity, this method ensures that the impact velocity will be between 0.8 and 1.6 m/s. This fulfills requirement 6.3.1. When the mechanical sensors on the legs register a vehicle height just before impact, the pulses will be stopped. The length of this sensor depends on the amount of time it takes for the electrical signal to travel from the sensor to the guidance computer, but a conservative estimate of a 0.25 m sensor was requested such that even if the guidance algorithm does not register sensor impact before the end of a pulse, the vehicle will still not bounce as the length is larger than a single pulse on + pulse off time.

With regards to horizontal velocity on landing, the minimum velocity is limited by the radar velocimeter precision. Similar systems achieve accuracies of approximately 0.2 m/s<sup>75</sup>, so the team felt comfortable assuming the final horizontal velocity would be less than 1 m/s, which the mechanical team was able to achieve. As shown in the pointing error analysis, the translational thrusters should have no problem achieving this with their minimum impulse bit, but a large margin was felt necessary as characterization of a custom doppler velocimeter system and the terminal descent algorithm were both outside the scope of the project. This fulfills requirement 6.3.1b.

For detecting the local vertical, the spacecraft will use its IMU to detect its acceleration vector. By comparing this to the expected acceleration from the well-characterized thrust of the main thrusters, the IMU will be able to detect the local gravitational vertical vector. Multiple short-range LiDAR sensors were examined as a way of detecting the actual ground slope, but the resolution on these sensors was deemed insufficient for detection. From the mission planning team, the site is expected to be flat, so deviation between the local gravitational vertical and the vector normal to the surface should be minimal.

---

<sup>74</sup> Li, Shuang, et al. Guidance Summary and Assessment of the Chang'e-3 Powered Descent and Landing. *Journal of Spacecraft and Rockets*, 2015. Accessed 5 May 2020.

[https://www.researchgate.net/publication/284345092\\_Guidance\\_Summary\\_and\\_Assessment\\_of\\_the\\_Chang'e-3\\_Powered\\_Descent\\_and\\_Landing](https://www.researchgate.net/publication/284345092_Guidance_Summary_and_Assessment_of_the_Chang'e-3_Powered_Descent_and_Landing)

<sup>75</sup> Polar, Brian. Radar Terminal Descent Sensor. Jet Propulsion Laboratory. Accessed 5 May 2020.  
<https://trs.jpl.nasa.gov/handle/2014/43075>

To determine the maximum rotational velocity, both the sensors and actuators were analyzed. With a minimum impulse bit of 0.1 Ns<sup>76</sup>, these thrusters change the lander's angular velocity by approximately 0.09 deg/sec. This represents the maximum uncorrectable error. This is presumed to be much larger than the angular velocity error of the IMU, which features an angle random walk of 0.06 deg/ $\sqrt{hr}$  implying a much lower angular velocity error than 0.09 deg/sec. Thus, the only unknown is the terminal descent control algorithm. A hefty safety factor of 5 was applied to get the 0.5 deg/sec maximum touchdown angular velocity given to the mechanical team, which was achievable with reasonable mass of landing legs. This fulfills requirement 6.3.5.

### Block Diagram

The following is a block diagram showing the overall concept of operations of the system.

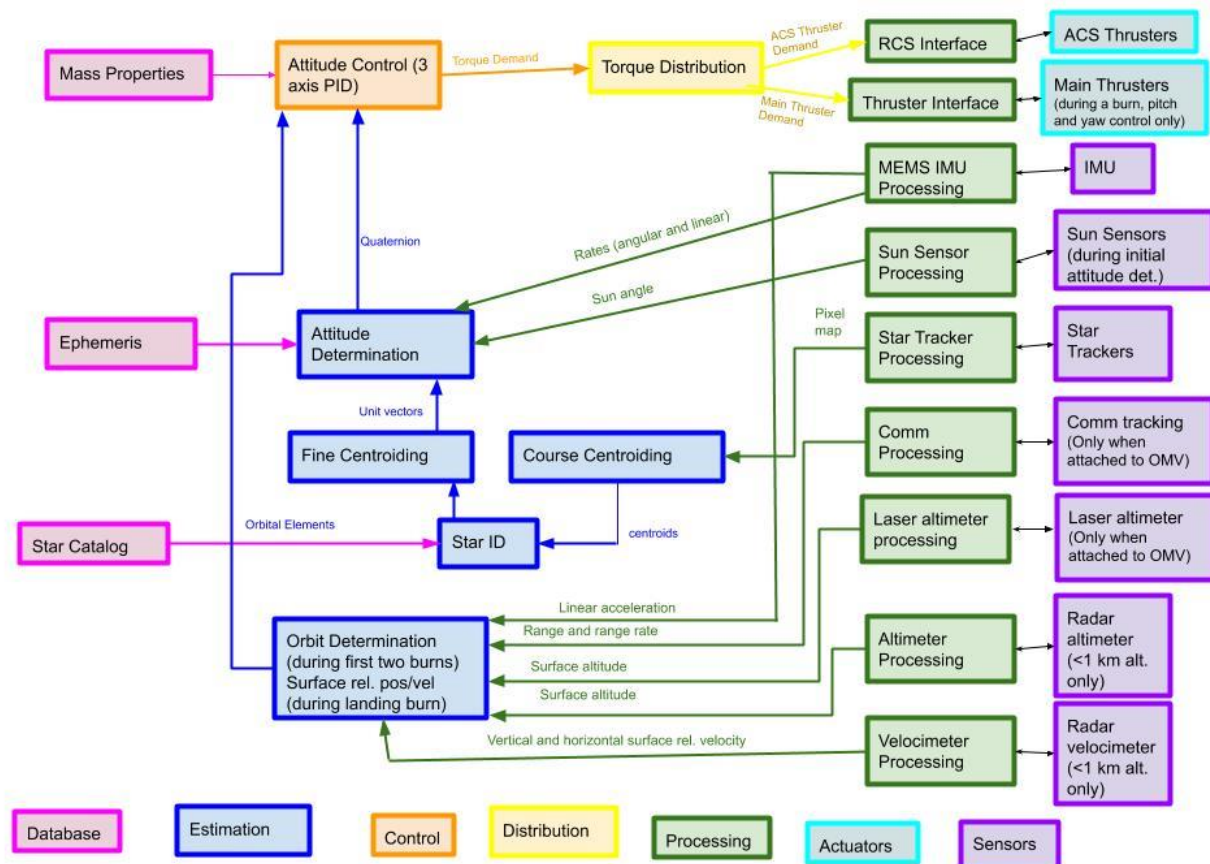


Figure 5.4.7. Lander GNC Block Diagram

### Detumble mode

Because of the moon's irregular (not dipolar) magnetic field, the spacecraft will not be using magnetic torquers to detumble. The spacecraft will thus rely on the IMU, targeting  $1 < \omega_z < 2$  deg/sec of angular

<sup>76</sup> Fick, M. et al. EADS-ST's Latest Bipropellant 10 N Thruster and 400 N Engine: The Fully European Solution.

Accessed 5 May 2020

<http://articles.adsabs.harvard.edu/full/2004ESASP.555E..92F/0000092.003.html>

velocity in the roll axis and 0 deg/sec angular velocity in all other axes. The 2 deg/sec limit is imposed by the capability of the star sensor to take images while the spacecraft is slewing. This enables one of the star sensors to sweep a band around the spacecraft, with ample warning from the sun sensors to avoid trying to get information from the sun. With the 360 degree sweep finishing in approximately 6 minutes, complete attitude determination should be complete within or before that time.

### Fuel Needed for Detumble

According to requirement 6.3.3, the expected angular velocity upon separation from the launch vehicle is expected to be less than 5 deg/sec. Assuming approximately 20 N, and thus 10 Nm of available thruster torque (2 10 N thrusters), and the  $64.5 \text{ kg m}^2$  inertia referenced earlier, this results in an angular acceleration of  $8.9 \text{ deg/s}^2$ , which results in a 0.56 s thruster burn needed for detumble, requiring 3.9 g of propellant.

### Slew Mode

The slew mode is activated immediately after the detumble and again immediately after each impulsive burn to reorient the spacecraft into the correct attitude for the next burn.

The first step in this mode is angular velocity targeting. The spacecraft targets an angular velocity (determined such that the spacecraft will reach the target attitude with significant margin before the next burn) with thrusters and cuts off when this angular velocity is met. After this, the spacecraft holds the current angular velocity, with only minor thruster corrections to null out angular velocity in unwanted axes.

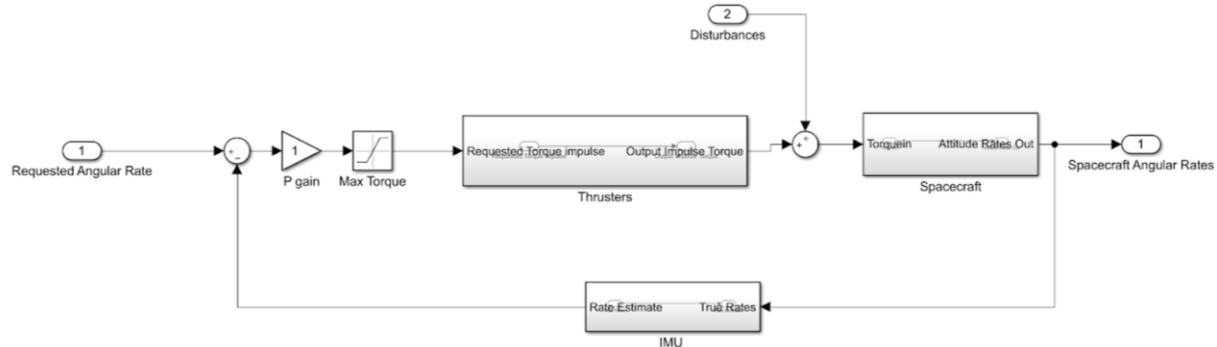


Figure 5.4.8. Block Diagram for Velocity Targeting Mode

Next, once the inequality in equation 5.4.4 is true, the spacecraft will target 0 angular velocity until the spacecraft has a small enough angular velocity and angle error to switch to hold mode. In the equation,  $\omega_{current}$  is the current angular velocity,  $\alpha$  is the maximum angular acceleration commandable in the axis of rotation, and  $\Delta\theta$  is the difference between the current and target attitudes. The equation represents the state at which a constant angular deceleration of  $\alpha$  will result in the spacecraft reaching the target attitude with no angular velocity.

$$\omega_{current}^2 \geq 2\alpha\Delta\theta \quad (5.4.4)$$

### Fuel Needed For Slew Mode

The time between OMV separation and the first burn is about 2 hours, the time between the first burn and

the second burn is 56 minutes, and the time between the second burn and the final burn is 18 minutes. Assume each slew is a 180 degree slew, which is the worst case. Clearly, as long as this slew can be accomplished in approximately 5 minutes, the lander will reach the desired orientation before the next burn. Thus the desired slew rate is 0.6 deg/sec. Assuming approximately 20 N, and thus 10 Nm of available thruster torque (2 10 N thrusters), and the  $64.5 \text{ kg m}^2$  inertia referenced earlier, this results in an angular acceleration of  $8.9 \text{ deg/s}^2$ , which results in two 0.068 s thruster burns required for each slew operation. With the nominal 3.5 g/s nominal thruster flow rate<sup>77</sup>, for two thrusters with two 0.068 s burns for three slew operations requires 42 grams of propellant.

### *Hold Mode*

The function of the hold mode is to maintain the current attitude between and before burns once reorientation is complete. This will use phase plane targeting, similar to what was done on the Apollo Lunar Lander<sup>78</sup>. This is a method for thruster-only attitude maintenance, which for reasonable fuel margins requires large angle deadbands. However, since for the vast majority of the time between burns the spacecraft does not have stringent attitude requirements (in fact, there are no attitude requirements since communications does not impose an attitude requirement), this scheme can be extremely fuel-efficient. During this mode, the spacecraft will be rolled at a rate of 0.6 deg/sec in the z-axis, so the phase plane diagram in figure 5.4.9 refers to pitch and yaw control only.

The phase plane diagram plots the angular rate vs the angle error. It consists of two curves that define when the vehicle uses its thrusters to correct its state. Figure 5.4.9 shows how these curves are determined. For further analysis, a nominal error of 1.3 degrees or a 2.5 degree total error cone was assumed. This could potentially increase, but was chosen so that the system could quickly reduce to 0.1 degrees of error just before the burn. Just before the burn, the phase plane diagram will narrow to a nominal error of 0.1 degrees.

---

<sup>77</sup> 10 N Bipropellant Thruster. ArianeGroup. Accessed 6 May 2020. <http://www.space-propulsion.com/spacecraft-propulsion/bipropellant-thrusters/10-bipropellant-thrusters.html>

<sup>78</sup> Stengel, Robert. Manual Attitude Control of the Lunar Module. AIAA Guidance, Control, and Flight Mechanics Conference. Retrieved 5 May 2020. <http://www.stengel.mycpanel.princeton.edu/AIAA69LM892.pdf>

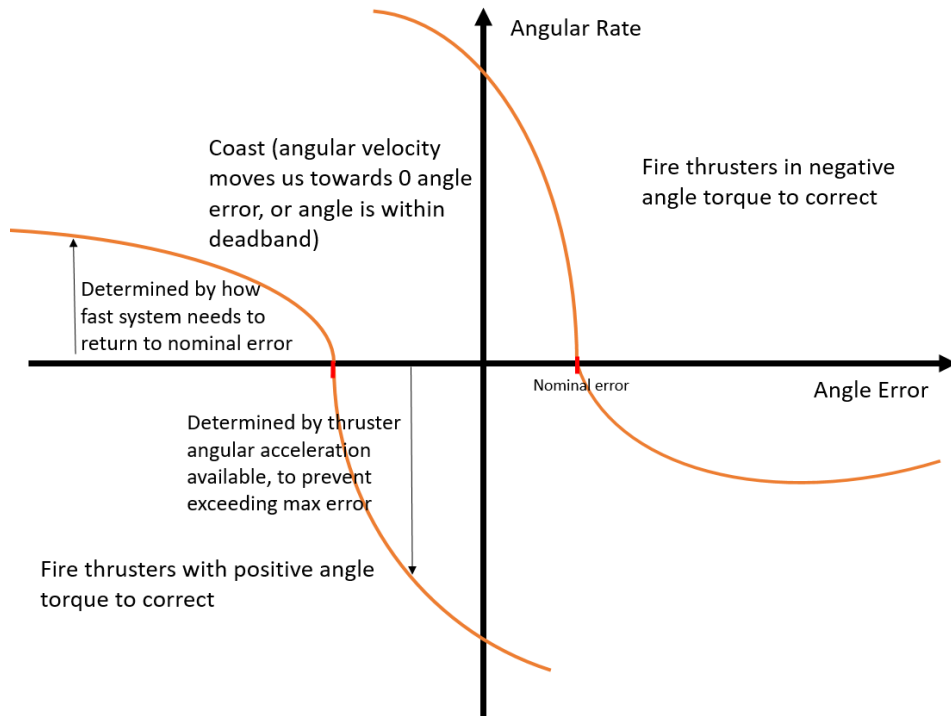


Figure 5.4.9. Phase Plane Targeting Diagram

#### *Fuel Needed During Hold Mode*

With a minimum bit of 0.1 Ns of thrust from each of the 2 torque thrusters<sup>79</sup> each acting with a lever arm of 0.5 m the minimum angular velocity change is 0.0015 rad/s or 0.088 deg/s. Assume that the spacecraft rotates at a rate of 0.044 deg/s between extremes of the deadband (see figure 5.4.10). Note that in the real world this varies but the average velocity will always be 0.044 deg/s since the angular velocity in each direction will sum to 0.088 deg/s. If the deadband is 2.5 degrees, this means the thrusters must be fired every 56 seconds at the minimum impulse bit. The minimum impulse bit takes 25 ms of thruster on time or 0.175 g of propellant. The total hold time from descent to landing, in the overestimate that the entire descent is hold time, is just over three hours. This results in 193 total thruster firings to maintain attitude, or 34 g of propellant.

---

<sup>79</sup> Fick, M. et al. EADS-ST's Latest Bipropellant 10 N Thruster and 400 N Engine: The Fully European Solution. Accessed 5 May 2020 <http://articles.adsabs.harvard.edu/full/2004ESASP.555E..92F/0000092.003.html>

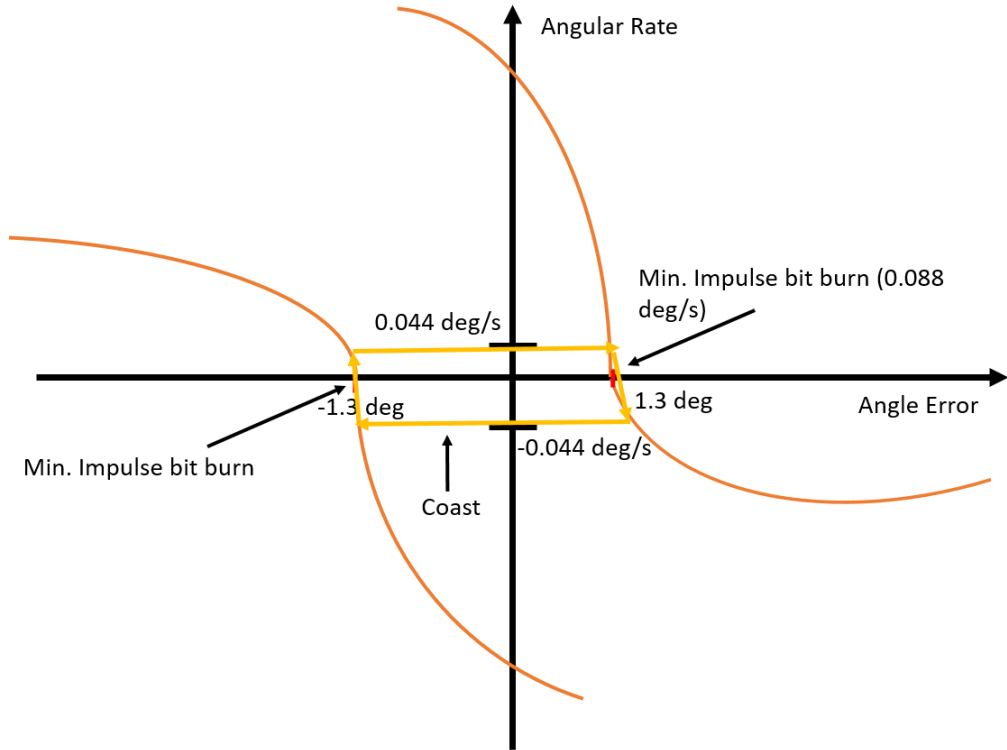


Figure 5.4.10. Stabilized Hold Mode On the Phase Plane

### *Descent and Burn Mode*

In the descent and burn mode, the spacecraft holds a commanded attitude based on the guidance algorithm's commands. This loop must be much faster than the guidance algorithm so that the guidance program's estimation algorithm is accurate, and thus will be run as fast as possible, most likely limited by the mechanical excitation limit of 35 hz and the minimum time between thruster pulses of 28 ms.

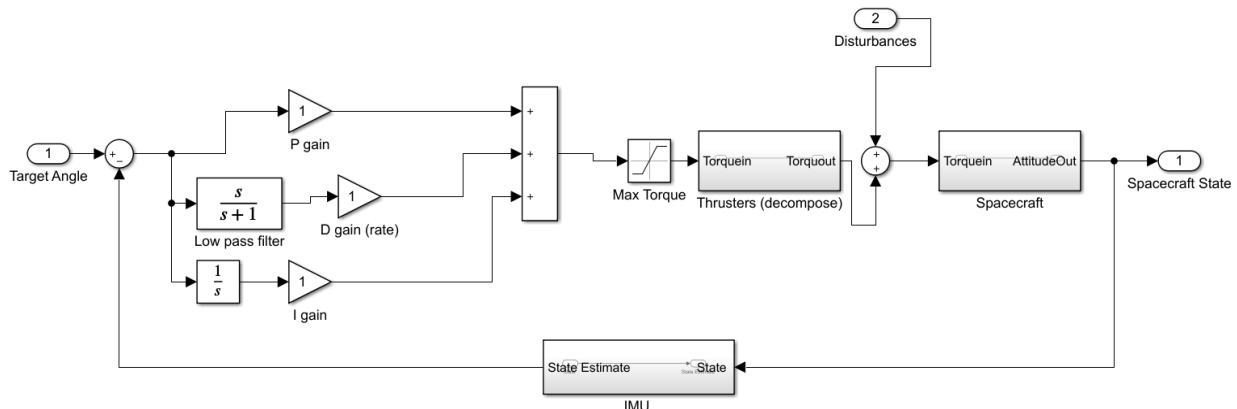


Figure 5.4.11. Descent and Burn Mode Block Diagram

Figure 5.4.11 represents the block diagram for this control phase. Note the addition of the integral term. This is because a constant torque from the main thrusters in the roll direction is expected to be accounted for by the attitude roll thrusters. Pitch and yaw control is via the off-pulsing and variable throttling of the main thrusters.

The initial orbit-lowering burn will be open-loop as it is essentially impulsive, approximately 8 seconds, holding a single attitude. Course correction maneuvers will be performed after this burn and before the final descent burn using the RCS system. The final descent burn will use closed-loop guidance, as detailed later in this chapter.

### *Fuel Needed During Descent Burn*

The total expected angular momentum change due to main thruster misalignment and translational thruster induced torque is 6000 Nms, as totaled from the disturbance environment section. With the standard 2 thrusters, 10 Nm of torque total, 3.5 g/s per thruster of propellant flow, this results in 600 seconds of thruster on-time or 4.2 kg of propellant.

### *Powered Explicit Guidance Algorithm*

As a potential candidate for the final finite burn and descent guidance algorithm, the team examined and tested an implementation of the Powered Explicit Guidance algorithm originally developed for Space Shuttle ascent guidance. The algorithm goes through stages as shown in figure 5.4.12.

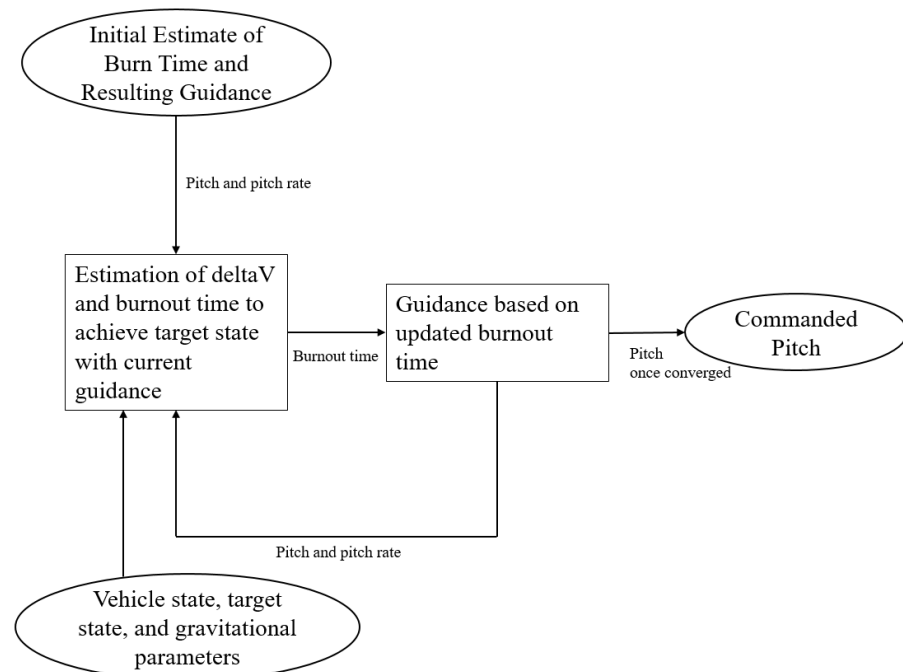


Figure 5.4.12. Powered Explicit Guidance Stages

The algorithm is initialized with an estimated burn time and the current position and velocity of the craft, and a target altitude, horizontal velocity, and vertical velocity. The guidance algorithm then calculates the ideal current pitch and rate of pitch change (which is constant) based on the burn time to

achieve the required vertical velocity and altitude. This initial guidance is then passed to the estimation algorithm, which estimates the delta-V and burnout time needed to achieve the target angular momentum change (horizontal velocity and altitude) based on the initial guidance. This burnout time is then passed back to the guidance algorithm, which recalculates pitch and pitch rate. This process continues until the updated burnout time in the estimation algorithm and previous burnout time have converged, and the commanded pitch is sent to the control algorithm<sup>80</sup>.

This algorithm was chosen for its simplicity - it is relatively high level and does not require extensive computation to implement. It does not ensure an optimal controller, as it is linear in the sin of the pitch angle over time, but it is commonly used because it is efficient enough for most purposes<sup>81</sup>.

To better characterize the algorithm, the team implemented the algorithm in MATLAB. While the algorithm was tested with parameters closer to a lunar ascent trajectory, the lessons learned informed the limitations of the algorithm. The full simulation program can be found in Appendix I.1.6.

In this test case, the spacecraft (with mass and thrust properties similar to the lander) was started in lunar orbit, with an initial radius of 1757 km, a horizontal speed of 1500 m/s, a target horizontal speed of 1656 m/s, a target vertical speed of 10 m/s, and a target radius of 1757 km. The guidance algorithm was run and simulated until time to burnout approached 0 seconds. Figure 5.4.13 shows the trajectory of the spacecraft during the duration of the burn and the commanded pitch vs time (zero pitch corresponds with the vehicle z axis parallel to the orbit tangent, and a negative pitch means the vehicle points “upwards”).

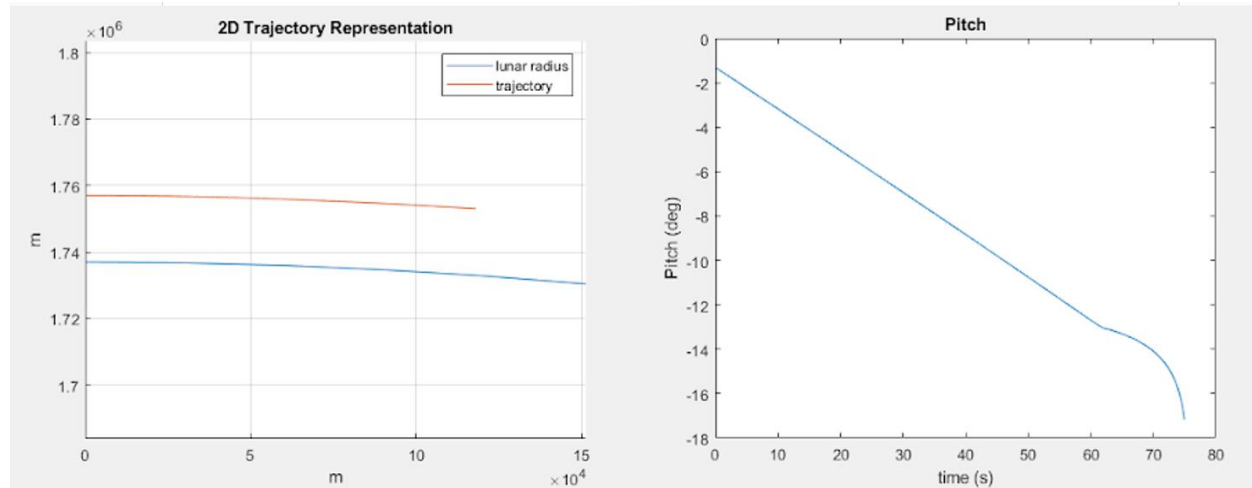


Figure 5.4.13. 2D Trajectory Under PEG and Pitch vs Time

Figure 5.4.14 showcases the algorithm’s performance. Approximately 1 second before burnout, the spacecraft is approximately 8 meters from the target altitude, 0.5 m/s from the target vertical velocity, and 4 m/s from the target horizontal velocity. The reason why the script is stopped shortly before burnout is because at times very close to burnout, the guidance constants become very large and could command

---

<sup>80</sup> Powered Explicit Guidance. Retrieved 6 May 2020.  
[https://www.orbiterwiki.org/wiki/Powered\\_Explicit\\_Guidance](https://www.orbiterwiki.org/wiki/Powered_Explicit_Guidance)

<sup>81</sup> Sostaric, Ronald R. Powered Descent Trajectory Guidance and Some Considerations For Human Lunar Landing.  
<https://ntrs.nasa.gov/archive/nasa/casi.ntrs.nasa.gov/20070004584.pdf>

very large pitch oscillations. Presumably, at the very end of the PEG algorithm, the spacecraft would switch to a PID controller or similar.

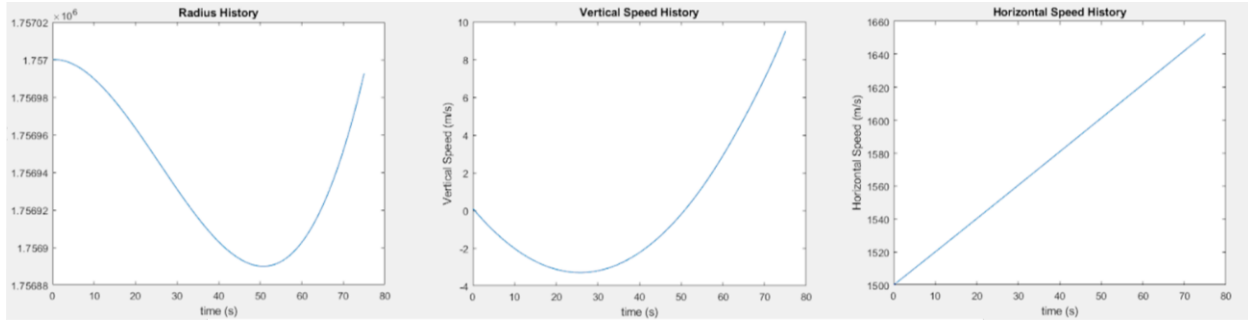


Figure 5.4.14. Spacecraft State History

One of the most important lessons from implementing this algorithm is that guidance convergence is dependent on an accurate initial burn time estimate. For cases like the test case, this can be approximated as the time needed if the required delta-V is simply equal to the total difference in velocity between the starting and ending conditions, but for the case of the lunar descent finding this approximation will be significantly more difficult. In addition, the algorithm does not target a certain downrange distance to reach the target state - this will have to be simulated ahead of time, and then the PEG portion of the descent initiated such that the expected downrange distance will land the vehicle in the center of the crater.

### *Future Work*

Now that the overall concept of operations and architecture of the guidance, navigation, and control system have been established, future work involves developing algorithms for the mission. This includes orbit determination and propagation based on Earth tracking, attitude, IMU, and laser altimeter data. This also includes interpreting and integrating star tracker, sun sensor, and IMU data for attitude determination. Each control algorithm described in this chapter must be implemented, and various gains must be calculated. A final touchdown controller must be selected (likely PID) and implemented. The closed-loop guidance algorithm, currently selected as the PEG algorithm, must be adapted for this spacecraft's specific scenario, and an estimated burn time made and ensured that the algorithm converges in simulation. More accurate inertia models must also be modeled for the spacecraft and torque/thruster matrices created.

### *Total Fuel Budget*

Fuel Needed For	Prop Mass (kg)	Notes
Detumble	0.003	Once in a mission
Slew Between Burns	0.042	3 slews required
Attitude Hold	0.034	3 hours of hold
Thruster Induced Torque	4.2	Main thruster + translational thruster torques
<b>Total</b>	<b>4.28</b>	

<b>Allocated</b>	5.00	
<b>Margin</b>	0.72 (17%)	While the fuel usage is relatively well characterized, exact details of the control and guidance algorithms may change it

Table 5.4.1. GNC Fuel Budget

#### 5.4.4 Components

- Radar Altimeter (TRL 7)

The FreeFlight RA-4000 radar altimeter<sup>82</sup> serves as a stand-in for a custom solution built by Honeywell, who produced radar systems for NASA's Mars landers<sup>83</sup>. It is assumed that the system will be very similar to the system they have produced for other planetary landers and will be very similar in mass to this commercial solution, however it will probably be slightly smaller and less massive than other systems it has produced at the expense of range. The accuracy of this component is assumed to be close to the commercial solution.

- Radar Velocimeter (TRL 7)

The FreeFlight RA-4000 radar altimeter again serves as a stand-in for a two-axis velocimeter custom solution built by Honeywell, who produced velocimeter systems for NASA's Mars landers. It is assumed that the system will be very similar to the system they have produced for other planetary landers and will be very similar in mass to this commercial solution, however it will probably be more massive than this commercial solution because of the increase in capabilities from single axis to two axis, and accounts for most of the included mass margin.

- HG1900 IMU<sup>84</sup> (TRL 9)

The HG1900 IMU is a commercially available component that has been widely deployed for military and commercial applications. 1 IMU is needed for the mission while a second one was included for redundancy. HG1900 utilizes a universal interface box and a flex tape connector, both of which are provided by the manufacturer, Honeywell.

- NST-3 Star Tracker<sup>85</sup> (TRL 9)

The NST-3 star trackers are currently put up as ready-to-order.

- NFSS 411 Sun Sensor<sup>86</sup> (TRL 9)

There are currently more than 100 NFSS-411 sun sensors in operation in space. The ADCS subsystem incorporates these specific sun sensors without any modifications. The sensor requires a 9-way female Micro-D connector and is interfaced with the M2 Socket Head Cap Screw. These are assumed to be delivered together with the sensors.

<sup>82</sup> *Radar Altimeters*. FreeFlight Systems. Accessed 5 May 2020.

<https://www.freelflightsystems.com/blog/product/radar-altimeters/>

<sup>83</sup> *Phases of Entry Descent and Landing*. NASA. Accessed 5 May 2020.

<https://mars.nasa.gov/MPF/mpf/realtime/edlstatus.html>

<sup>84</sup> *HG1900 Inertial Measurement Unit*. Accessed 4 May

2020. <https://aerospace.honeywell.com/en/learn/products/sensors/hg1900-inertial-measurement-unit>

<sup>85</sup> *NST-3 Nano Star Tracker*. Accessed 2 May 2020. <https://www.cubesatshop.com/product/nst-3-nano-star-tracker/>

<sup>86</sup> *NewSpace Sun Sensor 8\_a*. Accessed 2 May 2020. [http://www.newsacesystems.com/wp-content/uploads/2019/03/NewSpace-Sun-Sensor\\_8a.pdf](http://www.newsacesystems.com/wp-content/uploads/2019/03/NewSpace-Sun-Sensor_8a.pdf)

## 5.5 Propulsion

The lander propulsion system provides the thrust required to achieve a soft landing on the surface of the Moon from low lunar orbit. Its main goal is to reliably execute the  $\Delta V$  maneuvers required to decelerate, control, and correct the spacecraft during this mission. To successfully achieve this mission, it was determined that a conventional bi-propellant system with a multi-engine arrangement of 200N main thrusters and 10N control thrusters would be fitted on the lander. At various phases throughout the mission, these thrusters would be fired in both steady-state and pulsing mode to achieve variable thrust along descent.

### 5.5.1 Key Requirements and Assumptions

#### *Requirements*

- The propulsion system shall produce a  $\Delta V$  of  $>15.9\text{m/s}$  to insert the lander into a transfer orbit from the OMV detachment point to the landing altitude.
- The propulsion system shall produce a  $\Delta V$  of  $>1673\text{m/s}$  to decelerate the lander and achieve an approximate zero velocity above the landing site.
- The propulsion system shall produce sufficient  $\Delta V$  to achieve a soft landing on the Moon's surface.
- The propulsion system shall be compact and capable of securely fitting within the volume constraints of the ESPA ring (42" by 46" by 56").

#### *Assumptions*

- Given most of the  $\Delta V$  produced for the mission will be produced by thrusters operating in steady-state, propellant mass calculations were done assuming nominal specific impulse.
- Design of the components utilized in the control and distribution of the propulsion system fluid was outside of the scope of this project.

## 5.5.2 Mass and Power Budgets

### *Propulsion System Mass Budget*

Component	Mass (kg)	Notes
200 N biprop thrusters	7.6	
10 N biprop thrusters	3.15	
Propellant tanks	7.63	Does not include mounting
Helium tanks	5.09	Does not include mounting
Plumbing/valves	12.9	SMAD: lines/valves mass approximately 1-1.2x total mass of all thrusters (Table 10-37)
<b>Subsystem total</b>	<b>36.4</b>	
<b>Allocated Mass</b>	<b>41.8</b>	
<b>MGA</b>	<b>5.4 (15%)</b>	Medium margin for well characterized components

### *Propellant Mass Budget*

Given the assumption that there will be no significant losses due to drag or gravity, preliminary calculations for the propellant mass budget were done using the rocket equation:

$$m_{propellant} = m_{dry} (e^{\Delta v / u_{exhaust}} - 1) \quad (5.5.1)$$

The following calculations were made using nominal values for the 200N Bipropellant Thruster.<sup>87</sup> For a dry mass of 213.7 kg, a  $\Delta V$  of 1700m/s, and an exhaust velocity of 2650m/s, the propellant mass was calculated to be 192.3 kg. With an additional 5 kg of propellant on from the GNC team, 2% propellant mass added to account for residual propellant, and a margin of 10%, the total propellant mass for the mission was determined to be 220 kg. Using a nominal oxidizer/fuel flow rate (mixture ratio) of 1.65, the fuel and oxidizer masses were calculated to be about 86.3kg and 132.7kg respectively.

Purpose	Mass (kg)
Delta-V	192.3
ADCS	5.0
10% Margin	19.2
2%	3.5
<b>Total:</b>	<b>220.0</b>

Table 5.5.1: Propellant mass budget.

<sup>87</sup> 200 N Bipropellant Thruster. ArianeGroup. Accessed on May 5th, 2020

### *Power Budget*

The power budget for the lander propulsion system is assumed to be negligible. Hypercyclic propellants, unlike monopropellant systems, spontaneously ignite when they come into contact with each other. Thus, there is no need for a catalyst bed to release the propellant energy. Propellant thermal conditioning is also not needed as it is assumed the spacecraft will stay well above the -40°C freezing point of the propellants. Power is only drawn to the propulsion system through the opening and closing of valves within the plumbing of the system. This is usually done on the order of a couple hundred microseconds.

### *Margins and Contingency*

A substantial mass margin of 10%, alongside a 2% residual, allows the lander to produce a  $\Delta V$  of approximately 1960m/s.

## 5.5.3 Design

### *Selection of Rocket Propulsion System*

To determine the type of rocket propulsion system would be used on the lander, several chemical propellant engines were compared on several different criteria. These criteria include:

- 1) Efficiency: Minimizing mass was an important criterion in the design of the lander propulsion system. Thus, a propulsion system that uses propellant mass efficiently was important. Specific impulse was used for this comparison.
- 2) Volume: Minimizing volume was also an essential criterion in the design of the lander propulsion system. Due to ESPA ring size constraints, the effective sizing and complexity of each of the propulsion systems were important factors in choosing a propulsion system.
- 3) Throttability: Varying thrust must be applied during the final phase of landing. For this criterion, the variation of thrust can also be achieved with off-pulsing, or the firing of an engine in definite short pulses.

The propulsion systems compared include solid, hybrid, monopropellant, and bipropellant rocket engines. It should be noted that due to boil off susceptibility and refrigeration requirements, cryogenic propellants were not considered in this study. Below are the reasons behind the judgments from the trade study:

- Solid rocket propulsion has moderate efficiency, with a specific impulse of 280-300 second. It also has good size/little complexity. However, solid rockets are not actively throttleable and cannot be tested before the mission. This makes the solid rocket engine unsuitable for the lander propulsion system.
- Hybrid rocket propulsion has moderate efficiency, with a specific impulse of 300-320 seconds. It has moderate size/complexity as well as moderate throttability. However, hybrid rockets have limited multiple ignition capabilities compared to monopropellant and bipropellant engines. Thus, the hybrid rocket engine is unsuitable for the lander propulsion system.
- Monopropellant rocket propulsion has low efficiency, with a specific impulse of 155-205 seconds. It has good storability/less complexity. It also has good off-pulsing ability. However, its

low performance for large  $\Delta V$ 's makes the monopropellant rocket engine unsuitable for the lander propulsion system.

- Bipropellant rocket propulsion has good efficiency, with a specific impulse of 300-340 seconds. It has moderate size/high complexity. Like monopropellant engines, it also has good off-pulsing ability. Thus, despite its high complexity, a bipropellant rocket system, due to its good performance and extensive heritage, was chosen to provide the thrust for both the main and ACS engines.

### *200N Main Engines/10N ACS Engines*

The main thrusters for the lander were chosen to be four 200N Bipropellant Thrusters from ArianeGroup (shown in Figure 5.5.3.a). Our main engines have a capability of producing 864N nominally in steady-state. It has a max time on a single burn of 11,400 seconds. This will ensure the propulsion system can deliver enough steady-state thrust to effectively decelerate the lander during the large  $\Delta V$  braking burn.

These thrusters also have excellent pulsing capability, and they have been tested for more than 270,000 pulses.<sup>88</sup> This pulsing ability will allow the propulsion system to deliver precise thrust values given to by the guidance system.<sup>89</sup> This, in turn, will effectively make the propulsion system throttles to ensure it can effectively deliver the variable thrust needed to softly land on the moon.

One potential setback to utilizing this method to achieve variable thrust levels is spacecraft vibration. This will be greatest when the spacecraft is approximately 3.2 meters off the ground, where the lander will pulse its thruster about 117ms every 250ms while having a frequency of 4Hz (see Section 5.4.3). This is well below the minimum lander mechanical excitation frequency of 35Hz. Therefore, the impact of vibration on the lander will be negligible.



Figure

5.5.1:(a) 200N Main Engine  
RCS Engine

(b) 10N

<sup>88</sup> 200 N Bipropellant Thruster. ArianeGroup. Accessed on May 5th, 2020

<sup>89</sup> Sutton, George P. et al. Rocket Propulsion Elements, Seventh Edition. 2001



Figure 5.5.2: Engine Configurations

#### *Selection of Rocket Propellant*

Stringent mass, volume, and power constraints of the lander mean that it is undesirable to actively heat the propellant after launch. Propellant temperatures are known to drop significantly during the course of a deep space mission. In order to prevent the liquid propellants from freezing, the lander bipropellant oxidizer is nitrogen tetroxide (NTO) with twenty-five percent mixed oxides of nitrogen (25% nitric oxide, MON-25). For the bipropellant fuel, the lander utilizes monomethylhydrazine (MMH). This oxidizer was chosen instead of the standard NTO oxidizer which utilizes three percent mixed oxides of nitrogen (MON-3) because of its low freezing temperature below -50°C, which is similar to the freezing temperature of MMH. Research has also demonstrated that MMH/MON-25 have the capability of operating successfully at temperatures as low as -40°C with slightly reduced performance<sup>90</sup>.

This significantly reduces potential complications involving the lander's design constraints and reliability. First, it eliminates the need for active heating during the mission. It also reduces the overall mass of the propulsion system and its complexity. The reliability of the propulsion system is also greatly increased as there is little to no chance of the oxidizer freezing and thereby causing the system to fail.

---

<sup>90</sup> NASA, Mars Flyer Rocket Propulsion Risk Assessment. 2001. Retrieved from <https://ntrs.nasa.gov/archive/nasa/casi.ntrs.nasa.gov/20010047294.pdf>. Assessed on May 5th, 2020

### Tanks Material

Research showed that the most common tank materials used in space flight were aluminum, steel, titanium, and composites. Thus, to determine the best tank material, a small trade study was done comparing the strength, weight and manufacturability of these materials. A small table comparing these properties can be found below in Table 5.5.3. It should be noted that due to high cost for low production volume, composites were excluded from the tank material options table below.

Material Alloy <sup>91<sup>92</sup></sup>	Aluminum 7075-T73	Steel 17-4PH H1 150z	Titanium Ti-Al-4V
Ultimate Strength (MPa)	460	860	900
Density (kg/m <sup>3</sup> )	2,800	7,860	4,480
Strength to Density Ratio	0.164	0.109	0.201
Weld Efficiency (%)	85-95	50-65	>95
Ease of Fabrication	Easy to Machine	Most are Hard to Machine	Hard to Machine

Table 5.5.3: Material Alloys and their Properties

For a given working pressure, the lightest tank structure will be the one with the highest strength to density ratio. Given the tight mass constraints of the lunar lander, this was determined to be the most important factor in choosing a tank material. Thus, titanium was selected to be the tank material.

Although there is evidence that points toward the Ti-6Al-4V titanium alloy having a close to a 100%<sup>93</sup> weld efficiency under the right conditions, for the purpose of the design, stress calculations will be based on the minimum expected strength. Thus, a 95%<sup>94</sup> weld efficiency was used.

### Propellant Tank Design

Due to the sizable volume penalty of fitting multiple spherical fuel and oxidizer tanks inside the lander structure, it was determined that four cylindrically shaped tanks with spherical ends would be fitted in a multi-tank configuration around the center of mass of the lander. Since this is a positive expulsion system, it was also determined that a rolling diaphragm would be used in the tanks to ensure a low pressure

<sup>91</sup> Wertz, James R., et al. Space Mission Analysis and Design, Third Edition. Microcosm Press, El Segundo, CA, 1999. p. 466

<sup>92</sup> Huzel, D.K., Huang D.H. Design of Liquid Propellant Rocket Engines, NASA SP-125. 1971. Retrieved from <https://ntrs.nasa.gov/archive/nasa/casi.ntrs.nasa.gov/19710019929.pdf>. Accessed on May 5th, 2020

<sup>93</sup> Miranda, R.M, et al. Analysis of Beam Material Interaction in Welding of Titanium with Fiber Lasers. 2007. Retrieved from

[https://www.researchgate.net/publication/233267456\\_Analysis\\_of\\_Beam\\_Material\\_Interaction\\_in\\_Welding\\_of\\_Titanium\\_with\\_Fiber\\_Lasers](https://www.researchgate.net/publication/233267456_Analysis_of_Beam_Material_Interaction_in_Welding_of_Titanium_with_Fiber_Lasers). Accessed on May 5th, 2020

<sup>94</sup> Holko, Kenneth H. Hot Press and Roll Welding of Titanium. 1972. Retrieved from <https://ntrs.nasa.gov/archive/nasa/casi.ntrs.nasa.gov/19720023902.pdf>. Accessed on May 5th, 2020

difference during expulsion of the propellants.<sup>95</sup> This will reduce the differences in thrust and pulse levels during the mission. It is also low in weight.

### *Pressurant Tank Design*

To pressurize the system, the lander shall be equipped with four spherical helium pressurant tanks for the four separate propellant tanks. The spherical shape was decided upon because it has the smallest surface to volume ratio, making it the lightest possible configuration. Utilizing a pressure regulated system will allow the propulsion system to maximize the propellant expulsion efficiency and alternate pressurization approaches for the individual propellants.

### *Tank Sizing*

As a rule, the wall thickness of the propellant tanks is first calculated from the stresses caused by internal pressure loads.<sup>96</sup> Therefore, initial designs for the propellant and pressurant tanks were carried out by sizing the tanks to contain the propellant volumes calculated and designing the tanks to withstand the maximum internal pressure during the mission. A safety factor of 1.5 times the Maximum Expected Operating Pressure (MEOP) of the tanks was used to account for transient spikes in pressure. An additional 5% of volume was added to both the propellant and pressurant tanks to account for ullage and excess gas respectively.

It should be noted that these are preliminary results, and that a more in depth study using finite element analysis and qualification tests need to be done. Research shows that most failures in spacecraft occur at a local level.<sup>97</sup> Local stress analysis for the propellant and pressurant tanks, however, was beyond the scope of this project.

### *Propellant Tank Sizing*

The total mass of the fuel and oxidizer are 86.3kg and 132.7kg respectively. This means that the two fuel tanks would contain 43.1kg per tank and the oxidizer tanks would contain 66.4kg per tank. The volume of the 4 tanks were then calculated using their respective fuel and oxidizer densities at 21°C ( $\text{MMH} \approx 880\text{kg/m}^3$ ;  $\text{MON-25} \approx 1410\text{kg/m}^3$ ). Ultimately the required usable fuel and oxidizer volumes were determined to be  $0.049\text{m}^3$  and  $0.051\text{m}^3$ .

The mass of the fuel and oxidizer tanks was estimated using the equation for the wall thickness represented in 5.5.3<sup>98</sup>, where  $t_{cylinder}$  is the cylindrical tank shell thickness,  $r_{tank}$  is the cylindrical tank

---

<sup>95</sup> Wertz, James R., et al. *Space Mission Analysis and Design*, Third Edition. Microcosm Press, El Segundo, CA, 1999. p. 709

<sup>96</sup> Huzel, D.K., Huang D.H. *Design of Liquid Propellant Rocket Engines*, NASA SP-125. 1971. Retrieved from <https://ntrs.nasa.gov/archive/nasa/casi.ntrs.nasa.gov/19710019929.pdf>. Accessed on May 5th, 2020

<sup>97</sup> Sarafin, T., *Spacecraft Structures and Mechanisms: From Concept to Launch*. Microcosm, Inc., Torrance, CA, 1995.

<sup>98</sup> Wertz, James R., et al. *Space Mission Analysis and Design*, Third Edition. Microcosm Press, El Segundo, CA, 1999. p. 714

radius,  $\sigma$  is the ultimate strength of the material, and  $e_w$  is the weld efficiency. required to withstand the internal tank pressure:

$$t_{cylinder} = \frac{p_{tank}r_{tank}}{\sigma e_w} \quad (5.5.3)$$

The estimated values were calculated using a cylindrical tank radius of 0.175m, the weld efficiency of 0.95, an ultimate strength of 900MPa, and internal tank pressures of 27 bar and 22.5 bar for the oxidizer and fuel tanks respectively. The internal pressure values come from qualified inlet pressure values. Ultimately, both the fuel and oxidizer tank shells were determined to have a thickness of 0.61mm and mass of 1.94kg. Overall, for the tank shells plus mounting<sup>99</sup>, the mass of the propellant tanks are estimated to be about 9.3kg.

### *Pressurant Tank Sizing*

The total mass of the helium required to pressurize all four propellant tanks was calculated using a conservation of energy approximation<sup>100</sup>, where  $m_{He}$  is the helium mass,  $P_p$  is the propellant tank pressure,  $V_p$  is the propellant volume,  $R$  is the helium gas constant,  $T_0$  is the initial storage temperature,  $p_g/p_0$  is the ratio of the initial pressures in the propellant tanks to the helium tanks, and  $k$  is the specific heat ratio of helium:

$$m_{He} = \frac{P_p V_p}{RT_0} \left[ \frac{k}{1 - (p_g/p_0)} \right] \quad (5.5.3)$$

The estimated values were calculated using a propellant tank pressure of 18 bar (oxidizer) and 15 bar (fuel), a propellant volume of 0.051m<sup>3</sup>, a gas constant of 2077 J/kg K, a initial temperature of 294°C, a pressure ratio of 0.1, and a specific heat ratio of 1.66. Using these values, the masses of the pressurant tanks for the oxidizer and fuel came out to 0.27kg and 0.23kg respectively. Assuming an ideal gas, the volume of the helium inside of the pressurant tanks was estimated using the ideal gas law, where  $V_{He}$  is the helium volume and  $P_g$  is the the pressurant tank pressure:

$$V_{He} = \frac{m_{He}RT_0}{P_g} \quad (5.5.4)$$

The estimated values were calculated using a pressurant tank pressure of 180 bar (oxidizer) and 150 bar (fuel) as well as the values given previously. Using these values, the volumes of both the oxidizer and fuel pressurant tanks were determined to be about equal, with the helium utilizing approximately 0.0094m<sup>3</sup>.

Finally, the mass of the pressurant tanks was estimated using the equation for the wall thickness of a sphere represented in 5.5.3, where  $t_{sphere}$ is the spherical tank shell thickness,  $r_{tank}$ is the spherical tank radius,  $\sigma$  is the ultimate strength of the material, and  $e_w$  is the weld efficiency. required to withstand the internal tank pressure:

$$t_{sphere} = \frac{p_{tank}r_{tank}}{2\sigma e_w} \quad (5.5.3)$$

---

<sup>99</sup> Wertz, James R., et al. Space Mission Analysis and Design, Third Edition. Microcosm Press, El Segundo, CA, 1999. p. 714

<sup>100</sup> Wertz, James R., et al. Space Mission Analysis and Design, Third Edition. Microcosm Press, El Segundo, CA, 1999. P. 714

The estimated values were calculated using a spherical tank radius 0.13m, a weld efficiency of 0.95, an ultimate strength of 900MPa, and internal tank pressures,  $p_{tank}$ , of 270 bar and 225 bar for the oxidizer and fuel tanks respectively. The internal pressure values come from being ten times greater than the propellant tank pressure values. Ultimately, the helium tank pressurizing the oxidizer was determined to have the larger thickness given its higher internal pressure, with a value of approximately 2.1mm. To provide consistency and a higher safety margin for the fuel pressurant tanks, all four tanks were designed with this larger thickness. Thus, the mass for a single tank was calculated to be approximately 2.0kg. Overall, for the tank shells plus mounting, the mass of the pressurant tanks is estimated to be about 9.6kg.

#### 5.5.4 Propulsion System Layout

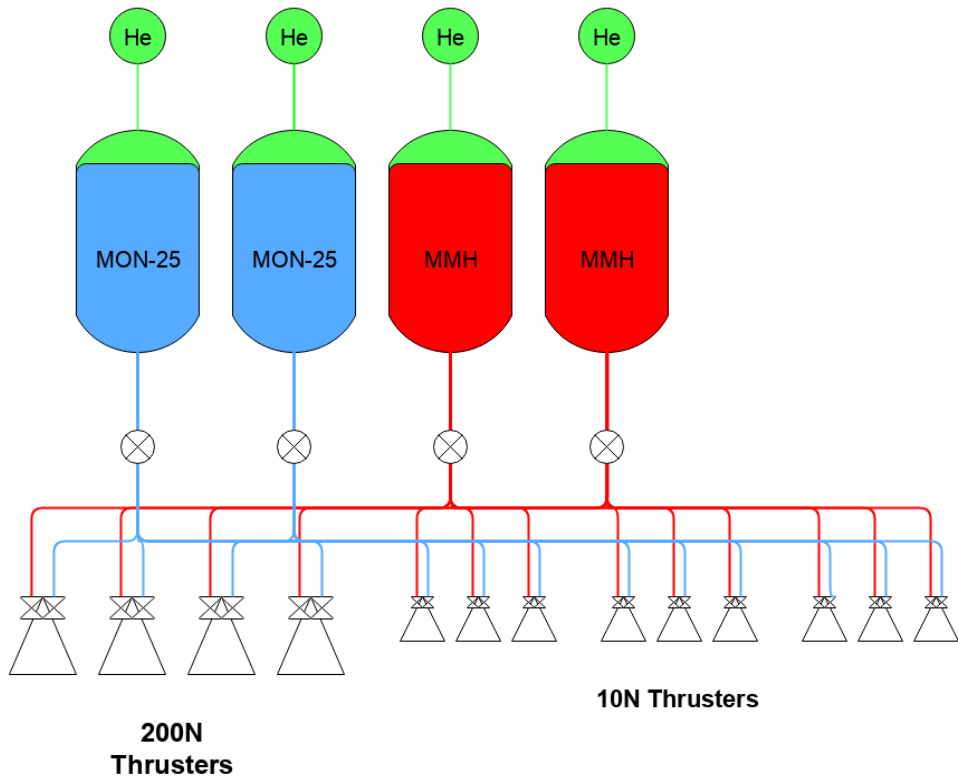


Figure 5.5.4: Simplified Flow Schematic of the Propulsion System.

#### 5.5.5 Components

All of the components used have extensive space flight heritage. Thus, every component has a TRL of 9.

- Titanium bipropellant tanks
- Titanium helium tanks
- 200N/10N Thrusters
- High pressure latch valve
- Low pressure latch valve
- Propellant biprop latch valve
- Filters
- Service valves
- Pressure regulator

- Titanium lines
- Pressure transducers

## 5.6 Power

The Electrical Power System (EPS) is vital for ensuring the successful operation of all lander components for the duration of the mission, providing lander components with electrical power from batteries. As described in Section 2.2, the lander will land within Shackleton Crater and thus operate in shade for the duration of the mission. Solar panels are therefore infeasible for power production; batteries must supply all energy. Critically, the batteries must provide high peak power for the drill at high specific energy to maintain a light weight.

### 5.6.1 Key Requirements and Assumptions

#### *Requirements*

- The EPS shall provide a minimum power of 546.25 W for lander component functions
- The EPS shall provide a minimum energy of 9280.1 Wh for lander component functions

Refer to Section 2.2.4 for Power budget table detailing power requirements for each subsystem.

#### *Assumptions*

- The battery pack size scales linearly with the number of parallel strings
- The voltage of the bus remains at a constant 28Vdc for all calculations on battery sizing

### 5.6.2 Mass Budget

Component	Mass (kg)	Notes
Batteries	23.6	
Computer	5	
Harnessing	--	1% - 4% lander dry weight
<b>Subsystem total</b>	<b>28.6</b>	
<b>Allocated Mass</b>	<b>35.8</b>	
<b>MGA</b>	<b>7.2 (25%)</b>	Margin accounts for harnessing and packaging

#### *Margins and Contingency*

The substantial margin of 25% accounts for additional harnessing mass as well as packaging and mounting of the battery. Harnessing includes cabling from the battery, through converters and to each component. The conducted battery calculations and the stated battery mass include only cell mass, thus packaging and mounting masses have been included in the mass growth allowance.

### 5.6.3 Design

The main challenge in designing the EPS was the absence of sunlight as a source of power. No prior lander has relied solely on batteries for power, making this mission a first. An initial trade study was conducted to compare batteries to fuel cells to determine which would be most suitable for the mission. Though fuel cells have the potential for a higher peak power, and are able to use the lander's onboard fuel to produce electricity, few implementations, and thus little documentation, exists for functioning fuel cells on landers. Fuel cells are also more complex, increasing the risk of malfunction. The lander would be forced to carry an extra fuel tank, which would take up much needed space for other components. Lastly, fuel cells are most applicable for long-duration missions. The lander's scheduled mission duration lasts only 25 hours, making this complicated system infeasible for this application.

Batteries were therefore chosen for their greater simplicity, higher variety in chemistries, and because of the lander's short mission duration. Apollo's Lunar Module made the same decision to switch from fuel cells to batteries amid concerns of complexity, time sensitivity and development costs.<sup>101</sup> Due to the drill's high peak power demand, the EPS must be able to provide a high peak power. The lander's size restrictions also mean the EPS must be as small and light as possible: a high specific power is necessary. An initial battery choice of Li-SOCl<sub>2</sub> was made due to its high specific energy, but among concerns of this specific chemistry being unable to produce a high enough discharge current, a switch to the Li-S cell was made. The cell of choice is the High Energy Li-S pouch cell manufactured by OXIS Energy, designed for satellite application<sup>102</sup>. An unregulated 28Vdc bus was chosen. The total power requirement remains low and so a low-voltage bus would be sufficient. An unregulated bus was chosen because of its high battery to load efficiency, as well as the small load variations experienced during operations.

Type	High Energy
Part Number	POA000343
Nominal Voltage (V)	2.1
Typical Capacity (Ah)	15
Gravimetric Energy (Wh/kg)	410
Cycle Life (Cycles)	60-100
Operating Temperature (°C)	0 to 30
Pouch format (mm) Length x width x height	145 x 78 x 10
Cell Weight (g)	85

Table 5.6.1: OXIS Energy Li-S cell specifications<sup>103</sup>

The total energy required by all subsystems (including margin) is 9280.1 Wh and the total power is 546 W. Using a 28 V bus gives a total energy capacity of 331.4 Ah for the 25 hr operation time. Fourteen

<sup>101</sup> Lunar Module Electrical Power Subsystem, NASA Technical Note TN D -6977 09/72 6977, 09/72

<sup>102</sup> <https://oxisenergy.com/products/>, Accessed on May 11, 2020

<sup>103</sup> <https://45uevg34gwlltnsf2plyua1-wpengine.netdna-ssl.com/wp-content/uploads/2019/07/OXIS-Li-S-Ultra-Light-Cell-spec-sheet-v4.2.pdf>, Accessed on May 5, 2020

series cells are required to match the 28 V bus, and an energy capacity of 15 Ah gives 23 parallel strings required to fulfil the 331.4 Ah capacity minimum. This size yields a mass of 23.6 kg and a raw battery volume of 36.4 L. More detailed calculations can be found in Appendix K. The battery will only be discharged once and so no consideration must be made of cycle life and fade.

#### 5.6.4 Components

- 322 Lithium-Sulfur cells (TRL 7)  
Cells need to be wired and housed from their off-the-shelf pouch format.
- Regulation circuit (TRL 6)  
Necessary to supply the variety of input voltages for different components.

## 5.7 Thermal

The thermal system on the lander is necessary to maintain all of the lander components within their operable temperatures for the duration of surface operations. As the craft will be in full darkness during these operations, there are limited sources of external heat. Thus, the thermal system must minimize heat loss by sufficiently insulating the craft from radiating to deep space and the lunar surface as well as from conducting to the lunar surface.

### 5.7.1 Key Requirements and Assumptions

#### *Requirements*

- The thermal system shall ensure that all lander subsystems remain above 0°C for a duration of 25 hours following touchdown on the lunar surface, per the battery's temperature requirement. This ensures systems are within their operable temperature ranges for that duration.
- The thermal system shall stay below a maximum temperature of 30°C for all system operations, due to the operable temperature range of the battery.

The thermal requirements come from the operable temperature ranges of equipment from other subteams. The most restrictive acceptable temperature range of 0 to 30°C came from the battery, in the power subsystem. The other thermally sensitive subsystems include the science payload and GNC. The only subsystems that needed to maintain their operable temperature ranges during lunar surface operations, however, were battery, science payload, mechanisms, and communications. GNC and chemical propellants are no longer needed at the lunar surface due to the short-life of the landers, and so their thermal requirements are not actually necessary to uphold at the lunar surface. Due to the restrictive nature of the battery, however, the lander is kept warm enough that the GNC and chemical propellants would remain operable on the moon, even though they would not be needed.

#### *Assumptions*

- Multinodal and transient analyses are outside the scope of this report and are classified as future work.
- Only radiation to the lunar surface and deep space as well as conduction to the lunar surface were analyzed. Sources of internal heat besides the added heaters and IR from the lunar surface were neglected to provide a worst-case estimate.
- The sides of the lander have a view factor of 1 to deep space, to provide a worst-case estimate. Likely some portion of the sides of the lander will have a view factor to the walls of Shackleton Crater.
- Due to single-node assumptions, conduction does not rely on the geometry, volume, or insulative capacity of lander legs, instead all heat transfer occurs directly from lander feet to the lander internals.

- The lunar surface in the Shackleton Crater has the same thermal and material properties as the lunar regolith tested in the Apollo 11 mission.<sup>104</sup>
- Due to single-nodal assumption, heaters are assumed to evenly heat the entire lander (no concentrations in heat or cold).

### 5.7.2 Mass and Power Budgets

#### *Mass Budget*

Component	Mass (kg)	Notes
Heater <sup>105</sup> /controller <sup>106</sup> /sensor <sup>107</sup>	0.35	Minco Products
Coating	0.71	3-mil Polyimide (Kapton) Film <sup>108</sup> : ITO <sup>109</sup> , VDA <sup>110</sup> , Kapton <sup>111</sup>
<b>Subsystem total</b>	<b>1.06</b>	
<b>Allocated Mass</b>	<b>4.24</b>	
<b>MGA</b>	<b>3.18</b> (300%)	Margin accounts for harnessing and other unknown components

#### *Power Budget*

Component	Power (W)	Energy (Wh)	Notes
Heaters	50	1250	25 hours of operations
<b>Subsystem total</b>	<b>50</b>	<b>1250</b>	
<b>Allocated</b>	<b>62.5</b>	<b>1562.5</b>	
<b>Margin</b>	<b>12.5 (25%)</b>	<b>312.5 (25%)</b>	

<sup>104</sup> Grott, M., Knollenberg, J. and Krause, C. *Apollo lunar heat flow experiment revisited: A critical reassessment of the in situ thermal conductivity determination*. Journal of Geophysical Research, Vol 115, November 2010, p. 4.

<sup>105</sup> Minco. *Thermal Solutions Design Guide*. Accessed April 20, 2020.

<<https://www.minco.com/~media/files/minco/productguides/heat/minco%20thermal%20solutions%20design%20guide.ashx>>

<sup>106</sup> Minco. *Multi-Function Prototype Controller: CT425B*. Accessed April 24, 2020.

<[http://catalog.minco.com/catalog3/d/minco/?c=products&cid=2\\_1\\_4-mutli-function-prototype-controller&id=CT425B](http://catalog.minco.com/catalog3/d/minco/?c=products&cid=2_1_4-mutli-function-prototype-controller&id=CT425B)>

<sup>107</sup> Minco. *Strip Sensing: S651PDY120A*. <[http://catalog.minco.com/catalog3/d/minco/?c=products&cid=1\\_8\\_1\\_2-strip-sensing&id=S651PDY120A](http://catalog.minco.com/catalog3/d/minco/?c=products&cid=1_8_1_2-strip-sensing&id=S651PDY120A)>

<sup>108</sup> Caplinq. “3-mil Polyimide (Kapton) Film.” Accessed April 6, 2020. <<https://www.caplinq.com/3-mil-polyimide-kapton-film-no-adhesive-pit3n-series.html?filter=26005.9871>>

<sup>109</sup> MIT. *Material: Indium Tin Oxide*. Accessed April 6, 2020. <<http://www.mit.edu/~6.777/matprops/ito.htm>>

<sup>110</sup> Dunmore. *The Vacuum Metalization Process*. Accessed April 6, 2020.

<<https://www.dunmore.com/technical/vacuum-metallizing.html>>

<sup>111</sup> Matweb. *DuPont™ Kapton® 500VN Polyimide Film, 125 Micron Thickness*. Accessed April 6, 2020.

<[http://www.matweb.com/search/datasheet\\_print.aspx?matguid=338573ad1bdf4586aa17fab95f3a57d7](http://www.matweb.com/search/datasheet_print.aspx?matguid=338573ad1bdf4586aa17fab95f3a57d7)>

### *Margins and Contingency*

The margin for the mass budget is 300% to account for harnessing and other unknown components. Harnessing consists of the material needed to attach all thermal components, such as the heaters, controllers, and sensors, to the lander. Other unknown components could be items like heat pipes or multi-layer insulation. This margin is significantly large because the scope of the analyses done to date are single-node and steady-state. Once the complexity of a multinodal transient analysis is applied to the system, additional components will need to be added to avoid unwanted uneven temperature distributions and/or to thermally isolate certain sections of the lander from other sections.

The general margin for the power budget is 25% to account for the fact the calculations done are single-nodal and non-transient, and there may be active components that are not accounted for in this report.

### 5.7.3 Design

#### *Calculation of Heating*

The selection of a coating was crucial to be able to calculate the amount of heat necessary to keep the lander above 0°C. In order to determine an ideal coating, and thereby the amount of heating, the scope of this report included a single-node thermal balance of the lander, which is also a steady-state analysis. The ultimate goal was to select a coating to minimize the amount of heat needed to keep the lander above 0°C.

Radiative heat transfer and conductive heat transfer were considered as the two possible heat losses from the lander. Radiative heat transfer is a function of temperature to the fourth power (Equation 5.7.1). The temperature of the surroundings was different based on whether the panel was radiating to deep space or to the lunar surface. In order to produce a worst-case heat requirement, the lander was assumed to have the maximum possible view factor of deep space (i.e., the top of the lander and all sides of the lander emit to deep space at 0 K). Only the bottom panel of the lander was assumed to radiate to the lunar surface (40 K). The conductive heat transfer is also a function of temperature, and heat is only conducted through the lander's feet which touch the lunar surface (Equation 5.7.2). Since this analysis was single-node, it neglected any insulating effect of the crush-core legs, to again give a worst-case estimate. The total amount of heat lost from the lander is equal to the amount of heat radiated plus the amount of heat conducted into the lunar surface (Equation 5.7.3).

$$q_{radiative} = \sigma \varepsilon A_{radiating\ surface} (T_{lander}^4 - T_{surroundings}^4)$$

(Equation 5.7.1)

$$q_{conducted} = (T_{lander} - T_{surface}) A_{contact}/R$$

(Equation 5.7.2)

$$q_{radiative} + q_{conducted} = q_{lost} = q_{heaters}$$

(Equation 5.7.3)

where  $\sigma$  = Stefan-Boltzmann constant,  $\varepsilon$  = emissivity, and  $R$  = thermal contact resistance of the lunar surface.

Since no other internal heat besides the possible addition of heaters was considered to be generated, the effect of lunar IR radiation was neglected for a worst-case assumption, and there is no

sunlight in Shackleton Crater, the sum of the heat lost from the lander via radiation and conduction is equal to the amount of heat needed to be generated by the heaters (Equation 3). To minimize this amount of heat, a coating needed to be chosen with the lowest possible emissivity, as this would reduce the contribution of radiative heat loss to the overall total. Once a coating was selected, these calculations could be done to determine the total amount of heat necessary. Commented MATLAB code containing these calculations can be found in Appendix L.2.

### *Trade Study of Coatings*

A preliminary assortment of 8 coatings with the lowest emissivities were chosen from two sources.<sup>112,113</sup> The factors considered when making a selection were cost per square meter, emissivity (and therefore the heat required), absorptivity, and other relevant factors such as fragility or risk of surface charging. The most important factor was to select the lowest possible emissivity, since reducing the emissivity and thereby the necessary heat input was the purpose of conducting this trade study. Secondary considerations were a robust, unchangeable coating (i.e. not fragile, no risk of surface charging, etc.) and a reasonably low cost per square meter of coating. A tertiary concern was the absorptivity of the coating, which although it would not affect the amount of heat needed for the lander while on the lunar surface, it would affect heating while in transit to the surface. During the descent into Shackleton Crater, the lander will be sunlit, absorbing solar radiation.

Future work would better qualify the thermal characteristics of the detachment and descent stage, but at this scope a selection of low-absorptivity coating was determined to be sufficient. Full details of this trade study can be found in Appendix L.2.

Kapton 3mil (ITO/VDA/Kapton) was chosen first and foremost for its extremely low emissivity of 0.02. This was the lowest possible emissivity out of all 8 coatings. In addition, Kapton 3mil (ITO/VDA/Kapton) displays relatively robust characteristics. The ITO outer layer gives a good balance between indestructibility on the lunar surface and durability in the space environment. During landing on the lunar surface, there is a concern that airborne lunar regolith could scratch the coating, thereby increasing its emissivity. ITO is ranked 5 on the Mohs hardness scale<sup>114</sup> and the two most abundant minerals in the regolith, anorthite and enstatite, have Mohs hardnesses of 6 and 5-6, respectively.<sup>115</sup> This does mean that the lunar regolith will be able to scratch the ITO, but the disparity in Mohs hardness between ITO and lunar regolith is lower than other possible coatings.

Although scratching the ITO outer layer is a concern during landing, the ITO does a very good job protecting from any surface charging and it has very low changeability in the space environment. Thus, the balance between surface indestructibility and space durability was deemed appropriate. Of the coatings for which a price was able to be estimated, Kapton 3mil (ITO/VDA/Kapton) was placed at a reasonable price point of \$44.59 per square meter. Finally, the tertiary concern of absorptivity was also satisfied, as it had the lowest absorptivity of all the coatings investigated.

---

<sup>112</sup> Kauder, Lonny. "Spacecraft Thermal Control Coatings References." NASA, December 2005.

<sup>113</sup> Choueiri, Edgar. "Spacecraft Thermal Control." *MAE 432 Lecture Notes*, 2020.

<sup>114</sup> Feldman, Bernard, Harm Tolner, and Douglas Mclean. "15.4: Tin Oxide Transparent Conductor for PDP." *SID Symposium Digest of Technical Papers* 39, no. 1 (2008): 194. <https://doi.org/10.1889/1.3069573>.

<sup>115</sup> Rickman, Doug, Kenneth W. Street, and Mohamed S. El-Genk. "Some Expected Mechanical Characteristics of Lunar Dust: A Geological View." *AIP Conference Proceedings*, 2008. <https://doi.org/10.1063/1.2845062>.

## *Heat/Power Requirement*

By using Kapton 3mil (ITO/VDA/Kapton) as the chosen coating, the necessary heat was calculated as per the prior section to be approximately 40 W for an exact calculation. The power requirement was therefore determined to be 50 W with a conservative 15°C margin.<sup>116</sup>

## *Heaters*

In choosing the Minco Polyimide Thermofoil patch heaters for the lander, two separate comparison studies were performed. First, different types of heaters were compared for their appropriateness for lander operations. The heater categories studied were: patch heaters, cartridge heaters, heat pipes, and RHU's. Due to single-nodal assumptions, all heat provided from heaters was assumed to be evenly distributed throughout the lander. Thus, cartridge heaters, which provide concentrated heat sources for thermally sensitive subsystems such as the battery, were deemed unnecessary. In reality, had a multi-nodal analysis been able to be completed with a thermal analysis software, cartridge heaters may have been needed for power subsystem operations. Similarly to cartridge heaters, heat pipes, which take waste heat from heat-exuding components such as the battery, and distribute it to other subsystems via fluid-filled pipes that are able transfer heat, were also considered outside the scope of this analysis. Therefore, the main two heater variations compared for the lander were RHU's and patch heaters.

RHU's, rather than rely on a battery for energy like patch heaters, contain a radioactive isotope which decays to provide heat.<sup>117</sup> Due to their radioactive nature, however, RHU's need extra governmental approval to go on a space mission, which can take time to apply for and receive.<sup>118</sup> They also provide very little heat (only 1 Watt per RHU). Patch heaters, which use electrical-resistance from power provided by the system's battery, are less expensive, and need no additional approval process. Because 50 W is easily available by the power subsystem's battery, patch heaters were determined as the best option for heating.

The next study in heaters became which brand and type of patch heater would be best. The manufacturer Minco quickly stood out, due to its long history providing NASA and ESA approved products for missions in space. Polyimide thermofoil heaters, in particular, have been approved since 1996.<sup>119</sup> These are chosen for the lander's use due to their thin, lightweight nature and their availability in many sizes. In order to spread out the heat provided, a total of five heaters (as specified in section 5.7.4) are chosen to provide 52 W, just over the necessary total of 50 W. Figure 5.7.1 below shows the watt density as it varies with mounting method and thermal environment.

---

<sup>116</sup> 10°C margin suggested by Mr. Thomas Grzymala of Lockheed Martin. Extra 5°C added because of uncertainty surrounding scratching of coating upon descent.

<sup>117</sup> Gilmore, David G. *Spacecraft Thermal Control Handbook, Volume 1 - Fundamental Technologies* (2nd Edition). American Institute of Aeronautics and Astronautics/Aerospace Press: 2002.

<sup>118</sup> McCallum, Peter. *Improving the Nuclear Approval Process; Progress and Plans*. ANS NETS 2018 – Nuclear and Emerging Technologies for Space.

<sup>119</sup> King, T. *S-311-P-079E - Procurement Specification for Thermofoil Heater*. NASA. 1996. Accessed April 20, 2020. <<https://nepg.nasa.gov/files/22932/S-311-P-079E.pdf>>

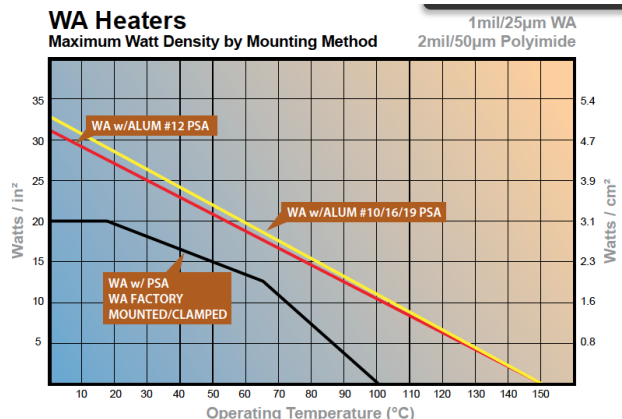


Figure 5.7.1: Watt density as provided by Minco.<sup>120</sup>

Since the targeted operating temperature of the lander is 0°C, and the preferable mounting option is PSA (Pressure Sensitive Adhesive) due to its approval for vacuum conditions, the maximum watt density of the heaters is 20 W/in<sup>2</sup>. Since heaters are an active, and not passive contribution to the thermal system of the lander, two more components are needed. In addition to the heaters themselves, a thermistor and a controller are required to provide data about the internal lander temperature, and to turn the heaters on, partially on, or completely off. The ability to turn the heaters on partially is useful because the total wattage available is 52 W, and no more than 50 W should ever be used at one time. These parts are also manufactured by Minco, in order to retain consistency between the entire heating system. All of these components are listed in the following Components section of this report.



Figure 5.7.2: Minco Polyimide Thermofoil Patch Heater.<sup>121</sup>

<sup>120</sup> Minco. *Thermal Solutions Design Guide*. Accessed April 20, 2020.

<<https://www.minco.com/~media/files/minco/productguides/heat/minco%20thermal%20solutions%20design%20guide.ashx>>

<sup>121</sup> Minco. *Polyimide Thermofoil Heaters*. Accessed April 20, 2020.

<<https://www.minco.com/products/heat/polyimidethermofoilheaters>>

### 5.7.4 Components

Below is a list of components needed for the lander, including coatings and heating elements.

- Kapton 3mil (ITO/VDA/Kapton) (TRL 9)  
Coating Kapton with various thin layers of metals is an established method for creating coatings of varying thermal properties. Design heritage derives from multiple international missions. For example, VDA-coated Kapton MLI was used in ESA's CHEOPS<sup>122</sup> and ITO/SiOx/VDA/Kapton was selected for NASA's Solar Plus Probe MAG Sensor<sup>123</sup>. No modifications of this established process will be necessary.
- Minco 12 Watt Polyimide Thermofoil Patch Heater (TRL 9)  
Polyimide thermofoil heaters have legacy flying on previous NASA missions, and have also gained materials approval from ESA. This heating patch is 3" by 0.5" and provides 12 Watts of heat. Four of these heaters will be needed per lander. The only additional modification that will be necessary to this heater will be to properly apply its adhesive to its desired location within the lander, and to wire it to the thermal controller.
- Minco 4 Watt Patch Heater (TRL 9)  
Similarly to the 12 Watt Patch heater, this heater is approved for NASA space missions. It provides 4 Watts of heat from a 1" by 0.5" patch. Only one of these heaters will be needed per lander. This patch only needs to be attached to the lander and wired to the thermal controller before it is ready for the mission.
- Minco Thermal Controller (TRL 7)  
This controller is not explicitly listed online as approved for space missions. It has, however, been demonstrated to work in conjunction with the chosen heaters and thermistor. This controller allows the heaters to be turned on, partially on, or off, from the data gathered by the thermistor.
- Minco RTD Thermal Ribbon Thermistor (TRL 7)  
The chosen thermistor is also not explicitly stated as approved for space missions. This thermistor comes in a long temperature averaging ribbon that is more accurate than a point-thermistor, because it gathers temperature data from a larger area of the lander.

---

<sup>122</sup> Melendo, Ignacio, and Romain Peyrou-Lauga. "CHEOPS Platform Thermal Architecture." *46th International Conference on Environmental Systems*, July 10, 2016.

<sup>123</sup> Choi, Michael. "Solar Probe Plus MAG Sensor Thermal Design for Low Heater Power and Extreme Thermal Environment." *45th International Conference on Environmental Systems*, July 12, 2015.

## 5.8 Command & Data Handling

The command and data-handling (C&DH) system control spacecraft function; process and disseminate all spacecraft data; and enable autonomous operation via response to environmental variables. C&DH is composed of a computational core, memory, and several peripheral boards that permit a broader variety of inputs and outputs.

### 5.8.1 Processor

#### *Key Requirements and Assumptions*

As the system design remains in its initial iterations, data and processing requirements are poorly defined. Specific choices of hardware have been made for ADCS but not communications and the scientific payload, both drivers of C&DH requirements. Only basic estimates of necessary memory are available (see requirements). More generally, the system had to satisfy mass and volume constraints imposed by the mechanical and electrical subteams: a mass less than 25 kg, volume small enough to fit within the frame, and minimal power consumption. Neither of the mechanical requirements narrowed the space of possible selections, though power became a deciding factor. Because of uncertainty in system requirements, hardware choices for C&DH were made principally through consideration of missions comparable in size, duration, data acquisition, and communication distance.

#### *Requirements*

The C&DH system shall...

- ...perform all computation required to meet other subsystem goals
- ...manage all spacecraft data: processing and storage of payload outputs, encoding for transmission, and management of ADCS and other sensor data.

#### *Assumptions*

- The RAD750's 260 MIPS performance is sufficient for the purposes of the lander:
  - There exist no defined performance requirements from ADCS or the science payload for the lander.
- Electronic components of other subsystems are capable of interface via Spacewire, RS422, or LVDS

### 5.8.2 Mass and Power Budgets

Note that the C&DH system is listed within the power section in the general mass and power requirements.

#### *Mass Budget*

Component	Mass (kg)	Notes
-----------	-----------	-------

RAD750 SBC <sup>124</sup>	0.549	-
RTIMS Flash Memory <sup>125</sup>	0.064	4 x 8 gb
3U-160 Compact PCI Board <sup>1</sup>	0.500	-
RADNET SWP-RB4 ASSP Chip Bridge <sup>1</sup>	0.200	< 100g + additional packaging
<b>Subsystem total</b>	1.295	
<b>Allocated Mass</b>	5	
<b>MGA</b>	3.705 (75%)	Margin accounts for harnessing, structure and additional, unforeseen, electronics

### *Power Budget*

Component	Power Consumption (W)	Notes
RAD750 SBC <sup>1</sup>	10.8	
RTIMS Flash Memory <sup>2</sup>	3	4 x 8 gb
3U-160 Compact PCI Board <sup>1</sup>	3	
RADNET SWP-RB4 ASSP Chip Bridge <sup>1</sup>	2.5	
<b>Subsystem total</b>	17.6	
<b>Allocated Power</b>	19.75	
<b>Margin</b>	2.15 (12%)	Margin consumed by last-minute addition of 3U-160 for Spacewire

### *Margins and Contingency*

Margins in mass are to support the harnessing required to link the computer to the other subsystems and the structure on which the boards are mounted.

Margins in power are to cover harnessing loss and account for operations that result in high power operation from several components simultaneously (above system averages). Margins also cover power requirements for the communications chip, which has not yet been selected.

### 5.8.3 Design

The RAD750 single board computer (SBC) is the computational center of the system (Fig. 5.8.1); all other components exist to provide additional storage or more versatile I/O, as the RAD750 is capable of interface only via PCI, UART, and JTAG. A trade study of processors is available in Appendix M.

Except the storage and communications board, components are selected from BAE's catalogue to ensure compatibility with the processor. RTIMs Flash Memory provides easily-expandable storage: units have almost negligible mass, volume, and power requirements. The 3U-160 Compact PCI Board and

---

<sup>124</sup> See BAE Space Web site.

<sup>125</sup> See 3D-Plus.com.

RADNET SWP-RB4 ASSP Chip Bridge enable Spacewire and RS422/LVDS communication, respectively, enabling the processor to control, receive data from, and transmit data to other spacecraft components (these connections are standard to most space rated electronics). Selection of a communications board or chip for the lander is pending, subject to receipt of data sheets from suppliers.

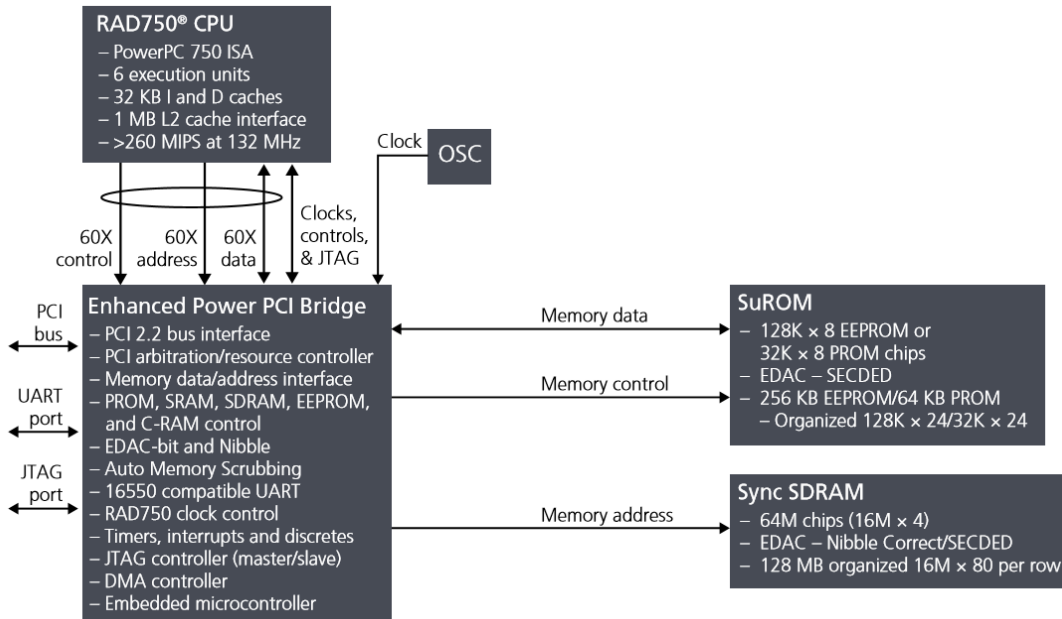


Figure 5.8.1: Detailed Schematic of RAD750 Architecture.<sup>126</sup>

Further design of the C&DH, after better definition of the driving requirements, will include specification of the wiring between the C&DH system and the components of other subsystems with which it interfaces and selection or manufacture of an enclosure for the boards.

#### 5.8.4 Components

- RAD750 (TRL 9)
- RTIMS Flash Memory (TRL 9)
- 3U-160 Compact PCI Board (TRL 9)
- RADNET SWP-RB4 ASSP Chip Bridge (TRL 9)

<sup>126</sup> Space Products Literature (2020). Retrieved from

<https://www.baesystems.com/en-us/our-company/inc-businesses/electronic-systems/product-sites/space-products-and-processing/radiation-hardened-electronics>

## 5.9 Communications

The lander-to-orbiter communications system relays data from the science payload and monitors the position and health data of the lander. After the lunar mission is complete, the orbiter will remain in operation for ten years as a communications satellite.

### 5.9.1 Key Requirements and Assumptions

#### *Requirements*

- The communications system shall provide a lander to orbiter connection via a patch antenna and S-band radio signals.
- The communications system shall support 0.07 Mbps uplink and downlink on the lander to orbiter connection.
- The communications system shall store information (via the flight computer) that becomes available between line of sight passes.

While S-band communications will limit the data rate of the lander-to-orbiter connection, S-band uses significantly less power than other bands, and, as the lander will be operating on battery power alone, this low power requirement is very important.<sup>127</sup> Though this may limit the allowable data rates of future lunar missions using this orbiter, it is likely that any lunar mission in this region will be performing similar research, and therefore have comparable data rates to the Erebus mission. An exception to this would be autonomous missions, which would have much higher data rates, but it is unlikely that these missions would choose to communicate using the Erebus orbiter as it has such a short connection period with the lunar South Pole during each orbit. Based on these considerations, S-band is both necessary and sufficient for the lander to orbiter connection.

The lander to orbiter data rate was chosen in order to upload the 1 MB of payload data that comes from one sample of the lunar surface within the 152 seconds of communication per orbit. A data rate of 0.07 Mbps allows a sample to be transmitted in 2 minutes, leaving a sufficient 32 seconds to transmit the position and health data.<sup>128</sup> If an additional safety margin proves desirable, the communications window can be extended with the orbiter's off-axis pointing capability as described in Section 6.3.

#### *Assumptions*

- Specific communications software is outside the scope of the course and is therefore classified as future work.
- Incorporation of a low gain antenna was suggested in feedback from the CDR, and is therefore classified as future work.
- The lander and orbiter will have a connection pattern of 152 seconds in line of sight and 2 hours and 16 minutes of no line of sight per orbit.

---

<sup>127</sup> “Spacecraft Subsystems IV- Communications and Power.” *Space Mission Engineering the New SMAD*, by James R. Wertz et al., Microcosm Press, 2011, p. 639.

<sup>128</sup> See Appendix N for a breakdown of this data.

- The communications system experiences a noise temperature of 290 K.<sup>129</sup>
- The average illumination factor is 70°.<sup>130</sup>

A low-gain antenna will be included on the orbiter and the lander as a backup in case either HGA has a failure. However, the inclusion of these antennas would require significant changes from the communications, thermal, power, and mechanical teams, so its inclusion was not possible in this report. It is classified as future work.

### 5.9.2 Mass and Power Budgets

#### *Mass Budget*

Component	Mass (kg)	Notes
Patch Antenna	0.4	Modeled after Endurosat product <sup>131</sup>
S-band Transmitter	0.25	Modeled after Endurosat product <sup>132</sup>
S-band Receiver	0.22	Modeled after Endurosat product <sup>133</sup>
Master Cable	2	Connects all components
<b>Subsystem total</b>	<b>2.87</b>	
<b>Allocated Mass</b>	<b>3.3</b>	
<b>MGA</b>	<b>0.43 (15%)</b>	Margin accounts for mounting materials

#### *Power Budget*

Component	Power (W)	Energy (Wh)	Notes
S-band Transmitter	7.20	2.74	Active only when line of sight is available with orbiter
S-band Receiver	2	0.76	Active only when line of sight is available with orbiter
<b>Subsystem total</b>	<b>9.20</b>	<b>3.5</b>	
<b>Allocated</b>	<b>11</b>	<b>4.2</b>	
<b>Margin</b>	<b>1.8 (15%)</b>	<b>0.7 (15%)</b>	Margin accounts for increased power consumption as equipment ages

<sup>129</sup> Ho, Christian, et al. “Atmospheric Noise Temperature Induced by Clouds and Other Weather Phenomena at SHF Band (1-45 GHz).” *Atmospheric Noise Temperature Induced by Clouds and Other Weather Phenomena at SHF Band (1-45 GHz)*, 11 Aug. 2005, descanso.jpl.nasa.gov/propagation/Ka\_Band/JPL-D32584\_1.pdf.

Accessed on April 23, 2020.

<sup>130</sup> Paluszek, Michael, “Spacecraft Communications,” Slide 35, Mae 342 2020, Accessed on May 6, 2020.

<sup>131</sup> <https://www.endurosat.com/cubesat-store/all-cubesat-modules/s-band-antenna-commercial/> Accessed May 1, 2020.

<sup>132</sup> <https://www.endurosat.com/cubesat-store/cubesat-communication-modules/s-band-transmitter/> Accessed May 1, 2020.

<sup>133</sup> <https://www.endurosat.com/cubesat-store/cubesat-communication-modules/s-band-receiver/> Accessed May 1, 2020.

### *Margins and Contingency*

As the communications components on the lander are all based off of existing designs, only a 15% margin is needed for the mass requirement of the lander, which will account for the mass of the mounting materials. Although the lander components are known, 15% power margins were allowable since the total communications power requirement was so low.

### 5.9.3 Design

#### *S-Band System*

After consideration of S-band, X-band, and UHF-band, S-band was selected as the best option for the lander-to-orbiter connection due to its low power requirement.<sup>134</sup> Though S-band has the lowest bandwidth of all of these bands, a link budget analysis determined that the S-band bandwidth would be sufficient for the Erebus and similar missions. A Lunar Gateway connection was also considered for connection with Earth, but the Gateway’s seven-day orbital period does not ensure that the Erebus mission would be able to use this connection during its twenty-hour lifetime.<sup>135</sup> S-band communication with the orbiter offers more guaranteed lunar coverage during the mission, and its low power requirement makes it ideal for the battery powered lander.

The communications system between the lander and the orbiter will consist of one patch antenna, one S-band receiver, and one S-band transmitter. Each of these components will be on both the lander and the orbiter. The S-band antenna will be a left hand circularly polarized patch antenna, with a gain of 11dB and an area of 110 square centimeters. This area was determined by the link budget, and each antenna is the same size in order to avoid either becoming too large or requiring too much power. The antenna is omnidirectional to allow the GN&C team sufficient pointing margins. The antenna is modeled after an Endurosat product, but will be modified to suit the mission’s needs. Both the receiver and transmitter are modeled after Endurosat products as well.

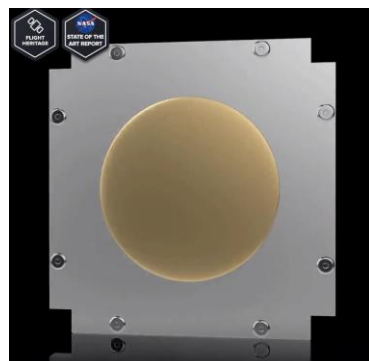


Figure 5.9.1: Endurosat S-band patch antenna<sup>136</sup>

---

<sup>134</sup> “Spacecraft Subsystems IV- Communications and Power.” *Space Mission Engineering the New SMAD*, by James R. Wertz et al., Microcosm Press, 2011, p. 639.

<sup>135</sup> Gerstenmaier, William. “Cislunar and Gateway Overview.” NASA, Mar. 2020, descanso.jpl.nasa.gov/propagation/Ka\_Band/JPL-D32584\_1.pdf. Accessed on May 6, 2020.

<sup>136</sup> Endurosat, “Commercial S-Band Patch Antenna”. Accessed on May 7, 2020. Retrieved from <https://www.endurosat.com/cubesat-store/all-cubesat-modules/s-band-antenna-commercial/>.

One set of components will be mounted on the top of the lander, while the other will be mounted on the moon-facing side of the orbiter. Components will be connected to each other and to the flight computer via a master cable.

### *S-Band Link Budget*

While creating the link budget, it was important to make the data rate as high as possible while keeping the power and mass requirements relatively low. This will ensure that future missions on the South Pole of the moon are able to use the Erebus orbiter for their own data needs, which may be greater than this mission. Based on the requirements from the Erebus mission, it was determined that a data rate of 0.07 Mbps would be sufficient for most of these missions. Again, it is not expected that autonomous missions would use the Erebus satellite due to its limited connection time. This bitrate will allow one sample from the Erebus mission to upload in 2 minutes during the 152 second connection period.

The resulting lunar link budget is -135 dB.<sup>137</sup> Though the budget is small, it is for a much higher bitrate than the mission will need, eliminating the need for a larger budget.

### *S-Band Pointing Requirements*

The omni-directional patch antenna has a  $\theta_{3dB}$  value of  $47.46^\circ$  and an allowable pointing error of  $13.70^\circ$ .<sup>138</sup> This allowable error is much larger than the expected pointing error from the GNC team. The radiation pattern of this antenna is shown below, although the specific values are slightly different.

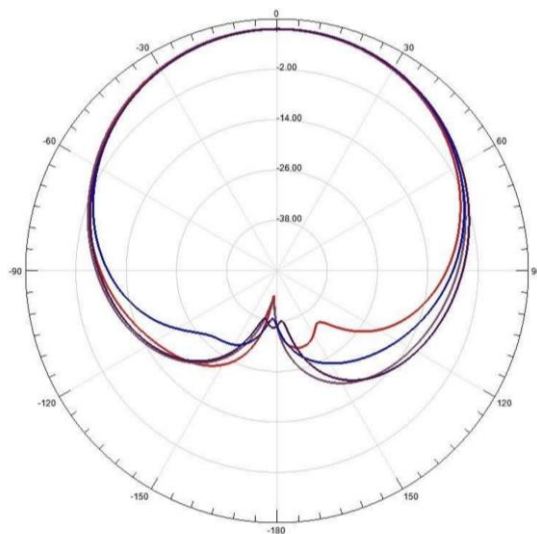


Figure 5.9.2: Radiation pattern for an Endurosat patch antenna<sup>139</sup>

#### 5.9.4 Components

- S-band Patch Antenna (TRL 8)

---

<sup>137</sup> See Appendix N for calculations.

<sup>138</sup> See Appendix N for calculations.

<sup>139</sup> <https://www.endurosat.com/cubesat-store/all-cubesat-modules/s-band-antenna-commercial/> Accessed May 1, 2020.

The S-band patch antennas will be based on an existing off-the-shelf solution, but will be customized to suit the link budget and pointing requirements of the mission.

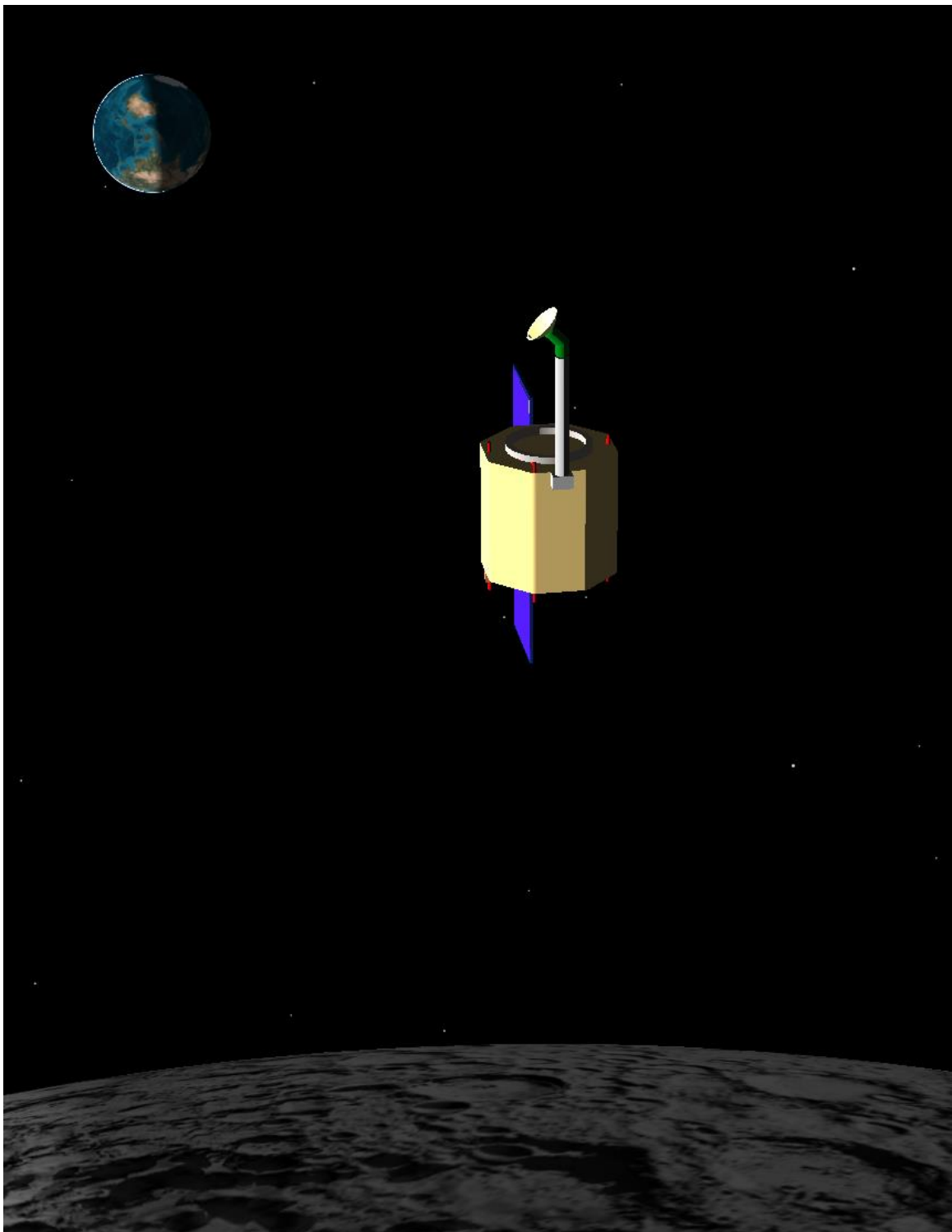
- **S-band Transmitter (TRL 9)**

The S-band transmitters will be based on an existing off-the-shelf solution, with few to no expected changes.

- **S-band Receiver (TRL 9)**

The S-band receivers will be based on an existing off-the-shelf solution, with few to no expected changes.

## 6. Lunar Orbiter



## 6.1 Structure

Similar to the lander, the orbiter must possess a structure which not only can withstand the various loads the orbiter will encounter throughout the mission but also accommodates the needs of each subsystem by providing protection, support, and attachment points. The orbiter structure will be in large part inherited from the lander structure and uses the same beam-and-panel model. The design of this structure will be dominated by launch loads in terms of strength and deflection. The structure also must conform to launch vehicle and ESPA guidelines by resisting "low frequency" (< 35 Hz) resonance and staying within a specified volume envelope. As with the lander, the packaging of components will be a primary concern when considering the dimensions of the structure, as the orbiter structure will be limited as much by volume as by weight (note: these components were not within the scope of this report). In addition to accommodating the components themselves, the structure must also allow for efficient electrical harnessing and propellant plumbing.

### 6.1.1 Key Requirements and Assumptions

#### *Requirements*

The structure shall...

- ...fit all other subsystems internally or externally as required.
- ...support all masses with a safety factor greater than 3.
- ...have no resonant modes below 35 Hz, per requirement 3.2.1.

As with the lander, many of the requirements placed on the orbiter structure will be defined by the needs of other subteams, whose subsystems must be integrated safely and efficiently. The worst case boundary conditions will be provided in large part by evaluating LV integration and loading scenarios. Within the weight allotted to the structure, it is desirable to have as great a safety factor as possible to increase platform security.

#### *Assumptions*

- LV launch load case condition is 8.5 g LV axial and 3 g LV lateral.
- LV launch volume envelope is 42”x46”x56” (ESPA volume envelope).
- Aluminum honeycomb paneling will not have significant structural impact.

The internal layout of this orbiter is beyond the scope of this report, so while there exist many components such as batteries, thrusters, propellant and relevant storage, the exact dimensions and masses that must be accommodated remain unknown. However, it can be assumed that these masses will not surpass those that the lander structure was designed to support, especially given that the orbiter wet mass is significantly lower than the lander wet mass.

### 6.1.2 Mass Budget

Component	Mass (kg)	Notes
-----------	-----------	-------

Frame	30.4	
Bracing	7.6	
Honeycomb Panels	1.1	Based on 3.62 kg/m <sup>2</sup> (see Appendix F.1)
Separation System	2.42	
<b>Subsystem total</b>	<b>41.5</b>	
<b>Allocated Mass</b>	<b>62.3</b>	
<b>Margin</b>	<b>20.8 (50%)</b>	

#### *Margins and Contingency*

Once again the total mass of the structure is dominated by the frame and bracing. The honeycomb panel mass is comparatively very small and thus should not significantly alter the structure mass, however it can be estimated; see Appendix F.1 for calculations of the panel mass.

With the orbiter structure—as with the lander structure—it is not expected that the real mass of the structure will deviate significantly from the predicted mass as the requisite materials are well known and documented and are available from a variety of reputable commercial suppliers. However, mounting hardware for the internal components can be expected to add some mass. This is accounted for by a total mass margin of 50%.

#### 6.1.3 Design

As previously stated, the orbital's base structure was inherited from that of the lander to reduce design and manufacturing associated costs while simultaneously mitigating potential failure modes which could result from the added complexity of a brand-new structure design. The structure was designed as an octagonal prism for a variety of reasons. This shape provides high rigidity and good overall strength as well as symmetry for convenient mounting while still being able to capitalize on the majority of the volume window allocated by the ESPA Grande's volume allotment specifications. In addition, this structure was designed to accommodate panels for mounting and protection. The structure was designed as a monocoque shell for strength and rigidity. Conveniently, this also provides for simple and easy wiring runs. The constraining volume window as defined by the LV envelope and the ESPA Grande's carrying capacity is 42"x46"x56". Aluminum 6061 was chosen for the structure for its high strength to weight ratio, large commercial availability and design heritage, and superb weldability as compared with other similarly high-strength alloys. Please see Appendix F.2 for a chart of Aluminum Alloy Characteristics.

The structure consists of 8 radially located 3"x3"x36" rectangular tubes with a wall thickness of  $\frac{1}{8}$ ". These are welded on either end to two 1" hollow octagonal plates, also with a wall thickness of  $\frac{1}{8}$ ". The structure is reinforced with 2"x0.3" aluminum cross bracing situated diagonally between each adjacent pair of aluminum square tubes. A drawing of the structure may be found in Appendix F.3.

The internal layout of the orbiter is beyond the scope of this report; however, the fuel mass and power storage requirements are known to be less than that of the lander, and no payload needs be accommodated, so it can be assumed that the internal components will be neither more massive nor more voluminous than those found in the lander, and thus the extant structure can be used without issue.

#### 6.1.4 Drawings and Layouts

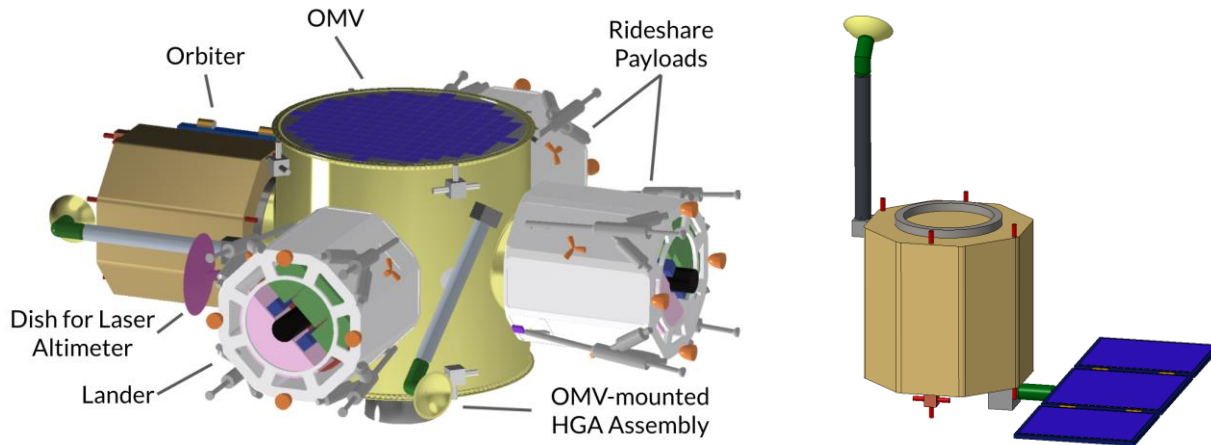


Figure 6.1.1: The OMV with orbiter and lander modules (left);  
the orbiter in its deployed configuration (right).

For images detailing the Finite Element Analysis of the structure, please see section 5.1.4.

#### 6.1.5 Components

- Aluminum 6061 Welded Hollow Frame (TRL 9)  
These are standard aluminum 6061 tubes made of a standard thickness and size, and should be readily available from mass manufacturers.
- Aluminum 6061 Welded Solid Bracing (TRL 9)  
These are standard aluminum 6061 bars made of a standard thickness and size, and should be readily available from mass manufacturers.
- Aluminum Honeycomb Panels (TRL 9)  
These are standard aluminum honeycomb panels of a standard thickness and size, and should be readily available from a variety of specialty manufacturers, including APCO Technologies and Collins Aerospace.

## 6.2 Mechanisms

The mission objectives and layout of the Erebus lunar orbiter require significant deployable structures, and continuous or near-continuous actuation to point those components mounted on those structures, in order to maximize communication time with Earth and power the spacecraft. The mechanisms subsystem is responsible for deploying the high gain antenna (HGA) mast and the solar array; pointing the HGA towards the Earth when required; and orienting the solar array towards the sun.

### 6.2.1 Key Requirements and Assumptions

#### *Requirements*

##### HGA Mast and Gimbal

- The HGA mast shall support the HGA gimbal assembly. From launch until orbiter separation, the mast shall be stowed against the side of the orbiter module, per requirement 3.4.5, supported by a latch near the gimbal end and a hinge at the other end. After orbiter separation, the hinge shall rotate by 180 degrees to deploy the mast. The mast shall then be rigidly supported at the hinge end and free at the gimballed end.
- The mast and gimbal assembly together shall displace the HGA from the main orbiter body a distance of 1 m to prevent the body from blocking RF signals and to isolate the HGA from EM waves emitted by other orbiter systems, per requirement 3.4.4.
- The mast, in the stowed state, shall have all resonant modes above 35 Hz, per requirement 3.2.1.
- The mast, in the deployed state, shall have all resonant modes above 20 Hz in order to avoid being excited by ADCS thruster firings, per requirement 3.3.1.
- The HGA gimbal shall provide 180 degrees of motion about two axes, per requirement 3.4.1, in order to be able to point the HGA at the Earth whenever there is line of sight between the orbiter and Earth, thus maximizing communication time.

The main reason for mounting the HGA on a large mast is to minimize the area of sky blocked by the body of the spacecraft, in order to avoid the need for periodic slewing of the spacecraft towards Earth. In addition, mounting the HGA on a long mast isolates it from other RF sources, including other antennas and various electronic components. It also eliminates the risk of passive intermodulation, where resonant re-radiation is generated from electronic and structural elements of the spacecraft.

##### Solar Array

- The solar array shall be stowed against the side of the orbiter module, per requirement 3.4.5, until deployment is required.
- The total area of the solar array shall be at least 2.26 m<sup>2</sup>, per requirement 3.4.6, in order to provide the required power to the orbiter.
- The solar array shall have full 360+ degree motion about two axes, per requirement 3.4.3, in order to align the surface normal of the solar array with the sun vector no matter the attitude of the orbiter relative to the sun.
- The solar array drive actuators (SADAs) shall be able to accommodate at least 628 W of power throughput, per requirement 3.4.2, in order to satisfy the power requirement of the orbiter.

### *Assumptions*

- Based on the heritage of the Lunar Reconnaissance Orbiter, 180 degrees of motion about two axes is sufficient to point a high gain antenna towards Earth given line of sight, no matter the spacecraft attitude; and two axes of freedom for the solar array allows it to be oriented towards the sun without constant slewing of the spacecraft.<sup>140</sup>
- The specific actuation commands and control schemes necessary to accomplish Earth-pointing of the HGA and sun-pointing of the solar array are outside the scope of this report.

### 6.2.2 Mass and Power Budgets

#### *Mass Budget*

Component	Mass (kg)	Notes
Moog EPGA	6.5	Full-size mass
Honeybee SADA (x2)	2.0	
Antenna mast	1.4	
Deployment mechanisms	5.0	Upper-bound estimate
<b>Subsystem total</b>	<b>14.9</b>	
<b>Allocated Mass</b>	<b>22.4</b>	
<b>Margin</b>	<b>7.5 (50%)</b>	

#### *Power Budget*

Component	Max Power (W)	Energy (Wh)	Notes
HGA gimbal	28	66	Operated over entire orbit
Solar array SADAs	28	66	Operated over entire orbit
<b>Subsystem total</b>	<b>56</b>	<b>132</b>	
<b>Allocated</b>	<b>72.8</b>	<b>171.6</b>	
<b>Margin</b>	<b>16.8 (30%)</b>	<b>39.6 (30%)</b>	

#### *Margins and Contingency*

The power required to operate the HGA gimbal and the solar array drive actuators is estimated at an average value of 10 W per axis, with a maximum of 14 W per axis, based on Moog's Enhanced Pointing

---

<sup>140</sup> Chernyakov, Boris, and Kamal Thakore, "Gimbals Drive and Control Electronics Design, Development and Testing of the LRO High Gain Antenna and Solar Array Systems," Proceedings of the 40th Aerospace Mechanisms Symposium, NASA Kennedy Space Center, May 12-14, 2010, accessed via the NASA Technical Reports Server, <https://ntrs.nasa.gov/archive/nasa/casi.ntrs.nasa.gov/20100021940.pdf>.

Gimbal Assembly (EPGA), a heritage unit used on Lockheed Martin’s A2100 satellites.<sup>141</sup> The orbiter’s HGA gimbal and SADAs will both be smaller than the EPGA, so 14 W per axis, 56 W in total, is an upper bound estimate. Furthermore, the HGA gimbal will not be continuously actuating; for example, when the orbiter is on the other side of the Moon opposite Earth, there is no reason for the HGA gimbal to draw power. Therefore, assuming the HGA gimbal is active for the entire orbit is an upper bound estimate for energy, in terms of Wh per orbit, as well.

The solar array mass is considered part of the power subsystem, with a mass of 25.1 kg. This is based on the empirical relation, based on active satellite solar arrays, that the specific power of spacecraft solar arrays is 25 W/kg; since the orbiter’s array produces 628 W, this comes out to 25.1 kg for the total mass of the solar array.<sup>142</sup>

### 6.2.3 Design

The overall mechanisms architecture involves three main phases: 1) the deployment of the HGA mast and the solar array from their stowed configurations; 2) the unfolding of the three-panel solar array; and 3) the two-axis articulation of the HGA and solar array.

Figure 6.2.1 shows how the HGA mast deploys, rotating 180 degrees from its stowed position to its deployed position. Once the mast is deployed, the 2-axis gimbal can be used to point the HGA towards Earth. For the solar array, the initial deployment involves a 90 degree rotation of the folded solar array away from the body of the orbiter; this is accomplished by the actuation of one of the solar array drive actuators (SADAs). Then, one after another, the two outer panels of the solar array unfold. The solar array will have full range of motion about two axes, as labeled in Figure 6.2.2. The release, deployment, and articulation mechanisms are detailed later in this section.

---

<sup>141</sup> Moog, “Enhanced Pointing Gimbal Assembly (EPGA)”, Moog Space and Defense Group, 2019. Accessed May 9, 2020.

[https://www.moog.com/content/dam/moog/literature/Space\\_Defense/Space\\_Access\\_Integrated\\_Systems/EPGA\\_0410.pdf](https://www.moog.com/content/dam/moog/literature/Space_Defense/Space_Access_Integrated_Systems/EPGA_0410.pdf).

<sup>142</sup> Nadir, Bill, “Satellite Engineering” (Boston, MA: MIT, 2003). [https://ocw.mit.edu/courses/aeronautics-and-astronautics/16-851-satellite-engineering-fall-2003/projects/portfolio\\_nadir1.pdf](https://ocw.mit.edu/courses/aeronautics-and-astronautics/16-851-satellite-engineering-fall-2003/projects/portfolio_nadir1.pdf)

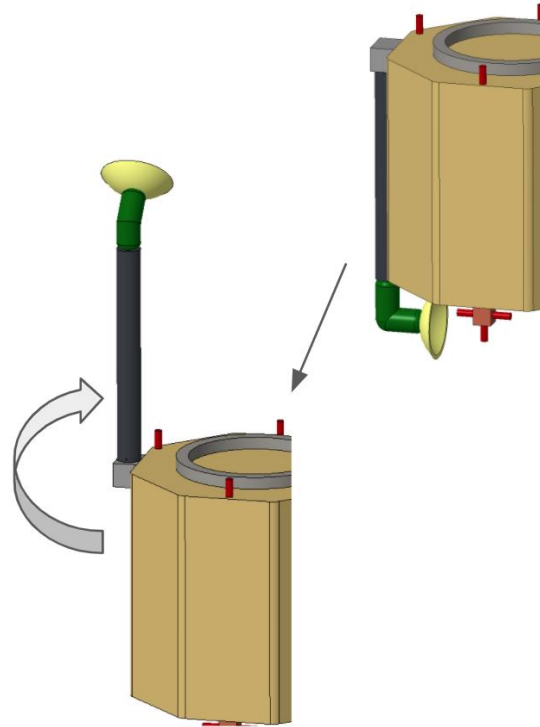


Figure 6.2.1: Deployment of HGA mast.

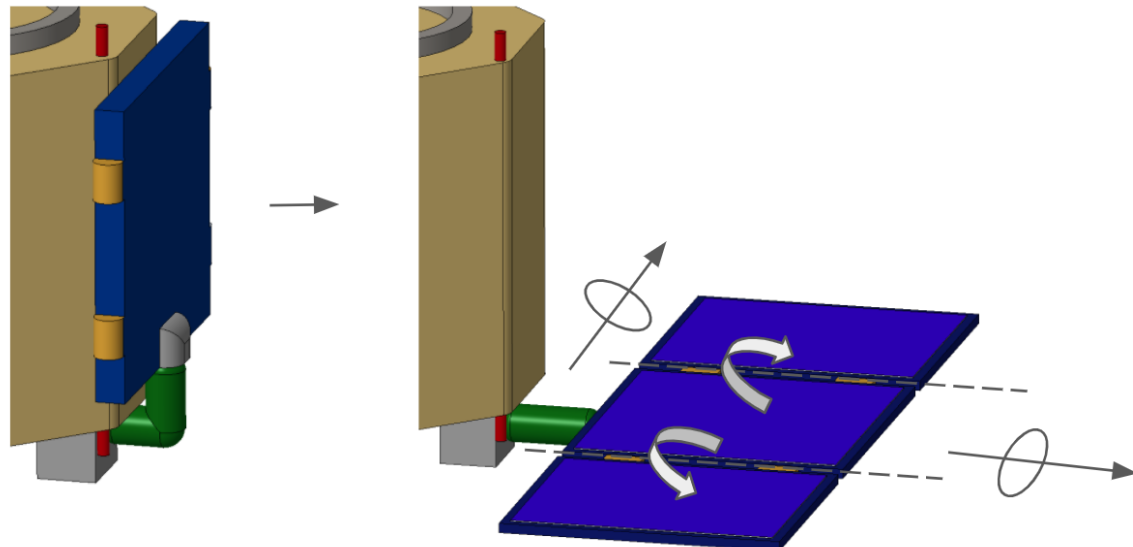


Figure 6.2.2: Deployment of solar array.

#### *Deployment Mechanism for HGA Mast and Solar Array*

Both the solar array panels and the HGA mast are required to be rotated 180 degrees from their stored to deployed configuration. For this deployment, two hinge mechanisms were considered: the HA-180 hinge and the camplate hinge.

The HA-180 hinge has a constant torque spring driven for uniform torque applications and has heated viscous dampers for rate control. It has redundant hard stops and latches on a large radius for

improved deployed repeatability. Its design allows it to be back-driven and it is highly precise. It is expensive to produce and is heavy.<sup>143</sup> On the other hand, the camplate hinge mechanism has a redundant torsion spring that is driven, with heated viscous dampers that control the rate of deployment. It has no free play in the deployed configuration and its non-reversible latching and high torque prevent back-driving. It is one sixth the cost of the HA-180 Hinge and one quarter the mass.<sup>144</sup> It is less precise than the HA-180 Hinge but, as the mechanism simply needs to go from storage to full deployment, and there is an additional gimbal to vary orientation, an extremely high level of precision was not required. Therefore, the camplate hinge was selected for these applications.

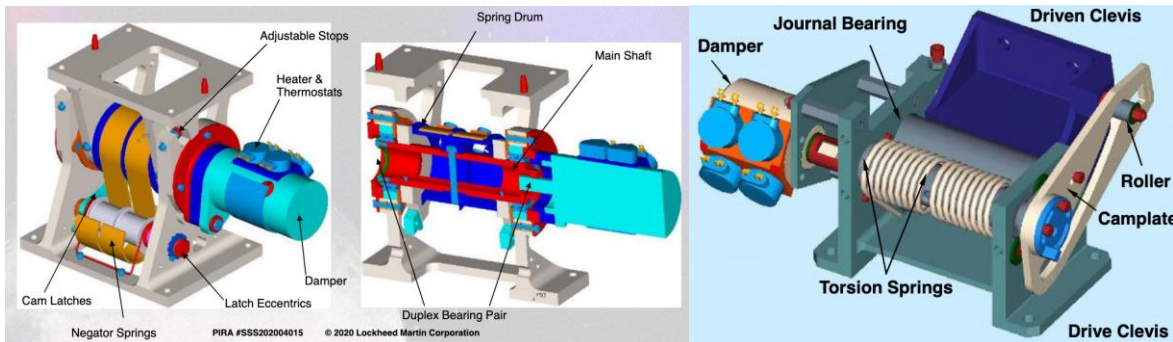


Figure 6.2.3: Hinge Mechanisms.<sup>145</sup> HA-180 Hinge (left) and Camplate Hinge (right).

#### Choosing the Spring Torque and Damping Rate

The critical parameters for the hinge are the damping rate needed and the stiffness of the spring. Ideally, the deployment would be at a slow constant velocity, as seen by the right side of the figure. It is important to note that these curves are for motors, but the same principles can be applied to the hinge. This is to ensure that the system is not shocked but releases in a controlled manner, which can be provided with a damper.

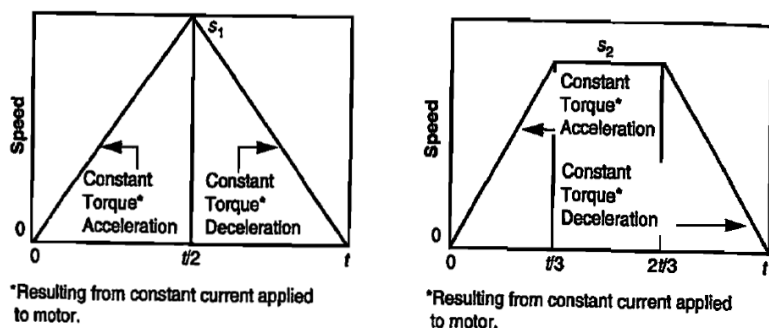


Figure 6.2.4: Release Mechanism Speed versus Time Curves<sup>146</sup>

First, the acceleration time was determined to be 0.25 seconds, before which the damper would act to ensure terminal velocity. The terminal velocity ( $s_2$  in Figure 6.2.4 above) required for the release

<sup>143</sup> Joe Munder, Spacecraft Design Course - Mechanisms Overview. Class lecture, given April 16 2020.

<sup>144</sup> Ibid.

<sup>145</sup> Ibid.

<sup>146</sup> Space Mission Analysis and Design, 3rd ed., ed. by James R. Wertz and Wiley J. Larson (Hawthorne, CA: Microcosm Press, 1999), 346.

was estimated to be 0.025 rad/s. A safety factor of 1.5 gives a terminal velocity of 0.0375 rad/s, which means that the damper would have to act even more aggressively. Additionally, this analysis assumes only one hinge, but in reality there will be two hinges. This ensures an overall safety factor of 200%. Next, a constant acceleration ramp-up to terminal velocity is assumed, allowing this acceleration ( $\alpha = 0.15 \text{ rad/s}^2$ ) and the distance travelled during this acceleration period (0.005 rad) to be estimated.

The torque needed to be produced by the spring is then given by  $T = I\alpha$ , where  $I$  is the moment of inertia of the solar array or mass. To achieve terminal velocity, the torque produced by the dampers needs to equal this torque produced by the spring, in order to have no angular acceleration. To calculate the damping rate, the torque is divided by the angular velocity. The results for both the torque and damping rate for the HGA Mast and Solar Array Panel are tabulated in Table 6.2.1.

Parameter	HGA Mast	Solar Array Panel
Moment of inertia ( $\text{kg}\cdot\text{m}^2$ )	9.0	2.14
Torque requirement (Nm)	1.35	0.32
Damping rate (Nm/rad/s)	36.0	8.56

Table 6.2.1: Deployment mechanism parameters.

It is important to note that the mast requires a more significant damping as its moment of inertia is much higher than the solar array. Finally, this gives results in a deployment time of 83.90 seconds, which can be tweaked after testing, but gives a proof of concept estimate for using these hinges for controlled deployment of the solar array and mast.

#### *Release Mechanism*

Shear ties will be used to keep the mast and solar array stowed against the body of the orbiter, and will also be used to keep the three-panel solar array folded up. When ready for deployment, the pyrotechnic cutters will activate, releasing the shear ties and allowing the solar array and mast to deploy, and the array panels to unfold.

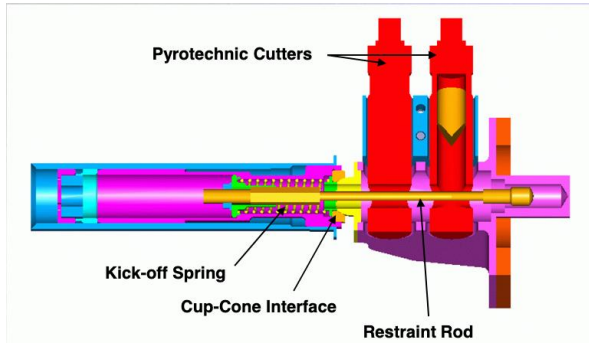


Figure 6.2.5: Pyrotechnic cutter for shear tie cables.<sup>147</sup>

#### *HGA Mast Sizing*

The form factor of the mast is chosen to be a hollow cylinder to minimize the mass needed to withstand buckling and cantilevered loads applied in any direction, offer maximal rigidity, and provide easy

<sup>147</sup> Joe Munder, Spacecraft Design Course - Mechanisms Overview. Class lecture, given April 16 2020.

mounting for the gimbal assembly. The outer diameter is chosen to be constant at 4" to maximally utilize the clearance offered by the gimbal assembly. The length is preliminarily chosen to be 36", with the length of the gimbal assembly bringing the antenna to 1m away from the vehicle, as required. The wall thickness of the mast is chosen to be 1/16" using a simple finite element analysis that tests for static loading stresses, buckling, and resonant modes, as detailed in Appendix G.6. Although a structure of this size may merit using carbon fiber reinforced composites, Al6061 is used as the material for the purpose of the FEA due to its isotropic nature and well-characterized and documented material properties. Therefore, the resulting mass estimate of 1.4 kg for the mast is the heaviest bound for what can be achieved using carbon fiber, and will serve as the baseline should this project move past CDR. FEA shows that in the stowed position, the von Mises stress experienced throughout the mast (aside from stress localization points that come as an artifact of defining constraints) does not exceed 10 ksi, which provides a 250% margin of safety from the tensile yield stress of 35 ksi of Al6061.<sup>148</sup> The buckling load factor of the first buckling mode was found to be 19, and the lowest resonant mode is at 89 Hz, satisfying requirement 3.2.1. Acceleration load factors are anticipated to be much smaller for the orbital (deployed) case compared to the launch (stowed) case, so only the modal analysis was performed, yielding a first resonant mode of 23 Hz, satisfying requirement 3.3.1.

### *HGA Gimbal Articulation*

The pointing of the HGA towards Earth will be accomplished by a downscaled version of Moog's Enhanced Gimbal Pointing Assembly (EPGA). The original EPGA, shown in Figure 6.2.6, is around six inches in diameter, and has a mass of 6.5 kg; it has an output step of 0.002 degrees. Two modifications are necessary to make the EPGA work with the Erebus lunar orbiter. First, actuators must be selected, and the gimbal geometry appropriately scaled down, so that it fits onto the four-inch-diameter mast; and running power and data to and from the HGA must be accommodated. To address the first modification, Moog would be contracted to adapt its existing product, or find a suitable substitute; however, for the purposes of this project, the EPGA serves as a heritage example from which parameters like power draw and mass can be derived. As for the second modification, given that the gimbal provides  $\pm 90$  degrees along each axis (for a total of 180 degrees along each axis), it would be possible to use a flex harness, as opposed to a series of slip rings, to transfer power and data. Flex harnesses providing  $\pm 90$  degrees, or even in some cases  $\pm 180$  degrees, of rotation have been flown on Earth-orbiting and interplanetary spacecraft, capable of upwards of 20,000 cycles of flexing over lifetimes of 15 years.<sup>149</sup>

---

<sup>148</sup> Metallic Materials Properties Development and Standardization (MMPDS): MMPDS-08, April 2013.

Washington, D.C.: Federal Aviation Administration, 2013. Table 3.6.2.0(c<sub>1</sub>).

<sup>149</sup> Patel, Mukund R., *Spacecraft Power Systems* (Cleveland, OH: CRC Press, 2005), 306.



Figure 6.2.6: Moog Enhanced Gimbal Pointing Assembly.<sup>150</sup>

#### *Solar Array Articulation*

The cells that make up the solar array are Spectrolab XTJ Prime triple junction solar cells, as detailed in the power subsystem chapter. The solar array will have a full 360+ degree range of motion about two axes of rotation, as required, through the use of two Honeybee ESPA Class SADAs, mounted within a gimbal geometry similar to the EPGA. Each SADA, shown in Figure 6.2.7, is 75 mm in diameter and 147 mm in length, so the overall solar array gimbal will be of comparable size to the downscaled EGPA, which will be about 4 inches in diameter. Each SADA has a slip ring, with a power throughput capacity of 1.7 kW, well beyond the power throughput requirement of 628 W. This SADA is derived from a heritage design for a pointing actuator built for the NASA/JPL Curiosity Rover.<sup>151</sup>

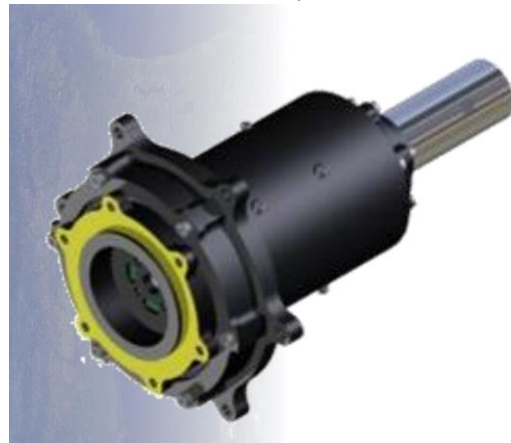


Figure 6.2.7: Honeybee ESPA Class Solar Array Drive Actuator.<sup>152</sup>

---

<sup>150</sup> Moog, “Enhanced Pointing Gimbal Assembly (EPGA)”, Moog Space and Defense Group, 2019. Accessed May 9 2020.

[https://www.moog.com/content/dam/moog/literature/Space\\_Defense/Space\\_Access\\_Integrated\\_Systems/EPGA\\_0410.pdf](https://www.moog.com/content/dam/moog/literature/Space_Defense/Space_Access_Integrated_Systems/EPGA_0410.pdf)

<sup>151</sup> “ESPA Class SADA,” Honeybee Robotics, 2013. Accessed May 9 2020. <https://honeybeerobotics.com/wp-content/uploads/2014/07/Honeybee-Robotics-ESPA-SADA.pdf>.

<sup>152</sup> Ibid.

## 6.2.4 Drawings and Layouts

### *Solar Array*

The following drawing shows the general size of the solar array; the dimensions are in inches. The total area is 1190 in<sup>2</sup>, or 0.768 m<sup>2</sup>. The height of 34" allows the array to fit inside the vertical ESPA envelope, given the structure height of 38"; the width of 35" leaves significant room within the horizontal part of the ESPA envelope.

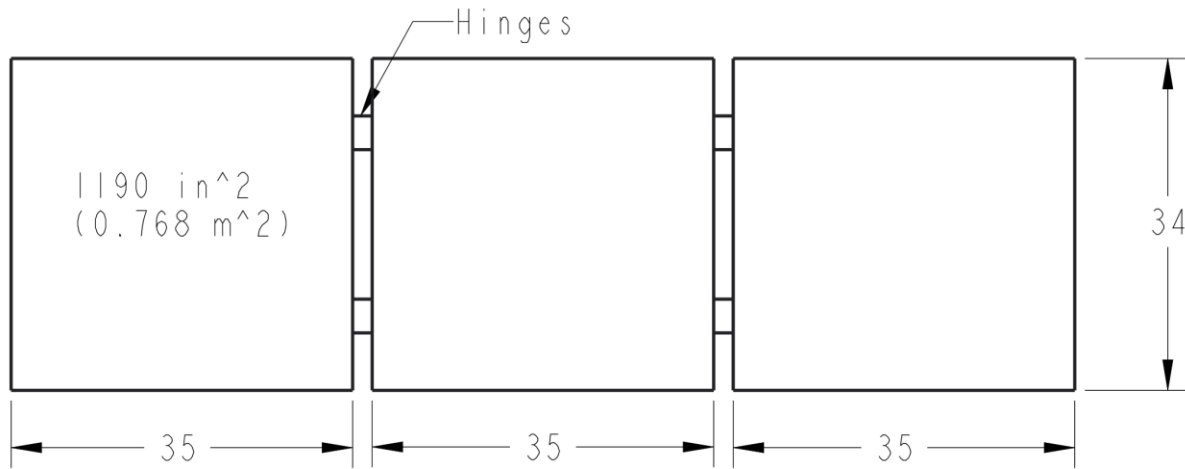


Figure 6.2.8: Basic dimensions of deployed solar array.

## 6.2.5 Components

### *HGA Mast and Gimbal*

- HGA mast (TRL 9)  
The HGA mast follows the precedent of many spacecraft, including the LRO, that have used deployable masts. It would be manufactured in-house.
- Downscaled Moog EPGA (TRL 7)  
While Moog's EPGA has flown on many space missions, modifying the gimbal architecture and selecting appropriate smaller actuators would require working closely with Moog to develop a new, smaller unit.
- Flex harness (TRL 9)  
As mentioned in the sections above, Earth-orbiting and interplanetary spacecraft have flown with flex harnesses. The particular flex harness for the HGA would be procured from a vendor.
- Camplate hinge (x1) (TRL 9)  
Camplate hinges are standard spacecraft mechanisms. Hinges with the appropriate torque and damping rates would be procured from a vendor.
- Shear tie release mechanism (TRL 9)  
As with the camplate hinge, shear tie release mechanisms are standard in deployable spacecraft structures. A suitable model would be procured from a vendor.

### *Solar Array*

- Honeybee ESPA Class SADA (x2) (TRL 8)

Honeybee's ESPA Class SADA is directly derived from a flight-proven pointing actuator used on the NASA/JPL Curiosity rover; however, it is unknown whether or not this specific actuator has been flight-proven.

- Gimbal mechanical assembly (TRL 6)

A mechanical gimbal assembly would have to be designed in-house in order to mount the SADAs to the solar array.

- Camplate hinge (x4) (TRL 9)

See above.

## 6.3 Guidance, Navigation, and Control

The GNC subsystem ensures accurate control and pointing of the spacecraft throughout the mission and will deorbit the system at the end of the mission. After stabilizing the vehicle post-OMV separation, the system will point the spacecraft nominally at the nadir. The capability will be included to point up to 15 degrees off-axis in order to facilitate target-of-opportunity pointing to increase the communications capability of the orbiter. Roll control will primarily be used to point the solar panel at the sun such that it does not block the nadir-facing antenna.

### 6.3.1 Key Requirements and Assumptions

#### *Requirements*

The GNC system shall...

- ... provide pointing accuracy of up to 14 deg towards the moon to ensure communications antenna access to both the Earth and the lunar surface throughout the entire mission life over the entire orbital period throughout the lifetime of the orbiter. (5.3)
- ... perform the final deorbit maneuver at the end of life. (5.1.2)
- ... perform spacecraft attitude stabilization (disturbance rejection) as required. (5.1.3).
- ... shall keep the maximum frequency of vehicle excitement by its instruments to be under 20 Hz as required by the Mechanical subsystems. (5.5.1)

The orbiter will be acting as a relay sat for the lander and possibly for future farside lunar missions. Therefore, it should be able to provide pointing accuracy at the lunar surface to the degree of accuracy determined by the communications team and ensure adequate attitude knowledge for the gimbaled antenna to point at the Earth.

The chosen lunar orbit is relatively stable but due to the various small external disturbances, disturbance rejection and momentum unloading have to be done occasionally (orbit disturbance analysis shows that this has to be done at least once every 95 hours).

The maximum excitement frequency is determined by the mechanical structure. The requirement originates with the minimum resonance frequency of the deployed boom.

#### *Assumptions*

- The design and simulation of the orbiter's control system were considered to be outside the scope of this project and classified as part of the future work. The time and expertise required for these sections of the subsystem exceeded the timeline within which the project had to be completed.
- The major perturbations are magnetic field, gravity gradient, and solar radiation pressure, as in SMAD III, and all others are ignored<sup>153</sup>.

---

<sup>153</sup> Wertz, James R., et al. *Space Mission Analysis and Design, Third Edition*. Microcosm Press, El Segundo, CA, 1999.

### 6.3.2 Mass and Power Budgets

#### *Mass Budget*

Component	Mass (kg)	Notes
Reaction Wheels (4)	16.4	Commercial off-the-shelf (COTS)
Star Tracker(2)	0.08	COTS
Sun Sensor(6)	0.20	COTS
IMU(2)	1.0	COTS
<b>Subsystem total</b>	<b>17.7</b>	
<b>Allocated Mass</b>	<b>26.6</b>	
<b>Margin</b>	<b>8.9 (50%)</b>	

#### *Power Budget*

Component	Power (W)	Energy (Wh)	Notes
Reaction Wheels	40	96	Active for the entire orbit, this is quadruple the average power over 95 hrs
Star Tracker	2	4.8	Active for 0.5 hrs per orbit
Sun Sensor	0.18	0.43	Active for 0.25 hrs per orbit
IMU	15	36	
<b>Subsystem total</b>	<b>57.2</b>	<b>137.23</b>	
<b>Allocated</b>	<b>74.3</b>	<b>178.4.9</b>	
<b>Margin</b>	<b>17.2 (30%)</b>	<b>41.2 (30%)</b>	Large margin considering the early stage of the design

#### *Margins and Contingency*

The mass of the reaction wheels is well-known because it is a commercial off the shelf component, and mass growth includes mounting equipment. The sun sensors, star trackers, and IMU are all off-the-shelf solutions and therefore require small margins. Some portion of the margins will be used towards acquiring or building in-house the mounting baffles that better fit the orbiter spacecraft.

The sensors and actuators power allotment is much larger than the expected value. This is the result of the power team accidentally using the maximum power draws, instead of the average power draws, of the sensors and actuators, both of which were communicated by the GNC team.

### 6.3.3 Design and Analysis

#### *Spacecraft Body-Centered Coordinate Frame Convention*

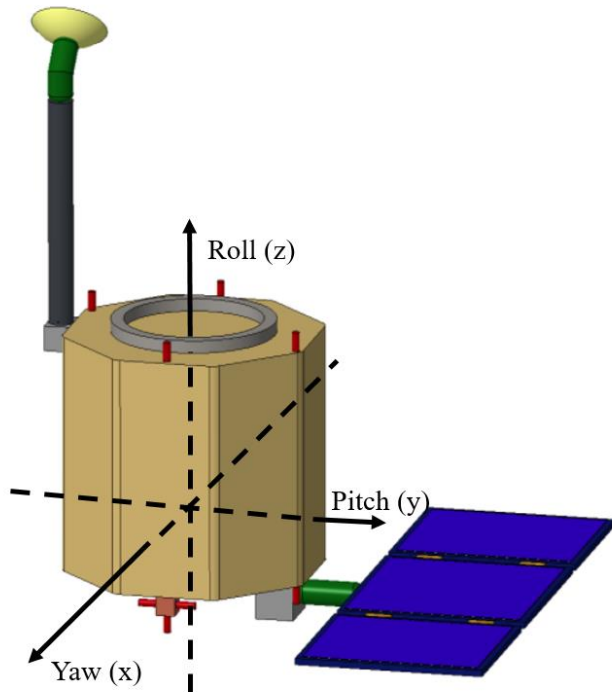


Figure 6.3.1. Orbiter Body Axis Diagram.

#### *Orbiter Disturbance Environment*

Because the vehicle will have no propulsion over its lifetime until the deorbit burn, all disturbances will be external. Recall that the orbit is 400 km in altitude, nearly circular, and has a 2.36 hr period.

#### *Magnetic Field*

The first disturbance analyzed is the magnetic field of the moon. This disturbance is unique because the moon's magnetic field is not dipolar, but irregular. It is assumed to be approximately random and thus does not create a net gain of angular momentum over the course of the mission<sup>154</sup>. According to SMAD III, equation 6.3.1 represents the torque generated by the magnetic field, where  $D$  is the residual dipole of the vehicle,  $M$  is the moon's magnetic moment, and  $R$  is the orbital radius<sup>155</sup>. The value of  $M$  is sourced from the paper referenced earlier in this section and is  $1.3 \times 10^{12} \text{ T m}^3$ . The spacecraft magnetic dipole was assumed to be  $1 \text{ A m}^2$ , which is the SMAD estimate for a small-sized, uncompensated vehicle. This

<sup>154</sup> Russell, C. T., et al. *The permanent and induced magnetic dipole moment of the moon*. Accessed 6 May 2020. <http://adsabs.harvard.edu/full/1974LPSC....5.2747R>

<sup>155</sup> Wertz, James R., et al. *Space Mission Analysis and Design, Third Edition*. Microcosm Press, El Segundo, CA, 1999.

results in a torque of  $1.37 \times 10^{-6}$  Nm.

$$T_m = D \frac{2M}{R^3} \quad (6.3.1)$$

### Solar Radiation Pressure

The torque generated by solar radiation pressure is significant because of the asymmetrical nature of the vehicle, which creates a significant difference between the center of mass and center of solar radiation pressure. With the final  $2.26 \text{ m}^2$  area solar panel, with the centroid of the solar panel located 1 m from the center of mass of the spacecraft, and assuming a  $1 \text{ m}^2$  body area (the worst torque case when the smallest body area is facing the sun), the result is that the difference between the center of mass and center of pressure is 0.68 m and a total surface area of  $3.26 \text{ m}^2$ . Equation 6.3.2 represents the equation for the force from solar radiation pressure, where  $F_s$  is the solar constant,  $1367 \text{ W/m}^2$ ,  $c$  is the speed of light,  $A_s$  is the surface area,  $q$  is the reflectance factor, and  $i$  is the sun angle of incidence. Zero angle of incidence was assumed, and the reflectance factor was assumed to be 0.6, the same as used in SMAD for initial estimates<sup>156</sup>. The torque is simply this force multiplied by the difference between the center of mass and the center of area. This came out to be  $1.66 \times 10^{-5}$  Nm.

$$F = \frac{F_s}{c} A_s (1 + q) \cos(i) \quad (6.3.2)$$

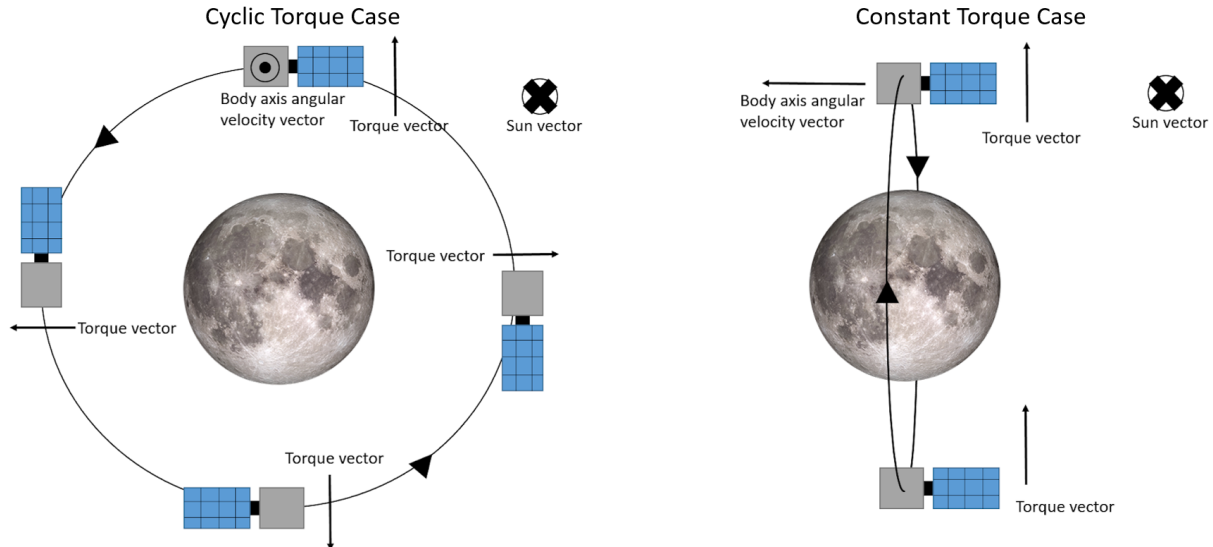


Figure 6.3.2. Cyclic vs Constant Torque Case

While SMAD states that solar radiation is cyclic for an Earth-oriented vehicle, further analysis shows this to be slightly more nuanced. As shown in figure 6.3.2, the torque is purely cyclic when the sun vector is normal to the plane of the orbit, and it is purely constant when the sun vector is parallel to the plane of the orbit. Over the course of the mission, it is expected that the sun vector will slowly alternate

<sup>156</sup> Wertz, James R., et al. *Space Mission Analysis and Design, Third Edition*. Microcosm Press, El Segundo, CA, 1999.

between these two extremes. In order to simplify analysis, the worst case scenario in which the torque is always constant was used.

### *Aerodynamics*

Negligible aerodynamics is assumed because the vehicle is in lunar orbit.

### *Gravity Gradient*

The gravity gradient torque represents the torque created by the decrease in lunar gravity as distance increases. This tends towards the minimum inertia axis of the spacecraft being oriented vertically. For the purposes of this analysis, the spacecraft is modeled as a cylinder with 300 kg of mass evenly distributed, 53 cm in radius and 142 cm in height. Note that this does not take into account the solar array, which would add inertia to  $I_z$  than  $I_y$  or  $I_x$  and thus decrease the gravity gradient torque - so this analysis is an overestimate. This represents the maximum ESPA envelope in case the mechanical team ever decides to stretch the final design, and a larger mass in order to account for potential mass growth. The equation for the gravity gradient torque is as represented in equation 6.3.3, where  $\mu$  is the gravitational parameter,  $R$  is the orbital radius,  $I_z$  and  $I_y$  are the moment of inertias of the spacecraft around its z and y axis respectively (it is assumed that  $I_y$  is approximately equal to  $I_x$ ), and  $\theta$  is the angle between the local vertical and spacecraft's z-axis<sup>157</sup>. The system will have to point 15 degrees of-axis as a mission requirement. The torque from gravity gradient comes out to  $9.88 \times 10^{-7}$  Nm.

$$T_g = \frac{3\mu}{2R^3} |I_z - I_y| \sin(2\theta) \quad (6.3.3)$$

### *Momentum Buildup*

Assuming the torque from the magnetic field is cyclic by orbit, the gravity gradient is a constant torque (the worst case scenario), and the solar radiation pressure is also a constant torque. Thus, in the worst case, total momentum buildup in one orbit is the sum of these torques multiplied by the full orbital period (because of the random direction of the lunar magnetic field, this probably accumulates to a maximum over half the orbital period but it is hard to be sure) or 0.16 Nms

The constant momentum buildup is at a rate of the gravity gradient plus SRP or  $1.76 \times 10^{-5}$  Nms/s. The spacecraft shall unload such that the maximum momentum needed to be stored by the reaction wheels (using the final 8 Nms capacity wheels) adds up to 6 Nms needed, keeping 2 Nms in the wheels as reserve for slewing for target of opportunity pointing since this allows for approximately 2.7 deg/s of rotation rate. Thus momentum unloading is done at a period of the momentum capacity divided by the torque, or every 340909 s or 95 hrs. Note that this is in the worst case in which all of the disturbances act in the axis of a single wheel, which will likely not be the case on-orbit, so the time between wheel unloadings will actually be far longer.

### *Torque Required for Disturbance rejection*

The worst-case torque required for rejecting the disturbance torques is the sum of all disturbance torques or  $1.9 \times 10^{-5}$  Nm.

---

<sup>157</sup> Wertz, James R., et al. *Space Mission Analysis and Design, Third Edition*. Microcosm Press, El Segundo, CA, 1999.

### *Sizing Force for Momentum Dumping*

Assuming 6 Nms of momentum needed to be unloaded, a 0.5 m moment arm for the thrusters, and 6 second burns (arbitrarily chosen), then 2 N of total force is required, or 1 N each assuming two thrusters are used in each axis. This requirement was passed on to the propulsion team.

### *Fuel Needed for Momentum Dumping*

Approximating a specific impulse of 220 seconds, for each 6 second burn of 2 N of thrust  $5.57 \times 10^{-3}$  kg of fuel is required every 95 hrs. This results in 92 momentum dumps per year or 0.51 kg of fuel per year for momentum dumping. Over 10 years, this is 920 thruster firings, which does not even come close to approaching thruster maximum pulse ratings. A 12% margin, moderate because the solar radiation pressure torque calculated is already a large overestimate, was added for a total 0.57 kg of fuel per year.

### *Actuator Trade Study*

Reaction wheels were the final choice of actuator. Magnetic torquers are not usable in the moon's orbit due to its random nature. Thrusters alone are not used for long-term pointing of spacecraft because they require constant fuel usage and generally have large deadbands. Control moment gyros were an option for the spacecraft, but these require a constant power input and their main advantage over reaction wheels, increased torque, is unnecessary. Two main companies were inspected, and a tradeoff between mass and momentum capacity was made (reference Appendix I.2.1 for the full study). The RW8 reaction wheel was chosen, with 8 Nms of momentum storage and 0.25 Nm of torque. The standard 4 reaction wheels configuration was chosen to allow for all-axis torque capability and single-wheel-out capability.

### *Power Required*

The reaction wheels build up from 0 to 6 Nms of momentum every 95 hrs, linearly (not taking into account cyclic disturbances, which are small). Thus the average power required is for 3 Nms of momentum, about 0.375 of the full momentum of a single wheel. The power of the reaction wheel varies approximately linearly with momentum storage, so this corresponds to about 3.75 W as the average power need over the lifetime of the spacecraft<sup>158</sup>. This will probably be a bit higher in reality as this momentum will be spread over several wheels. Note that this does not correspond with the power team's given number, which is a vast overestimate resulting from the power team using the maximum possible power of all four reaction wheels instead of average power, both of which were communicated to the power team by the GNC team.

### *Sensor Trade Study*

The sensor combination for the orbiter was chosen to be similar to the lander combination. The trade study for the lander was then expanded to cover more sensors that specifically targeted for the fulfillment of the orbiter requirements. The ST200 star tracker was chosen as it had a much greater lifetime (15+ years) and an accuracy of 30 arcseconds 3 sigma accuracy on both the roll, pitch and yaw which was sufficient for the required pointing requirements (5.3.1). The major differences between the two missions are that the sensors chosen for the orbiter had to have a much greater lifetime compared to those chosen

---

<sup>158</sup> Reaction Wheels. Blue Canyon Technologies. Accessed 6 May 2020.

[https://www.bluecanyontech.com/static/datasheet/BCT\\_DataSheet\\_Components\\_ReactionWheels.pdf](https://www.bluecanyontech.com/static/datasheet/BCT_DataSheet_Components_ReactionWheels.pdf)

for the lander. This informed the need to change the star tracker. The sun sensors chosen had an accuracy of 0.2 deg which fulfilled the required pointing requirement (5.3.1) . The IMU selected for the lander, HG1900, remained the best option available for the orbiter given its small mass and low power draw, and was therefore retained. As with the lander, redundancy was included in the sensor consideration. Four sun sensors are enough to cover the whole sky since each has a field of view of 140 degrees, however, for redundancy, two more sun sensors were included, an extra sensor was included for both the IMU and the star tracker.

### Block Diagram

The following is a block diagram showing the overall concept of operations of the system.

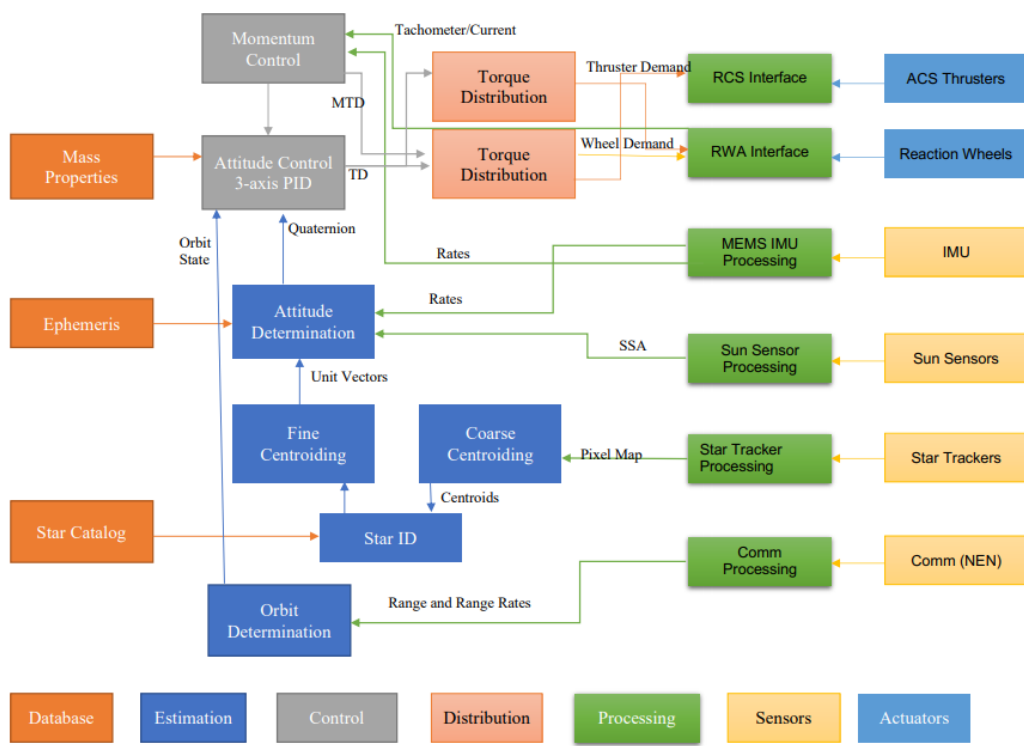


Figure 6.3.3. Block Diagram of Orbiter GNC.

### Navigational Accuracy Impact on Pointing Accuracy

For orbit determination of the orbiter, ground tracking from Earth will be used. This tracking has an accuracy of approximately 70 m in position<sup>159</sup>. Using equation 6.3.4, where  $s$  is the position error,  $r$  is the distance between the orbiter and the target of its antenna, and  $\theta$  is the angular error, the impact of this position error in the worst case (normal to the radial direction) on both the orbiter-Earth and orbiter-moon

<sup>159</sup>Mazarico, Erwan, et al. *Orbit Determination of the Lunar Reconnaissance Orbiter*. Accessed 5 May 2020. [http://www-geodyn.mit.edu/mazarico\\_LROPOD\\_jgeod11.pdf](http://www-geodyn.mit.edu/mazarico_LROPOD_jgeod11.pdf)

pointing can be determined. For a target on the lunar surface, this is 0.01 degrees, and for a target on Earth this is on the order of  $10^{-4}$  degrees, which is well within the pointing requirements imposed by communications (requirement 5.3).

$$s = r\theta \quad (6.3.4)$$

### *Detumble*

Just as in the lander, because of the moon's irregular (not dipolar) magnetic field, the spacecraft will not be using magnetic torquers to detumble. The spacecraft will thus rely on the IMU, targeting  $1 < \omega < 2$  deg/sec of angular velocity in the sun-facing axis and 0 deg/sec angular velocity in all other axes. The sun sensors will be used for initial pointing of the spacecraft in two axes, followed by the star trackers for the third axis and fine pointing in the original two axes. The specific face of the vehicle that points at the sun will depend on power and communications requirements. According to requirement 5.5.2, the maximum angular velocity of the spacecraft on separation is 2 deg/sec. This is so that the star trackers are immediately able to begin attitude determination. With the 0.25 Nm torque rating of the wheels, and assuming the spacecraft is a sphere with radius 0.5 m and a point-mass solar panel of 25 kg 1 m from the center of rotation, this results in a 0.26 deg/sec<sup>2</sup> angular acceleration, taking 7.7 sec to null out the imparted torque. This will take about 1.5 Nms of the available 8 Nms in the worst case that all of the angular velocity is imparted in the axis of a single reaction wheel, leaving plenty of momentum available for the initial pointing routine. Thrusters will not be used during the detumble operation. After detumble, the orbiter will rotate to its nominal nadir-pointing orientation.

### *Deorbit*

As the final function of the orbiter GNC, it will be required to deorbit the vehicle. To do this, it will use the reaction wheels to point the +z axis in the desired thrust axis, and then fire the -z facing thrusters, which are appropriately placed so as to produce nominally pure translation. The onboard IMU will measure this burn and cut off when the desired change in velocity has been achieved. In the event of a failure of one of the -z thrusters, the spacecraft will point the -z axis in the thrust direction and use the +z facing thrusters. Attitude control will be done with both reaction wheels and the thrusters when necessary to account for any small disturbances due to imperfect thrust alignment or placement. In the event one thruster has failed on each side, then two collinear thrusters on one of the sides will be used. In this way, the system can withstand 3 worst-case thruster failures and still de-orbit.

### *Future Work*

Now that the overall concept of operations of the guidance, navigation, and control system have been established, future work involves describing and implementing algorithms for the mission and finalizing component placement. This includes orbit determination and propagation based on Earth tracking, attitude, and IMU data. This also includes interpreting and integrating star tracker, sun sensor, and IMU data for attitude determination. The reaction wheel control algorithm must be designed, implemented, and various gains must be calculated. Finally, the exact reaction wheel configuration must be chosen to maximize momentum distribution between the wheels while retaining wheel-out capability.

### 6.3.4 Components

- RW8 Reaction Wheel<sup>160</sup> (TRL 8)  
The RW8 Reaction Wheel is a commercial off the shelf solution from Blue Canyon Technologies and will require no modifications before use. These have a lifetime of over 10 years. The minimum required wheels for full 3-axis control is three, but there is one redundant wheel included for a total of 4 wheels.
- HG1900 IMU<sup>161</sup> (TRL 9)  
The HG1900 IMU is a commercially available component that has been widely deployed for military and commercial applications. 1 IMU is needed for the mission while a second one was included for redundancy. HG1900 utilizes a universal interface box and a flex tape connector, both of which are provided by the manufacturer, Honeywell.
- ST200 Star Tracker<sup>162</sup> (TRL 9)  
These Star Trackers are flight proven with an heritage on 14 missions since 2015. The manufacturer will provide any additional interfaces if need be.
- SS-411 Sun Sensor<sup>163</sup> (TRL 9)  
The SS-411 sun sensor is an off the shelf sensor with a good heritage (22 in orbit, 58 awaiting launch)

---

<sup>160</sup> *Reaction Wheels*. Blue Canyon Technologies. Accessed 6 May 2020.

[https://www.bluecanyontech.com/static/datasheet/BCT\\_DataSheet\\_Components\\_ReactionWheels.pdf](https://www.bluecanyontech.com/static/datasheet/BCT_DataSheet_Components_ReactionWheels.pdf)

<sup>161</sup> *HG1900 Inertial Measurement Unit*. Accessed 4 May 2020.

<https://aerospace.honeywell.com/content/dam/aero/en-us/documents/learn/products/sensors/brochures/N61-1468-000-001-HG1900-InertialMeasurementUnit-bro.pdf?download=true>

<sup>162</sup> *ST 200*. Accessed 4 May 2020. <https://hyperiontechnologies.nl/products/miniatuised-star-tracker/>

<sup>163</sup> *State of the Art Small Spacecraft Technology*. Accessed 4 May 2020 .

[https://www.nasa.gov/sites/default/files/atoms/files/soa2018\\_final\\_doc-6.pdf](https://www.nasa.gov/sites/default/files/atoms/files/soa2018_final_doc-6.pdf).

## 6.4 Propulsion

The objective of the lunar orbiter propulsion system is to provide the total impulse needed for attitude control over the duration of the mission and EOL delta-V.

### 6.4.1 Key Requirements and Assumptions

#### *Requirements*

The propulsion system for the lunar orbiter shall...

- ...provide EOL delta-V of 30 m/s (Appendix J.1).
- ...be able to provide at least 15000 firings (Appendix B.2.6).
- ...be rated for the necessary propellant throughput.
- ...minimize propellant mass.

#### *Assumptions*

- Plumbing design is outside the scope of this report.

### 6.4.2 Mass and Power Budgets

#### *Mass Budget*

Component	Mass (kg)	Notes
Thrusters	3.48	
Propellant lines/valves	4.18	1.2x thruster mass
Propellant tanks	1.27	
<b>Subsystem total</b>	<b>8.93</b>	
<b>Allocated Mass</b>	<b>13.4</b>	
<b>Margin</b>	<b>4.5 (50%)</b>	

#### *Power Budget*

Component	Power (W)	Energy (Wh/orbit)	Notes
Thruster cat beds	60	0.13	Duration: 5 min every 95 hours
Thruster FCV	60	Negligible	Duration: 5 s every 95 hours
<b>Subsystem total</b>	<b>120</b>	<b>0.13</b>	
<b>Margin</b>	<b>36 (30%)</b>	<b>0.04 (30%)</b>	
<b>Total</b>	<b>156</b>	<b>0.17</b>	

### *Margins and Contingency*

The propellant line and valve mass value was based on a SMAD estimate. Likewise, fuel mass is not included in this table, but comes to 12.7 kg (Appendix J.1).

### 6.4.3 Design

#### *Thruster and Propellant Choice*

To select a thruster that would meet all of the requirements, a trade study between cold gas, electrothermal, and decomposition thrusters was conducted (Appendix J.1). The merits of cold gas thrusters are their simple design and reliability, but they are generally low  $I_{sp}$  (~70s) and require high pressure tanks to operate. The electrothermal thrusters examined had very high  $I_{sp}$  but the power requirement would well oversize the solar array. Hydrazine decomposition thrusters have good  $I_{sp}$  but dealing with hydrazine comes with added challenges. Ultimately, Hydrazine decomposition with catalyst beds was decided upon, specifically twelve 1N monopropellant hydrazine thrusters from the Ariane group (figure 6.4.1).<sup>164</sup> This unit produces a nominal  $I_{sp}$  of 220s, and has a low dry mass of 0.290kg. This  $I_{sp}$  leads to a low propellant mass of 12.7 kg (Appendix J.1). It is able to operate for 59000 cycles of momentum dump maneuvers which reaches the functional requirements of the propulsion system. The thruster is also rated for 67 kg of propellant throughput, plenty for our mission which is taking only 13 kg of fuel total. Furthermore, these thrusters have proven space heritage which demonstrates their capability and reliability for the mission. The freezing temperature of hydrazine is around 2° C, so the tanks and piping must be kept above this temperature.



Figure 6.4.1. 1N monopropellant hydrazine thruster from the Ariane Group<sup>165</sup>

#### *Tank Sizing*

The thermal range of the orbiter is 2-40C, so the tanks must be sized to properly hold the hydrazine in its most expanded case: at the max of 40C. As calculated in appendix J.1, based on a density curve of hydrazine, a minimum tank volume of 14.1L is needed. With margin for a worst case body temperature of 50C, a 15 L tank will be utilized.

<sup>164</sup>“1N Monopropellant Hydrazine Thruster,” retrieved from <http://www.space-propulsion.com/spacecraft-propulsion/hydrazine-thrusters/1n-hydrazine-thruster.html>

<sup>165</sup> Ibid.

#### 6.4.4 Drawings and Layouts

##### *Thruster Configuration*

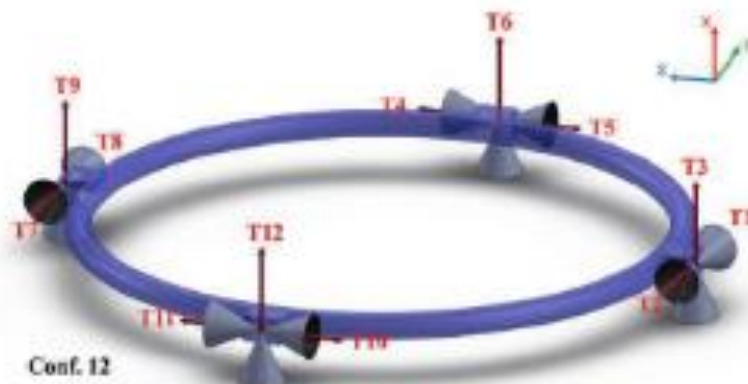


Figure 6.4.2 Configuration 12 from “A Study of Spacecraft Reaction Thruster Configurations for Attitude Control System.”<sup>166</sup>

Based on a study done by Pasand, Hassani, and Ghorbani, this configuration shown in Figure 6.4.2 offers a level of redundancy of two, thus two thrusters may be lost before attitude control is lost.<sup>167</sup> In addition, it has below average fuel consumption, well below average translational error, and low tracking error.

#### 6.4.5 Components

- 12 1N monopropellant hydrazine thrusters (TRL 9)
- 15 L Hydrazine tank (TRL 9)
- Plumbing and valves: outside scope, but COTS components should suffice.

---

<sup>166</sup> Hassani, Ali & Ghorbani, Mehrdad & Pasand, Milad. (2017). A Study of Spacecraft Reaction Thruster Configurations for Attitude Control System. IEEE Aerospace and Electronic Systems Magazine. 32. 10.1109/MAES.2017.160104.

<sup>167</sup>Ibid.

## 6.5 Power

Similar to the lander's EPS, the orbiter's EPS is equally vital for ensuring the successful operation of all components for the duration of the mission. Unlike the lander, the orbiter will have access to sunlight for a period of its orbit and can therefore use solar panels for energy production and batteries for energy storage and discharge during eclipse periods. The EPS consists of solar arrays, batteries, a shunt system for power regulation, as well as distribution assemblies. These ensure that each component receives the specific power amounts it needs to function as desired. The solar panels will be deployed from their initial stowed position along the satellite body.

### 6.5.1 Key Requirements and Assumptions

#### *Requirements*

- The solar cells shall provide a minimum power of 628 W to the load and for battery recharge at end of life (EOL).
- The battery shall provide a minimum of 620.33 W to the load at EOL.

The thermal system will only be drawing power during eclipse periods, and as its power value of 300W is significantly larger than any other subsystem, the battery must provide a much higher power output during eclipse than the solar arrays during sun time. Please refer to section 2.3.4 for the power budget table detailing power requirements for each subsystem.

#### *Assumptions*

- The solar array power outputs assume an operating temperature of 65°C.
- The solar arrays will always be angled facing the sun.
- The battery sizing assumes an operating temperature between 0°C - 30°C.

The operating temperature of the solar panels can at this point not be guaranteed to remain at 65°C, and further calculations must therefore be completed with this in mind.

## 6.5.2 Mass and Power Budgets

### *Mass Budget*

Component	Mass (kg)	Notes
Batteries	16.02	Internal harnessing and mounting included
Solar Cells	25.12	Based on a specific power of 25 W/kg <sup>168</sup>
Computer	6	
Harnessing	--	Included in margin
<b>Subsystem total</b>	<b>47.14</b>	
<b>Allocated Mass</b>	<b>70.7</b>	
<b>Margin</b>	<b>23.6 (50%)</b>	Margin accounts for harnessing

### *Margins and Contingency*

Battery mass calculations were conducted based on a flight 8S3P for the Quallion 1.43Ah cell (the cell of choice), a manufactured off-the-shelf product including internal harnessing and mounting. The 30% margin was applied to all power requirements from subsystems for the lunar orbiter.

## 6.5.3 Design

The EPS system of the orbiter will rely on solar panels for powering the load during sunlit periods, as well as to recharge the battery that has been discharged during eclipse periods. The orbital period is 2.4 hrs, of which 1.595 hrs is in sunlight and 0.805 hrs is in shade. A 28Vdc regulated bus was chosen as a higher voltage wasn't necessary, and because we will be discharging the batteries to voltages considerably below peak voltage. The thermal control will be passive during sunlit periods, and only draw power during eclipse. The battery decision was based on a tested Quallion 1.43 Ah cell produced by Enersys. During discharge it would have to provide a power output of 635.9 W to the load, including harnessing losses as can be seen in Figure 6.5.2b.

To supply 28V from a nominal cell voltage of 2.6V<sup>169</sup>, 8 series cells are required. A 60% depth of discharge (DoD) was chosen to achieve a smaller battery mass (as compared to 40% DoD), resulting in a 24% fade over the 36,500 cycles experienced by the orbiter. This yields a total capacitance of 37.78 Ah, and 27 parallel strings. Since the battery discharges over a shorter period than it charges, the charging power is lower. A charging time margin of 0.08 hr is applied to find a charging power of 380.82 W, leading to a total solar panel power requirement of 628 W.

---

<sup>168</sup>[https://ocw.mit.edu/courses/aeronautics-and-astronautics/16-851-satellite-engineering-fall-2003/projects/portfolio\\_nadir1.pdf](https://ocw.mit.edu/courses/aeronautics-and-astronautics/16-851-satellite-engineering-fall-2003/projects/portfolio_nadir1.pdf), Accessed on May 7, 2020

<sup>169</sup> Joe Troutman, Electrical Systems Lecture. Class lecture, given March 2 2020

Spectrolab XTJ-Prime Cell EOL P-V graph

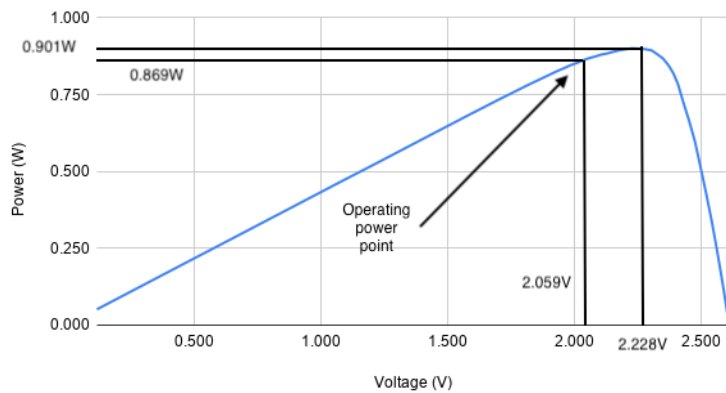


Figure 6.5.1: Power-Voltage graph for the XTJ-Prime solar cell.<sup>170</sup>

Spectrolab's XTJ-Prime cell was chosen for its superior efficiency and lower operating temperature. As described above, as can be seen in figure 6.5.2a, the power output required for the solar panels during exposure to sunlight is 628 W. 19 series cells are required for the bus voltage along with 44 parallel strings for a sufficient power output. This yields a final area of  $2.26m^2$ . Using a power density of 25 W/kg we achieve an estimated mass of 25.12 kg.

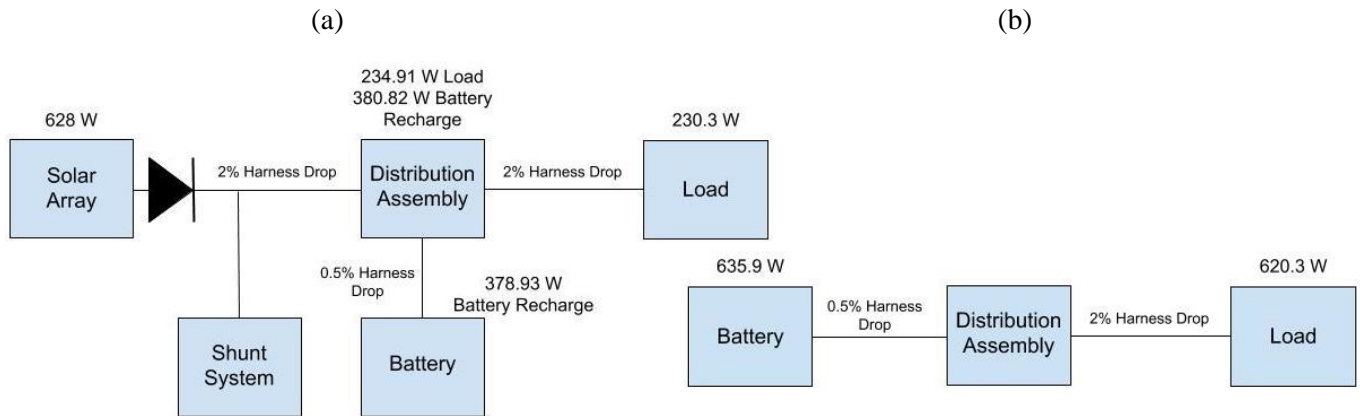
Spectrolab XTJ-Prime Cell Specifications <sup>171</sup>	
Operating Voltage (V)	2.059
Operating Current (A)	0.422
Operating Power (W)	0.869
Voltage Fade	11%
Current Fade	1%
Power Fade	11.89%
Cell Area ( $cm^2$ )	27
Max. Cell mass ( $mg/cm^2$ )	84

Table 6.5.1: XTJ-Prime Solar Cell Specifications.

<sup>170</sup> Joe Troutman, from personal correspondence on April 26th, 2020

<sup>171</sup> Spectrolab, "XTJ Prime Space Quallion Cell". Retrieved from [https://www.spectrolab.com/photovoltaics/XTJ-Prime\\_Data\\_Sheet.pdf](https://www.spectrolab.com/photovoltaics/XTJ-Prime_Data_Sheet.pdf), Accessed on May 7, 2020

#### 6.5.4 Drawings and Layouts



Figures 6.5.2a and 6.5.2b: Power layout for orbiter during sunlit period (a) and eclipse period (b)

#### 6.5.5 Components

- **836 Solar Cells (TRL 7)**  
Solar Cells will be purchased from Spectrolab, and are currently in full production and readily available off-the-shelf. It will require in-house assembly to mount and harness to the deployment mechanism.
- **216 Quallion 1.43Ah cells (TRL 7)**  
Cells can be purchased off the shelf and organised in a 8S27P pack. Assembly required for harnessing if service not offered by Enersys.
- **Regulation circuit (TRL 6)**  
Necessary to supply the variety of input voltages for different components. A shunt type regulator will be included in the regulation circuit.

## 6.6 Thermal

The thermal system on the orbiter is necessary to maintain all of the orbiter components within their operable temperatures for the duration of its time in lunar orbit. Due to frequent transitions from sunlight to umbra, the thermal subsystem will need to have states that alternately reject heat during sunlit periods and maintain internal heat during umbrae.

### 6.6.1 Key Requirements and Assumptions

#### *Requirements*

- The thermal system shall keep the interior of the orbiter between 2°C (requirement for hydrazine fuel) and 40°C (requirement for batteries). This will ensure that all orbiter subsystems remain within their operable temperature ranges for the duration of its lunar orbit, including while passing through areas of umbra.
- The thermal system shall not draw more than 300W for all operations. This is a requirement because of the maximum possible size of the solar array.

#### *Assumptions*

- Multinodal and transient analyses are outside of the scope of this report and are classified as future work.
- Lunar albedo, lunar IR effects, radiation to deep space, internal heat, and incident solar energy are assumed to account for all gains and losses of heat.
- Solar radiation is assumed to be incident on the largest possible area, in order to make worst-case calculations.
- Louvers are assumed to be baffled, such that their usage incurs no area change.
- Shape factors to the lunar surface are assumed to be equivalent to the shape factors for a sphere of the moon's average radius.

### 6.6.2 Mass and Power Budgets

#### *Mass Budget*

Component	Mass (kg)	Notes

Louvers	15	Calculated based on ROSETTA design heritage <sup>172</sup>
Coating	1	Calculated based off Kapton <sup>173</sup> , black, and green paint <sup>174</sup> weight
<b>Subsystem total</b>	16	
<b>Allocated Mass</b>	24	
<b>Margin</b>	8 (50%)	Margin is system-level

### *Power Budget*

Component	Power (W)	Energy (Wh/orbit)	Notes
Heaters	300	195	Average duration: 1800 seconds per orbit
<b>Subsystem total</b>	300	195	
<b>Allocated</b>	390	253.5	
<b>Margin</b>	90 (30%)	58.5 (30%)	Margin is system-level

### *Margins and Contingency*

The margin for the mass budget is 50% due to the likelihood of additional components being necessary.

### 6.6.3 Design

#### *Determination of Coatings*

The orbiter passes through regions of sunlight for durations of 1h30 to 2h15, depending on where the orbiter is in its lifetime. In between these regions of sunlight, regions of umbra between 3 and 50 minutes long are traversed; the longest umbra for the entire mission is a 3 hour, 15 minute eclipse period, which is the driving thermal case. Although this thermal oscillation will produce transient effects, the scope of this report includes a single-node thermal balance of the orbiter, which is also a steady-state analysis. Using a steady-state analysis allows for a worst-case estimation of this long eclipse period, since it is likely that the orbiter will not come to a steady state during these short periods of passing between sunlight and umbra.

The heat balance consists of terms for the internal heat of components, the added heating, the lunar IR radiation, the incident solar energy, and the lunar albedo. The internal heat of components was passed by the power team and was not dependent on any other factor considered here. The added heating was given a maximum of 300 W by the power team, due to maximum sizing of the solar array. The lunar IR radiation (Equation 6.6.2) is dependent on the portion of the orbiter that has a view of the lunar surface

<sup>172</sup> Domingo, Miguel, and José Julián Ramírez. “Mechanical Design and Test of ROSETTA Platform Louvres.” Proceedings of the 10th European Space Mechanisms and Tribology Symposium, September 24, 2003, 289–92.

<sup>173</sup> Caplinq. “3-mil Polyimide (Kapton) Film.” Accessed April 6, 2020. <https://www.caplinq.com/3-mil-polyimide-kapton-film-no-adhesive-pit3n-series.html?filter=26005,9871>.

<sup>174</sup> AZ Technology. “Spacecraft Thermal Control and Conductive Paints/Coatings and Services Catalog.” January 2008, iv-v.

(Equation 6.6.1), which is radiating into deep space. Percentage view of the lunar surface on horizontal and vertical surfaces was determined by using the view factors to a sphere with the same average radius as the moon, from the average altitude that the orbiter orbits<sup>175</sup>. The incident solar energy on the craft was assumed to be at a maximum, for worst-case calculations, and is calculated as in Equation 6.6.3 Finally, the lunar albedo (Equation 6.6.4) is the portion of the sun's energy that is reflected off the lunar surface, and therefore this is also dependent on the portion of the orbiter with a view of the lunar surface (Equation 6.6.1).

The temperature of the orbiter is dependent upon the emissivity and absorptivity of the coating scheme, since all other values are fixed (including the 300 W maximum heating capability). Emissivity and absorptivity are calculated by a weighted average of the two coatings. The temperature while in sunlight accounts for heat from internal heat, lunar IR radiation, incident solar energy, and lunar albedo. It also accounts for radiation of the orbiter to deep space. This balance is shown in Equation 6.6.5. When in the umbra, the orbiter will no longer experience incident solar energy or lunar albedo. However, there is the addition of extra heat from the heaters in the orbiter. This balance is shown in Equation 6.6.6. By adjusting the emissivity and absorptivity through the percentage of primary coating used, a coating scheme was selected where the steady-state temperature in the sunlit portion of the orbit was 40°C.

$$A_{lunar\ view} = 8A_{sides}f_v + A_{bottom}f_h \quad (Equation\ 6.6.1)$$

$$q_{lunar\ IR} = A_{lunar\ view}\sigma\varepsilon_{moon}T_{moon}^4 \quad (Equation\ 6.6.2)$$

$$q_{solar} = A_{max}H_{su} \quad (Equation\ 6.6.3)$$

$$q_{lunar\ albedo} = f_{albedo}A_{lunar\ view}H_{su} \quad (Equation\ 6.6.4)$$

$$T_{orbiter\ in\ sunlight} = ((q_{internal} + \varepsilon q_{lunar\ IR} + \alpha q_{solar} + \alpha q_{lunar\ albedo})/\sigma\varepsilon A_{total})^{0.25} \quad (Equation\ 6.6.5)$$

$$T_{orbiter\ in\ umbra} = ((q_{internal} + q_{heaters} + \varepsilon q_{lunar\ IR})/\sigma\varepsilon A_{total})^{0.25} \quad (Equation\ 6.6.6)$$

where  $f_v$  =view factor for surfaces vertical with respect to the moon's surface,  $f_h$  =view factor for surfaces horizontal with respect to the moon's surface,  $\sigma$  =Stefan-Boltzmann constant,  $A_{max}$  =maximum possible projected area in the direction of the sun vector (therefore worst-case),  $H_{su}$  =solar constant,  $f_{albedo}$  =lunar albedo,  $\varepsilon$  =emissivity, and  $\alpha$  =absorptivity.

Once the coatings analysis was performed for the sunlit case, where the temperature must remain below 40°C, a similar analysis was run to determine what portion of the spacecraft surface required louvers during the umbra case in order to maintain a temperature above 2°C. For this analysis, the weighted average emissivity and absorptivity values for the sunlit coating scheme was considered as one type of coating, and the umbra coating scheme was the secondary coating. A second weighted average was taken, which allowed for the determination of what percentage of the surface needed to be covered in louvers that revealed the secondary coating during umbra. With these calculations, along with the results from the trade studies discussed later in this section, the coating scheme for the sunlit portions of orbit was determined to be 96.4% Aeroglaze Z306 black paint and 3.6% AMJ-400-IG green paint. During the

---

<sup>175</sup> Karam, Robert D.. Satellite Thermal Control for Systems Engineers. United States: American Institute of Aeronautics & Astronautics, 1998. p. 76.

umbra, 52.6% of the surface will become Kapton 3mil (ITO/VDA/Kapton) because of the passive thermal-driven louvers. The umbra will also require the maximum 300W of heating. Commented MATLAB code containing these calculations can be found in Appendix L.5.

### Louvers

When choosing louvers, there are two main types to decide between: vane and pinwheel. Pinwheels louvers are less common and although thinner than vane louvers, the drawback is that the radiator only covers 5% of the surface of the mechanism, making it impractical for the orbiter's application. Because a large amount of area needs to be covered in louvers for the orbiter, the vane or "venetian blind" louvers are chosen. Although it seems this mechanism would need to be actively controlled and powered by a battery source, an ingenious application of bimetallic spring actuation flips the "blinds" or rectangular areas, when a certain temperature threshold is reached.<sup>176</sup> By changing the metals that make up the springs, the louvers can be adjusted to flip to maintain the orbiter's unique operable temperature range. The figure on the left below shows louvers that are on the ESA Rosetta spacecraft, which is similarly designed to withstand wide variations in temperature like this report's lunar orbiter.<sup>177</sup> The figure on the right shows a CAD mock-up of a Cubesat covered in louvers, showing the potential of having spacecraft with the majority of their surfaces utilizing this technology, such as the application described here.

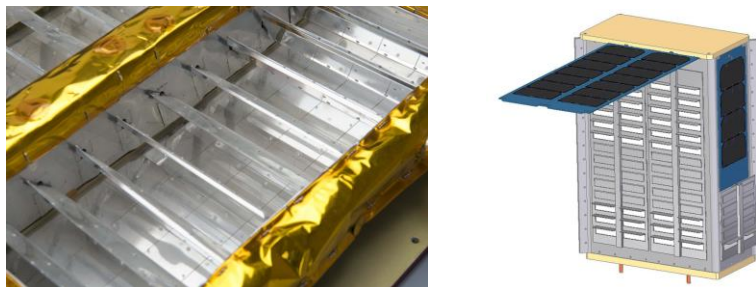


Figure 6.6.1: Rosetta louvers<sup>178</sup> (left) and Cubesat louvers<sup>179</sup> (right).

Using louvers helps minimize the power the thermal subsystem monopolizes, and lets all the power that is allocated to thermal go to powering the heaters during the extremely cold umbra sections. As mentioned in the louver coating section of this report, the louvers are covered in three coatings in total: on one side is black and green paint, which shows during the sunlit portion of the orbit, and on the other side, is Kapton, the same material used on the landers, which the louvers will change to during the umbras of the orbit.

<sup>176</sup> Gilmore, David G. *Spacecraft Thermal Control Handbook, Volume 1 - Fundamental Technologies* (2nd Edition). American Institute of Aeronautics and Astronautics/Aerospace Press: 2002.

<sup>177</sup> ESA. *Rosetta Thermal Louvres*. August 19, 2019. Accessed April 20, 2020.

<[https://www.esa.int/ESA\\_Multimedia/Images/2015/08/Rosetta\\_thermal\\_louvres](https://www.esa.int/ESA_Multimedia/Images/2015/08/Rosetta_thermal_louvres)>

<sup>178</sup> Ibid.

<sup>179</sup> NASA. *CubeSat Form Factor Thermal Control Louvers*. Accessed April 20, 2020.

<<https://technology.nasa.gov/patent/GSC-TOPS-40>>

### *Trade Study of Coatings for Orbiter*

In order to maintain a steady-state temperature of 40°C during the sunlit portions of the orbit, a coating scheme with an absorptivity to emissivity ratio of 1.04 was necessary. This ratio could not be achieved with one coating alone, so the purpose of this trade study was to choose two coatings for the orbiter. When combined in a particular ratio, one coating with an absorptivity to emissivity ratio above that desired and one coating with an absorptivity to emissivity ratio below that desired will combine to create the desired ratio.

Four coatings from two sources<sup>180,181</sup> were investigated in this trade study. Aeroglaze Z306 black paint was chosen as the base coating, since its absorptivity to emissivity ratio was already very close to the desired 1.04. For the secondary coating, the main consideration was whether its absorptivity to emissivity ratio was also close to 1.04. This maximizes the amount of the secondary coating necessary, which functionally means that it is more easily distributed over the entire surface of the craft. The current calculations are unable to account for multi-nodal features, and so it is crucial that minimizing any areas of possible heat variation due to coating differences be accomplished in this manner. The second most important consideration was whether the material was available at the desired TRL. With these two factors in mind, AMJ-400-IG green paint was chosen as the secondary coating.

In order to achieve the necessary absorptivity to emissivity ratio, a coating scheme of 96.4% Aeroglaze Z306 black paint and 3.6% AMJ-400-IG green paint was chosen.

### *Trade Study of Coatings for Louvers*

The trade study of coatings for the lander was repurposed for use with the louvers. The louvers' required characteristics were very similar to that of the lander coating. In order to maintain heat while in the umbra, a very low emissivity coating was needed for the louvers. Kapton 3mil (ITO/VDA/Kapton) was chosen due to having the lowest emissivity of 0.02. Secondarily, it is a very robust material in the space environment, which lays to rest any fragility concerns stemming from the fact that the louvers are moving. See section 5.7.3 for more details on the lander trade study.

---

<sup>180</sup> Kauder, Lonny. "Spacecraft Thermal Control Coatings References." NASA, December 2005.

<sup>181</sup> Choueiri, Edgar. "Spacecraft Thermal Control." MAE 432 Lecture Notes, 2020.

#### 6.6.4 Components

Below is a list of the components needed for the orbiter.

- Aeroglaze Z306 Black Paint (TRL 9)  
This paint has legacy flying on several of NASA's missions including the Geostationary Operational Environmental Satellites.<sup>182</sup> No modifications of this established coating will be necessary.
- AMJ-400-IG Green Paint (TRL 7)  
This paint has been demonstrated on the Materials International Space Station Experiment<sup>183</sup>, but has limited information on whether it has yet been used on a spacecraft. However, other similar green paints have been developed and used proprietarily by NASA.<sup>184</sup> Some development would be required before flight.
- Kapton 3mil (ITO/VDA/Kapton) (TRL 9)  
Coating Kapton with various thin layers of metals is an established method for creating coatings of varying thermal properties. Design heritage derives from multiple international missions. For example, VDA-coated Kapton MLI was used in ESA's CHEOPS<sup>185</sup> and ITO/SiOx/VDA/Kapton was selected for NASA's Solar Plus Probe MAG Sensor<sup>186</sup>. No modifications of this established process will be necessary.
- Louvers (TRL 9)  
The louvers for this orbiter would have to be manufactured specially. Coatings, sizing, and the bimetallic springs are a few of the factors that would be tailored to fit the orbiter's operable temperature range and structural needs. Louvers such as the ones planned for this mission have flown before (as mentioned previously the Rosetta spacecraft is an example of this), and so have the required legacy to be considered for use in a lunar orbiter.

---

<sup>182</sup> Persky, M. J. "Review of Black Surfaces for Space-Borne Infrared Systems." *Review of Scientific Instruments* 70, no. 5 (1999): 2193–2217. <https://doi.org/10.1063/1.1149739>.

<sup>183</sup> "Spacecraft Thermal Control and Conductive Paints/Coatings\* and Services Catalog ." AZ Technology, January 2008, 16.

<sup>184</sup> Kauder, Lonna. "Spacecraft Thermal Control Coatings References." NASA, December 2005.

<sup>185</sup> Melendo, Ignacio, and Romain Peyrou-Lauga. "CHEOPS Platform Thermal Architecture." *46th International Conference on Environmental Systems*, July 10, 2016.

<sup>186</sup> Choi, Michael. "Solar Probe Plus MAG Sensor Thermal Design for Low Heater Power and Extreme Thermal Environment." *45th International Conference on Environmental Systems*, July 12, 2015.

## 6.7 Command & Data Handling

The command and data-handling characteristics of the orbiter are virtually identical to those of the lander, save a more powerful communications board, as the requirements of the former are essentially undefined and both are intended for spacecraft of approximately the same size and complexity.

### 6.7.1 Processor

#### *Key Requirements and Assumptions*

Requirements are grafted from the previous section. Though the spacecraft no longer has the computational load of the science payload, its communications requirements are higher, and the complexity of most other subsystems is approximately constant.

As before (in Section 5.8.1):

#### *Requirements*

The C&DH system shall:

- perform all computation required to meet other subsystem goals
- manage all spacecraft data: processing and storage of payload outputs, encoding for transmission, and management of ADCS and other sensor data.

#### *Assumptions*

- The RAD750's 260 MIPS performance is sufficient for the purposes of both the orbiter:
  - We have no defined performance requirements from ADCS or communications for the orbiter.
- Electronic components of other subsystems are capable of interface via Spacewire, RS422, or LVDS
- Communications performance requirements are met by the Aitech S910

## 6.7.2 Mass and Power Budgets

Note that the C&DH system is listed within the power section in the general mass and power requirements.

### *Mass Budget*

Component	Mass (kg)	Notes
RAD750 SBC <sup>187</sup>	0.549	-
RTIMS Flash Memory <sup>188</sup>	0.064	4 x 8 gb
3U-160 Compact PCI Board <sup>1</sup>	0.500	-
RADNET SWP-RB4 ASSP Chip Bridge <sup>1</sup>	0.200	< 100g + additional packaging
Aitech S910 <sup>189</sup>	0.318	Dependent on number of I/O ports
<b>Subsystem total</b>	<b>1.613</b>	
<b>Allocated Mass</b>	<b>6</b>	
<b>Margin</b>	<b>4.369 (72%)</b>	Margin accounts for harnessing, structure and additional, unforeseen, electronics

### *Power Budget*

Component	Power Consumption (W)	Notes
RAD750 SBC <sup>1</sup>	10.8	
RTIMS Flash Memory <sup>2</sup>	3	4 x 8 gb
3U-160 Compact PCI Board <sup>1</sup>	3	
RADNET SWP-RB4 ASSP Chip Bridge <sup>1</sup>	2.5	
Aitech S910 <sup>3</sup>	2.14	Dependent on number of I/O ports configured and operational
<b>Subsystem total</b>	<b>19.3</b>	
<b>Allocated Power</b>	<b>29.75</b>	
<b>Margin</b>	<b>10.45 (35%)</b>	Margin for cable losses and additional boards required for communication beyond the scope of the lander (requires further research)

<sup>187</sup> See BAE Space Web site.

<sup>188</sup> See 3D-Plus.com.

<sup>189</sup> See Aitech Web site.



### 6.7.3 Design

Because the orbiter is only in the earliest iterations of development, its systems are identical to those of the lander save the Aitech S910, an interface board for communications. The S910 is not suitable for use on the lander. The S910's performance unnecessarily exceeds communications requirements of the lander at the cost of significant mass and power requirements. Further design of the C&DH will include complete definition of data and computation requirements; specification of the wiring between the C&DH system and the components of other subsystems with which it interfaces; selection or manufacture of an enclosure for the boards; and optimization of the orbiter electronics as additional system requirements materialize.

### 6.7.4 Components

- RAD750 (TRL 9)
- RTIMS Flash Memory (TRL 9)
- 3U-160 Compact PCI Board (TRL 9)
- RADNET SWP-RB4 ASSP Chip Bridge (TRL 9)
- Aitech S910 (TRL 9)

## 6.8 Communications

The orbiter communications system relays data from the science payload and monitors the position and health data of the lander and the orbiter. After the lunar mission is complete, the orbiter will remain in operation for ten years as a communication satellite.

### 6.8.1 Key Requirements and Assumptions

#### *Requirements*

The communications system shall...

- ...provide an orbiter to Earth connection via a parabolic reflector antenna and Ka-band radio signals.
- ...support 40 Mbps uplink and downlink on the orbiter-Earth connection.
- ...store information (via the flight computer) that becomes available between line of sight passes.

The orbiter to Earth data rate was chosen as the maximum possible data rate with the available link budget in order to support other missions that may be relaying from places other than the lunar South Pole, and have a higher data requirement. The Earth to orbiter data rate was chosen to match the downlink rate, as it is unlikely that missions using the Erebus communications satellite will require an uplink larger than their downlink. Based on previous NASA missions, a data rate of 40 Mbps seems reasonable.<sup>190</sup>

#### *Assumptions*

- The specific communications software is outside the scope of the course and is therefore classified as future work.
- The incorporation of a low gain antenna was suggested in feedback from the CDR, but due to time constraints that has been deferred to future work (see section 9.1), as it presents an interesting opportunity.
- The orbiter and Earth will have a connection pattern of 1 hour and 45 minutes in line of sight and 30 minutes of no line of sight per orbit.
- The parabolic reflector antenna and Ka-band receiver and transmitter will be custom made, so mass and power estimates are made using data from existing missions.
- The communications system experiences a noise temperature of 290 K<sup>191</sup>
- The average illumination factor is 70°<sup>192</sup>

---

<sup>190</sup> “PDS: Instrument Information.” NASA, NASA, Mar. 2020, pds.nasa.gov/ds-view/pds/viewInstrumentProfile.jsp?INSTRUMENT\_ID=RSS&INSTRUMENT\_HOST\_ID=LRO. Accessed on April 30, 2020.

<sup>191</sup> Ho, Christian, et al. “Atmospheric Noise Temperature Induced by Clouds and Other Weather Phenomena at SHF Band (1-45 GHz).” *Atmospheric Noise Temperature Induced by Clouds and Other Weather Phenomena at SHF Band (1-45 GHz)*, 11 Aug. 2005, descanso.jpl.nasa.gov/propagation/Ka\_Band/JPL-D32584\_1.pdf. Accessed on April 23, 2020.

<sup>192</sup> Paluszek, Spacecraft Communications, Slide 35, Mae 342 2020, Accessed on May 6, 2020.

A low gain antenna will be included on the orbiter as a backup in case the HGA has a failure. However, the inclusion of this antenna would require significant changes from the communications, thermal, power, and mechanical teams, so its inclusion was not possible in this report. It is classified as future work.

## 6.8.2 Mass and Power Budgets

### *Mass Budget*

Component	Mass (kg)	Notes
Patch Antenna	0.4	Modeled after Endurosat product
S-band Transmitter	0.25	Modeled after Endurosat product
S-band Receiver	0.22	Modeled after Endurosat product
Parabolic Reflector Antenna	3	Estimate from similar antenna <sup>193</sup>
Ka-band Transmitter	0.3	Modeled after Endurosat product
Ka-band Receiver	0.3	Modeled after Endurosat product
Master Cable	3	Connects all components
<b>Subsystem total</b>	<b>7.47</b>	
<b>Allocated Mass</b>	<b>11.2</b>	
<b>Margin</b>	<b>3.74 (50%)</b>	Margin accounts for uncertainty in parabolic reflector weight and mounting materials

### *Power Budget*

Component	Power (W)	Energy (Wh)	Notes
S-band Transmitter	7.20	11,984	Active during line of sight with lunar south pole for full 10 years
S-band Receiver	2	3329	Active during line of sight with lunar south pole for full 10 years
Ka-band Transmitter	30	2,044,000	Active during line of sight with Earth for full 10 years
Ka-band Receiver	10	681,333	Active during line of sight with Earth for full 10 years
<b>Subsystem total</b>	<b>49.2</b>	<b>2,740,646</b>	
<b>Allocated</b>	<b>60</b>	<b>3,151,743</b>	
<b>Margin</b>	<b>10.8 (18%)</b>	<b>411,097 (18%)</b>	Margin accounts for increased power consumption as equipment ages

<sup>193</sup> “PDS: Instrument Information.” NASA, NASA, Mar. 2020, pds.nasa.gov/ds-view/pds/viewInstrumentProfile.jsp?INSTRUMENT\_ID=RSS&INSTRUMENT\_HOST\_ID=LRO. Accessed on April 17, 2020.

### *Margins and Contingency*

A 30% margin is needed for the mass requirement of the orbiter, since these components will be custom made. The orbiter power requirements are taken from a similar communications system, and are given an 18% margin to account for decreased efficiency as the components age over the 10 years of operation.<sup>194</sup>

### 6.8.3 Design

#### *Ka-Band System*

After consideration of X-band, UHF-band, Ka-band, and lunar lasers, Ka-band was selected as the best option for the orbiter to earth connection due to its substantial bandwidth and its current and upcoming use by NASA.<sup>195</sup> <sup>196</sup> This will allow future missions to transmit substantial data through the orbiter connection, though it is not expected that south pole lunar missions will require it. However, since the solar array provides the orbiter with substantial power, the higher power requirement of Ka-band is not a problem, and may provide useful connections for non-polar lunar missions.

To communicate with Earth, the orbiter will use a parabolic reflector antenna, a Ka-band receiver, and a Ka-band transmitter. The orbiter will communicate with the TDRS network, which will then relay to a dish antenna in New Jersey.<sup>197</sup> The parabolic reflector antenna is left hand circularly polarized with a gain of 37 dB and a diameter of 30 cm. This diameter was determined by balancing the available space on the orbiter and the required antenna size as dictated by the link budget. The Ka-band receiver and transmitter will be custom made, but reasonable estimates on their mass and power requirements can be made from data from similar missions.<sup>198</sup>

The antenna will be mounted on a two-axis gimbal on the Earth-facing side of the orbiter to allow communication during the entire line of sight period.<sup>199</sup> Components will be connected to each other and to the flight computer via a master cable.

#### *Ka-Band Link Budget*

While creating the link budget, the data rate to Earth was maximized in order to support future missions. The uplink was then matched to this, as it is unnecessary for the type of mission Erebus anticipates supporting to have an uplink that exceeds the downlink capacity. A bitrate of 40 Mbps is the maximum downlink, so both uplink and downlink are 40 Mbps. This will allow one Erebus sample to dowlink to Earth in under a second.

---

<sup>194</sup> “PDS: Instrument Information.” NASA, NASA, Mar. 2020, pds.nasa.gov/ds-view/pds/viewInstrumentProfile.jsp?INSTRUMENT\_ID=RSS&INSTRUMENT\_HOST\_ID=LRO. Accessed on April 17, 2020.

<sup>195</sup> “Spacecraft Subsystems IV- Communications and Power.” *Space Mission Engineering the New SMAD*, by James R. Wertz et al., Microcosm Press, 2011, p. 639.

<sup>196</sup> Miranda, Félix, et al. “A Review of Antenna Technologies for Future NASA Exploration Missions.” NASA, Mar. 2020, ntrs.nasa.gov/archive/nasa/casi.ntrs.nasa.gov/20110000847.pdf.

<sup>197</sup> See 7.3 for more details.

<sup>198</sup> “PDS: Instrument Information.” NASA, NASA, Mar. 2020, pds.nasa.gov/ds-view/pds/viewInstrumentProfile.jsp?INSTRUMENT\_ID=RSS&INSTRUMENT\_HOST\_ID=LRO.

<sup>199</sup> See 6.2.2-3 for more details.

The resulting link budget is -129 dB for downlink and -86 dB for uplink.<sup>200</sup> Again, though these margins are small, they are sufficient for the types of missions Erebus will support.

#### *Ka-Band Pointing Requirements*

The directional antenna has a  $\theta_{3dB}$  value of  $2.33^\circ$  and an allowable pointing error of  $0.2^\circ$ .<sup>201</sup> The radiation pattern of this antenna is shown below, although the specific values are slightly different.

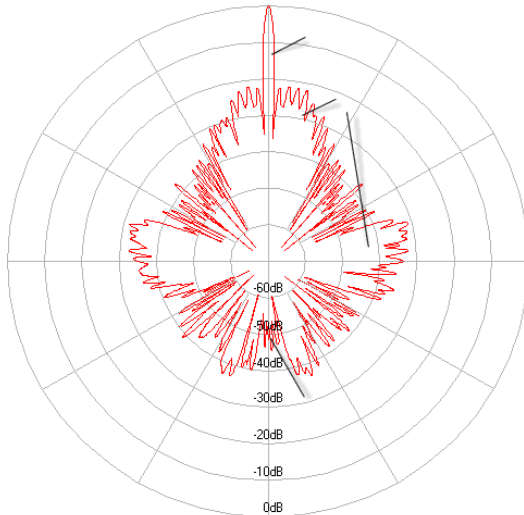


Figure 6.8.1: Radiation pattern for a left hand circularized parabolic reflector antenna.<sup>202</sup>

#### 6.8.4 Components

- Parabolic Reflector Antenna (TRL 6)

The parabolic reflector antenna will be built completely in-house, founded on existing designs from previous lunar missions.

- Ka-band Transmitter (TRL 7)

The Ka-band transmitter will be built completely in-house, founded on existing designs from previous missions.

- Ka-band Receiver (TRL 7)

The Ka-band receiver will be built completely in-house, founded on existing designs from previous missions.

---

<sup>200</sup> See Appendix N for calculations.

<sup>201</sup> See Appendix N for calculations.

<sup>202</sup> <https://www.radartutorial.eu/06.antennas/Parabolic%20Antenna.en.html>

# 7. Systems Integration

## 7.1 Reliability, Survivability and Safety

The Erebus Mission has three major segments: separation, lander operations, and orbiter operations.

### 7.1.1 Separation

The lander utilizes a MkII Lightband to separate from the ESPA ring. The Lightband uses a motor and spring to release the lander without the use of explosives. Eliminating explosives reduces possible damage to the lander or the orbiter during separation. Unlike explosives the Lightband does not have easily built in redundancy, but it has operated successfully in flight over 65 times proving reliability. In addition, it can be tested more thoroughly than explosives. In the event that lander separation fails, the OMV will proceed to enter stable lunar orbit with the lander attached, and the orbiter would then separate as planned.

### 7.1.2 Lander

#### *Thruster*

A mission threatening failure would be one that prevents the lander from being able to land. Therefore issues with the thrusters or the landing mechanism pose the greatest threat to the mission. There are four main thrusters providing a total of 800 N of thrust. If one thruster failed, the remaining three thrusters could still provide enough thrust to slow and land the lander with additional stabilization from the RCS thrusters.

#### *Landing Mechanism*

If there is failure in landing gear extension, the margins for landing are greatly reduced. The lander will cut into fuel margins to land slower and depend less on the legs for final deceleration. Without one of the legs, the lander will also have less stable footing, but the suspension and anti-torque spikes will allow the lander to hold its position and do some science and data collection.

#### *Impact Damage*

Even without failures to the landing system, there is a risk of damage on impact. To mitigate risk of damage on landing there are several ground sensors. The legs also have sacrificial material to provide dampening up to 5 m/s which is 3 times the maximum expected final descent velocity.

#### *Science Instruments*

Once successfully landed, several circumstances could prevent performing the science analysis. The largest possible failure would be if the drill does not operate. The drill has been tested on faux lunar regolith and will be tested additionally before launch to ensure that it is operational. However, due to weight and space constraints redundant drills are not possible. The science data from the mission could be rendered unusable if the instruments are damaged or contaminated. These risks will be mitigated by following testing and decontamination procedures during assembly.

### *Communications*

The last major potential failure is with communications. This is an additional reason to include a low gain antenna in addition to the already present HGA (as described in section 6.8.3), as that would mean communications can continue if one of the two antennas fail. Additionally, the communications system will remain active for a few hours after the science payload turns off. The lander will transmit data when the orbiter is overhead as it gathers data, but will also have at least one final pass after the science payload is done and before the lander runs out of power. This final pass gives the lander an extra chance to transmit data. If there are still issues in data transmission, the lander can be put into safe mode to extend its life long enough for it to reach another communication window and retry sending the data.

### 7.1.3 Orbiter

#### *Radiation*

The greatest threat to the long term survival of the orbiter is radiation in the form of SPE and GCR. With no shielding, the orbiter will be doused with over 100 Mrad over its lifetime. The computer and other electronics are rated to 1 Mrad. With Al shielding of 10 mm, the radiation is reduced to 550 Krad. To save on weight the shielding will not completely surround the electronics. Instead shielding will be between the electronics and the side of the orbiter facing away from the moon. In addition, there will be some additional spot shielding around more delicate components.

#### *Solar Panels*

If the solar panel fails to deploy, then the orbiter will run out of power very quickly. However, the solar panels deploy automatically when the restraining wire is broken by one of two redundant heating elements. If the solar panels positioning motor breaks, some of the functionality can be taken over by the reaction wheels.

#### *Control Systems*

The orbiter has a redundant reaction wheel and multiple redundant thrusters so can survive a reaction wheel failure or up to two thruster failures.

### 7.1.4 Safety

No humans are involved after launch. The EOL plan for the orbiter ensures that it will not pose a danger to other manned or unmanned missions. Both the lander and the orbiter will avoid other current and forecasted moon missions by a wide margin.

## 7.2 Parts/Processes

A major consideration in making the mission cost-effective and reliable was to use off-the shelf parts and modules for various sections of the mission. The parts used have been outlined in the subsections above. In terms of manufacturing, the ease of creating the parts was also a consideration in designing some of the mechanical parts and choice of material for the structure (Aluminium 6061). Manufacturing times and delays have been accounted for while planning the schedule of the mission. In terms of components and subsystem integration or assembly, see section 7.5.

## 7.3 Ground Systems Integration

The ground system communications system is a key part of the mission that allows data to be transmitted from the TDRS network to Earth, and then to Princeton University for analysis. The main goals of this system are relaying data from the science payload and monitoring the position/health data of the lander and orbiter. After the Erebus mission is complete, this connection will remain open for 10 years, though it is expected that many future missions will direct their data elsewhere.

In the case that more communications time is needed with the lander, the GN&C system has a 15° off-axis pointing capability. This will allow the orbiter to provide greater communication windows with on-surface missions, thereby allowing for more data transfer. This can be used to accommodate a wider variety of lunar missions with their respective data link requirements, and it provides generous margins for the data transmission of this mission. It does require active mission control from a ground station on Earth, as these off-axis pointing maneuvers will only be executed if demanded by ground support.

### 7.3.1 Key Requirements and Assumptions

#### *Requirements*

- The ground system shall support a connection from TDRS to the satellite antenna in Wall Township, NJ for a 10 year period.<sup>203</sup>
- The ground system shall support an uplink bitrate of 40 Mbps, which is expected to be sufficient for future missions using the Erebus orbiter.
- The ground system shall be able to maintain a connection to the orbiter for the 1 hour and 45 minutes of line of sight each orbit.

The Wall Township antenna is a parabolic reflector with an 18 meter diameter and 6 kW of transmission power. This antenna is sufficient to support the desired bitrate, as seen in the link budget analysis.<sup>204</sup>

The TDRS system supports Ka-band and will offer coverage for the Erebus orbiter as long as it is not behind the moon. This will allow for a Princeton to orbiter connection for the full time that the orbiter has a line of sight with Earth.

#### *Assumptions*

- The specifics of the communications software/data processing details are outside the scope of this report and are classified as future work.

---

<sup>203</sup><https://www.princeton.edu/news/2016/08/25/cold-war-era-satellite-dish-restored-princeton-scientists-becomes-teaching-tool>

<sup>204</sup> See Appendix N for calculations.

## 7.4 Mass Properties Details

### 7.4.1 Lunar Lander

To compute the center of mass of the lander, the packaging mockup was used to find the coordinates of the geometric center of all components greater than 2 kg in mass, in relation to the center of the top surface of the structure. Then, the center of mass was computed for two scenarios (propellant tanks full, representing the first part of the mission, and propellant tanks empty, representing the final phase of the mission) using the following formula:

$$\vec{r}_{cm} = \frac{1}{M} \sum_{i=1}^n m_i \vec{r}_i \quad (\text{Equation 7.4.1})$$

where  $\vec{r}_{cm}$  is the position of the center of mass,  $M$  is the total mass,  $n$  is the total number of components, and  $m_i$  and  $\vec{r}_i$  are the mass and position of an individual component.

Parameter	Value when Full	Value when Empty	Units
COM distance from top surface	46.4	62.0	cm
COM distance from ESPA attachment plane	20.4 (51.8)	26.5 (67.3)	in (cm)
COM offset from central axis	0.21	0.59	cm

Table 7.1: Lunar lander center of mass.

The ESPA attachment plane is 2.1" above the top surface of the lander. As shown in Table 7.1, the lander's center of mass drops by more than six inches as the propellant is depleted. This is due to the placement of the propellant tanks closer to the top surface of the lander, and makes the center of mass closer to the ESPA attachment plane at launch (in order to reduce the total moment) and closer to the lunar surface when landing (in order to provide stability).

In terms of moment of inertia, calculations involving the GNC subsystem used abstracted models of the lander as an ellipsoid or cylinder, with uniformly distributed mass and taking up the full ESPA volume envelope (see Section 5.4). This results in a greater moment of inertia about all three axes than the actual model of the lander, ensuring that the GNC subsystem components have a significant additional margin to control the motion and attitude of the spacecraft.

### 7.4.2 Lunar Orbiter

Because a detailed packaging layout has not yet been made for the orbiter, detailed center of mass and moment of inertia calculations are not yet feasible. As with the lander, the GNC subsystem used an abstracted model for calculations, which included consideration of the effects of the large solar array, including its offset from the central axis of the orbiter (for moment of inertia) and its area and moment arm in regards to solar radiation pressure. Treating the orbiter in this manner results, as in the case of the lander, in the GNC subsystem's capabilities having a significant margin. See Section 6.3 for more details.

## 7.5 Qualification

This section is not intended to provide a detailed, in-depth analysis of all spacecraft qualification steps. Rather, it serves to provide a high-level overview of general testing steps in the development of the Erebus Mission's spacecraft. Further qualification details are classified as future work (Section 9.1). In the subsections below, some important system-specific tests have been outlined, but generally, most subsystems will follow an integration and testing procedure as outlined in Figure 7.5.1, stemming from NASA's Goddard Space Flight Center. The remainder of this section is based on the guidelines outlined in one of their documents.<sup>205</sup>

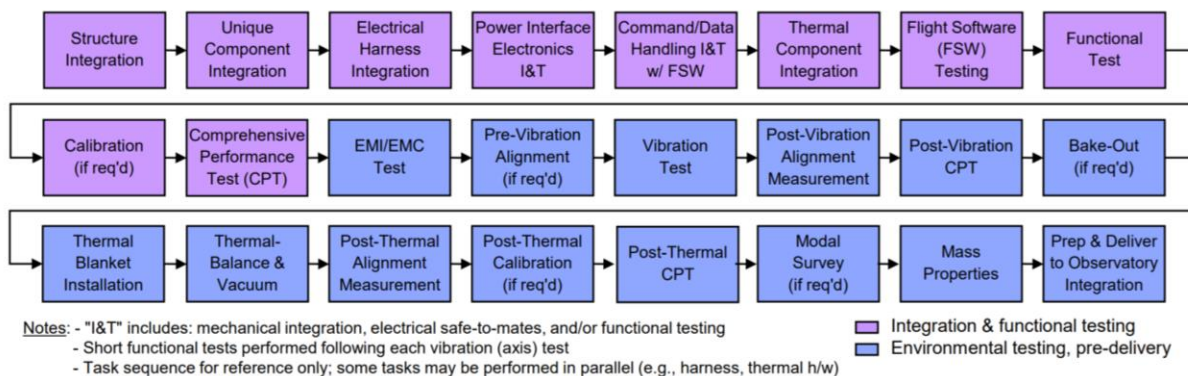


Figure 7.5.1: General Subsystem Integration and Testing Procedure.<sup>206</sup>

### 7.5.1 Components Testing

All components will be tested for resonant frequency to confirm that launch vehicle vibrations will not damage the component, usually 20 - 20,000 Hz at a random spectrum (SMAD3). All components will be tested in temperature cycling 11 °C beyond their operational extremes (SMAD3) to confirm that they will survive the space environment. The lander components will undergo shock testing to determine maximum impacts they can survive.

Subsystems will receive additional testing before being integrated into the overall system.

- Structural tests: Structural tests confirm that parts are strong enough to withstand all the stresses of the mission. There will be static, modal and resonant frequency tests of the frame and the lander legs. The fuel tanks will undergo pressure testing.
- Deployment tests: Deployment tests confirm that compact components can safely expand. The landing system, solar arrays, antenna and boom will be tested. The drill will be tested to confirm extension and functionality on simulant lunar regolith.
- Separation Tests: The MKLightband for orbiter and lander will be tested to the extent possible, to make sure it functions and will not damage other components.
- The antennas will be tested for signal strength, reception, and tracking.

<sup>205</sup> Wright, Michael. "Flight Systems Integration and Test", for NASA/Goddard Space Flight Center. Retrieved from <https://ntrs.nasa.gov/archive/nasa/casi.ntrs.nasa.gov/20110022499.pdf>. Accessed on May 11, 2020.

<sup>206</sup> Ibid.

- The ADCS will be tested to calibrate sensors and confirm functionality of the control system in different modes
- Contamination: As contamination is a potential risk for the science payload functionality, throughout the process all contamination must be closely monitored and avoided where possible.

### 7.5.2 Assembly Testing

The assembled craft will undergo additional testing. Crucially, the craft's power bus will be thoroughly tested generally, and specifically for leaks, vibrations and environmental compatibility. Apart from all hardware tests, another essential component of the qualification procedure is the execution of flight software testing, as well as the different operational modes. Before deployables are installed, all subsystems will be tested under normal conditions followed by testing in a temperature chamber while thermal cycling.

Once deployables are installed, the craft will undergo mass properties testing, as well as vibration and acoustic tests in an acoustic chamber to simulate launch conditions. Deployables will be tested to confirm functionality and that they do not interfere with each other. There will be additional subsystem tests with the deployables extended, and then the deployables will be stowed.

Finally the craft will undergo thermal vacuum testing in launch, transit, landing, and orbit configurations. After all tests are completed, the orbiter and lander will be carefully shipped to the launch facility.

### 7.5.3 Launch Vehicle Integration Testing

The full assembly will be tested with the launch vehicle attachment surfaces to confirm that everything fits and can detach properly at the correct time. At the launch site, the spacecraft will undergo rigorous final testing to make sure there was no damage during transit.

Upon arrival, the craft will first undergo visual inspection for damages during transit. Next it will be checked for leaks. There will be final subsystem tests. Propellant will be loaded and the craft.

Mating interfaces will be checked and then the lander and orbiter will be loaded into the ESPA ring. The ESPA ring will be loaded into the shroud and loaded onto the launch vehicle. The batteries will be charged on the launch pad and there will be a final test of the computer electronics.

## 7.6 Cost & Schedule

### 7.6.1 Mission Development Cost Estimation

To determine the total development cost for the Erebus mission, several components must be considered individually. The calculations used to estimate the development costs for both the lander and orbiter use the following equation from the new SMAD<sup>207</sup>:

$$Y = 2.829 \times \text{Dry mass}^{0.457} \times \text{Power}^{0.157} \times 2.718^{0.171 \times \text{Data\%}} \times \\ 2.718^{0.00209 \times \text{Life}} \times 2.718^{1.52 \times \text{New}} \times 2.718^{0.258 \times \text{Planetary}} \times \\ \frac{1}{2.718^{0.0145 \times (\text{Year} - 1960)}} \times 2.718^{0.467 \times \text{InstrComp\%}} \times \frac{1}{2.718^{0.237 \times \text{Team}}} \quad (\text{Equation 7.6.1})$$

Most of these variables can readily be filled in with values from this report, but some of them require an explicit justification here. All the values, as they were used in the equation above, can be found in Appendix O: Cost Estimation. The main factors that require justification are the percentage of new technology and the component complexity. While both the lander and orbiter rely heavily on heritage and off-the-shelf solutions, the lander has a higher percentage of new technology (which includes how much existing technology needs to be modified) of 50%, while the orbiter requires less new technology and was therefore given a 30% estimate. One factor that contributes to these variables being estimated on the lower side is the fact that the lander and orbiter share certain parts of their design, such as the main structure and the separation system.

In terms of component complexity, most of the components on the lunar lander have a low complexity, and many of its payload components have been flight-proven. However, since a dedicated payload laboratory will need to be developed, the lander has an associated overall 50% component (median) complexity. The orbiter has no such instrument complexity and was estimated to have a 20% factor (below median) of complexity.

The cost estimation for the OMV is a lot more difficult. Part of the development cost will be for Moog, and a significant part of the craft has been readily developed, but the OMV does require some Erebus-specific modifications that will bring with them significant costs. To determine an overall cost estimate, the OMV development costs were simply determined using a ballpark estimate.

In terms of launch cost, the following scenarios are reflected in the estimate: A co-primary payload launch opportunity on a Falcon 9, with a dropoff at GTO, where the minimum launch costs represent the ideal scenario (in which the two open OMV ESPA slots are taken by rideshares), the maximum launch costs represent a worst-case scenario in which no rideshares join the launch. Altogether, the results of the Erebus Mission cost estimation can be found in Table 7.6.1, and they come out to an estimated total cost of \$255M ± \$80M.

---

<sup>207</sup> “Cost Estimating” *Space Mission Engineering the New SMAD*, by James R. Wertz et al., Microcosm Press, 2011, p.302

Component	Cost (Millions USD)
Erebus lander development & production cost	69 ± 28
Erebus orbiter development & production cost	61 ± 24
OMV modification & production cost	60 ± 20
Launch cost to GTO with Falcon 9	15-30
<b>Total Erebus Mission Cost (including +20% overhead)</b>	<b>255 ± 80</b>

Table 7.6.1. Overview of Erebus Mission costs.

## 7.6.2 Erebus Mission Development Schedule

This section is not intended to go into a high level of detail on the development timeline for the Erebus mission. Rather, its main function is to provide a very rough outline of what a potential spacecraft development timeline could look like, with lander and orbiter development happening in parallel. This outline is represented in Figure 7.6.1, with a preliminary launch window in Q2 of the year 2025. The timeframes in this sequence are based on estimates from the AIAA Aerospace Design Engineers Guide.<sup>208</sup>

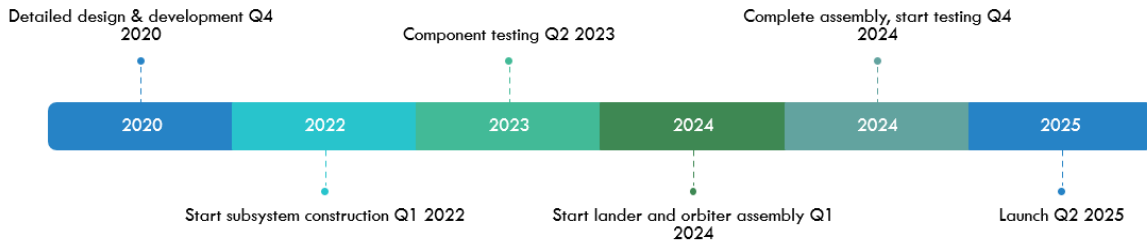


Figure 7.6.1. Preliminary Erebus Mission development timeline.

<sup>208</sup> AIAA *Aerospace Design Engineers Guide*, 6th ed., ed. by Charles R. Dauwalter, Draper Laboratories and E. Russ Althof. (American Institute of Aeronautics and Astronautics, 2012), pp. 52-55

# **8. Project Management**

## **8.1 Guiding principles**

The mission we tackled was ambitious. To achieve this goal we needed to function as a cohesive unit of 23 members moving towards the same goal. During the initial phase of our semester, we brainstormed as a team in coming up with our team values which proved extremely helpful to look back, especially during difficult times during the course of this project. Our values consisted of three major components - Transparency, Communication and Accountability:

- *Transparency* - To ensure that there is no miscommunication we ensured all communication took place through the designated slack channels resorting to one to one communication only when necessary.
- *Communication* - Represented by close to 10000 messages sent via slack, we emphasized from the beginning that communicating the work is as important as doing it. Hence, through the use of Important updates slack channels and other means, even the smallest of details was relayed to the team.
- *Accountability* - We ensured that all team members believed in our mission and through allowing them to set their own weekly goals, we ensured there was no feeling of directed tasks but rather a feeling of empowerment. However as a leadership group, we held members accountable to the goals set and did not shy away from tackling technical and other problems head on.

## **8.2 Communication channel**

All communication was done via slack to ensure transparency. The mentors were also actively involved and engaged through slack answering questions in the subteam channels. This ensured that all members were aware of updates and feedback.

## **8.3 Documentation**

### **8.3.1 Data Storage**

In terms of making sure no information is lost, we ensured storage of all of our files in a single shared Google Drive. To ensure clean organization, each sub-team had its own folder. Keeping up with our transparency principle, all members had access to every part of the google drive so that they may view the work of team mates and understand the working of the whole mission rather than their individualised component. Cloud storage ensured that data would not be lost even if there is damage of physical property of any of the members.

### **8.3.2 Use of an all-encompassing live requirements page**

While functioning as a large group, we wanted to prevent misinformation especially when mass, volume and performance requirements changed from the various subsystems. Especially while going through the

iterative process, these values changed continuously in an iterative process and hence we created a centralized document where all changes would be updated in real-time. In this document, all requirements were organized by subteam and had individual ownership. In this way, it was always known who was in charge of a certain requirement, as well as to which subteam it had any implications. This helped ensure smooth flow of information through the various subteams and keeping everyone on the same page.

The centralized collection of requirements and mass and power budgets also allowed for a rapid switch between the lander and orbiter spacecraft. While having some learning curve, after full team adoption the system proved to be a generalized format through which the team could efficiently operate. The lander and orbiter live requirements spreadsheets can be found in Appendix B.1 and B.2, respectively.

## 8.4 Team Organization and Flow of Information

In terms of the various subteam assignments and the overall organizational structure, there were some differences between the lander and orbiter part of the project. This is represented in the two diagrams below, Figure 8.4.1 and 8.4.2. Apart from showing the different teams, they also represent the interconnectedness of the various subteams, highlighting important communication links.

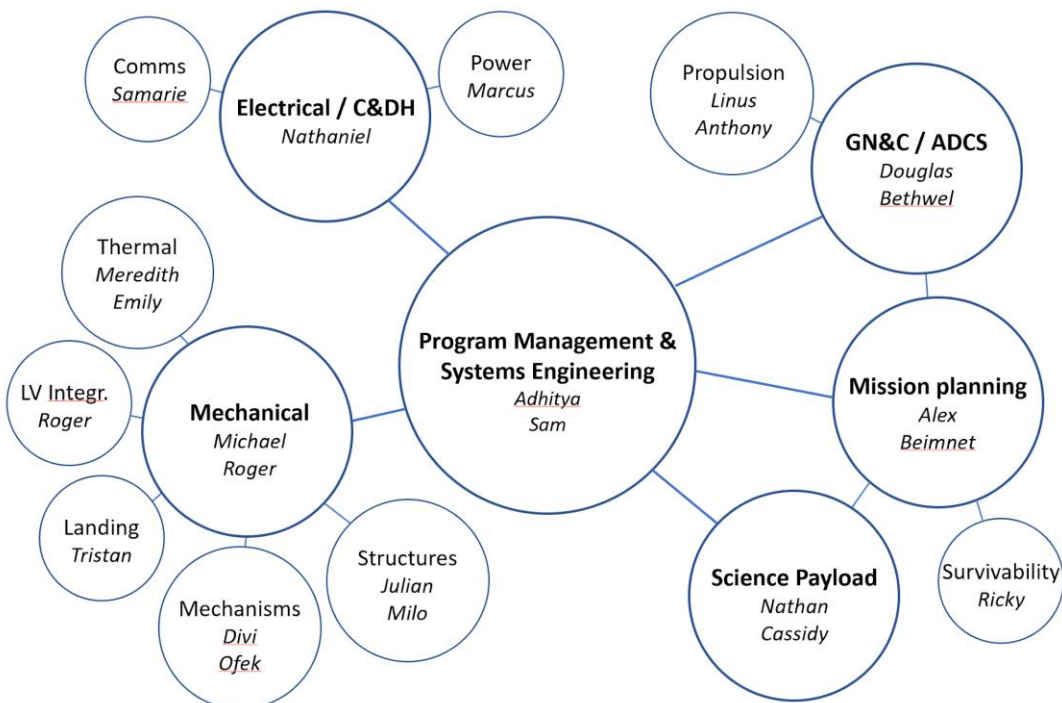


Figure 8.4.1. Lunar Lander Team Organization

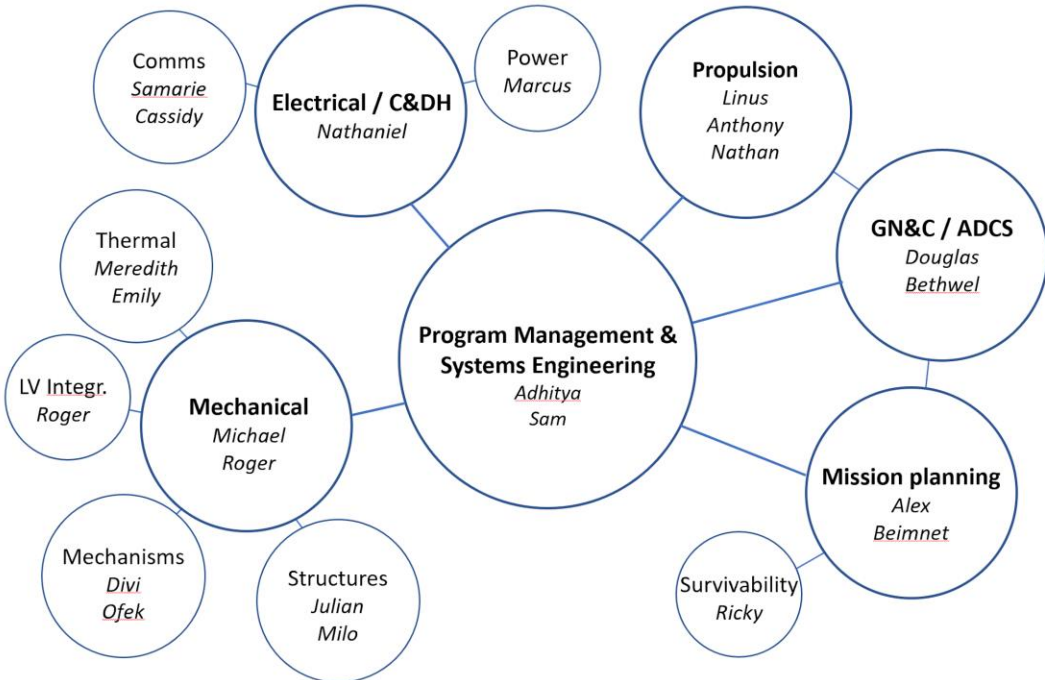


Figure 8.4.2. Lunar Orbiter Team Organization. The main difference is the absence of the landing gear and science payload subteams.

During the initial phase of our project it was made abundantly clear that there would not be a top down hierarchy within the team but rather different roles for all the members. The project managers facilitated conversation within different subteams and any issues raised within subteams would be brought out through the subteam leaders. This ensured that the information flow is organized while giving all members this opportunity to voice their thoughts and ideas.

## 8.5 Meetings and Discussions

Our top priority was to keep meetings time-efficient and at the same time ensure everyone was aware of the updates, requirements and deadlines. Ensuring that the whole team functioned as a single cohesive unit. In that regard, particular emphasis was put into taking meeting notes in all types of interactions and updating the important updates slack channel. This made information accessible to all members of the team irrespective of whether they could attend the meeting or not.

### 8.5.1 Weekly full-team meetings

These meetings were used to provide logistical information and share high level updates from the different subteams. In addition, it facilitated conversation between the different subteams. It was also used to debrief feedback received in the various stages of the project and discuss them with our mentors, making sure they do not go unaddressed.

### 8.5.2 Subteam Meetings

These meetings were primarily used to brainstorm ideas and more technical details pertaining to the particular group. While weekly meetings were used to transfer information around , these meetings focused on making progress and completing the various tasks.

### 8.5.3 Meetings with mentors

Individual meetings took place with mentors to get feedback and ideas on particular components of the project. While these conversations ensured efficient use of time, the lessons learned were shared through the important updates slack channel.

### 8.5.4 Leadership group meetings

The leadership group consisting of project managers and subteam leads met regularly to discuss the overall direction of the whole group. The meeting was used to review PDR and CDR presentations and other material before submission providing feedback for each other. This ensured that while 23 different people contributed to the various submittable documents, it is submitted as a cohesive document with a natural flow. As with the other meetings, all updates were posted to the rest of the team following our principle of transparency and ensuring that there is no hierarchy felt within our team.

## 9. Conclusions

We would like to sincerely thank you for reading our report in full. This project has been a significant challenge for everyone on Team Goddard, and this document represents roughly nine weeks of hard work, analysis, design decisions, and meetings. Considering the original objective of this project--gaining familiarity with systems engineering and experiencing the design process and budgeting associated with space systems--that goal has absolutely been achieved.

The two spacecraft that we've presented in this report (or three, with the OMV) have taught us the importance of clear communication, central documentation, and individual ownership, as is also reflected in the project management chapter (8). One of the main challenges throughout this project has been the interdependence of many subsystems, which can lead to everyone waiting for each other to start. In those moments, initiating the cycle with a ballpark (or SMAD) estimate can really kick the design process off. Another thing this project has really shown is the power of digital collaboration tools and the possibility of working with team members across the globe, in a time where in-person meetings were impossible. It took a certain amount of resilience and flexibility, but with sufficient effort it can work, as is again represented by this report.

However, no project is perfect, and this report is far from a finished mission design. In many cases, the scope was narrowed to accommodate for time and knowledge constraints. Nevertheless, by explicitly setting such scope and having it reflected in the assumptions as they have been established throughout this report, the number of loose ends is limited. However, a lot of work remains to be done if the Erebus mission were to be developed further. Some tasks have to this end been laid out in the section below.

### 9.1 Future Work

Some specific tasks that were classified as future work, either because of time or project scope constraints are listed below. This is by no means an exhaustive list, but it gives an indication of steps that would be next in the process of further developing the Erebus mission concept.

- Analyze possibility to equip the orbiter with a low-gain antenna in addition to the currently present Ka-band antenna
- Research possible additional instruments for the orbiter, expanding its functionality beyond solely communications. This could add a science, exploration or mapping component to its purpose
- Design the internals of the lander's science payload laboratory module
- Detailed design steps, suchs as the design of harnessing, wiring, and fastening
- Multi-node thermal analysis
- Rigorous quantitative survivability/reliability analysis for the orbiter's 10-year mission lifetime

More generally, following this report, the next main steps in the Erebus mission development would be the following:

- Move lander from CDR level towards FDR level
  - Detailed design of individual components and science lab
  - Further narrowing down margins on mass & power
- Move orbiter from PDR level towards CDR level
  - Further narrowing down margins on mass & power
  - Detailed design of the thermal system, designing individual solutions per component
  - Design packaging of all components and determination of overall spacecraft layout
  - In-depth end-of-life analysis
- Design modifications for off-the-shelf OMV: Work with Moog on its development
- Design detailed qualification procedures for all three of the spacecraft

# References

- 10 N Bipropellant Thrusters.* Accessed 7 May 2020. Retrieved from <http://www.space-propulsion.com/spacecraft-propulsion/bipropellant-thrusters/10-bipropellant-thrusters.html>
- “1N Monopropellant Hydrazine Thruster.” Retrieved from <http://www.space-propulsion.com/spacecraft-propulsion/hydrazine-thrusters/1n-hydrazine-thruster.html>
- 2000785G MkII MLB User Manual.* Planetary Systems Corporation. Accessed April 10, 2020. Retrieved from <https://www.planetarysystemscorp.com/wp-content/uploads/2018/07/2000785G-MkII-MLB-User-Manual.pdf>
- AIAA, *AIAA Aerospace Design Engineers Guide*, 6th ed., ed. by Charles R. Dauwalter, Draper Laboratories and E. Russ Althof. (American Institute of Aeronautics and Astronautics, 2012)
- Andreas, Edgar L., “New estimates for the sublimation rate for ice on the Moon.” *Icarus* 186 (2007) 24–30.
- Arevalo, R., Ni, Z., & Danell, R., (2019), “Mass spectrometry and planetary exploration: A brief review and future projection.” Retrieved from <https://onlinelibrary.wiley.com/doi/full/10.1002/jms.4454>
- “ARGUS IR Spectrometers.” Retrieved from <http://thothx.com/products/argus-ir-spectrometers>
- Assad Anis (2012). Cold Gas Propulsion System - An Ideal Choice for Remote Sensing Small Satellites, Remote Sensing - Advanced Techniques and Platforms, Dr. Boris Escalante (Ed.), ISBN: 978-953-51-0652-4, InTech, Available from: <http://www.intechopen.com/books/remote-sensing-advanced-techniques-andplatforms/cold-gas-propulsion-system-an-ideal-choice-for-remote-sensing-small-satellites>
- Auriga CP.* Accessed 4 May 2020. Retrieved from [http://www.sodern.com/website/docs\\_wsw/RUB\\_315/tile\\_685/Auriga-CP.pdf](http://www.sodern.com/website/docs_wsw/RUB_315/tile_685/Auriga-CP.pdf).
- “Auto-Gopher Drill,” Honeybee Robotics. Accessed May 10, 2020. Retrieved from <http://honeybeerobotics.com/portfolio/auto-gopher-drill/>.
- AZ Technology. “Spacecraft Thermal Control and Conductive Paints/Coatings and Services Catalog.” January 2008, iv-v.
- “Buckling of Circular Thin-Walled Cylinders,” NASA SP-8007, 1968. Accessed via the NASA Technical Reports Server, May 9, 2020. Retrieved from <https://ntrs.nasa.gov/archive/nasa/casi.ntrs.nasa.gov/19690013955.pdf>.
- Caplinq. “3-mil Polyimide (Kapton) Film.” Accessed April 6, 2020. Retrieved from <https://www.caplinq.com/3-mil-polyimide-kapton-film-no-adhesive-pit3n-series.html?filter=26005,9871>.
- Chernyakov, Boris, and Kamal Thakore, “Gimbals Drive and Control Electronics Design, Development and Testing of the LRO High Gain Antenna and Solar Array Systems,” Proceedings of the 40th Aerospace Mechanisms Symposium, NASA Kennedy Space Center, May 12-14, 2010. Retrieved from the NASA Technical Reports Server, <https://ntrs.nasa.gov/archive/nasa/casi.ntrs.nasa.gov/20100021940.pdf>.
- Choi, Michael. “Solar Probe Plus MAG Sensor Thermal Design for Low Heater Power and Extreme Thermal Environment.” 45th International Conference on Environmental Systems, July 12, 2015.
- Choueiri, Edgar. “Spacecraft Thermal Control.” MAE 432 Lecture Notes, 2020.
- CMG 4-6s.* Accessed 7 May 2020. Retrieved from <https://spaceequipment.airbusdefenceandspace.com/avionics/control-momentum-gyroscopes/cmg-4-6s/>

“Cost Estimating” *Space Mission Engineering the New SMAD*, by James R. Wertz et al., Microcosm Press, 2011, p.302

“D-Series Linear Dampers,” Taylor Devices, Inc. Accessed May 11, 2020. Retrieved from <https://www.taylordevices.com/custom/pdf/brochures/D%20Series%20Linear%20Dampers.pdf>.

De Almeida, Bruno, “Testemunho,” Projecto Situ, 2015. Accessed May 10, 2020. Retrieved from <https://projetositu.wordpress.com/2015/08/07/situ-2-daniel-de-paula-2/>.

“Delta IV.” United Launch Alliance. Accessed April 10, 2020. Retrieved from <https://www.ulalaunch.com/rockets/delta-iv>.

Derewa, C. et al. “LOTUS: Standardized ESPA Propulsion System.” *AIAA Propulsion and Energy Forum*. July 2015.

Deutsch, Head III, Neumann, (2019), “Analyzing the ages of south polar craters on the Moon: Implications for the sources and evolution of surface water ice,” retrieved from: <https://doi.org/10.1016/j.icarus.2019.113455>

Domingo, Miguel, and José Julián Ramírez. “Mechanical Design and Test of ROSETTA Platform Louvres.” Proceedings of the 10th European Space Mechanisms and Tribology Symposium, September 24, 2003, 289–92.

Dunmore. The Vacuum Metalization Process. Accessed April 6, 2020. Retrieved from <https://www.dunmore.com/technical/vacuum-metallizing.html>.

Elts, Ekaterina & Windmann, Thorsten & Staak, Daniel & Vrabec, Jadran. (2012). Fluid phase behavior from molecular simulation: Hydrazine, Monomethylhydrazine, Dimethylhydrazine and binary mixtures containing these compounds. *Fluid Phase Equilibria*. s 322–323. 79–91. 10.1016/j.fluid.2012.03.008.

Endurosat, “Commercial S-Band Patch Antenna”. Accessed on May 7, 2020. Retrieved from <https://www.endurosat.com/cubesat-store/all-cubesat-modules/s-band-antenna-commercial/>

ESA. Rosetta Thermal Louvres. August 19, 2019. Accessed April 20, 2020. Retrieved from [https://www.esa.int/ESA\\_Multimedia/Images/2015/08/Rosetta\\_thermal\\_louvres](https://www.esa.int/ESA_Multimedia/Images/2015/08/Rosetta_thermal_louvres).

“ESPA Class SADA,” Honeybee Robotics, 2013. Accessed May 9 2020. Retrieved from <https://honeybeerobotics.com/wp-content/uploads/2014/07/Honeybee-Robotics-ESPA-SADA.pdf>.

“Falcon 9.” Space Exploration Technologies Corp. Accessed April 10, 2020. Retrieved from <https://www.spacex.com/falcon9>.

Feldman, Bernard, Harm Tolner, and Douglas Mclean. “15.4: Tin Oxide Transparent Conductor for PDP.” SID Symposium Digest of Technical Papers 39, no. 1 (2008): 194. <https://doi.org/10.1889/1.3069573>.

Feng, J. et. al., (2019), “An imaging method for Chang'e-5 Lunar Regolith Penetrating Radar,” doi: <https://doi.org/10.1016/j.pss.2019.01.008>

Foessel-Bunting, Alex, et al. *MMW-Scanning Radar for Descent Guidance and Landing Safeguard*. Accessed 7 May 2020. Retrieved from [https://ri.cmu.edu/pub\\_files/pub2/foessel\\_alex\\_2001\\_1/foessel\\_alex\\_2001\\_1.pdf](https://ri.cmu.edu/pub_files/pub2/foessel_alex_2001_1/foessel_alex_2001_1.pdf)

*FreeFlight Systems RA-4000*. Accessed 7 May 2020. Retrieved from <https://sarasaotaavionics.com/avionics/ra-4000>

Glavin D. et al., (2010), “In Situ Biological Contamination studies of the Moon: Implications for Future Planetary Protection and Life Detection Missions.” Retrieved from <https://ntrs.nasa.gov/archive/nasa/casi.ntrs.nasa.gov/20100036597.pdf>

Gerstenmaier, William. “Cislunar and Gateway Overview.” NASA, Mar. 2020, descanso. Accessed on May 6, 2020. Retrieved from [jpl.nasa.gov/propagation/Ka\\_Band/JPL-D32584\\_1.pdf](jpl.nasa.gov/propagation/Ka_Band/JPL-D32584_1.pdf).

Gilmore, David G. Spacecraft Thermal Control Handbook, Volume 1 - Fundamental Technologies (2nd Edition). American Institute of Aeronautics and Astronautics/Aerospace Press: 2002.

Grott, M., Knollenberg, J. and Krause, C. *Apollo lunar heat flow experiment revisited: A critical reassessment of the in situ thermal conductivity determination*. Journal of Geophysical Research, Vol 115, November 2010, p. 4.

Hassani, Ali & Ghorbani, Mehrdad & Pasand, Milad. (2017). A Study of Spacecraft Reaction Thruster Configurations for Attitude Control System. IEEE Aerospace and Electronic Systems Magazine. 32. 10.1109/MAES.2017.160104.

Hereath, Anuradha, (2009), “How to Protect Other Planets from Earth Microbes.” <https://www.space.com/7410-protect-planets-earth-microbes.html>

“HexWeb CR III Corrosion Resistant Specification Grade Aluminum Honeycomb,” Hexcel Corporation, 2017. Accessed May 9, 2020. Retrieved from [https://www.hexcel.com/user\\_area/content\\_media/raw/HexWeb\\_CRIII\\_DataSheet.pdf](https://www.hexcel.com/user_area/content_media/raw/HexWeb_CRIII_DataSheet.pdf).

“HexWeb Honeycomb Selector Guide,” Hexcel, 2017. Accessed 11 May 2020. Retrieved from [https://www.hexcel.com/user\\_area/content\\_media/raw/HexWeb\\_SelectorGuide\\_2017.pdf](https://www.hexcel.com/user_area/content_media/raw/HexWeb_SelectorGuide_2017.pdf).

Ho, Christian, et al. “Atmospheric Noise Temperature Induced by Clouds and Other Weather Phenomena at SHF Band (1-45 GHz) .” *Atmospheric Noise Temperature Induced by Clouds and Other Weather Phenomena at SHF Band (1-45 GHz)* , 11 Aug. 2005. Accessed on April 23, 2020. [descanso.jpl.nasa.gov/propagation/Ka\\_Band/JPL-D32584\\_1.pdf](descanso.jpl.nasa.gov/propagation/Ka_Band/JPL-D32584_1.pdf).

“Honeybee Robotics - HD Mars 2020 Sample Acquisition and Caching Concept.” Honeybee Robotics, <www.youtube.com/watch?v=NphWPvi9cy4>.

Honeywell, *HG1900 Inertial Measurement Unit*. Accessed 4 May 2020. <https://aerospace.honeywell.com/en/learn/products/sensors/hg1900-inertial-measurement-unit>

“Honeycomb Characteristics,” APCO Technologies, 2018. Retrieved from <https://www.apco-technologies.eu/apco-content/uploads/2018/04/Catalogue-PdV-LR.pdf>.

Indyk, Stephen. “TRIDENT: The Regolith and Ice Drill for Exploration of New Terrains.” Honeybee Robotics Spacecraft Mechanisms Corporation. Retrieved from <www.hou.usra.edu/meetings/leag2017/presentations/wednesday/zacny2.pdf>.

Joe Munder, Spacecraft Design Course - Mechanisms Overview. Class lecture, given April 16 2020.

Joe Troutman, Electrical Systems Lecture. Class lecture, given March 2 2020

“JPL’s NDEAA Ultrasonic/Sonic Driller/Corer Homepage,” NASA JPL, 2002. Accessed May 9, 2020. Retrieved from <https://ndeaa.jpl.nasa.gov/nasa-nde/usdc/usdc.htm>.

Karam, Robert D.. Satellite Thermal Control for Systems Engineers. United States: American Institute of Aeronautics & Astronautics, 1998. p. 76.

- Kauder, Lonny. "Spacecraft Thermal Control Coatings References." NASA, December 2005.
- King, T. S-311-P-079E - Procurement Specification for Thermofoil Heater. NASA. 1996. Accessed April 20, 2020. Retrieved from <https://nepg.nasa.gov/files/22932/S-311-P-079E.pdf>.
- KU Leuven Star Tracker.* Accessed 2 May 2020. Retrieved from <https://www.cubesatshop.com/wp-content/uploads/2018/10/KULST-Datasheet.pdf>
- LiDAR Specification Comparison Chart.* Accessed 7 May 2020. Retrieved from [https://autonomoustuff.com/wp-content/uploads/2018/04/LiDAR\\_Comparison.pdf](https://autonomoustuff.com/wp-content/uploads/2018/04/LiDAR_Comparison.pdf).
- "Lunar regolith simulant," Wikipedia. Accessed May 8, 2020. Retrieved from [https://en.wikipedia.org/wiki/Lunar\\_regolith\\_simulant](https://en.wikipedia.org/wiki/Lunar_regolith_simulant).
- Lunar Sourcebook*, ed. by Grant H. Heiken, David T. Vaniman, and Bevan M. French (Cambridge: Cambridge University Press, 1991).
- Matweb. DuPont™ Kapton® 500VN Polyimide Film, 125 Micron Thickness. Accessed April 6, 2020. Retrieved from [http://www.matweb.com/search/datasheet\\_print.aspx?matguid=338573ad1bdf4586aa17fab95f3a57d7](http://www.matweb.com/search/datasheet_print.aspx?matguid=338573ad1bdf4586aa17fab95f3a57d7).
- Mazarico, Erwan, et al. *Orbit Determination of the Lunar Reconnaissance Orbiter*. Accessed 5 May 2020. Retrieved from [http://www-geodyn.mit.edu/mazarico\\_LROPOD\\_jgeod11.pdf](http://www-geodyn.mit.edu/mazarico_LROPOD_jgeod11.pdf)
- McCallum, Peter. Improving the Nuclear Approval Process; Progress and Plans. ANS NETS 2018 – Nuclear and Emerging Technologies for Space.
- Melendo, Ignacio, and Romain Peyrou-Lauga. "CHEOPS Platform Thermal Architecture." 46th International Conference on Environmental Systems, July 10, 2016.
- Metallic Materials Properties Development and Standardization (MMPDS): MMPDS-08, April 2013. [Washington, D.C.]: Federal Aviation Administration, 2013. Table 3.6.2.0(c1).
- Minco. Multi-Function Prototype Controller: CT425B. Accessed April 24, 2020. Retrieved from [http://catalog.minco.com/catalog3/d/minco/?c=products&cid=2\\_1\\_4-mutli-function-prototype-controller&id=CT425B](http://catalog.minco.com/catalog3/d/minco/?c=products&cid=2_1_4-mutli-function-prototype-controller&id=CT425B).
- Minco. *Polyimide Thermofoil Heaters*. Accessed April 20, 2020. Retrieved from <https://www.minco.com/products/heat/polyimidethermofoilheaters>.
- Minco. Strip Sensing: S651PDY120A. Retrieved from [http://catalog.minco.com/catalog3/d/minco/?c=products&cid=1\\_8\\_1\\_2-strip-sensing&id=S651PDY120A](http://catalog.minco.com/catalog3/d/minco/?c=products&cid=1_8_1_2-strip-sensing&id=S651PDY120A).
- Minco. Thermal Solutions Design Guide. Accessed April 20, 2020. Retrieved from <https://www.minco.com/~/media/files/minco/productguides/heat/minco%20thermal%20solutions%20design%20guide.ashx>.
- Miranda, Félix, et al. "A Review of Antenna Technologies for Future NASA Exploration Missions." NASA, Mar. 2020. Retrieved from [ntrs.nasa.gov/archive/nasa/casi.ntrs.nasa.gov/20110000847.pdf](https://ntrs.nasa.gov/archive/nasa/casi.ntrs.nasa.gov/20110000847.pdf)
- MIT. Material: Indium Tin Oxide. Accessed April 6, 2020. Retrieved from <http://www.mit.edu/~6.777/matprops/ito.htm>.
- Moog, "Enhanced Pointing Gimbal Assembly (EPGA)", Moog Space and Defense Group, 2019. Accessed May 9, 2020. Retrieved from

[https://www.moog.com/content/dam/moog/literature/Space\\_Defense/Space\\_Access\\_Integrated\\_Systems/E\\_PGA\\_0410.pdf](https://www.moog.com/content/dam/moog/literature/Space_Defense/Space_Access_Integrated_Systems/E_PGA_0410.pdf).

Moog Space and Defense Group. *ESPA User's Guide*. November 2018. Accessed March 30, 2020. Retrieved from [https://www.moog.com/content/dam/moog/literature/Space\\_Defense/spaceliterature/structures/moog-espa-users-guide-datasheet.pdf](https://www.moog.com/content/dam/moog/literature/Space_Defense/spaceliterature/structures/moog-espa-users-guide-datasheet.pdf)

"MR-501B." Retrieved from <http://www.astronautix.com/m/mr-501b.html>

NASA. CubeSat Form Factor Thermal Control Louvers. Accessed April 20, 2020. Retrieved from <https://technology.nasa.gov/patent/GSC-TOPS-40>.

Nadir, Bill. *Satellite Engineering*. Accessed on May 7, 2020. Retrieved from [https://ocw.mit.edu/courses/aeronautics-and-astronautics/16-851-satellite-engineering-fall-2003/projects/portfolio\\_nadir1.pdf](https://ocw.mit.edu/courses/aeronautics-and-astronautics/16-851-satellite-engineering-fall-2003/projects/portfolio_nadir1.pdf)

*nanoSSOC-D60 digital sun sensor*. Accessed: 2 May 2020. Retrieved from <https://www.cubesatshop.com/product/nanossoc-d60-digital-sun-sensor/>

NASA, "LCROSS Impact Data Indicates Water on Moon," (2009). Retrieved from <https://ntrs.nasa.gov/archive/nasa/casi.ntrs.nasa.gov/20110014548.pdf>

NASA, *Lunar Module Electrical Power Subsystem*, NASA Technical Note D-6977 09/72 6977, 09/72. Retrieved from <https://45uevg34gwlltnbsf2plyua1-wpengine.netdna-ssl.com/wp-content/uploads/2019/07/OXIS-Li-S-Ultra-Light-Cell-spec-sheet-v4.2.pdf>. Accessed on May 5, 2020

NASA, "RIMFAX." Retrieved from <https://mars.nasa.gov/mars2020/spacecraft/instruments/rimfax/>

NASA, *State of the Art Small Spacecraft Technology*. Date accessed: 2 May 2020. Retrieved from [https://www.nasa.gov/sites/default/files/atoms/files/soa2018\\_final\\_doc-6.pdf](https://www.nasa.gov/sites/default/files/atoms/files/soa2018_final_doc-6.pdf).

"New VIPER Lunar Rover to Map Water Ice on the Moon," NASA, 2020. Accessed May 10, 2020. Retrieved from <https://www.nasa.gov/feature/new-viper-lunar-rover-to-map-water-ice-on-the-moon>.

*NewSpace Sun Sensor\_6a*. Date accessed: 2 May 2020. Retrieved from [https://www.cubesatshop.com/wp-content/uploads/2016/06/NewSpace-Sun-Sensor\\_6a-1.pdf](https://www.cubesatshop.com/wp-content/uploads/2016/06/NewSpace-Sun-Sensor_6a-1.pdf)

*NewSpace Sun Sensor 8\_a*. Accessed 2 May 2020. Retrieved from [http://www.newspacesystems.com/wp-content/uploads/2019/03/NewSpace-Sun-Sensor\\_8a.pdf](http://www.newspacesystems.com/wp-content/uploads/2019/03/NewSpace-Sun-Sensor_8a.pdf)

*NST-3 Nano Star Tracker*. Accessed 2 May 2020. Retrieved from <https://www.cubesatshop.com/product/nst-3-nano-star-tracker/>

"The Orbital Maneuvering Vehicle." Moog Inc. Accessed April 25, 2020. Retrieved from <https://www.moog.com/markets/space/omv.html>

"Orbital Maneuvering Vehicle | Comet" Moog Inc. Accessed April 25, 2020. Retrieved from [https://www.moog.com/content/dam/moog/literature/Space\\_Defense/spaceliterature/omv/moog-omv-comet-datasheet.pdf](https://www.moog.com/content/dam/moog/literature/Space_Defense/spaceliterature/omv/moog-omv-comet-datasheet.pdf)

OXIS Energy, Standar, Accessed on May 11, 202. Retrieved from <https://oxisenergy.com/products/>

Paluszek, Spacecraft Communications, Slide 35, Mae 342 2020, Accessed on May 6, 2020.

- Patel, Mukund R., *Spacecraft Power Systems* (Cleveland, OH: CRC Press, 2005), 306.
- Paulsen, Gale et al. "The Regolith and Ice Drill for Exploration of New Terrains (TRIDENT); a One-Meter Drill for the Lunar Resource Prospector Mission." Proceedings of the 44th Aerospace Mechanisms Symposium, NASA Glenn Research Center, May 16-18, 2018.
- "PDS: Instrument Information." NASA, NASA, Mar. 2020. Accessed on April 17, 2020. Retrieved from [pds.nasa.gov/ds-view/pds/viewInstrumentProfile.jsp?INSTRUMENT\\_ID=RSS&INSTRUMENT\\_HOST\\_ID=LRO](https://pds.nasa.gov/ds-view/pds/viewInstrumentProfile.jsp?INSTRUMENT_ID=RSS&INSTRUMENT_HOST_ID=LRO).
- Pearson, C. et al. "Extending Rideshare: Mission Case Studies Using Propulsive ESPA." *31st Space Symposium*. April 13, 2015.
- Pearson, C. et al. "Rideshare and the Orbital Maneuvering Vehicle: the Key to Low-cost Lagrange-point Missions." *29th Annual AIAA/USU Conference on Small Satellites*. August 2015.
- Persky, M. J. "Review of Black Surfaces for Space-Borne Infrared Systems." *Review of Scientific Instruments* 70, no. 5 (1999): 2193–2217. Retrieved from <https://doi.org/10.1063/1.1149739>.
- "Planetary Deep Drill Completes Second Field Test," The Planetary Society Blog. Accessed May 10, 2020. Retrieved from [www.planetary.org/blogs/jason-davis/pdd-completes-second-field-test.html](https://www.planetary.org/blogs/jason-davis/pdd-completes-second-field-test.html).
- Reaction Wheels*. Blue Canyon Technologies. Accessed 6 May 2020. Retrieved from [https://www.bluecanyontech.com/static/datasheet/BCT\\_DataSheet\\_Components\\_ReactionWheels.pdf](https://www.bluecanyontech.com/static/datasheet/BCT_DataSheet_Components_ReactionWheels.pdf)
- Rickman, Doug, Kenneth W. Street, and Mohamed S. El-Genk. "Some Expected Mechanical Characteristics of Lunar Dust: A Geological View." AIP Conference Proceedings, 2008. Retrieved from <https://doi.org/10.1063/1.2845062>.
- "ROPEC Drill." Honeybee Robotics. Accessed May 10, 2020. Retrieved from <http://honeybeerobotics.com/portfolio/ropec-drill/>.
- "Rover Curiosity finds Mars rocks more porous than thought," The Week, 2019. Accessed May 9, 2020. Retrieved from <https://www.theweek.in/news/sci-tech/2019/02/02/Rover-Curiosity-finds-Mars-rocks-more-porous-than-thought.html>.
- RSI 12 Momentum and Reaction Wheel*. Accessed 7 May 2020. Retrieved from [http://www.electronicnote.com/media/downloads/RSI%202012\\_A4.pdf](http://www.electronicnote.com/media/downloads/RSI%202012_A4.pdf)
- RSI 45 Momentum and Reaction Wheel*. Accessed 7 May 2020. Retrieved from <https://www.yumpu.com/en/document/read/35491907/rsi-45-momentum-and-reaction-wheels-15-45-nms-with->
- RSI Momentum and Reaction Wheels 15-45 Nms*. Accessed 7 May 2020. Retrieved from [http://www.electronicnote.com/media/downloads/RSI%202045\\_A4.pdf](http://www.electronicnote.com/media/downloads/RSI%202045_A4.pdf)
- RUAG Space. "PAS 610S (24") Separation System." Accessed April 10, 2020. Retrieved from [https://www.ruag.com/sites/default/files/media\\_document/2019-03/PAS%20610S%20Separation%20System.pdf](https://www.ruag.com/sites/default/files/media_document/2019-03/PAS%20610S%20Separation%20System.pdf)
- Russell, C. T., et al. *The permanent and induced magnetic dipole moment of the moon*. Accessed 6 May 2020. Retrieved from <http://adsabs.harvard.edu/full/1974LPSC....5.2747R>
- S910. Accessed 04 May 2020. Retrieved from <https://aitechsystems.com/product/s910-3u-compactpci-mil-std-1553b-board/>

Sanders, G.B. et al., (2011), “RESOLVE for Lunara Polar Ice/Volatile Characterization Mission.” Retrieved from <https://ntrs.nasa.gov/archive/nasa/casi.ntrs.nasa.gov/20110014548.pdf>

Santiago-Bond, Jo., (2015), “INFICON Transpector MPH Mass SPectrometer Random Vibration Test Report.” Retrieved from <https://ntrs.nasa.gov/archive/nasa/casi.ntrs.nasa.gov/20160012024.pdf>

Smith, D. et al. “Mars Orbiter Laser Altimeter: Experiment summary after the first year of global mapping of Mars.” Journal of Geophysical Research. Vol. 106, No. E10, p23689-722. October 25, 2001.

Space Exploration Technologies Corp. *Falcon User’s Guide*. Accessed May 1, 2020.

Space Mission Analysis and Design, 3rd ed., ed. by James R. Wertz and Wiley J. Larson (Hawthorne, CA: Microcosm Press, 1999), 346.

*Space Products Literature* (2020). Retrieved from

<https://www.baesystems.com/en-us/our-company/inc-businesses/electronic-systems/product-sites/space-products-and-processing/radiation-hardened-electronics>

“Spacecraft Subsystems IV- Communications and Power.” *Space Mission Engineering the New SMAD*, by James R. Wertz et al., Microcosm Press, 2011, p. 639.

“Spacecraft Thermal Control and Conductive Paints/Coatings\* and Services Catalog .” AZ Technology, January 2008, 16.

Spectrolab, *XTJ Prima Space Qualified Triple Junction Solar Cell*. Accessed on May 7, 2020. Retrieved from [https://www.spectrolab.com/photovoltaics/XTJ-Prime\\_Data\\_Sheet.pdf](https://www.spectrolab.com/photovoltaics/XTJ-Prime_Data_Sheet.pdf)

*SS-411 Two-Axis Digital Sun Sensors*. Accessed: 2 May 2020. Retrieved from [https://7846f86-a-744dbb28-s-sites.googlegroups.com/a/sinclairinterplanetary.com/www/digitalsunsensors/sunsensor2011a.pdf?attachauth=ANoY7coQ6\\_r-7ZowJtPM9xOEaElVk19oLZU-KI5AhUH0lapJUYReqK7of3mPN5UOlrvCtp4tKJh7SRXpGXYI\\_lam1-S8\\_L3xW-qf4MvPXv6\\_jBzVqVZbATrBibxQMvO08NU6Vl6Ei8AjuuuNpofo0I8eg\\_8qtBPH8WRw96bNjNev8g\\_2\\_GaLWycZ9yo03YgTS-RpP2lQCvR1477c7tMY2A5nfnk\\_-Dev6dSZVdGuSjxr7SdLyVq9fCCVXejdf9u\\_0nUrPCd0dhwZ&attredirects=1](https://7846f86-a-744dbb28-s-sites.googlegroups.com/a/sinclairinterplanetary.com/www/digitalsunsensors/sunsensor2011a.pdf?attachauth=ANoY7coQ6_r-7ZowJtPM9xOEaElVk19oLZU-KI5AhUH0lapJUYReqK7of3mPN5UOlrvCtp4tKJh7SRXpGXYI_lam1-S8_L3xW-qf4MvPXv6_jBzVqVZbATrBibxQMvO08NU6Vl6Ei8AjuuuNpofo0I8eg_8qtBPH8WRw96bNjNev8g_2_GaLWycZ9yo03YgTS-RpP2lQCvR1477c7tMY2A5nfnk_-Dev6dSZVdGuSjxr7SdLyVq9fCCVXejdf9u_0nUrPCd0dhwZ&attredirects=1)

*ST 200*. Accessed 4 May 2020. Retrieved from <https://hyperiontechnologies.nl/products/miniatrised-star-tracker/>

S. X. Shen et al., (2018). “Lunar Regolith Penetrating Radar on the Lander for Chang’E-5 Mission,” 2018 17th International Conference on Ground Penetrating Radar (GPR), Rapperswil, 2018, pp. 1-4, doi: 10.1109/ICGPR.2018.8441614

*TF03 Single-Point Long-Distance LiDAR Product Specification*. Accessed 7 may 2020. Retrieved from [https://acroname.com/sites/default/files/assets/tf03\\_datasheet\\_v0.4\\_en.pdf](https://acroname.com/sites/default/files/assets/tf03_datasheet_v0.4_en.pdf)

“Transpector MPH High Performance Residual Gas Analyzer For Semiconductor Manufacturing,” retrieved from <https://products.inficon.com/getattachment.axd/?attaName=118b3bc1-dacb-49c4-b563-ef752c7f5799>

United Launch Alliance, *Atlas V Launch Services User’s Guide* - March 2010. Accessed May 01, 2020. Retrieved from <https://www.ulalaunch.com/docs/default-source/rockets/atlasvusersguide2010.pdf>

United Launch Alliance, *Delta IV Launch Services User’s Guide* - June 2013. Accessed May 01, 2020. Retrieved from <https://www.ulalaunch.com/docs/default-source/rockets/delta-iv-user's-guide.pdf>

United Launch Alliance. “ULA Rocket Rundown.” Originally retrieved from <https://www.ulalaunch.com/docs/default-source/rockets/atlas-v-and-delta-iv-technical-summary.pdf>, Accessed April 10, 2020. Contents have changed. Refer to archived version: <https://web.archive.org/web/20200404202142/https://www.ulalaunch.com/docs/default-source/rockets/atlas-v-and-delta-iv-technical-summary.pdf>

Wertz, J. *et al.* “Mass and Power Distribution for Spacecraft.” *Space Mission Engineering the New SMAD*. Microcosm Press, 2011.

Wright, Michael. “Flight Systems Integration and Test”, for NASA/Goddard Space Flight Center. Retrieved from <https://ntrs.nasa.gov/archive/nasa/casi.ntrs.nasa.gov/20110022499.pdf>. Accessed on May 11, 2020.

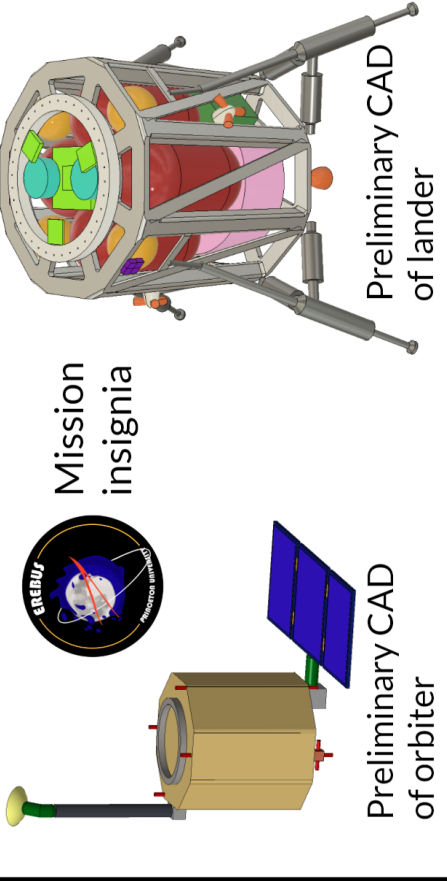
Zupp, George A., “ An Analysis and a Historical Review of the Apollo Program Lunar Module Touchdown Dynamics,” NASA SP-2013-605. Accessed May 11 2020. <http://ston.jsc.nasa.gov/collections/TRS>.

# Table of Appendices

<b>Appendix A: Quad Chart</b>	<b>183</b>
<b>Appendix B: Requirements</b>	<b>185</b>
B.1 Lander Requirements	184
B.1.1 Mission Planning	184
B.1.2 Payload	184
B.1.3 LV Integration	185
B.1.4 Mechanical	18786
B.1.5 Thermal	18887
B.1.6 Guidance, Navigation & Control	18988
B.1.7 Propulsion	19089
B.1.8 Power	190
B.1.9 Communications	191
B.1.10 C&DH	191
B.2 Orbiter Requirements	192
B.2.1 Mission Planning	192
B.2.2 LV Integration	193
B.2.3 Mechanical	194
B.2.4 Thermal	195
B.2.5 Guidance, Navigation & Control	196
B.2.6 Propulsion	196
B.2.7 Power	197
B.2.8 Communications	197
B.2.9 C&DH	197
<b>Appendix C: Detailed Mass Budgets</b>	<b>198</b>
C.1 Lander Mass Budget	198
C.2 Orbiter Mass Budget	199
<b>Appendix D: Mission Planning</b>	<b>200</b>
D.1 Launch Option Visualizations	200
<b>Appendix E: LV Integration</b>	<b>20201</b>
E.1 OMV Dry Mass Estimation	20201
E.2 OMV Launch Mass and Propellant Mass Calculation	20302
E.3 OMV Tank Sizing and Validation	20504
E.4 Separation System	20606
E.5 OMV as Communications Link during Lander Descent	20807
<b>Appendix F: Structures</b>	<b>20908</b>
F.1 Aluminum Honeycomb Panels	20908
F.2 Aluminum Alloy Characteristics	21009
F.3 Lander/Orbiter Structure Drawing	21110
<b>Appendix G: Mechanisms</b>	<b>21211</b>
G.1 Landing System Calculations	21211
G.2 Landing System Release Mechanism Trade Study	21514

G.3 Drill Mechanism Trade Study Details	21615
G.3.1 Auto-Gopher	21716
G.3.2 ROPEC	21717
G.3.3 Ultrasonic Drill	21817
G.4 Danger of Sublimating Ice with the TRIDENT Drill	22019
G.5 Landing System Member Sizing	22221
G.6 Finite Element Analysis for HGA Mast	22423
<b>Appendix H: Payload</b>	<b>22726</b>
<b>Appendix I. Guidance, Navigation, and Control</b>	<b>22827</b>
I.1 Lander Guidance, Navigation, and Control	22827
I.1.1 Sun Sensor Trade Study	22827
I.1.2 Star Tracker Trade Study	22928
I.1.3 IMU Trade Study	22929
I.1.4 Actuator Trade Study	23029
I.1.5 LiDAR/RADAR	23130
I.1.6 Powered Explicit Guidance	23231
I.1.7 Navigational Accuracy Analysis	23736
I.1.8 Pointing Error Propagation	23938
I.2 Orbiter Guidance, Navigation, and Control	24040
I.2.1 Reaction Wheel Trade Study	24140
<b>Appendix J: Propulsion</b>	<b>24241</b>
J.1 Orbiter propulsion	24241
<b>Appendix K: Power</b>	<b>24443</b>
<b>Appendix L: Thermal</b>	<b>24846</b>
L.1 Lander Coating Trade Study	24846
L.2 Walkthrough of Lander Thermal Code	24947
L.3 Lander Thermal Requirements	25048
L.4 Orbiter Coating Trade Study	25149
L.5 Walkthrough of Orbiter Code	25250
L.6 Walkthrough of TLI Code	25452
L.7 Orbiter Thermal Requirements	25654
<b>Appendix M: Command &amp; Data Handling</b>	<b>25755</b>
<b>Appendix N: Communications</b>	<b>25856</b>
N.1 State Data	25856
N.2 Antenna Sizing	25856
N.3 Link Budget Calculations	25856
<b>Appendix O: Cost Estimation</b>	<b>26159</b>
<b>Appendix P: Technology Readiness Levels</b>	<b>259</b>

## MAE342: Erebus Mission - Quest for Water

<p><b>Mission Description and Innovation</b></p> <ul style="list-style-type: none"> <li>• ESPA Class lunar lander (198 kg dry) with a ~20 hour on-surface lifetime</li> <li>• Analyze lunar ice composition in Shackleton Crater, where there's no sunlight</li> <li>• Payload analysis - Mass &amp; IR Spectrometers, Lunar Regolith Penetrating Radar</li> <li>• Orbiter module to relay data to Earth, stays in lunar orbit for 10 years as comms sat</li> </ul>	 <p>Mission insignia</p> <p>Preliminary CAD of lander</p> <p>Preliminary CAD of orbiter</p>
<p><b>Applications &amp; Importance</b></p> <ul style="list-style-type: none"> <li>• Novel, low-cost, replicable ESPA-class lunar lander &amp; orbiter</li> <li>• First lander powered solely by batteries</li> <li>• Cheap, reliable and repeatable concept</li> <li>• Provide crucial data on resources for future lunar base</li> <li>• Orbiter to provide comms link from lunar surface to Earth for future missions</li> </ul>	<p><b>Salient Features and Challenges</b></p> <ul style="list-style-type: none"> <li>• Design features: Octagonal structure, core drill mechanism, extendable landing gear, multi-axis thrusters, compact size</li> <li>• Low-risk design: mostly based on existing, proven and cost-effective technologies</li> <li>• Challenges: Safe landing, retrieving sample, to sustain under given power constraints</li> <li>• Orbiter to cover full lunar surface</li> </ul>

## Appendix A: Quad Chart

# Appendix B: Requirements

## B.1 Lander Requirements

### B.1.1 Mission Planning

No.	Requirement	Dimension	Unit	Duplicates
<b>1.1 General Mission Planning Requirements</b>				
1.1.1	End transfer orbit latitude	89.9	deg. South	
1.1.2	End transfer orbit longitude	0	deg. West	
1.1.3	Maximum velocity in moon's inertial frame above landing site	0	m/s	
1.1.4	Duration of nominal surface operations	20	hours	5.3.3
<b>1.2 Requirements from other teams</b>				
1.2.1	Maximum distance between actual and intended lander site	6000	m	6.2.1
	Maximum commanded angular acceleration for required maneuvers		1 deg/s <sup>2</sup>	6.2.2
1.2.3	Fastest commanded slew in time	180 deg/60 sec	deg/sec	6.2.3
1.2.4	Maximum acceleration of deltaV thrusters	5	m/s <sup>2</sup>	7.2.3

### B.1.2 Payload

No.	Requirement	Dimension	Unit	Duplicates
<b>2.1 Time requirements</b>				
2.1.1	Maximum duration of scientific analysis	20	min/analysis	
2.1.2	Duration of radar analysis			
<b>2.2 Power requirements</b>				
2.2.1	Power consumption of NIR spectrometer	5	W	
2.2.2	Power consumption of GC-MS	20	W	
2.2.3	Power consumption of LGPR	5-10	W	
<b>2.3 Analysis requirements</b>				
2.3.1	Minimum drilling depth	50	cm	4.4.2
2.3.2	Sample delivery form	Powdered	-	4.4.3
<b>2.4 Data requirements</b>				
2.4.1	Scientific data package size	1	MB	9.2.1
<b>2.5 Mass and Volume requirements</b>				
2.5.1	mass of payload, max	36	kg maximum	
2.5.1a	Mass NIR spectrometer	1	Kg	
	Mass GC-MS	8	Kg	
	Mass GPR	3	Kg	
	Total mass of instrumentation	12	Kg	
2.5.2	volume NIR spectrometer	18	in <sup>3</sup>	
	volume GC-MS	356	in <sup>3</sup> (large upper bound)	
	Volume GPR	88	in <sup>3</sup>	
	total instrument volume	462	in <sup>3</sup>	

### B.1.3 LV Integration

No.	Requirement	Dimension	Unit	Duplicates	Driven By
<b>3.1 General LV Integration requirements</b>					
3.1.1	Max lander height in stowed config (in LV coord. sys)	42	Inch		
3.1.1b	Max lander width in stowed config (in LV coord. sys)	46	Inch		
3.1.1c	Max lander length in stowed config (in LV coord. sys)	56	Inch		
3.1.2	ESPA ring diameter	24	Inch		
3.1.3	ESPA ring fastener size	1/4	Inch		
3.1.4	All resonant frequencies above	35	Hz	4.2.1	
3.1.5	Number of 15-pin inflight-disconnect (IFD) connectors	2	-		
3.1.6	Maximum lander launch mass	450	kg		
3.1.7	Maximum distance between COG and interface plane	22	Inch		
3.1.8	Tolerable Launch vehicle load factor in lateral & Axial directions*	8.5	g		
3.1.9	Dormant wait time after deployment (No RF or deployables)**	30	s		
*This requirement is superseded by req. 3.3.1-3					
**Originally 30 minutes, but can be set arbitrarily since RF interference can be coordinated and avoided now that Erebus mission has assumed total control of the OMV, and that thrusters are angled away from OMV to prevent impingement.					
<b>3.2 Requirements for Separation System</b>					
3.2.1	Lander orientation at deployment	-			GN&C
3.2.2	Separation velocity range	0.3-0.4	m/s	6.3.3b	GN&C
3.2.3	Max. rotation rate induced by separation	5	Deg	4.5.2, 6.3.3	GN&C
3.2.4	Maximum shock from separation	200	g		Mechanical
3.2.5	Separation system min operating temperature	-54	C	5.4.3	
3.2.6	Separation system max operationg temperature	128	C	5.4.3	
3.2.7	Minimum Payload Capacity (CoM at 20")	500	kg		
3.2.8	Maximum Stack Height	2.5	in		
3.2.9	Max. full System Mass	10	kg		
3.2.10	Max. flyaway mass	3	kg		
3.2.11	Separation system thermal resistance	0.13	deg C/W	5.5.7	
<b>3.3 Launch Environment (Load factors based on Falcon 9 (which presents worst case), all else based on Atlas V)</b>					
3.3.1	Max combined (static+dynamic) axial load factor	8.5	g	4.2.2	
3.3.2	Min combined (static+dynamic) axial load factor	-4	g		
3.3.3	Max combined (static+dynamic) lateral load factor	3	g	4.2.3	
3.3.4	Max vectorially summed load factor	8.73	g		
3.3.5	<a href="#">Acoustic - See Figure 3.2.2-2 and table 3.4.4-2</a>	-	-	4.2.4	
3.3.6	<a href="#">Sinusoidal vibration - See Figure 3.2.3-1</a>	-	-	4.2.5	
3.3.7	Primary Payload Separation shock at 100 Hz	100	g	4.2.6	
3.3.8	Primary Payload Separation shock at 1000 Hz	4500	g	4.2.7	
3.3.9	Max emittance of Payload Fairing Interior Wall	0.9	-	5.5.1	
3.3.10	Max temp of PLF Interior Wall	88	C	5.5.2	
3.3.11	Max peak heat flux radiuated by PLF surfaces	536	W/m^2	5.5.3	
3.3.12	Max emittance of PLF Acoustic suppression system	0.1	-	5.5.4	
3.3.13	Max temp of Payload Fairing Interior Wall	60	C	5.5.5	
3.3.14	Payload adapter temperature range	0 - 49	C	5.5.6	
3.3.15	Max depressurization rate	6.2	kPa/s		
3.3.16	Typical depressurization rate	2.5	kPa/s		

## B.1.4 Mechanical

No.	Requirement	Dimension	Unit	Duplicate	Driven By
4.1	<i>Overall requirements</i>				
4.1.1	Maximum overall mass of structure	50	kg		
4.1.2	Maximum distance between CoM and central axis	3	cm		
4.2	<i>Structure requirements</i>				
4.2.1	All resonant frequencies of lander structure above	35	Hz	3.1.4	
4.2.2	Withstand combined (static+dynamic) axial load factor of	8.5	g	3.3.1	
4.2.3	Withstand combined (static+dynamic) lateral load factor of	3	g	3.3.3	
	Withstand acoustic environment described in Fig. 3.2.2-2 and				
4.2.4	Table 3.4.4-2			<a href="https://www.ulalaunch.com">https://www.ulalaunch.com</a>	3.3.5
4.2.5	Withstand sinusoidal vibration described in Fig. 3.2.3-1			<a href="https://www.ulalaunch.com">https://www.ulalaunch.com</a>	3.3.6
4.2.6	Primary Payload Separation shock at 100 Hz	100	g	3.3.7	
4.2.7	Primary Payload Separation shock at 1000 Hz	4500	g	3.3.8	
4.3	<i>Landing system requirements</i>				
4.3.1	Survive impact on lunar surface with vertical velocity of	1.6	m/s	6.3.1	GNC
4.3.2	Survive impact on lunar surface with horizontal velocity of	1	m/s	6.3.1b	GNC
4.3.3	landing system will extend from center axis of lander	1.15	m		
	Maximum angle between center axis of lander and surface				
4.3.4	normal	5	deg		
4.3.5	Minimum counter-torque provided by landing system	10	Nm		
4.4	<i>Drill apparatus requirements</i>				
4.4.1	Target Material Density	~1.5	g/cc		
4.4.2	Drilling depth	60	cm		
4.4.3	Sample delivery form	Crushed	-		
4.4.4	Drilling Apparatus Power Requirement	250	W		
4.4.5	Drilling Apparatus Mass Requirement	16	kg		
4.4.7	Drilling operation time	125	mins		
4.4.8	Retain volatiles in sample	75	%		
4.5	<i>Requirements from other subteams</i>				
4.5.1	Maximum frequency of vehicle excitement by GNC system	35	Hz	6.3.2	Mechanical
4.5.2	Maximum angular velocity on vehicle separation	5	deg/sec	6.3.3	Mechanical
4.5.3	Maximum landing angular velocity in roll	0.5	deg/sec	6.3.4	GNC
4.5.4	Maximum landing angular velocity in pitch/yaw	0.5	deg/sec	6.3.5	GNC

## B.1.5 Thermal

No.	Requirement	Dimension	Unit	Duplicates
<b>5.1 Constraints</b>				
5.1.1	Maximum thermal system mass	11	kg	
5.1.2	Maximum thermal system power consumption	50	W	
<b>5.2 Reliability Requirements</b>				
5.2.1	Minimum reliability	0.99	-	
5.2.2	Safety Factor	1.2	-	
<b>5.3 Environment requirements</b>				
5.3.1	Minimum operable temperature	0	deg C	
5.3.2	Maximum operable temperature	30	deg C	
5.3.3	Minimum duration of operations	20	hours	1.4
<b>5.4 Requirements from other teams</b>				
5.4.1	Payload Requirements			
	NIR spectrometer min operable temperature	-20	deg C	-30 to 50 survivable
	NIR spectrometer max operable temperature	40		
	Inficon transpector max operating temperature	70	deg C	20C nominal
5.4.3	GNC Requirements			
	GNC sensors minimum operating temperature	-25	C	6.7.1
	GNC sensors maximum operating temperature	50	C	6.7.2
	Roll rate of lander during descent	0.6	deg/s	6.7.3
5.4.4	LV Int. Requirements			
	Separation system min operating temperature	-54	C	
	Separation system max operating temperature	128	C	
5.4.5	Power System Requirements			
	Battery min operating temperature	0	C	
	Battery max operating temperature	30	C	
5.4.6	Computer Requirements			
	Computer min operating temperature	-30	C	
	Computer max operating temperature	50	C	
5.4.7	Propulsion Requirements			
	Propellants Freezing Points	-50	C	
5.4.8	Comms requirements			
	Comms min operating temperature	-50	C	
	Comms max operating temperature	70	C	
<b>5.5 Launch Environment (Based on Atlas V 5YZ)</b>				
5.5.1	Max emittance of Payload Fairing Interior Wall	0.9	-	3.3.9
5.5.2	Max temp of PLF Interior Wall	88	C	3.3.10
5.5.3	Max peak heat flux radiated by PLF surfaces	536	W/m^2	3.3.11
5.5.4	Max emittance of PLF Acoustic suppression sy	0.1	-	3.3.12
5.5.5	Max temp of Payload Fairing Interior Wall	60	C	3.3.13
5.5.6	Payload adapter temperature range	0 - 49	C	3.3.14
5.5.7	Separation system thermal resistance	0.13	deg C/W	3.2.11

## B.1.6 Guidance, Navigation & Control

No.	Requirement	Dimension	Unit	Duplicates	Driven By
6.1	<b>INTERNAL</b>				
6.1.1	Maximum navigation system error of lander altitude above lunar surface estimation	1.66	m		GNC
6.1.2	Total maximum commanded angular accelerations due to 6.2.3 and disturbances	2	deg/s <sup>2</sup>	6.5.3	GNC
6.1.3	Maximum attitude deviation from commanded attitude	0.1	deg		GNC
6.1.4	Maximum attitude sensing deviation from commanded attitude	0.1	deg		GNC
6.2	<b>MISSION PLANNING</b>				
6.2.1	Maximum distance between actual and intended lander site	6000	m	1.2.1	MP
6.2.2	Maximum commanded angular acceleration for required maneuvers	1	deg/s <sup>2</sup>	1.2.2	MP
6.2.3	Fastest commanded slew in time	180 deg/60 sec	deg/sec	1.2.3	MP
6.3	<b>MECHANICAL</b>				
6.3.1	Maximum vertical impact velocity	1.6	m/s	4.3.2	GNC
6.3.1b	Maximum horizontal impact velocity	1	m/s	4.3.2b	GNC
6.3.2	Maximum frequency of vehicle excitement by GNC system	35	Hz	4.5.1	Mechanical
6.3.3	Maximum angular velocity on vehicle separation	5	deg/sec	4.5.2, 3.2.3	Mech, LV
6.3.3b	Separation velocity Range	0.3 - 0.4	m/s	3.2.2	GNC
6.3.4	Maximum impact angular velocity in roll	0.5	deg/sec	4.5.3	GNC
6.3.5	Maximum landing angular velocity in pitch/yaw	0.5	deg/sec	4.5.4	GNC
6.4	<b>POWER</b>				
6.4.1	Maximum GNC system algorithms & databases storage space occupation	10	MB	8.5.1	GNC
6.4.2	Maximum GNC sensor power draw	31.6	W	8.2.2	GNC
6.5	<b>PROPELLION</b>				
6.5.1	Maximum frequency of thruster pulses	35	Hz	7.1.1	Propulsion
6.5.2	Maximum commandable angular acceleration	17	deg/s <sup>2</sup>	7.2.2, 6.1.2	GNC
6.5.3	Maximum thruster pulse length	10	s	7.2.3	Propulsion
6.5.4	Fuel needed for attitude corrections	5	kg	7.2.4	GNC
6.6	<b>COMMUNICATIONS</b>				
6.6.1	Maximum download rate on descent	1.1	kb/s	9.3.1	GNC
6.6.2	Maximum upload rate on descent	1.1	kb/s	9.3.2	GNC
6.7	<b>THERMAL</b>				
6.7.1	GNC sensors minimum operating temperature	-25	C	5.4.3	GNC
6.7.2	GNC sensors maximum operating temperature	50	C	5.4.3	GNC
6.7.3	Roll rate of lander during descent	0.6	deg/s	5.4.3	Thermal

## B.1.7 Propulsion

No.	Requirement	Dimension	Unit	Duplicates	Driven By
<b>7.1 General propulsion requirements</b>					
7.1.1	Perform propulsive maneuvers for spacecraft of mass around	400	kg		
7.1.2	Dormant wait time after deployment (No RF or deployables)	30	sec	3.8	
7.1.3	Maximum frequency of thruster pulses	35	Hz	6.5.1	
<b>7.2 Requirements from other teams</b>					
7.2.1	Maximum frequency of thruster pulses	35	Hz	6.5.1	Prop
7.2.2	Maximum commandable angular acceleration	17	deg/s <sup>2</sup>	6.5.2, 6.1.2	GNC
7.2.3	Maximum thruster pulse length	10	s	6.5.3	Prop
7.2.4	Maximum acceleration of deltaV thrusters	5	m/s <sup>2</sup>	1.2.4	Mission Planning
7.2.5	Fuel needed for attitude corrections	5	kg	6.5.4	GNC
7.2.6	Longest burn time	200	s		Mission Planning
<b>7.3 LV Integration (Per AFSPCMAN 91-710V3 Ch 12.)</b>					
7.3.1	Minimum number of faults for critical failure	2	-		
7.3.2	Minimum number of faults for catastrophic failure	3	-		
7.3.3	Pressure vessels shielded from heat sources (i.e. combustor)	-	-		
7.3.4	Minimum design burst pressure of pressure vessels	1.5			
7.3.5	Minimum design burst pressure of lines and fittings (< 1.5")	4			
7.3.6	Minimum design burst pressure of other pressure components	2.5			

## B.1.8 Power

No.	Requirement	Dimension	Unit	Duplicates
8.1	<i>General Requirements</i>			
8.1.1	Total power required for mission	546.25	W	
8.1.2	Total energy required for mission	9280	Wh	
8.1.3	Thermal Range	0-30	C	
8.2	<i>Landing operation</i>			
8.2.1	Power required for processing unit	20	W	
8.2.2	Maximum GNC sensor power draw	31.6	W	6.4.2
8.2.3	Power required for thermal system	50	W	
8.3	<i>Nominal surface operations</i>			
8.3.1	Power required for drilling	250	W	4.4.5
8.3.2	Power required for scientific processing	55	W	2.2.1
8.3.3	Power required for communications	9.4	W	
8.3.4	Power required for thermal system	50	W	
8.4	<i>Margins</i>			
8.4.1	Minimum power margin	0.05	-	
8.4.2	Maximum power margin	0.25	-	
8.4.3	Fractional power losses, voltage conversion	0.2	-	
8.4.4	Minimum power loss fraction due to wiring	0.02	-	
8.4.5	Maximum power loss fraction due to wiring	0.05	-	
8.5	<i>LV Integration (Per AFSPCMAN 91-710V3 Ch 14.)</i>			
8.5.1	Wiring Material	Copper	-	
8.5.2	Batteries readily accessible for disconnection and removal	-	-	
8.5.3	Battery case burst pressure safety factor	3	-	
8.5.4	All external components grounded	-	-	
8.5.5	Interface with IFD connector for charging (pre T=0) and sep. confirmation	-	-	

## B.1.9 Communications

No.	Requirements	Dimension	Unit	Duplicates	Driven By
9.1	<i>General requirements</i>				
9.1.1	Frequency range	2-4	GHz		
9.1.2	Distance to transmit	3500-4000	Km		Mission Planning
9.2	<i>Payload requirements</i>				
9.2.1	Scientific data package size	1	MB/analysis	2.4.1	Payload
9.3	<i>GNC requirements</i>				
9.3.1	Maximum download rate on descent	1.1	kb/s	6.6.1	GNC
9.3.2	Maximum upload rate on descent	1.1	kb/s	6.6.2	GNC

## B.1.10 C&DH

No.	Requirements	Dimension	Unit	Duplicates	Driven By
10.1	<i>Constraints</i>				
10.1.1	Mass	5	kg		
10.1	<i>General Requirements</i>				
10.1.1	Total Memory	200	MB		
10.1.2	Power Consumption	20	W		
10.2	<i>Other Team's Requirements</i>				
10.2.1	Maximum GNC Memory	10	MB	6.4.1	GNC
10.2.2	Maximum Payload Memory	100	MB		Payload

## B.2 Orbiter Requirements

### B.2.1 Mission Planning

No.	Requirement	Dimension	Unit	Duplicates
1.1	<i>General Mission Planning Requirements</i>			
1.1.1	Orbital elements at lander separation			
1.1.1a	<i>Eccentricity</i>	0		
1.1.1b	<i>Inclination</i>	86	degrees	
1.1.1c	<i>Semi-major axis</i>	2138	km	
1.1.2	Orbital operational lifetime beyond lander mission	10	years	4.3.3

## B.2.2 LV Integration

No.	Requirement	Dimension	Unit	Duplicates	Driven By
<b>2.1 LV Integration requirements FOR ORBITER</b>					
2.1.1	Max module height in stowed config (in LV coord. sys)	42	Inch		
2.1.1b	Max module width in stowed config (in LV coord. sys)	46	Inch		
2.1.1c	Max module length in stowed config (in LV coord. sys)	56	Inch		
2.1.2	ESPA payload interface ring diameter	24	Inch		
2.1.3	ESPA ring fastener size	1/4	Inch		
2.1.4	All resonant frequencies above	35	Hz	3.2.1	
2.1.5	Number of 15-pin inflight-disconnect (IFD) connectors	2	-		
2.1.6	Maximum module launch mass	450	kg		
2.1.7	Maximum distance between COG and interface plane	20	Inch		
2.1.8	Tolerable Launch vehicle load factor in lateral & Axial directions*	8.5	g		
2.1.9	Dormant wait time after deployment (No RF or deployables)**	30	s		
*This requirement is superseded by req.2.2.1-3					
**Originally 30 minutes, but can be set arbitrarily since RF interference can be coordinated and avoided now that Erebus mission has assumed total control of the OMV, and that thrusters are angled away from OMV to prevent impingement.					
<b>2.2 Launch Environment (Load factors based on Falcon 9 (which presents worst case), all else based on Atlas V 5YZ)</b>					
2.2.1	Max combined (static+dynamic) axial load factor	8.5	g	3.2.2	
2.2.2	Min combined (static+dynamic) axial load factor	-4	g		
2.2.3	Max combined (static+dynamic) lateral load factor	3	g	3.2.3	
2.2.4	Max vectorially summed load factor	8.73	g		
2.2.5	<a href="#">Acoustic - See Figure 3.2.2-2 and table 3.4.4-2</a>	-	-	3.2.4	
2.2.6	<a href="#">Sinusoidal vibration - See Figure 3.2.3-1</a>	-	-	3.2.5	
2.2.7	Primary Payload Separation shock at 100 Hz	100	g	3.2.6	
2.2.8	Primary Payload Separation shock at 1000 Hz	4500	g	3.2.7	
2.2.9	Max emittance of Payload Fairing Interior Wall	0.9	-	5.5.1	
2.2.10	Max temp of PLF Interior Wall	88	C	5.5.2	
2.2.11	Max peak heat flux radiated by PLF surfaces	536	W/m^2	5.5.3	
2.2.12	Max emittance of PLF Acoustic suppression system	0.1	-	5.5.4	
2.2.13	Max temp of Payload Fairing Interior Wall	60	C	5.5.5	
2.2.14	Payload adapter temperature range	0 - 49	C	5.5.6	
2.2.15	Max depressurization rate	6.2	kPa/s		
2.2.16	Typical depressurization rate	2.5	kPa/s		
<b>2.3 LV Integration Requirements for ENTIRE ORBITAL MANEUVERING VEHICLE (ESPA RING + LANDERS + MODULES)</b>					
2.3.1	Max vehicle height in stowed config (in LV coord. sys)	42	Inch		
2.3.2	Max vehicle radius in stowed config (in LV coord. sys)	90	Inch		
2.3.3	ESPA primary interface bolt circle diameter	62.01	Inch		
2.3.4	ESPA ring fastener size	1/4	Inch		
2.3.5	All resonant frequencies above	35	Hz		
2.3.6	Number of 37 or 61-pin inflight-disconnect (IFD) connectors	2	-		
2.3.7	<a href="#">Electrical Current Limits - See Table 5.2.1-1</a>	-			

### B.2.3 Mechanical

No.	Requirement	Dimension	Unit	Duplicate	Driven By
3.1	<i>Overall requirements</i>				
3.1.1	Maximum overall mass of structure	50	kg		
3.1.2	Maximum distance between CoM and central axis	1	cm		
3.2	<i>Structure requirements</i>				
3.2.1	All resonant frequencies of lander structure above	35	Hz	2.1.4	
3.2.2	Withstand combined (static+dynamic) axial load factor of	8.5	g	2.2.1	
3.2.3	Withstand combined (static+dynamic) lateral load factor of	3	g	2.2.3	
3.2.4	Withstand acoustic environment described in Fig. 3.2.2-2 and Table 3.4.4-2	<a href="https://www.ulalaunch.com/docs/dl">https://www.ulalaunch.com/docs/dl</a>		2.2.5	
3.2.5	Withstand sinusoidal vibration described in Fig. 3.2.3-1	<a href="https://www.ulalaunch.com/docs/dl">https://www.ulalaunch.com/docs/dl</a>		2.2.6	
3.2.6	Primary Payload Separation shock at 100 Hz	100	g	2.2.7	
3.2.7	Primary Payload Separation shock at 1000 Hz	4500	g	2.2.8	
3.3	<i>Requirements from other subteams</i>				
3.3.1	Maximum frequency of vehicle excitement by GNC system	20	Hz	5.5.1	Mechanical
3.3.2	Maximum angular velocity on separation from OMV	2	deg/sec	5.5.2	
3.4	<i>Mechanisms requirements</i>				
3.4.1	Range of motion about both axes of HGA gimbal	180	deg		
3.4.2	Power throughput of solar array drive assembly	628	W		Power
3.4.3	Range of motion about both axes of solar array drive assembly	360+	deg		
3.4.4	HGA offset from spacecraft body	1	m		
3.4.5	All deployables must stow within the ESPA volume envelope.	-	-		
3.4.6	Solar array area	2.26	m^2		Power

## B.2.4 Thermal

No.	Requirement	Dimension	Unit	Duplicates
4.1	<i>Constraints</i>			
4.1.1	Maximum thermal system mass	16	kg	
4.1.2	Maximum thermal system power consumption	300	W	
4.2	<i>Reliability Requirements</i>			
4.2.1	Minimum reliability	0.99	-	
4.2.2	Safety Factor	1.2	-	
4.3	<i>Environment requirements</i>			
4.3.1	Minimum temperature	0	deg C	
4.3.2	Maximum temperature	40	deg C	
4.3.3	Minimum duration of operations	10	years	1.1.2
4.4	<i>Requirements from other teams</i>			
4.4.1	GNC Requirements			
	GNC sensors minimum operating temperature	-20	C	5.4.1
	GNC sensors maximum operating temperature	50	C	5.4.2
4.4.2	LV Int. Requirements			
	Separation system min operating temperature	-54	C	
	Separation system max operationg temperatur	128	C	
4.4.3	Power System Requirements			
	Battery min operating temperature	0	C	
	Battery max operating temperature	40	C	
4.4.4	Computer Requirements			
	Computer min operating temperature	-30	C	
	Computer max operating temperature	50	C	
4.4.5	Propulsion Requirements			
	Propellants Freezing Points	2	C	
4.4.6	Gimbal Requirements			
	Gimbal min operating temperature	-45	C	
	Gimbal max operating temperature	95	C	
4.4.7	Comms Requirements			
	Antenna min operating temperature	-50	C	
	Antenna max operating temperature	70	C	
4.5	<i>Launch Environment (Based on Atlas V 5YZ)</i>			
4.5.1	Max emittance of Payload Fairing Interior Wall	0.9	-	2.2.9
4.5.2	Max temp of PLF Interior Wall	88	C	2.2.10
4.5.3	Max peak heat flux radiuated by PLF surfaces	536	W/m^2	2.2.11
4.5.4	Max emittance of PLF Acoustic suppression sy	0.1	-	2.2.12
4.5.5	Max temp of Payload Fairing Interior Wall	60	C	2.2.13
4.5.6	Payload adapter temperature range	0 - 49	C	2.2.14

## B.2.5 Guidance, Navigation & Control

No.	Requirement	Dimension	Unit	Duplicates	Driven By
<b>5.1 POWER</b>					
5.1.1	Maximum GNC system algorithms & databases storage space occupation	100	MB		GNC
5.1.2	Maximum GNC system power draw	16.4	W		GNC
5.1.3	Average GNC system power draw	57.18	W		
<b>5.2 PROPULSION</b>					
5.2.1	Torque per momentum unloading firing	6	Nms	6.2.1	GNC
5.2.2	Maximum thruster pulse length	6	s	6.2.2	Propulsion
5.2.3	Fuel needed for attitude corrections	0.5	kg/year	6.2.3	GNC
5.2.4	Total pulses	92	pulses/year	6.2.4	GNC
<b>5.3 COMMUNICATIONS</b>					
5.3.1	Pointing accuracy towards Earth	360	deg	8.1.3	Comms
5.3.2	Pointing accuracy towards Moon	14	deg	8.1.4	Comms
<b>5.4 THERMAL</b>					
5.4.1	GNC sensors minimum operating temperature	-20	C	4.4.1	GNC
5.4.2	GNC sensors maximum operating temperature	50	C	4.4.1	GNC
<b>5.5 MECHANICAL</b>					
5.5.1	Maximum frequency of vehicle excitement by GNC system	20	Hz	3.3.1	Mechanical
5.5.2	Maximum angular velocity on separation from OMV	2	deg/sec	3.3.2	GNC

## B.2.6 Propulsion

No.	Requirement	Dimension	Unit	Duplicates	Driven By
<b>6.1 General propulsion requirements</b>					
6.1.1	Power requirement of cat bed/thruster	10	W		Thruster spec
6.1.2	Power requirement of FCV/thruster	10	W		Thruster spec
6.1.3	Propellant throughput max/thruster	67	kg		Thruster spec
6.1.4	Pulses / thruster				Thruster spec
6.1.5	Thrust range	0.320-1.1	N		Thruster spec
6.1.6	Isp, nominal	220	s		Thruster spec
6.1.7	Voltage input thruster	28+-4	V		Thruster spec
6.1.8	Propellant	Hydrazine			
6.1.9	Qualified Operating Temperature Range(Cat Bed)	10-50	deg C		
6.1.10	Freezing Point of Hydrazine	2	deg C		
6.1.11	Mass of thruster, unfuelled	0.29	kg		
<a href="http://www.space-propulsion.com/spacecraft-propulsion/hydrazine-thrusters/1n-hydrazine-thruster.html">http://www.space-propulsion.com/spacecraft-propulsion/hydrazine-thrusters/1n-hydrazine-thruster.html</a>					
<b>6.2 Requirements from other teams</b>					
6.2.1	Torque per momentum unloading firing	6	Nms	5.2.1	GNC
6.2.2	Maximum thruster pulse length	6	hr	5.2.2	Prop
6.2.3	Fuel needed for attitude corrections	0.06	kg/year	5.2.3	GNC
6.2.4	Longest burn time		s		Mission Planning
6.2.5	Total pulses	92	pulses/year	5.2.4	GNC
<b>6.3 LV Integration (Per AFSPCMAN 91-710V3 Ch 12.)</b>					
6.3.1	Minimum number of faults for critical failure	2	-		
6.3.2	Minimum number of faults for catastrophic failure	3	-		
6.3.3	Pressure vessels shielded from heat sources (i.e. combustor)	-	-		
6.3.4	Minimum design burst pressure of pressure vessels	1.5			
6.3.5	Minimum design burst pressure of lines and fittings (< 1.5")	4			
6.3.6	Minimum design burst pressure of other pressure components	2.5			

## B.2.7 Power

No.	Requirement	Dimension	Unit
7.1 General Requirements			
7.1.1	Total power required in shade	620	W
7.1.2	Total power required in sun	230	W
7.1.3	Total energy required in shade (per orbit)	671	Wh
7.1.4	Total energy required in sun (per orbit)	476	Wh
7.1.5	Thermal Range	0-30	C
7.2 Margins			
7.2.1	Minimum power margin	0.05	-
7.2.2	Maximum power margin	0.25	-
7.2.3	Fractional power losses, voltage conversion	0.2	-
7.2.4	Minimum power loss fraction due to wiring	0.02	-
7.2.5	Maximum power loss fraction due to wiring	0.05	-
8.5 LV Integration (Per AFSPCMAN 91-710V3 Ch 14.)			
8.5.1	Wiring Material	Copper	-
8.5.2	Batteries readily accessible for disconnection and removal	-	-
8.5.3	Battery case burst pressure safety factor	3	-
8.5.4	All external components grounded	-	-
8.5.5	Interface with IFD connector for charging (pre T=0) and sep. confirmation	-	-

## B.2.8 Communications

No.	Requirements	Dimension	Unit	Duplicates	Driven By
8.1 General requirements					
8.1.1	Frequency range	26-40	GHz		Comms
8.1.2	Distance to transmit	406,004.67	Km		Mission Planing
8.1.3	Pointing accuracy towards Earth	0.2	deg	5.3.1	Comms
8.1.4	Pointing accuracy towards Moon	14	deg	5.3.2	Comms

## B.2.9 C&DH

No.	Requirements	Dimension	Unit	Duplicates
9.1 Constraints				
9.1.1	Mass	6	kg	
9.2 General Requirements				
9.2.1	Total Memory	200	MB	
9.2.2	Power Consumption	20	W	
9.3 Other Team's Requirements				
9.3.1	Maximum GNC Memory	10	MB	

# Appendix C: Detailed Mass Budgets

## C.1 Lander Mass Budget

Subsystem	Component	Mass (kg)	Volume (L)		Subsystem	Component	Mass (kg)	Volume (L)
Communications	Broadband antenna	0.4	0.11		Payload	Laboratory structure	14	16.4
	S-band transmitter	0.25	0.38			NIR spectrometer	1	--
	S-band receiver	0.22	0.3			NASA RIMFAX	3	1.3
	Master cable	2	0.6			Mass spectrometer	2	--
	<b>Subsystem total</b>	<b>2.87</b>	<b>1.39</b>			<b>Subsystem total</b>	<b>20</b>	<b>17.7</b>
Mechanisms	<b>MGA (%)</b>	<b>15</b>				<b>MGA (%)</b>	<b>25</b>	
	<b>Total with margin</b>	<b>3.3</b>				<b>Total with margin</b>	<b>25.0</b>	
	TRIDENT drill	16	23		Propulsion	200 N biprop thrusters	7.6	3.1
	Landing system legs	5.33	5			10 N biprop thrusters	3.15	0.75
	Crush cores	0.2	--			Propellant tanks	7.63	200
Structure/LV Integration	Dampers	2	--			Helium tanks	5.09	36.8
	Landing pads	2.23	--			Plumbing/valves**	12.9	--
	<b>Subsystem total</b>	<b>25.76</b>	<b>28</b>			<b>Subsystem total</b>	<b>36.37</b>	<b>240.65</b>
	<b>MGA (%)</b>	<b>25</b>				<b>MGA (%)</b>	<b>15</b>	
	<b>Total with margin</b>	<b>32.2</b>				<b>Total with margin</b>	<b>41.8</b>	
Power/C&DH	Frame	30.4	770 (total available)		Thermal	Heater/controller/sensor	0.35	0.36
	Bracing	7.6	--			Coating	0.71	--
	Aluminum panels	1.1	6.35			<b>Subsystem total</b>	<b>1.06</b>	<b>0.36</b>
	Separation system	2.42	9.5			<b>MGA (%)</b>	<b>300</b>	
	<b>Subsystem total</b>	<b>41.52</b>	<b>15.85</b>			<b>Total with margin</b>	<b>4.2</b>	
	<b>MGA (%)</b>	<b>15</b>	(not including structure)		GNC	Radar (x2)	1.72	2.15
	<b>Total with margin</b>	<b>47.7</b>				IMU (x2)	1	2.69
	Batteries	23.6	35.3			Star tracker (x2)	0.7	0.25
	Harnessing*	--	--			Sun sensor (x6)	0.21	0.13
	Flight computer	5	2.5			<b>Subsystem total</b>	<b>3.63</b>	<b>5.22</b>
	<b>Subsystem total</b>	<b>28.6</b>	<b>37.8</b>			<b>MGA (%)</b>	<b>15</b>	
	<b>MGA (%)</b>	<b>25</b>				<b>Total with margin</b>	<b>4.2</b>	
	<b>Total with margin</b>	<b>35.8</b>						

\* = accounted for in Power/C&DH margin

\*\* = based on plumbing lines/valves ~1.2x mass of thrusters (SMAD)

<b>Dry Mass:</b>	<b>194.2 kg</b>
<b>System-Level Margin:</b>	<b>10 %</b>
<b>Total Dry Mass:</b>	<b>213.7 kg</b>
<b>Propellant Mass:</b>	<b>220 kg</b>
<b>Total Wet Mass:</b>	<b>433.7 kg</b>

<b>Propellant Budget</b>	
For given dry mass:	<b>192.3 kg</b>
ADCS:	<b>5 kg</b>
Margin (10% + 2% res.):	<b>22.7 kg</b>
Total propellant mass:	<b>220 kg</b>

## C.2 Orbiter Mass Budget

<b>Subteam</b>	<b>Component</b>	<b>Mass (kg)</b>
Structures	Frame	30.4
	Bracing	7.6
	Paneling	1.1
	Separation system	2.42
	<b>Total</b>	41.52
Mechanisms	Moog EPGA	6.5
	Honeybee SADA (x2)	2
	Antenna mast	1.4
	Deployment mechanisms	5
	<b>Total</b>	14.9
Communications	Patch antenna	0.4
	S-band Rx/Tx	0.47
	Parabolic reflector antenna	3
	Ka-band Rx/Tx	0.6
	Master cable	3
	<b>Total</b>	7.47
Power&DH	Batteries	16.02
	Flight computer	6
	Solar array*	25.12
	Harnessing**	--
	<b>Total</b>	47.14
Propulsion	Thrusters	3.48
	Propellant lines + valves	4.18
	Propellant tanks	1.27
	<b>Total</b>	8.93
Thermal	Louvers	15
	Coating	1
	<b>Total</b>	16
GNC/ADCS	Reaction wheels (x4)	16.4
	Sun sensors (x6)	0.20
	Star trackers (x2)	0.1
	IMUs (x2)	1
	<b>Total</b>	17.70

\* Solar Array Mass Calculation

Solar array power:	628 W
Specific power:	25 W/kg
Total array mass:	25.12 kg

Dry mass:	153.7 kg
System-level margin:	50 %
Total dry mass:	230.5 kg
Propellant mass:	12.7 kg
Total wet mass:	243.2 kg

\*\* = accounted for in margin

## Appendix D: Mission Planning

### D.1 Launch Option Visualizations

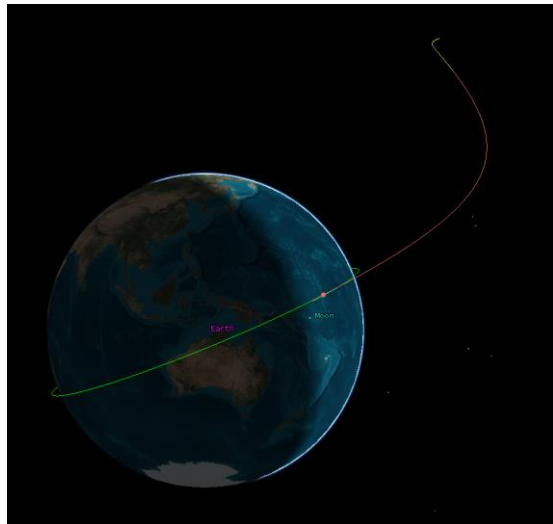


Figure D.1.1: Launch from LEO

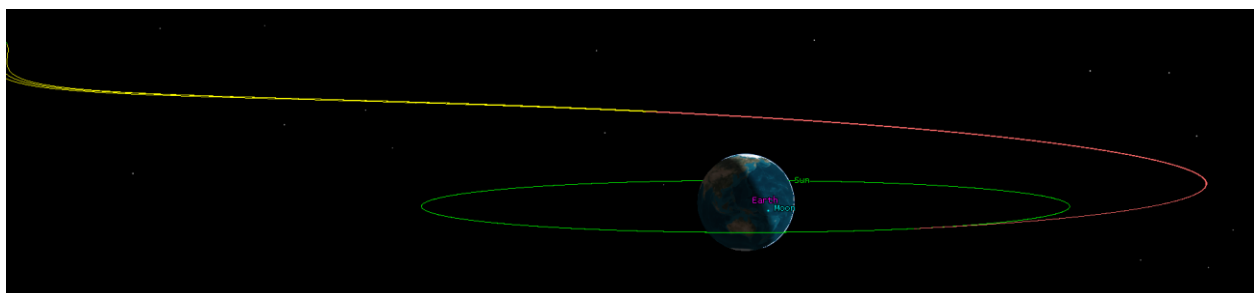


Figure D.1.2: Launch from GEO

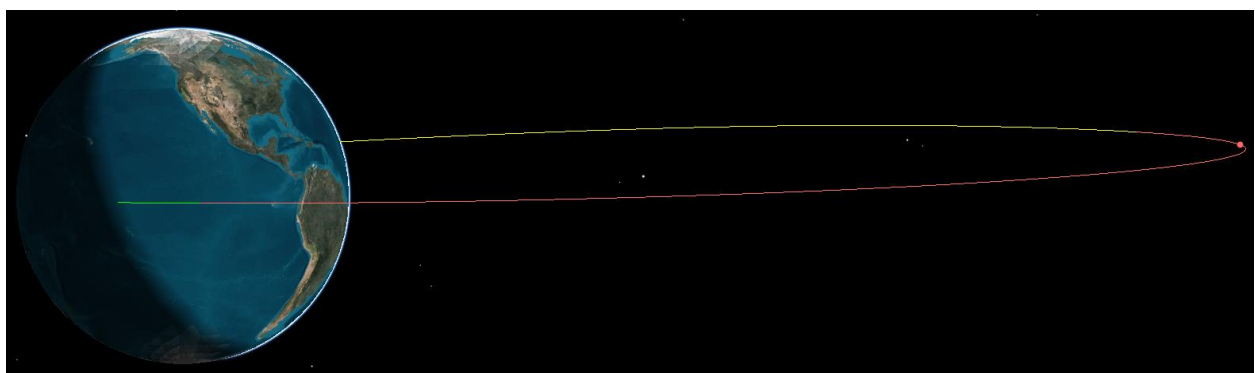


Figure D.1.3: Launch from GTO

# Appendix E: LV Integration

## E.1 OMV Dry Mass Estimation

Component	Mass (kg) - GTO Case	Mass (kg) - TLI Case
ESPA Grande Ring	286.6	211.0
Laser Altimeter	23	23
High gain antenna and gimbal	7.5	7.5
Transmitter and receiver chips for HGA	2	2
Additional DeltaV Capability (i.e. larger thrusters, heavier valves and plumbing to deal with larger tanks)	20	20
Total "Payload" Mass	<b>339.1</b>	<b>263.5</b>

Table E.1.1: OMV “payload” mass estimation.

OMV Dry Mass Estimation (Based on SMAD Avg. Dry mass distribution for Planetary spacecraft <sup>209*</sup> )			
Subsystem	Proportion of dry mass	Mass (kg) - GTO Case	Mass (kg) - TLI Case
OMV "Payload" (Extra Comms + ESPA Ring + Impulsive Prop. System)	0.45	339	264
Structure (Non-ESPA) and Mech	0.05	38	29
Thermal Control	0.03	23	18
Power (inc. Harness)	0.17	128	100
TT&C	0.05	38	29
On-Board Processing	0.03	23	18
ADCS	0.05	38	29
Propulsion	0.14	105	82
Other (Balance + launch)	0.03	23	18
Mass growth margin	0.25	188	146
<b>Tug Dry Mass (With Margin, no modules):</b>	<b>1.25</b>	<b>942</b>	<b>732</b>

\*Note: Mass distribution differs from SMAD because some mass is proportionally redistributed to “payload” to account for ESPA ring mass

Table E.1.2: OMV dry mass estimation.

<sup>209</sup> Wertz, J. et al. “Mass and Power Distribution for Spacecraft.” *Space Mission Engineering the New SMAD*. Microcosm Press, 2011, p. 948.

## E.2 OMV Launch Mass and Propellant Mass Calculation

	Impulsive Maneuver from TLI to LLO	Impulsive Transfer from LEO to LLO	Impulsive Maneuver from LLO to Frozen Orbit	Impulsive Transfer from GTO to LLO	Deorbit from Frozen Orbit
<b>Delta-V req (m/s)</b>	828.9	4040	200.75	1160.9	29.6
<b>Specific Impulse, <math>I_{sp}</math> (s)</b>	270	270	270	270	270
<b>Exhaust Velocity, <math>u_e</math> (m/s)</b>	2648.7	2648.7	2648.7	2648.7	2648.7
<b>Rocket mass ratio, <math>mf/mi</math></b>	0.73	0.22	0.93	0.65	0.99
<b>Source for Delta-V Requirement</b>	Calculations from TLI to LLO from mission planning, plus GTO to TLI deltaV using a Hohmann transfer	Calculations from Mission Planning	Calculations from Mission Planning	Calculations from Mission Planning	Calculations from Mission Planning

Table E.2.1: Delta-V and propellant characteristics (assuming the same MON/MMH propellant and Isp values as the lander, described in Section 5.5.1).

The rocket mass ratio in Table E.2.1 for each maneuver was calculated starting from  $I_{sp}$ ,  $u_e$ , and Delta-V using the Tsiolkovsky rocket equation:

$$\frac{m_i}{m_{i+1}} = e^{\Delta V/u_e} \quad . \quad (\text{E.2.1})$$

The rocket mass ratio for each maneuver was then used to propagate the dry mass of the OMV to the launch mass in Table E.2.2.

Item or Event	Mass (GTO Case)	Mass (TLI Case)	Unit
Number of Propellant Modules	0	0	-
Number of Orbiters	1	1	-
Number of Landers	1	1	-
Number of other rideshare payloads	2	2	kg
Dry Mass of Propellant Module	129	129	kg
Wet mass of lander	434	434	kg
Wet mass of other rideshare payloads	<b>340</b>	<b>400</b>	kg
Orbiter Module Mass (estimate)	249	249	kg
Tug Dry Mass (No Modules)	942	732	kg
OMV mass post deorbit maneuver (i.e. tug dry mass)	942	732	kg
OMV mass post orbiter separation (@ frozen orbit)	952	740	kg
OMV mass pre orbiter separation (@ frozen orbit)	1201	989	kg
OMV Mass post Lander Separation (@ LLO)	1295	1067	kg
OMV Mass pre Lander Separation (@ LLO)	2409	2300	kg
OMV mass before transit from drop-off, without fuel margin	3734	3145	kg
Minimum necessary propellant mass	1430	931	kg
Propellant margin mass (20%)	286	186	kg
<b>Propellant mass with margin</b>	<b>1716</b>	<b>1117</b>	kg
<b>OMV mass before transit, with all margins</b>	<b>4020</b>	<b>3332</b>	kg

Table E.2.2 OMV mass propagation.

### E.3 OMV Tank Sizing and Validation

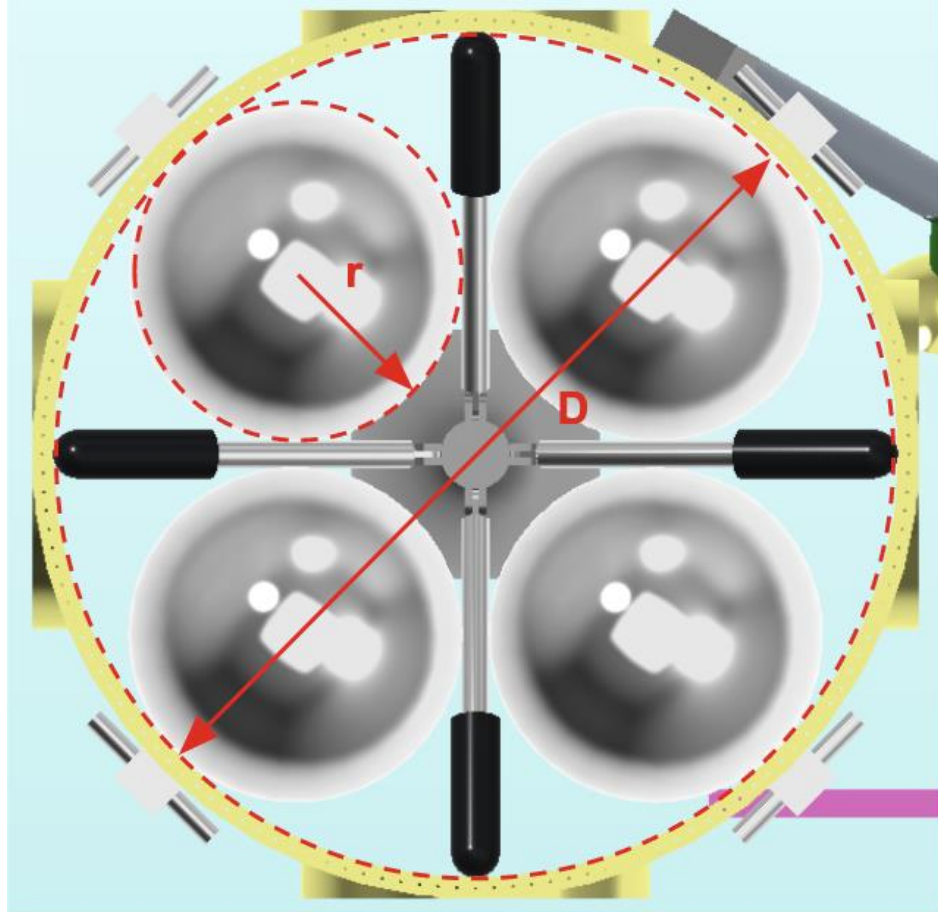


Figure E.3.1. Top view of OMV mockup, showing tank arrangement and visually defining variables relevant to tank sizing.

$$r_{max} = \frac{D}{2(1 + \sqrt{2})} \quad (\text{E.3.1})$$

$$V_{domed\ cylinder} = \pi r^2 \left( h - \frac{2}{3}r \right) \quad (\text{E.3.2})$$

Dimension	Value for Stretched ESPA (GTO case)	Value for Standard ESPA (TLI case)	Units
-----------	--	---------------------------------------	-------

ESPA Grande Interior diameter, $D$	60	60	in
Height, $h$	59	42	in
Mass of custom ESPA Grande	286.6	211	kg
Max propellant tank radius (4 tanks), $r$	12.43	12.43	in
Volume per domed cylindrical tank, $V$	24603	16356	in <sup>3</sup>
Volume per domed cylindrical tank	<b>0.403</b>	<b>0.268</b>	m <sup>3</sup>
Total internal tank volume (4 tanks)	<b>1.613</b>	<b>1.072</b>	m <sup>3</sup>

Table E.3.1: Calculating maximal internal propellant capacity from ESPA height and width. Equations E.3.1 and E.3.2 were used.

Dimension	Value for Stretched ESPA Grande (GTO config.)	Value for Standard ESPA Grande (TLI config.)	Units
Propellant Mass, from TLI	1188	1117	kg
Propellant Mass, from GTO	1716	1622	kg
Propellant Mass, from LEO	12457	11877	kg
Propellant density (average)	1065		kg/m <sup>3</sup>
Total Propellant Volume, from TLI	1.116	1.049	m <sup>3</sup>
Total Propellant Volume, from GTO	1.612	1.523	m <sup>3</sup>
Total Propellant Volume, from LEO	11.697	11.152	m <sup>3</sup>
Available Volume of ESPA Interior	<i>1.61</i>	<i>1.07</i>	m <sup>3</sup>
Exterior Propellant Volume needed, from TLI	-0.497	-0.023	m <sup>3</sup>
Exterior Propellant Volume needed, from GTO	-0.001	0.450	m <sup>3</sup>
Exterior Propellant Volume needed, from LEO	10.084	10.080	m <sup>3</sup>
Available Volume of 1 lander-sized module	0.838		m <sup>3</sup>
External propellant modules needed, from TLI	-0.59	<b>-0.03</b>	-
External propellant modules needed, from GTO	<b>0.00</b>	0.54	-
External propellant modules needed, from LEO	12.03	12.03	-

Table E.3.2: Validation that the propellant required for the entire OMV mission can fit inside the internal fuel tanks.

## E.4 Separation System

Product	<u>SNC QwkSep 24"</u> (Pyro)	<u>SNC QwkSep 24"</u> (Non-Pyro)	<u>RUAG PAS 610S</u>	<u>PSC Lightband</u>
Core Tech	CBOD	CBOD	CBOD	CBOD
Payload Capacity (@20" CoM)(kg)	300	300	500	900
Stack Height (in)	2.1	2.1	2.87	2.1
Full system mass (kg)	9.5	9.5	5.8	8.95
Flyaway mass	2.3	2.3	1.0	2.42
Source Shock near actuator	1000g @ 1-2 kHz	100g @ 10 Hz - 10 kHz	<100g @ 1kHz	~100g @ 1-2 kHz
Tip-off rate (max) (deg/s)	0.5	0.5	No Info	Adjustable: 0-5
Separation velocity (min) (m/s)	0.3	0.3	No Info	Adjustable: .2-.5
Operating Temperature (deg C)	-68 to 104	-65 to 75	No Info	-40 to 70 35 (optimal)
Heritage	100+ flights (diff. sizes)	660+ flights (diff. sizes)	60+ flights (diff sizes)	45+ (diff sizes)

Table E.4.1: ESPA payload separation system product study.

		Lander	2nd Payload	3rd Payload	Orbiter	
Inputs	Desired relative velocity, $V$	0.3	0.3	0.3	0.22	m/s
	Lander Mass, $m$	434	340	340	249	kg
	OMV Mass (post-sep), $M$	1975	1635	1295	952	kg
	PE per spring, $E_s$	0.85	0.85	0.85	0.85	J
	CM offset, $d$	0.03	0.03	0.03	0.01	m
	Moment of Inertia, $I$	70.0	70.0	70.0	40.0	kg*m^2
Calculated Quantities	PE needed, $E$	16.01	12.67	12.12	4.78	J
	Springs needed	18.84	14.90	14.26	5.62	-
	<b>Springs equipped, <math>n</math></b>	<b>19</b>	<b>15</b>	<b>15</b>	<b>6</b>	-
	<b>Actual relative velocity</b>	<b>0.301</b>	<b>0.301</b>	<b>0.308</b>	<b>0.227</b>	m/s
	Rotation rate, $\omega$	0.056	0.044	0.045	0.014	rad/s
	<b>Rotation rate</b>	<b>3.212</b>	<b>2.514</b>	<b>2.570</b>	<b>0.810</b>	deg/s

Table E.4.1: Calculations for the number of springs required per separation event (GTO Case).

## E.5 OMV as Communications Link during Lander Descent

The OMV will remain in LLO for as long as necessary to guide the lander's descent. Figure E.5.1 depicts the OMV with the laser altimeter pointing towards the lunar nadir, the orbiter module's low-gain antenna pointing towards the lander, and the OMV's HGA pointing towards Earth. The orbiter's solar arrays may be deployed as shown if additional power is found to be necessary in future work.

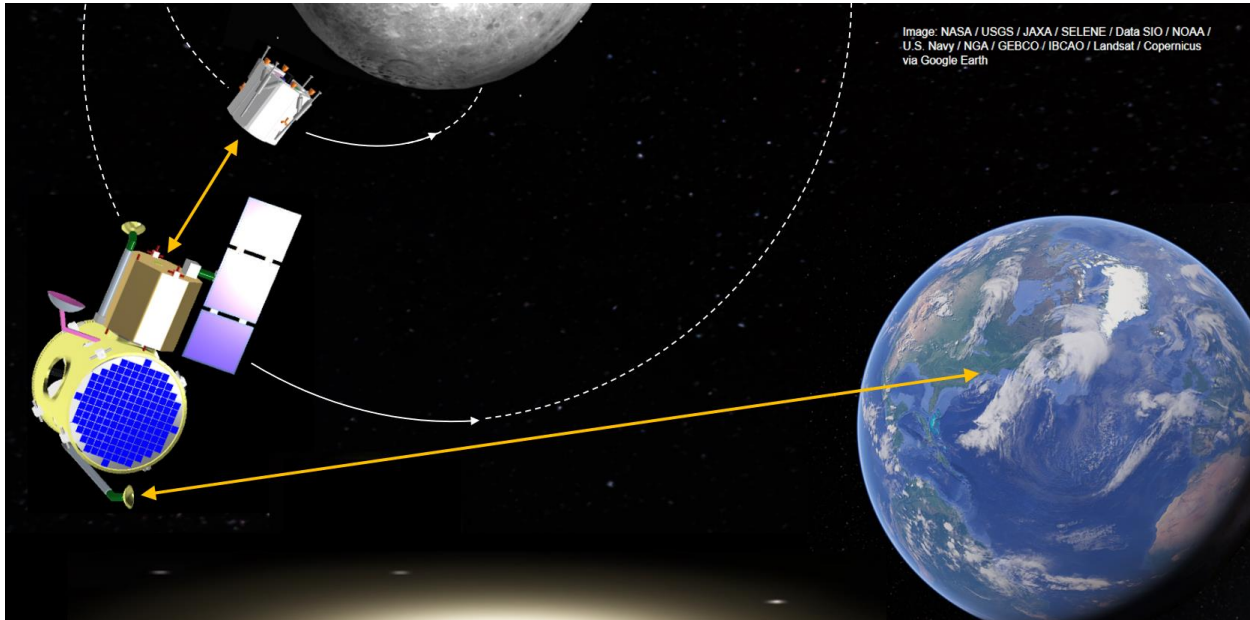


Figure E.5.1: The OMV in as a communications link during lander descent.

# Appendix F: Structures

## F.1 Aluminum Honeycomb Panels

The makeup of the honeycomb panels is assumed to be two 0.5 mm thick sheets of Al 2024 T3, with 0.5" (12.7 mm) of Al 5056 honeycomb between them, based on the highest-density aluminum honeycomb available from APCO Technologies. The two sheets have a density of 2710 kg/m<sup>3</sup>; the aluminum honeycomb has a density of 72 kg/m<sup>3</sup>.<sup>210</sup>

$$\text{Mass} = \text{Area} * \text{Height} * \text{Density}$$

$$\begin{aligned}\text{Mass per unit area} &= \text{Height} * \text{Density} = 1 \text{ mm} * 2710 \text{ kg/m}^3 + 12.7 \text{ mm} * 72 \text{ kg/m}^3 \\ &= 0.001 \text{ m} * 2710 \text{ kg/m}^3 + 0.0127 \text{ m} * 72 \text{ kg/m}^3 \\ &= 3.62 \text{ kg/m}^2\end{aligned}$$

The panels on the lander and orbiter structures have an area of 468 in<sup>2</sup> = 0.3 m<sup>2</sup>. Given the mass per unit area of 3.62 kg/m<sup>2</sup>, this comes to a total panel mass of 1.1 kg.

---

<sup>210</sup> "Honeycomb Characteristics," APCO Technologies, 2018. <https://www.apco-technologies.eu/apco-content/uploads/2018/04/Catalogue-PdV-LR.pdf>.

## F.2 Aluminum Alloy Characteristics

The following chart compares a variety of material properties across several Aluminum alloys. Up for consideration for the structure were Al 2024, 6061, and 7075. 6061, as stated previously, was selected for its weldability.

ALUMINUM ALLOY CHARACTERISTICS																			
Alloy	Temper	Gen'l. Availability			Typical Characteristics*				Specified Mechanical Properties										
		Flat Sheet	Coil Sheet	Cut to Length Sheet	Corrosion Resistance	Cold Workability	Machinability	Brazability	Gas	Arc Resistance, spot and seam	Where range is shown, property varies with specific width and/or thickness dimensions								
		Plate																	
Non-Heat Treatable Alloys	1100	O	x	x	x	-	A	A	D	A	A	B	11	15.5	3.5 <sup>1</sup>	-	15-30	-	
		H14	X	X	X	-	A	A	C	A	A	A	16	21	14 <sup>1</sup>	-	3-9	-	
		F	-	-	X	-	A	-	-	-	-	-	-	-	-	-	-	-	
	3003	O	X	X	X	-	A	A	D	A	A	B	14	19	5 <sup>1</sup>	-	14-25	-	
		H14	X	X	X	-	A	B	C	A	A	A	20	26	17 <sup>1</sup>	-	1-7	-	
		F	-	-	X	-	A	-	-	-	-	-	-	-	-	-	-	-	
	5052	O	X	X	X	-	A	A	D	C	A	B	25	31	9.5 <sup>1</sup>	-	15-20	-	
		H32	X	X	X	X	A	B	C	C	A	A	31	38	23 <sup>1</sup>	-	4-9	11-12	
		H34	X	X	X	-	A	B	C	C	A	A	34	41	26 <sup>1</sup>	-	3-7	-	
Heat-Treatable Alloys	Bare 2024	O <sup>3</sup>	X	-	-	X	C	B	D	D	C	B	-	32	-	14	12	12	-
		T3	X	-	-	-	C	C	B	D	D	C	63-64	-	42	-	10-15	-	
		T351	-	-	-	X	C	C	B	D	D	C	56-64	-	40-41	-	-	4-12	
	Alclad 2024	T42 <sup>2</sup>	-	-	-	-	C	C	B	D	D	C	58-62	-	38	-	12-15	4-12	
		O <sup>3</sup>	X	X	-	X	A	B	D	D	C	B	-	30-32	-	14	10-12	12	-
		T3	X	-	-	-	A	D	B	D	D	C	58-63	-	39-40	-	10-15	-	
	6061	T351	-	-	-	X	A	D	B	D	D	C	56-63	-	40-41	-	-	4-8	
		T42 <sup>2</sup>	-	-	-	-	A	D	B	D	D	C	55-61	-	34-38	-	10-15	4-12	
		O <sup>31</sup>	X	X	-	X	A	A	D	A	A	B	-	22	12	12	10-18	16-18	-
	7075	T4	X	-	-	-	A	C	C	A	A	A	30	-	16	-	10-16	-	
		T6	X	-	-	-	A	C	C	A	A	A	42	-	35	-	4-10	-	
		T651	-	-	-	X	A	C	C	A	A	A	40-42	-	35	-	-	6-10	
	Alclad 7075	T42 <sup>2</sup>	-	-	-	-	A	C	C	A	A	A	30	-	14	-	10-16	16-18	
		O <sup>1</sup>	X	-	-	-	C	D	D	D	D	B	-	40	-	21	10	-	
		T6	X	-	-	-	C	D	B	D	D	B	76-77	-	65-66	-	7-8	-	
	Alclad 7075	T651	-	-	-	X	C	D	B	D	D	B	67-77	-	53-66	-	-	2-8	

Ratings A, B, C, D are relative in decreasing order of merit. weldability and brazability ratings are specifically defined as:

A - Generally weldable by all commercial procedures and methods.

B - Weldable with special technique or specific applications which justify preliminary trials or testing to develop welding procedure and weld performance.

C - Limited weldability because of crack sensitivity or loss on resistance to corrosion, and all mechanical properties.

D - No commonly used welding methods have so far been developed.

1 - These yield strengths not determined unless specifically requested.

2 - Although sheet and plate are not sold in this temper, material heat treated from any temper by the user should attain the mechanical properties applicable to this temper.

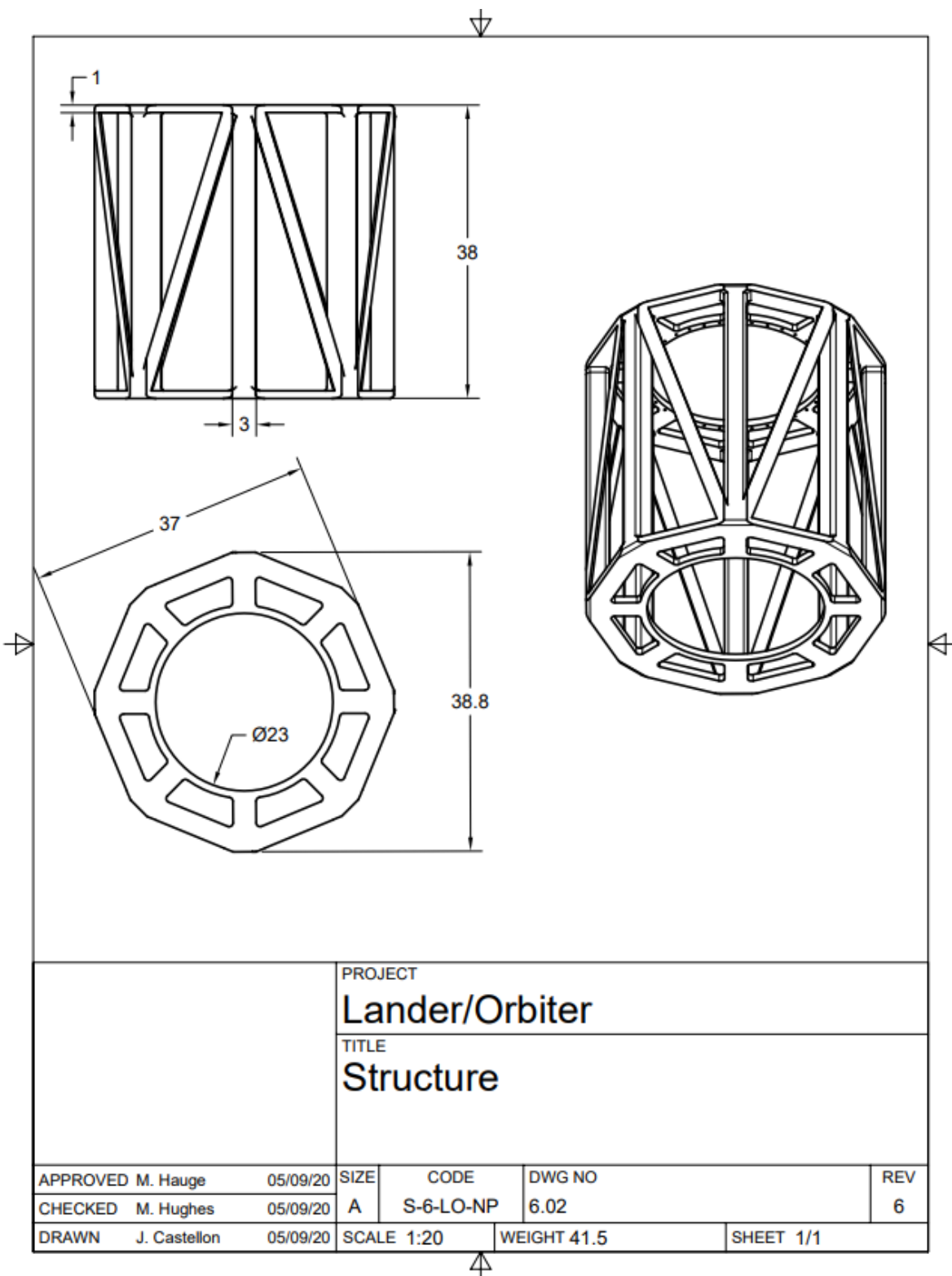
3 - Annealed (O temper) material shall, upon heat treatment, be capable of developing the mechanical properties applicable to T 42 temper material.

4 - Annealed (O temper) material shall, upon heat treatment and aging, be capable of developing the mechanical properties applicable to T 67 temper material.

Figure F.1: Weldability of aluminum alloys.<sup>211</sup>

<sup>211</sup> "Aluminum Alloy Characteristics," Aircraft Spruce and Specialty Co., 2020. <https://www.aircraftspruce.com/pdf/2015Individual/Cat15056.pdf>.

### F.3 Lander/Orbiter Structure Drawing



# Appendix G: Mechanisms

## G.1 Landing System Calculations

### Determining Footing Diameter

The section below outlines the iterative process that was used to determine the landing system's footing diameter. All references in this section stem from the Lunar Sourcebook.<sup>212</sup>

For rover wheel footing width ~0.2m, the ultimate bearing strength is >100kPa.

Maximum allowable static bearing capacity is 2 kPa per cm of settlement.

Safety factor of 2: 1kPa.

Lander Mass at touchdown: less than 251kg (assuming 1/4 the fuel remains).

Weight: 407N (~92lbf)

Vertical velocity of 5 m/s (worst case): kinetic energy of 3140 J

Desired: less than 3cm of settlement

Force supported by ground is proportional to settling depth:  $F/A = 2\text{kPa}/\text{cm} \cdot d$

Energy absorbed by ground is force integrated over depth settled:  $E = F \cdot d = 2\text{kPa}/\text{cm} \cdot d^2/2 * A$

$E = 1\text{kPa}/\text{cm} \cdot d^2$  If  $d^2 = 0.03\text{m} \cdot 3\text{cm}$ ,  $E = 0.09 \cdot A [\text{kPa} \cdot \text{m}] = 90A [\text{J}/\text{m}^2]$

$A = 3140/90 \text{ m}^2 = 35\text{m}^2 \leftarrow \text{Too large - unphysical!}$

According to the Lunar Sourcebook, "The dynamic ultimate bearing capacity defines the maximum resistance to impact loading. This dynamic capacity is always greater than the static capacity because of the inertial resistance of the soil."

From lunar landing gear design: Bearing capacity was assumed to be about 7 kPa

If the suspension can compress during landing impact, the maximum force transmitted to the soil will be small since the impulse is distributed over a longer time. The energy can be dissipated over 0.2m of travel.

$E = F \cdot d$ ,  $F = 15700\text{N}$ . At 7kPa bearing capacity, the total footpad area would need to be  $2.24\text{m}^2$ .

If it's drifting horizontally at 1 m/s and about to tip over, only 2 of the 4 feet would be supporting this impact. So each footpad needs  $1.12 \text{ m}^2$  of area. Circular pad w/ diameter: 1.2m. Still too large!

From lunar landing gear design:  $k = 5.0 \cdot 10^8 \text{ N/m}$  (Ground Stiffness Coefficient), assuming footpad diam. of 0.94m (pg. 62)  $\Rightarrow A = 0.693 \text{ m}^2$ . This results in a bearing strength per cm of settling of: 7215 kPa / cm. That's much greater than the footprint data (Fig. 9.37) suggests, but Fig. 9.36 shows that bearing strength increases with footing width. (Figures from Lunar Sourcebook, not included in this report).

---

<sup>212</sup> *Lunar Sourcebook*, ed. by Grant H. Heiken, David T. Vaniman, and Bevan M. French (Cambridge: Cambridge University Press, 1991).

If the footing diameter was 0.3m, the ultimate bearing capacity is around 400 kPa.  
 $15700\text{N}/400,000\text{Pa} = 0.039\text{m}^2$ . Smaller; further iteration necessary.

Footing diameter: 0.2m → Bearing strength: 300kPa. → Footing diameter needed (two circular pads): 0.18m. Convergence! Chosen footing diameter: 0.2 m = 8".

Check static loading: Sitting under the Moon's gravity, stress on all four feet is  $407\text{N}/0.125\text{m}^2 = 3.2\text{kPa}$ . At 2kPa/cm settling, that's 1.6cm of settling, which is acceptable.

## Primary Damper

**Candidate 1:** Based on the Hexcel's honeycomb selector guide, the landing system will use Aluminum Hexagonal Honeycomb crush core, since it is "Recommended for Energy Absorption."<sup>213</sup> The best core for this is the one with the highest crush strength (psi) per density (pcf). Cell size has no effect on this ratio, it is only a function of density.<sup>214</sup>

The best of these is the 5/32" core with a density of 8.4lb/ft<sup>3</sup> and crush strength of 800 psi (3600N/in<sup>2</sup>). If landing on two feet, the 15700N force will be split, and each crush core will have to hold (about, suspension geometry slightly alters; neglected for now) 7900 N (1775lbf). Area would be 2.2 in<sup>2</sup>, or 1.67" diameter.

For 8" of stroke and 20% pre-crushing, a 10" long core would be used, weighing 0.107lb or 0.0485kg. One for each leg would be a total of 0.194kg of core, assuming crush strength doesn't depend on length.

**Candidate 2:** From Taylor Devices<sup>215</sup>: 8 inch stroke, 1.5 inch diameter, 25" overall length damper. 2000 lbf max. No weight specified, min temp is -40C, probably not meant for space. Approximate weight by 0.44dia tube 25" long, that's over 1lb per damper, or around 2kg for all 4 dampers. It seems unlikely that any damper could be as light as the crush core.

Candidate	Weight (kg)	Volume	Re-usable?	Reliability	Rank:
Al hex core	0.194	same	No	High	1
Viscous damper	2	same	Yes	Medium	2

Table G.1.1: Primary damper trade study.

Based on this trade study, Aluminum hex crush core will be used for primary damping due to its very light weight and high reliability.

<sup>213</sup> "HexWeb Honeycomb Selector Guide," Hexcel, 2017. Accessed 11 May 2020. Retrieved from [https://www.hexcel.com/user\\_area/content\\_media/raw/HexWeb\\_SelectorGuide\\_2017.pdf](https://www.hexcel.com/user_area/content_media/raw/HexWeb_SelectorGuide_2017.pdf).

<sup>214</sup> "HexWeb CR III Corrosion Resistant Specification Grade Aluminum Honeycomb," Hexcel Corporation, 2017. Accessed May 9, 2020. [https://www.hexcel.com/user\\_area/content\\_media/raw/HexWeb\\_CRIII\\_DataSheet.pdf](https://www.hexcel.com/user_area/content_media/raw/HexWeb_CRIII_DataSheet.pdf).

<sup>215</sup> "D-Series Linear Dampers," Taylor Devices, Inc. Accessed May 11, 2020.

<https://www.taylordevices.com/custom/pdf/brochures/D%20Series%20Linear%20Dampers.pdf>.

## Stance

“At the Apollo 11 landing site, the nominal value for lunar surface bearing strength was 1.88 psi per inch depth with an associated nominal sliding friction coefficient between the footpad and the lunar surface of 0.33.”<sup>216</sup>

Tipping over:

5 degree tilt, 3cm offset, CG is 20” from top(56” height), legs extend 8” down (allow 0.2m bounce), extra **10 degree safety margin**, coefficient of friction 0.33. To have combined normal and friction force vector intercept CG, angle must be 56degrees, giving 31.6 inches of spread from the central axis. Add in the 3cm offset, accounting for a 45 degree rotated case, the legs **must extend 45” from the axis**.

When the lander height was shortened, the landing gear design remained the same, ultimately increasing the safety margin. It is assumed, conservatively, that the landing pads slide and the anti-torque spikes do not catch on rocks or soil.

## Leveling Springs

Leveling Spring operation:

Worst case for leveling is a 0-velocity landing where the honeycomb is not crushed (beyond the 20% initial as installed), this minimizes the available travel of the springs. With 12” long springs, the available travel is 4 inches.

If landing on a flat surface, all four legs compress the same amount, 2” (half of the total leveling travel). The extreme case is when two diagonal legs are compressed 4” and the others are at full extension.

This sets the spring rate:  $\frac{1}{4}$  of the landed weight should compress the spring by 2”.

$$k = 50\text{kg} \times 1.625 \text{ m/s}^2 / 0.0508 = 1600 \text{ N/m}$$

This analysis has been done assuming the primary dampers are approximately vertical. The deployed angle is approximately 60 degrees.

---

<sup>216</sup> Zupp, George A., “An Analysis and a Historical Review of the Apollo Program Lunar Module Touchdown Dynamics,” NASA SP-2013-605. Accessed May 11 2020. <http://ston.jsc.nasa.gov/collections/TRS>.

## G.2 Landing System Release Mechanism Trade Study

<b>Release Option</b>	<b>Pyrotechnic Pin Pusher</b>	<b>Split Spool (Non-Pyro)</b>	<b>Pyrotechnic Cable Cutter</b>
<b>Description</b>	Uses a controlled explosion to push a mechanical "pin" from point A to B	Upon electrical command, a fuse wire breaks in tension and the restraining wire unwinds, allowing the spools to separate and release the load.	Uses a controlled explosion to cut through a wire, releasing the mechanism
<b>Mass</b>			
<b>Activation Power</b>	3.5 amps	1.5 amps	3.5 amps
<b>Operating Temperature</b>	-65°C to +105°C	-245°C to +392°C	-54°C to +71°C
<b>Integration with wishbone deployment</b>	Easily integratable; beneficial linear motion	Integration of spool into mechanism needed	Will need to integrate cable into the mechanism
<b>Reliability</b>	High	Low Force Margins	High
<b>Release Time</b>	< 20 milliseconds	< 25 milliseconds	< 20 milliseconds
<b>Shock</b>	High	Low	High
<b>Complexity</b>	Simple, only one moving part	Complex, many moving parts	Simple, only one moving part
<b>Availability of Published Specs</b>	Available	Available	Available
<b>Pros (Summary)</b>	Integration ease, low complexity and high reliability	Low shock, large operating temperature range	High reliability and low complexity
<b>Cons (Summary)</b>	Explosion, can go wrong and cause damage with high shocks	Complex and not as reliable	Explosion, can go wrong and cause damage with high shocks
<b>Rank</b>	1	3	2

### G.3 Drill Mechanism Trade Study Details

Drill Option	Honeybee Auto-Gopher	Honeybee TRIDENT	Honeybee ROPEC	NASA/JPL Ultrasonic
<b>Description</b>	Large Core Type: rotary hammer drill	Auger type: rotary hammer drill	Bit Changable, small depths	Piezoelectric actuation, small depths
<b>Target Material Density</b>	2.96 g/cm^3	1.5 g/cm^3	2.81 g/cm^3	3.0 g/cm^3
<b>Drilling Depth</b>	Drill length: upto 3.3 meters	1 m	10 cm	1 inch
<b>Preservation of Volatiles</b>	Core: good	Powder: risk of sublimation	Core/Powder	Powder: risk of sublimation
<b>Power</b>	500 Watts	250 Watts	90 Watts	~30W
<b>Mass</b>	70 kg	16 kg	4 kg	4kg
<b>Ease of Sample Handling</b>	Complex: Need core processing hardware	Moderate: Need two attachments to drill	One-bit one core; need bit changing hardware	Undetermined path of delivery to analysis. Might need complex robotic system to assist with delivery
<b>Autonomy</b>	Can integrate in-drill sensors	Temperature Sensors, Hammer/Rotation alternating	Designed to work with bit changing architecture and a robotic arm	Custom designed system required
<b>Availability of Published Specs</b>	Moderate availability	Readily Available	Moderate; in development for Mars rover	Moderately Available
<b>Pros (Summary)</b>	Great depth sampling, with core type	Depth, Mass, Sample Handling	Light, Low power, Core Type	
<b>Cons (Summary)</b>	500 W, too much power & complex robotics for core	Powder type rather than core	Small Depth, potentially complex bit changing	Complex system to get extract powder from drill
<b>Rank</b>	3	1	2	5      4

### G.3.1 Auto-Gopher

The Honeybee Robotics Auto-Gopher Drill was the first drill explored for the mission. It extracts a core type sample which is excellent for preserving volatiles in the sample, as explained previously. It can drill through gypsum (density of  $2.96 \text{ g/cm}^3$ ), has a drill length of 3.3 meters and a tether length of 120 meters, requires less than 500W of power, and weighs 70 kg. The Auto-Gopher is able to integrate in-drill sensors and has a moderate amount of information, including published specifications, available.<sup>217</sup>



Figure G.3.1: Honeybee Robotics Auto-Gopher Drill

The Auto-Gopher is an excellent choice for exploring the composition of ice in lunar regolith as it hits all of the major physical requirements. It is able to drill through lunar regolith, has an excellent drilling depth, and preserves volatiles in its core type sample.

However, the Auto-Gopher was not selected due to the additional layer of complex robotics required to handle a core type sample, and its massive size and power requirements.

The Auto-Gopher has been tested by Honeybee Robotics in collaboration with NASA on drilling through gypsum, which has a consistency similar to cryogenic ice, as well as through ice in Greenland. The Auto-Gopher's intended missions are to drill on Mars or Europa.<sup>218</sup>

### G.3.2 ROPEC

Another alternative drill explored was the Honeybee ROPEC drill. The ROPEC is a core type sample drill, but has much smaller depths, meaning it is more compact and requires less power. It is designed to drill through Martian regolith, has a depth of 5-10 cm, requires 90 W of power and weighs 4 kg. It

---

<sup>217</sup> “Auto-Gopher Drill,” Honeybee Robotics. [honeybeerobotics.com/portfolio/auto-gopher-drill/](http://honeybeerobotics.com/portfolio/auto-gopher-drill/).

<sup>218</sup> “Planetary Deep Drill Completes Second Field Test,” The Planetary Society Blog. [www.planetary.org/blogs/jason-davis/pdd-completes-second-field-test.html](http://www.planetary.org/blogs/jason-davis/pdd-completes-second-field-test.html).

integrates well with a rover as it has a changeable drill bit that captures a core. The core then needs to be extracted from the drill bit and for drilling to continue a new drill bit must be attached. As such, a complex system must be created to autonomously swap out drill bits, extract samples from drill bits, and deliver the core type sample to the onboard science lab.

The ROPEC was determined to be the preliminary backup due to its small size and core type sample. In the event that the TRIDENT drill became unviable, the ROPEC drill could be utilized to deliver a single core type sample for analysis of Shackleton Crater.<sup>219,220</sup>

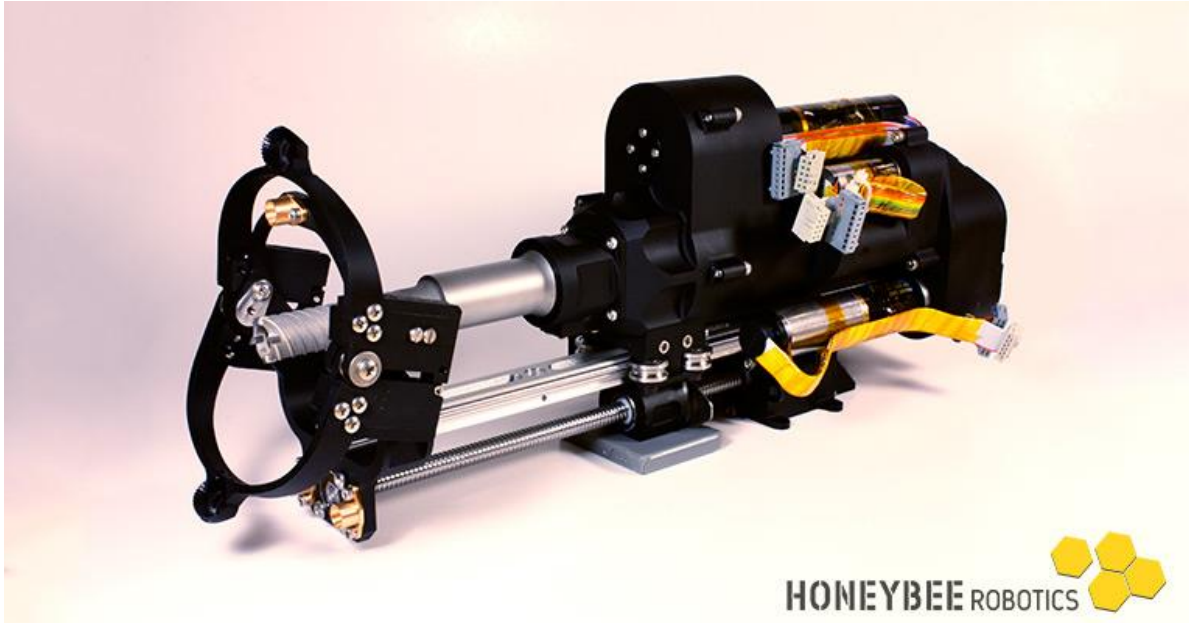


Figure G.3.2: Honeybee Robotics ROPEC Drill.<sup>221</sup>

### G.3.3 Ultrasonic Drill

The final drill explored was the NASA/JPL Ultrasonic drill. It is limited in depth due to its small size but is able to drill through basalt, with a density of  $3.0 \text{ g/cm}^3$ . Its drilling depth is 25 mm, it has a powder type sample, requires 3W of power, and weighs 400 g. It has readily available published specifications but doesn't have a clear path of sample delivery for analysis.

This drill was determined to be a worst-case backup option as its small nature allowed it to be powered by a flashlight battery. Its lack of delivery mechanism would require a custom built robotic system to handle the sample, and its shallow depth would not give the required insight for the depth vs composition study of lunar regolith that is the goal of this mission.

NASA modified this drill and created a GOPHER version that was demonstrated to drill 1.76 meters deep in ice at Lake Vida, Antarctica. This testing shows that if required, a modified custom design

<sup>219</sup> Honeybee Robotics - HD Mars 2020 Sample Acquisition and Caching Concept. Honeybee Robotics, [www.youtube.com/watch?v=NphWPvi9cy4](http://www.youtube.com/watch?v=NphWPvi9cy4).

<sup>220</sup> "Rover Curiosity finds Mars rocks more porous than thought," *The Week*, 2019. <https://www.theweek.in/news/sci-tech/2019/02/02/Rover-Curiosity-finds-Mars-rocks-more-porous-than-thought.html>

<sup>221</sup> "ROPEC Drill." Honeybee Robotics, [honeybeerobotics.com/portfolio/ropec-drill/](http://honeybeerobotics.com/portfolio/ropec-drill/).

of the NASA Ultrasonic Drill could fulfill the mission requirements, but this research and development would delay the mission and significantly increase costs.<sup>222</sup>



Figure G.3.3: NASA/JPL Ultrasonic Drill.

---

<sup>222</sup> “JPL’s NDEAA Ultrasonic/Sonic Driller/Corer Homepage,” NASA JPL, 2002. <https://ndeaa.jpl.nasa.gov/nasa-nde/usdc/usdc.htm>

## G.4 Danger of Sublimating Ice with the TRIDENT Drill

Based on previous testing of the TRIDENT drill in lunar regolith simulant, -100 °C was identified as an achievable target temperature for the drill bit.<sup>223</sup> At this temperature, the sublimation rate of ice on the Moon is 0.001 g/cm<sup>2</sup>/hr.<sup>224</sup> The anticipated drilling rate is 1.87 min/cm (see Figure G.4.1), which results in 0.31 hr to drill a 10 cm sample. Therefore, the sublimation rate with respect to area is 3.1x10<sup>-4</sup> g/cm<sup>2</sup>.

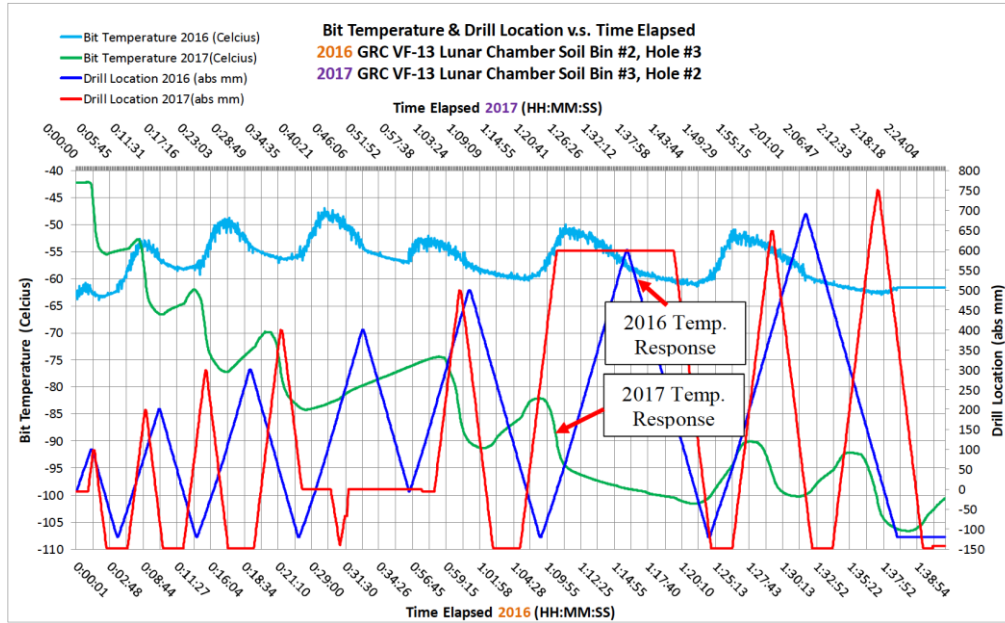


Figure G.4.1: Drilling rate and drill bit temperature for the TRIDENT drill in lunar regolith simulant.<sup>225</sup>

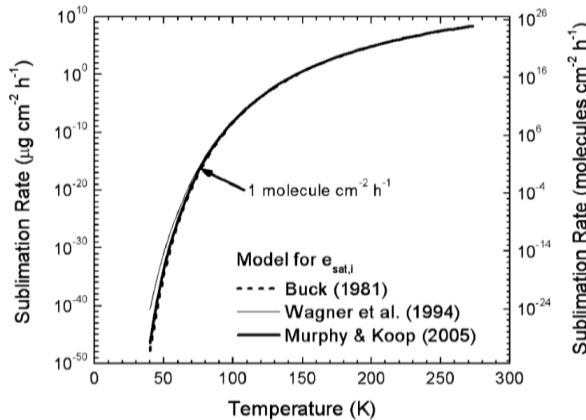


Figure G.4.2: Sublimation rates of ice on the Moon.<sup>226</sup>

<sup>223</sup> Paulsen, Gale et al. “The Regolith and Ice Drill for Exploration of New Terrains (TRIDENT); a One-Meter Drill for the Lunar Resource Prospector Mission.” Proceedings of the 44th Aerospace Mechanisms Symposium, NASA Glenn Research Center, May 16-18, 2018.

<sup>224</sup> Andreas, Edgar L., “New estimates for the sublimation rate for ice on the Moon.” Icarus 186 (2007) 24–30.

<sup>225</sup> Paulsen, Gale et al.

<sup>226</sup> Andreas, Edgar L.

The median particle size of lunar regolith within a few meters of the surface is 70  $\mu\text{m}$ .<sup>227</sup> Given the density of icy lunar regolith of 1.5 g/cc, for an ice particle 70  $\mu\text{m}$  in size, 17.7% of the mass of the particle would sublime over the 0.31 hr spent at -100 °C, as shown below. For larger particles, on the order of 0.1 cm in size, the sublimated mass is around 1%.

$$\begin{aligned}\text{Sublimation rate: } & 0.001 \text{ g/cm}^2/\text{hr} (\text{at around } -100 \text{ deg C or } 175 \text{ K}) \\ \text{Time to drill } 10 \text{ cm: } & 1.87 \text{ min/cm} * 10 \text{ cm} * 1 \text{ hr} / 60 \text{ min} = 0.31 \text{ hr} \\ \text{Sublimation w.r.t. area: } & 0.001 \text{ g/cm}^2/\text{hr} * 0.31 \text{ hr} = 3.1 \times 10^{-4} \text{ g/cm}^2 \\ \text{Median particle size: } & 70 \mu\text{m} = 0.007 \text{ cm} \\ \text{Particle surface area} & = 4 * \pi * (0.0035 \text{ cm})^2 = 1.54 \times 10^{-4} \text{ cm}^2 \\ \text{Mass sublimated per particle} & = 3.1 \times 10^{-4} \text{ g/cm}^2 * 1.54 \times 10^{-4} \text{ cm}^2 = 4.77 \times 10^{-8} \text{ g} \\ \text{Particle volume} & = 4/3 * \pi * (0.0035 \text{ cm})^3 = 1.8 \times 10^{-7} \text{ cm}^3 \\ \text{Density} & = 1.5 \text{ g/cm}^3 \\ \text{Initial particle mass} & = 1.5 \text{ g/cm}^3 * 1.8 \times 10^{-7} \text{ g} = 2.7 \times 10^{-7} \text{ g}\end{aligned}$$

$$\% \text{ loss} = \text{Mass Sublimated per particle} / \text{Initial particle mass} = (4.77 \times 10^{-8} \text{ g}) / (2.7 \times 10^{-7} \text{ g}) = 17.7\%.$$

Not all of the regolith is expected to reach -100 °C, because the thermal conductivity of lunar regolith is very low, and only the regolith at the top of the sample will be in contact with the drill for the whole drilling time. This analysis is merely an upper bound for the amount of sublimated ice. Therefore, the estimate for ice mass will have a lower bound of only the ice mass measured, and an upper bound of  $1/(1-0.177) = \sim 120\%$  of the ice mass measured.

The lunar lander will follow other lunar drilling missions by combining the temperature history of the drill bit with established models of lunar ice sublimation. In addition, testing will be conducted on lunar regolith simulant mixed with ice in order to better characterize the amount of sublimation.

---

<sup>227</sup> *Lunar Sourcebook*, ed. by Grant H. Heiken, David T. Vaniman, and Bevan M. French (Cambridge: Cambridge University Press, 1991).

## G.5 Landing System Member Sizing

The primary driver of the sizing of the members that will make up the linkages in the deployable landing system is buckling. The following analysis is based on a worst-case load of 7900 N on one leg, and only the longest member is analyzed, as it will be most likely to buckle. The formulas that appear in this appendix are derived from NASA SP-8007, “Buckling of Thin-Walled Circular Cylinder,” part of a series on space vehicle design criteria.<sup>228</sup>

The critical buckling load per unit width of circumference,  $N_x$ , is given by the following equation:

$$N_x = k_x \frac{\pi^2 D}{l^2}$$

where  $k_x$  is the buckling coefficient,  $l$  is the length of the cylinder, and  $D$  is the flexural rigidity of the cylinder, defined in terms of the Young's modulus  $E$ , Poisson's ratio  $\mu$ , and the thickness  $t$ :

$$D = \frac{Et}{12(1 - \mu^2)}$$

The buckling coefficient is defined in terms of the correlation factor,  $\gamma$ , and the curvature parameter,  $Z$ :

$$k_x = \frac{4\sqrt{3}}{\pi^2} \gamma Z$$

The correlation factor is defined in terms of the ratio of the radius,  $r$ , to the thickness  $t$ :

$$\gamma = 1 - 0.901(1 - e^\phi), \phi = \frac{1}{16} \sqrt{\frac{r}{t}}$$

The curvature parameter is defined as follows:

$$Z = \frac{l^2}{rt} \sqrt{1 - \mu^2}$$

All of this can be combined to once again define the critical buckling load per unit width of circumference:

$$N_x = \frac{4\sqrt{3}\gamma Z D}{l^2}$$

The relevant parameters of the longest linkage are listed below, assuming Aluminum 7075 as the material:

$$l = 1.18 \text{ m}$$

$$E = 71.7 \text{ GPa}$$

$$\mu = 0.33$$

For a leg diameter of 1 ½”, and a thickness of 3/32”, the critical buckling load per unit width of circumference is  $N_x = 11.1 \text{ MN/m}$ . The actual load, given by 7900 N /  $t$ , is 3.3 MN/m, giving a safety factor of approximately 3.36.

For completeness, the average normal stress on the cross-section of the leg is given by  $7900 \text{ N} / 2\pi rt = 27.7 \text{ MPa}$ . Compared to the compressive yield strength of Al 7075, 500 MPa, this gives a safety factor of 18. This safety factor is significantly higher than for buckling because buckling is an instability and therefore can cause problems well below the yield stress of the material.

---

<sup>228</sup> “Buckling of Circular Thin-Walled Cylinders,” NASA SP-8007, 1968. Accessed via the NASA Technical Reports Server. <https://ntrs.nasa.gov/archive/nasa/casi.ntrs.nasa.gov/19690013955.pdf>.

The total mass of the legs can be calculated by multiplying the cross-sectional area by total length of all linkages on all four legs (6.9 m), and multiplying that by the density of aluminum ( $2710 \text{ kg/m}^3$ ) to arrive at a total leg mass of 5.33 kg.

Additionally, the mass of the landing pads can be calculated in a similar way; They are 8" in diameter, and  $\frac{1}{4}$ " thick, so their volume can be calculated; assuming they are made of aluminum as well gives a total mass of 2.23 kg.

## G.6 Finite Element Analysis for HGA Mast

Physical description:

- 36" L x 4" OD hollow cylinder.
- 6061 Aluminum
- 1/16" wall thickness
- Axis of cylinder is along the Z direction in following images (arbitrary)
- Mass: 1.4 kg

Constraints:

- Stowed state: Pinned joint (free rotation about x-axis in Figure G.6.1) at hinged end
- Stowed state: Fixed translation spot 6" from gimbal end to simulate latch
- Deployed state: Fixed support at hinged end

Loads (conservative combination of various worst cases):

- 8.5 g acceleration load in y direction
- 3 g in z and x directions
- 7.5 kg mass simulator placed at end (0.7 kg antenna + 6.8 kg dual-axis gimbal assembly)

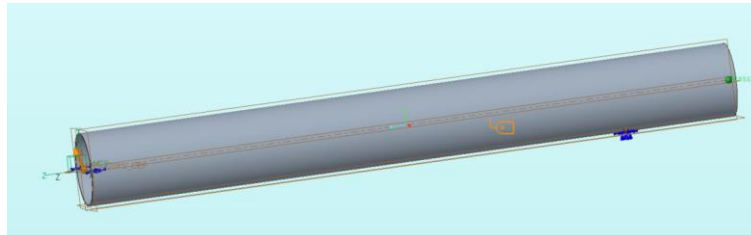


Figure G.6.1. Coordinate system, constraint locations, and load directions for the HGA mast FEA analysis in stowed state.

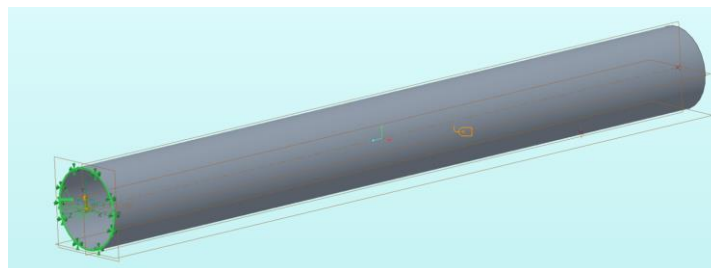


Figure G.6.2. Coordinate system and constraint location for the HGA mast modal analysis in deployed state.

Static analysis for stowed state:

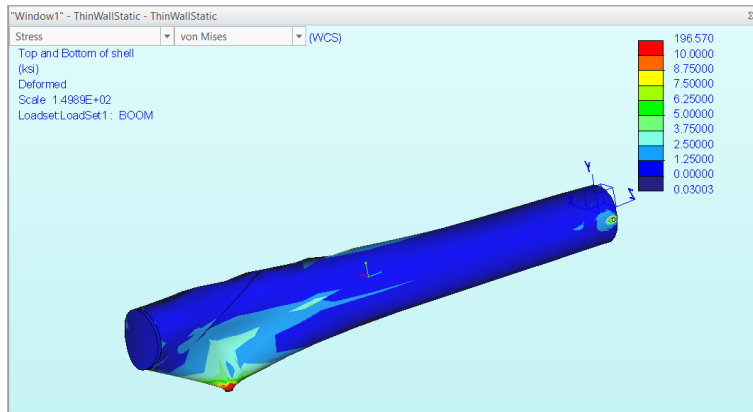


Figure G.6.3. FEA static analysis results for the HGA mast in the stowed state.

The mast is practically unstressed except for near the attachment points, as is consistent with its light weight. The analysis shows that the maximum von mises stress experienced is 196 ksi. This is artifact that results from placing a fixed constraint on a spot of arbitrary size to simulate the latch. In reality, the latch interface would be designed to avoid such a large stress concentration. One can see that the von mises stress remains below 10 ksi at all other locations.

Buckling analysis for stowed state:

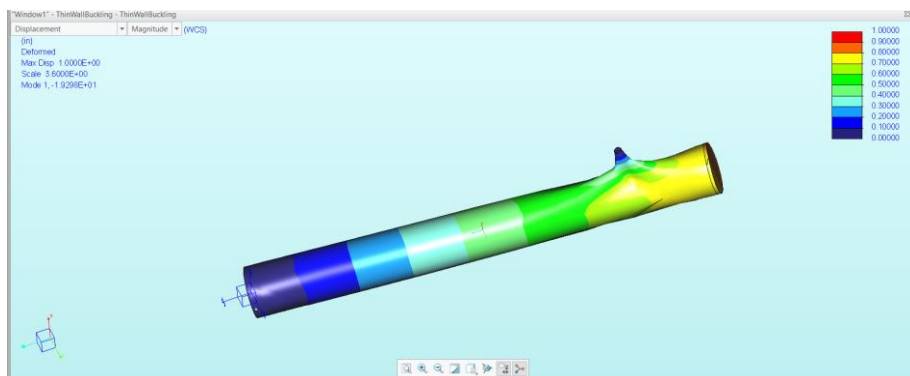


Figure G.6.4. FEA buckling analysis results for the HGA mast in stowed state, with the first buckling mode pictured.

The buckling load factor of the first buckling mode is around 19, meaning that the structure will not fail due to buckling until the currently applied loads are increased 19-fold. Note that this buckling mode occurs at the latch attachment point, which might not be the case after a detailed design of the latch mechanism. Nevertheless, the analysis shows mast buckling neither poses a major risk nor limits the design.

Modal analyses:

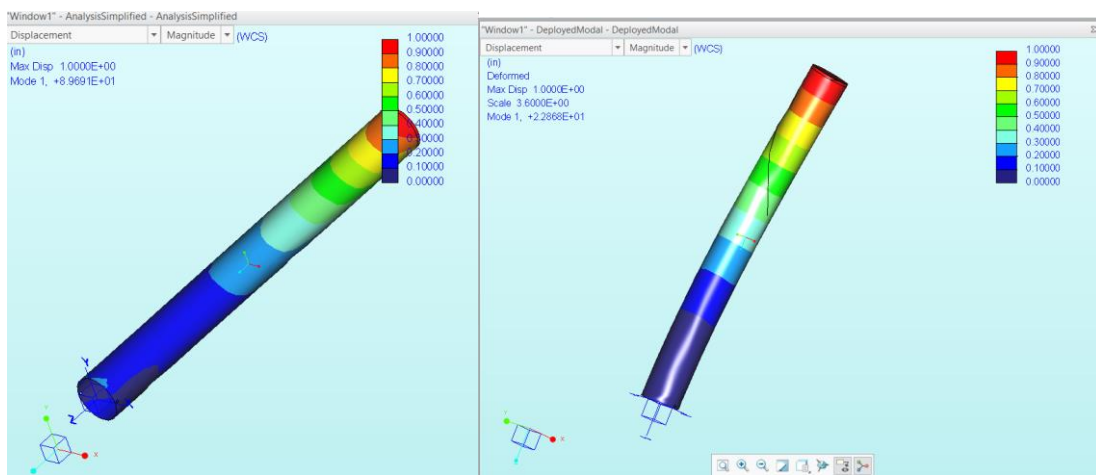


Figure G.6.5. FEA modal analysis results for the HGA mast in stowed state, with the lowest resonant mode (at 89.68 Hz) pictured (left), and the same analysis for the deployed state, with the lowest resonant mode (at 22.86 Hz) pictured (right).

## Appendix H: Payload

Component	Purpose	Advantages	Disadvantages/Possible Setbacks
SONAR	Ice thickness measurement	Well-known/often used technology → reliable way to collect data	When transmitting b/w 2 solid surfaces, liquid/semi-liquid layer required b/w two solids to account for surface irregularities Lack of atmosphere destroys soundwave transmission.
Mass Spectrometer/ Residual Gas Analyzer	Analyze concentration of volatiles	High sensitivity/accuracy	Limited scope to certain materials (not great for hydrocarbons) Expensive to put in space. Research being done into them but low space heritage.
Imaging Spectrometer	Provide a map of lunar surface	Good for collecting data on a specific area (i.e drilling site) Full coverage of spectral ranges Good for areas with large spatial variations	Image quality can change depending on range, chromatic aberrations, and complexity of system Possibility of distortion of images at different wavelengths, not vital to mission objectives
Lunar Regolith Penetrating Radar (LRPR)	Study structure of lunar regolith at landing site	Cleaner results than ground penetrating radar (GPR) Only 1 transmitter and 1 receiver needed to send & receive signals from all 12 antennae	Clutter, ground reflections, and small, irregular rocks can be difficult to image Structure information within the top 20 cm of regolith is masked by ringing effect of the ground reflections. No data sheet available (as of 3/30) Large size (12 antennae + original scope is for much larger Chang'e 5 mission)

Table H.1 Science Payload component class functionality trade study

# Appendix I. Guidance, Navigation, and Control

## I.1 Lander Guidance, Navigation, and Control

### I.1.1 Sun Sensor Trade Study

Sun Sensor	Manufacturer	Pointing Accuracy	Power Consumption	Mass	Notes
NSS CubeSat Sun Sensor <sup>229</sup>	NewSpace Systems	<0.5 deg	< 10 mA	< 5 g	Lower accuracy
BiSon64 <sup>230</sup>	Lens Research	<0.5 deg	-	<33g	Low accuracy
nanoSSOC-D60 digital sun sensor <sup>231</sup>	SolarMEMS	<0.5 deg	<23 mA	6.5 g	Low accuracy
NFSS-411 <sup>232</sup>	NewSpace Systems	$\leq 0.1 \text{ deg}$	<30 mA	<35 g	Best accuracy; Four sensors can achieve full-sky coverage; chosen for the lander
SS-411 <sup>233</sup>	Surrey (Sinclair)	$\leq 0.2\text{deg}$	<30mA	<34 g	Good accuracy; chosen for the orbiter

<sup>229</sup> NewSpace Sun Sensor\_6a. Date accessed: 2 May 2020. [https://www.cubesatshop.com/wp-content/uploads/2016/06/NewSpace-Sun-Sensor\\_6a-1.pdf](https://www.cubesatshop.com/wp-content/uploads/2016/06/NewSpace-Sun-Sensor_6a-1.pdf)

<sup>230</sup> State of the Art Small Spacecraft Technology. NASA. Date accessed: 2 May 2020. [https://www.nasa.gov/sites/default/files/atoms/files/soa2018\\_final\\_doc-6.pdf](https://www.nasa.gov/sites/default/files/atoms/files/soa2018_final_doc-6.pdf)

<sup>231</sup> nanoSSOC-D60 digital sun sensor. Accessed: 2 May 2020. <https://www.cubesatshop.com/product/nanossoc-d60-digital-sun-sensor/>

<sup>232</sup> NewSpace Sun Sensor 8\_a. Accessed 2 May 2020. [http://www.newspacesystems.com/wp-content/uploads/2019/03/NewSpace-Sun-Sensor\\_8a.pdf](http://www.newspacesystems.com/wp-content/uploads/2019/03/NewSpace-Sun-Sensor_8a.pdf)

<sup>233</sup> SS-411 Two-Axis Digital Sun Sensors. Accessed: 2 May 2020. [https://78462f86-a-744dbb28-sites.googlegroups.com/a/sinclairinterplanetary.com/www/digitalsunsensors/sunsensor2011a.pdf?attachauth=ANoY7coQ6\\_r-7ZowJtPM9xOEaElVk19oLZU-K15AhUH0lapJUYReqK7of3mPN5UOlrvCtp4tKJh7SRXpGXYI\\_lam1-S8\\_L3xW-qf4MvPXv6\\_jBzVqVZbBAtrBibxQMvO08NU6Vl6Ei8AjuuuNpof0I8eg\\_8qtBPH8WRw96bNjNev8g\\_2GaLWycZ9yo03YgTS-RpP2lQCvR1477c7tMY2A5nfnk\\_-Dev6dSZVdGuSjxr7SdLyVq9fCCVXejdf9u\\_0nUrPCd0dhwZ&attredirects=1](https://78462f86-a-744dbb28-sites.googlegroups.com/a/sinclairinterplanetary.com/www/digitalsunsensors/sunsensor2011a.pdf?attachauth=ANoY7coQ6_r-7ZowJtPM9xOEaElVk19oLZU-K15AhUH0lapJUYReqK7of3mPN5UOlrvCtp4tKJh7SRXpGXYI_lam1-S8_L3xW-qf4MvPXv6_jBzVqVZbBAtrBibxQMvO08NU6Vl6Ei8AjuuuNpof0I8eg_8qtBPH8WRw96bNjNev8g_2GaLWycZ9yo03YgTS-RpP2lQCvR1477c7tMY2A5nfnk_-Dev6dSZVdGuSjxr7SdLyVq9fCCVXejdf9u_0nUrPCd0dhwZ&attredirects=1)

### I.1.2 Star Tracker Trade Study

Star Sensor	Manufacturer	Geometry /sigma error	Power Consumption	Mass	Comments
KU Leuven Star Tracker <sup>234</sup>	KU Leuven	2 arcseconds 1-sigma	< 1W	250g	Accuracy wanting
NST-3 Nano Star Tracker <sup>235</sup>	Blue Canyon Technologies	50x50x50 /5 arcseconds point 3-sigma	<1W	165g	best accuracy; a slight mass trade-off; chosen for the lander
s3s	Sinclair	59x56x31.5 / 3-sigma	<1W, ~0.5W	90g	Ended up being not so accurate after deployment
ST-200 <sup>236</sup>	Hyperion Technologies	29 x 29 x 38.1/30 arcseconds 3-sigma	1W, ~0.6W	45g	15+ years; good accuracy; great lifetime; chosen for orbiter
Auriga <sup>237</sup>	Sodern Ariane Group	(56 x 66x 94)/6.6 3-sigma	1.1W, ~0.8W	210g	7+ years

### I.1.3 IMU Trade Study

IMU	Mass	Gyro Bias	Accelerometer	Power	Notes
-----	------	-----------	---------------	-------	-------

<sup>234</sup> KU Leuven Star Tracker. Accessed 2 May 2020. <https://www.cubesatshop.com/wp-content/uploads/2018/10/KULST-Datasheet.pdf>

<sup>235</sup> NST-3 Nano Star Tracker. Accessed 2 May 2020. <https://www.cubesatshop.com/product/nst-3-nano-star-tracker/>

<sup>236</sup> ST 200. Accessed 4 May 2020. <https://hyperiontechnologies.nl/products/miniaturised-star-tracker/>

<sup>237</sup> Auriga CP. Accessed 4 May 2020. [http://www.sodern.com/website/docs\\_wsw/RUB\\_315/tile\\_685/Auriga-CP.pdf](http://www.sodern.com/website/docs_wsw/RUB_315/tile_685/Auriga-CP.pdf)

			<b>Bias</b>		
IMU-LN200	4.5kg	1 deg/hr	0.3	16W	Greater mass; larger power draw.
HG1900 <sup>238</sup>	0.50 kg	1 deg/hr	0.3	3 W	Same accuracy; lower power draw; chosen for the small mass, and lower power draw; chosen for both lander and orbiter

## I.1.4 Actuator Trade Study

### *Reaction wheels*

The RSI 45 reaction wheel was used as an example of a large reaction wheel for the satellite, as it is intended for satellites 500 - 1500 kg<sup>239</sup>. It is relatively large volume-wise at 31 cm diameter and 16 cm height. It can store up to 45 Nms angular momentum at max speed and has 0.215 Nm torque at 2000 rpm. While the torque from a single wheel would be good for normal disturbance rejection and is actually sufficient for rough slew requirements, is insufficient for thruster misalignment disturbance torque and is extremely massive at 7.7 kg per wheel, ruling out reaction wheels as a useful addition to the vehicle.

### *Control Moment Gyros*

The Airbus CMG 4-6s<sup>240</sup> was used as an example of a large control moment gyro for this size of satellite. These can contain a maximum of 4 Nms momentum and exert 6 Nm torque. They weigh 13 kg, and are again large at 31 cm x 23 cm x 27 cm. Their torque is at reasonable values, but the maximum momentum change is far too small for required purposes.

---

<sup>238</sup> HG1900 Inertial Measurement Unit. Accessed 4 May 2020. <https://aerospace.honeywell.com/en/learn/products/sensors/hg1900-inertial-measurement-unit>

<sup>239</sup> RSI Momentum and Reaction Wheels 15-45 Nms. Accessed 7 May 2020. [http://www.electronicnote.com/media/downloads/RSI%2045\\_A4.pdf](http://www.electronicnote.com/media/downloads/RSI%2045_A4.pdf)

<sup>240</sup> CMG 4-6s. Accessed 7 May 2020. <https://spaceequipment.airbusdefenceandspace.com/avionics/control-momentum-gyrosopes/cmg-4-6s/>

### *Thrusters*

The main characterization necessary for thrusters was propellant needed for slews, which could potentially have been accomplished with other actuators. Using the ariane group 10 N thrusters<sup>241</sup> as a baseline, these produce 20 Nm torque or approximately 0.3 rad/s<sup>2</sup> of angular acceleration. Thus with the 3.5 g/s of propellant flow the fuel for the 180 degrees slew in 60 seconds is 4.2 g of propellant. This is very reasonable.

Thrusters are the only solution with reasonable torque and momentum change ability, thus a thruster-only system was chosen.

### I.1.5 LiDAR/RADAR

The overall conclusion of this trade study is that radar is far lighter than lidar for similar range capability without too significant of an accuracy penalty.

For example, there is a 1000 m range commercial lidar system, but it is fairly large and heavy (13 kg, over 10x the mass of comparable range radar solutions)<sup>242</sup>.

As a heritage mission example, the Mars pathfinder had a radar with 1520 m of range, 0.3 m resolution<sup>243</sup>. The commercial solution chosen as an analogue for a custom solution was the FreeFlight Systems RA-4000<sup>244</sup>. Because this is chosen as an analogue system and not a final component, an extensive trade study was not done on choosing the precise radar aside from mass, range, and accuracy appropriate for the mission.

Short-range LiDAR was examined as a way of sensing the spacecraft angle with respect to the ground. 4 single-point TF03 lidar sensors spaced around the craft were considered<sup>245</sup>. These have up to 180 m range and 1% accuracy. However, assuming dust obscures the LiDAR system below 20 m, this turns out to be a 0.2 m or 20 cm accuracy, which is useless with regards to sensing the local vertical as the vehicle could be at very large angles relative to the ground and this accuracy would make it unable to detect them reliably.

---

<sup>241</sup> *10 N Bipropellant Thrusters*. Accessed 7 May 2020. <http://www.space-propulsion.com/spacecraft-propulsion/bipropellant-thrusters/10-bipropellant-thrusters.html>

<sup>242</sup> *LiDAR Specification Comparison Chart*. Accessed 7 May 2020. [https://autonomoustuff.com/wp-content/uploads/2018/04/LiDAR\\_Comparison.pdf](https://autonomoustuff.com/wp-content/uploads/2018/04/LiDAR_Comparison.pdf)

<sup>243</sup> Foessel-Bunting, Alex, et al. *MMW-Scanning Radar for Descent Guidance and Landing Safeguard*. Accessed 7 May 2020. [https://ri.cmu.edu/pub\\_files/pub2/foessel\\_alex\\_2001\\_1/foessel\\_alex\\_2001\\_1.pdf](https://ri.cmu.edu/pub_files/pub2/foessel_alex_2001_1/foessel_alex_2001_1.pdf)

<sup>244</sup> *FreeFlight Systems RA-4000*. Accessed 7 May 2020. <https://sarasonaavionics.com/avionics/ra-4000>

<sup>245</sup> *TF03 Single-Point Long-Distance LiDAR Product Specification*.

[https://acroname.com/sites/default/files/assets/tf03\\_datasheet\\_v0.4\\_en.pdf](https://acroname.com/sites/default/files/assets/tf03_datasheet_v0.4_en.pdf)

## I.1.6 Powered Explicit Guidance

*Matlab R2020a code.*

```
%Author: Douglas Chin
%For Erebus Mission, MAE 342 Guidance, Navigation, and Control Team
%Powered Explicit Guidance Simulator

%coordinate system: +z = initial orbit radial, +x = initial velocity
%direction, y = initial orbit normal, right hand coordinate sys

close all;

timestep = 1/60; %
simtime = 75; %s, max sim time
lunarMass = 7.35 * 10^22; %kg
G = 6.67 * 10^(-11); %m^3kg^-1s^-2
simulationEnd = false;
thrust = 700; %N
r = [0.1 0.1 1757*1000.0]; %initial pos in m relative to central body
v = [1500 0.1 0.1]; %m/s %initial velocity
rhistory = zeros(3, simtime*1/timestep);
vhistory = zeros(3, simtime*1/timestep);
ahistory = zeros(3, simtime*1/timestep);
pitchhistory = zeros(1,simtime*1/timestep);
timeToBurnoutHistory = zeros(1,simtime*1/timestep);
horizontalSpeedHistory = zeros(1,simtime*1/timestep);
verticalSpeedHistory = zeros(1,simtime*1/timestep);
radiusHistory = zeros(1,simtime*1/timestep);
landerMass = 350; %kg
isp = 270; %
g0 = 9.8; %m/s^2
ve = isp*g0;
rT = 1757*1000; %target radius m
rdotT = 10; %target vertical speed m/s
vthetaT = 1656.0; %target horizontal speed m/s

initialLoop = true;

for t = 1:simtime/timestep

    firstLoop = true; %first guidance/estimation loop of this timestep
```

```

rhistory(:,t) = r;
vhistory(:,t) = v;
accel = thrust/landerMass; %current acceleration

if (initialLoop) %guidance based on first estimates
    timeToBurnout = (landerMass - landerMass*exp(-abs(v(1) -
vthetaT)/(ve)))*ve/thrust; %rocket equation for estimated burnout time
    rhat = r/norm(r);
    rdot = dot(r,v)/(norm(r));

    tau = ve/accel;
    b0 = -ve*reallog(1 - timeToBurnout/tau);

    b1 = b0*tau - ve*timeToBurnout^(1)/1;

    c0 = b0*timeToBurnout - b1;
    c1 = c0*tau - ve*timeToBurnout^(1+1)/1/1+1);

    MB = [rdotT - rdot; rT - norm(r) - rdot*timeToBurnout];
    MA = [b0 b1; c0 c1];
    MX = MA\MB;
    Anew = MX(1);
    Bnew = MX(2);
end

if (initialLoop == false) %initial loop is the first loop in entire
simulation
    timeToBurnout = Tnew;
end

if (initialLoop)
    deltaT = 0; %for the initial loop, there is no time difference
between guiding and estimating
else
    deltaT = timestep; %time between guidance iterations
end

%update guidance
Anew = Anew + deltaT*Bnew; %update pitch
Tnew = timeToBurnout - deltaT; %update time to burnout
Tplus = 0; %placeholder

```

```

%repeat estimation and guidance until converged
while (firstLoop || abs(Tplus - Tnew) > 1)
    if (firstLoop == false)
        Tnew = Tplus; %update time to burnout
    end
    %estimate
    h = (cross(r,v));
    rhat = r/norm(r);
    thetahat = (cross(h/norm(h), rhat));
    hT = vthetaT*rT;
    deltaH = hT - norm(h);
    rmean = (rT + norm(r))/2;
    rdot = dot((v),(rhat));
    vtheta = dot((v),(thetahat));
    tau = ve/norm(accel);

    omega = dot(v,thetahat)/norm(r);
    C = ((G*lunarMass/norm(r)^2 - omega^2*norm(r))/norm(accel));
    fr = (Anew + C);

    omegaT = vthetaT/rT;
    aTnew = norm(accel)/(1 - Tnew/tau);
    CT = (G*lunarMass/(rT)^2 - omegaT^2*(rT))/norm(aTnew);
    frT = Anew + Bnew*Tnew + CT;
    frdot = (frT - fr)/Tnew;
    ftheta = 1 - (fr^2)/2;
    fthetaDot = -(fr*frdot);
    fthetaDoubleDot = -(frdot^2)/2;
    deltaV = ((deltaH/rmean + ve*Tnew*(fthetaDot + fthetaDoubleDot*tau)
+ fthetaDoubleDot*ve*(Tnew^2)/2)/(ftheta + fthetaDot*tau +
fthetaDoubleDot*tau^2));
    %pause(1)
    Tplus = tau*(1 - exp(-deltaV/ve));
    %pause(.00001)

    %guidance Loop

    rhat = r/norm(r);
    rdot = dot(r,v)/(norm(r));

    tau = ve/norm(accel);
    b0 = -ve*log((1 - Tplus/tau));

```

```

b1 = b0*tau - ve*Tplus^(1)/1;

c0 = b0*Tplus - b1;
c1 = c0*tau - ve*Tplus^(1+1)/1/(1+1);

MB = [rdotT - rdot; rT - norm(r) - rdot*Tplus];
MA = [b0 b1; c0 c1];
MX = MA\MB;
Anew = MX(1);
Bnew = MX(2);
firstLoop = false;
%guidance end
end
Tplus;
timeToBurnoutHistory(t) = Tplus;
initialLoop = false;
pitch = -(asin(fr));

pitchhistory(t) = (pitch);
thrustVector = [cos(pitch) 0 sin(pitch); 0 1 0; -sin(pitch) 0
cos(pitch)] * thetahat.'; %transform from angle to thrust vector
thrustVector = thrust*thrustVector/norm(thrustVector);
aThrust = thrustVector/landerMass;

horizontalSpeedHistory(t) = dot(v, thetahat);
verticalSpeedHistory(t) = dot(v, rhat);
radiusHistory(t) = norm(r);
%update vehicle state, basic integrator

a = -rhat*G*lunarMass/(norm(r))^2 + aThrust.';
r = r + timestep*v;
v = v + a*timestep;
landerMass = landerMass - thrust/ve*timestep;
ahistory(:,t) = a;

end

%plot results
figure(1);
hold on;
axis equal;

```

```

th = 0:pi/180:pi/32;
xunit = 1737*1000 * sin(th);
zunit = 1737*1000 * cos(th);
yunit = zeros(length(th));
plot(xunit,zunit);
plot(rhistory(1,:),rhistory(3,:))
title('2D Trajectory Representation');
legend('lunar radius','trajectory');
xlabel('m');
ylabel('m');

grid on;

%plot((1:simtime/timestep)*timestep, rhistory(3,:))

figure(2);
vmaghist = zeros(1,simtime/timestep);
for t = 1:simtime/timestep
    vmaghist(t) = norm(vhistory(:,t));
end
plot((1:simtime/timestep)*timestep, horizontalSpeedHistory)

title('Horizontal Speed History');
xlabel('time (s)');
ylabel('Horizontal Speed (m/s)');

figure(3);
plot((1:simtime/timestep)*timestep,verticalSpeedHistory)
title('Vertical Speed History');
xlabel('time (s)');
ylabel('Vertical Speed (m/s)');

figure(4);
plot((1:simtime/timestep)*timestep, asin(pitchhistory)*180/pi)
title('Pitch');
xlabel('time (s)');
ylabel('Pitch (deg)');

figure(5);
plot((1:simtime/timestep)*timestep, timeToBurnoutHistory)
title('Time To Burnout');
xlabel('time (s)');
ylabel('Time To Burnout (s)');
figure(6);

```

```

plot((1:simtime/timestep)*timestep, radiusHistory)

title('Radius History');
xlabel('time (s)');
ylabel('Radius (m)');

```

### I.1.7 Navigational Accuracy Analysis

*Matlab R2020a code.*

```

%Author: Bethwel Kiplimo
%For Erebus Mission, MAE 342 Guidance, Navigation, and Control Team
%Navigation Accuracy Analysis
% max error due to a positive vertical tracking error
clc
clear
b = 10;
a = 350;
for y = 1:10
x1(y) = sqrt((a^2 * b^2 - a^2 * y^2)/ b^2);
x2(y) = sqrt((a^2 * b^2 - a^2 * (y+0.0015)^2)/ b^2);
if(y > 1)
    % disp(A(y-1))
    A(y) = x2(y) - x1(y) + A(y-1);
    g = A(y);
else
    A(y) = x2(y) - x1(y);
end
end
t = 1:1:10;
subplot(2,2,1);
plot(A, t)
title('+0.0015km vertical error')
xlabel(' max error(km)')
ylabel('vertical distance(km)')

% max error due to a negative vertical tracking error
c = 10;
a = 350;
%iterate over the ellipse
for y = 1:10
x1(y) = sqrt((a^2 * c^2 - a^2 * y^2)/ c^2);

```

```

x2(y) = sqrt((a^2 * c^2 - a^2 * (y-0.0015)^2)/ c^2);
if(y > 1)
    disp(A(x-1))
    A(y) = x2(y) - x1(y) + A(y-1);
    h = A(y);
else
    A(y) = x2(y) - x1(y);
end
end
t = 1:1:10;
subplot(2,2,2);
plot(A, t)
title('-0.0015km vertical error')
xlabel('max error(km)')
ylabel('vertical distance(km)')

% resulting max horizontal error due to negative tracking error
b = 10;
a = 350;
for x = 1:1:350
y1(x) = sqrt((a^2 * b^2 - b^2 * x^2)/ a^2);
y2(x) = sqrt((a^2 * b^2 - b^2 * (x-0.045)^2)/ a^2);
if(x > 1)
    disp(B(x-1))
    B(x) = y2(x) - y1(x) + B(x-1);
    i = B(x);
else
    B(x) = y2(x) - y1(x);
end
end
t = 1:350;
subplot(2,2,3);
plot(B, t)
title('-0.045km horizontal error')
xlabel('max error(km)')
ylabel('horizontal distance(km)')

% calculate the maximum horizontal error due to a positive tracking error
b = 10;
a = 350;
for x = 1:1:350
y1(x) = sqrt((a^2 * b^2 - b^2 * x^2)/ a^2);
y2(x) = sqrt((a^2 * b^2 - b^2 * (x+0.045)^2)/ a^2);

```

```

if(x > 1)
    disp(B(x-1))
    B(x) = y2(x) - y1(x) + B(x-1);
    j = B(x); % current maximum error
else
    B(x) = y2(x) - y1(x);
end
end
t = 1:350;
subplot(2,2,4);
plot(B, t)
title('0.045km horizontal error')
xlabel('max error(km)')
ylabel('horizontal distance(km)')

```

### I.1.8 Pointing Error Propagation

Assume the attitude error is 1/10 of a degree off of the ideal thrust axis. The burn in the correct direction is then  $\Delta V \times \cos(1/10)$  or  $\Delta V \times (1 - 1.523 \times 10^{-6})$ , a negligible amount. The burn normal to the correct direction is  $\Delta V \times \sin(1/10)$  or  $\Delta V \times 1.7453 \times 10^{-3}$ . This is 3 orders of magnitude greater in error than the error in the correct direction, so it will be examined.

The main impulsive burn lowers the vehicle's orbit from circular 50 km altitude to a 15 km altitude perilune. This requires a delta-V of 8.2 m/s, of which 0.014 m/s is normal to the expected thrust direction. It is assumed that this velocity is in the normal direction of the orbit, resulting in a plane change (a presumably more difficult problem for the spacecraft to overcome than if the velocity was in the radial direction, which would only result in an altitude change). Using the plane change equation<sup>246</sup>, equation I.0.1, in which  $v_1$  is the initial velocity,  $v_2$  is the final velocity, and  $\Delta_i$  is the plane change, the (approximate) plane change is 0.065 degrees, assuming the initial and final velocities are approximately the same.

$$\Delta v = \sqrt{v_1^2 + v_2^2 - v_1 v_2 \cos(\Delta_i)} \quad (\text{I.0.1})$$

This results in a positional error of approximately 1.98 km at the worst point (90 and 270 degrees ahead of the plane change), as seen in figure 5.4.5, which shows how the orbital radius, inclination difference, and total position difference are related.

This position error is too much to leave unaccounted for. The onboard IMU will be able to detect this improper thrust with the accelerometer and attempt to correct for it before the final descent.

Approximately 2500 s before the final descent burn starts, or with approximately 38% of the orbit left to

---

<sup>246</sup> Owens, Steve and Macdonald, Malcolm. Hohmann Spiral Transfer With Inclination Change Performed By Low-Thrust System. Accessed 5 May 2020.

[https://pure.strath.ac.uk/ws/portalfiles/portal/22210390/Owens\\_S\\_Macdonald\\_M\\_Pure\\_Hohmann\\_spiral\\_transfer\\_with\\_inclination\\_change\\_performed\\_by\\_low\\_thrust\\_system\\_Feb\\_2013.pdf](https://pure.strath.ac.uk/ws/portalfiles/portal/22210390/Owens_S_Macdonald_M_Pure_Hohmann_spiral_transfer_with_inclination_change_performed_by_low_thrust_system_Feb_2013.pdf)

go, the lander will perform a course correction burn. Approximate the amount of position 45 degrees ahead of the lander by dividing the maximum positional error caused by a plane change by 2. Thus, a plane change of double the original error is required, or 0.13 degrees. Assume a circular 15 km orbit with orbital velocity about 1.676 km/s. This plane change requires a delta-V (to an orbit of the same orbital radius) of about 0.0038 m/s, which is easily achieved by the translational thrusters in a less than 1 second pulse. These have a minimum impulse bit of 0.1 Ns, and if the spacecraft masses 300 kg (half-fuel depleted) with 2 thrusters firing for translational control then the minimum delta-V translational bit is  $6.67 \times 10^{-4}$  m/s, which means that the plane change can be commanded without the thrusters overcorrecting. Thus, off-nominal thrust during the approximately impulsive maneuvers will present a large translational error, but with course-correction maneuvers this error is easily nullified.

## I.2 Orbiter Guidance, Navigation, and Control

### I.2.1 Reaction Wheel Trade Study

Reaction Wheel	Manufacturer	Momentum (Nms)	Torque (Nm)	Mass (kg)
RSI 12 <sup>247</sup>	Collins	12	0.075	4.85
RSI 15 <sup>248</sup>	Collins	15	0.215	7.7
RW 4 <sup>249</sup>	Blue Canyon	4	0.25	3
RW 8	Blue Canyon	8	0.25	4.1

Four different reaction wheels were considered. It was eventually decided that the RW8 from Blue Canyon was the best overall wheel. It has double the momentum of the RW4 with a very low mass penalty, and triple the torque of the RSI 12. While this torque is not needed for disturbance rejection, it is desired for target-of-opportunity pointing capability. The Collins wheel with comparable torque, the RSI 15, is almost double the mass of the RW8 and was thus discarded for being more massive and, while it would have reduced momentum unloading firings needed, the mission is not expected to go anywhere near the maximum thruster firings.

---

<sup>247</sup> *RSI 12 Momentum and Reaction Wheel*. Accessed 7 May 2020.

[http://www.electronicnote.com/media/downloads/RSI%2012\\_A4.pdf](http://www.electronicnote.com/media/downloads/RSI%2012_A4.pdf)

<sup>248</sup> *RSI 45 Momentum and Reaction Wheel*. Accessed 7 May 2020.

<https://www.yumpu.com/en/document/read/35491907/rsi-45-momentum-and-reaction-wheels-15-45-nms-with->

<sup>249</sup> *Reaction Wheels*. Blue Canyon Technologies. Accessed 6 May 2020.

[https://www.bluecanyontech.com/static/datasheet/BCT\\_DataSheet\\_Components\\_ReactionWheels.pdf](https://www.bluecanyontech.com/static/datasheet/BCT_DataSheet_Components_ReactionWheels.pdf)

# Appendix J: Propulsion

## J.1 Orbiter propulsion

*Orbiter Thruster Trade Study*

Thruster	Power requirement	I <sub>sp</sub>	Dry mass	Notes
MR-501 1N electrothermal <sup>250</sup>	500 W	303s	0.89 kg	Power consumption far too high
Ariane group 1N hydrazine with cat bed <sup>251</sup>	10W FCV 10W cat bed heater	220s	0.29 kg	Hydrazine freezing point 2C
Cold gas <sup>252</sup>	10W FCV	30-70s	~0.1 kg	Must maintain high pressure tanks

Table J.1.1 Orbiter Thruster Trade Study

### EOL Analysis

Orbital elements of interest after 10 years in moon inertial frame (based on STK simulation of perturbations):

$$\begin{aligned} a &= 2045.26 \text{ km} \\ e &= 0.099961 \end{aligned}$$

Based on the elliptic equations of orbit:

$$r_a = a(1 + e) = 2249.7 \text{ km}$$

Based on the vis-viva equation:

$$v_a = (\mu_{moon}(2/r_a - 1/a))^{1/2} = 1400 \text{ m/s}$$

r<sub>moon</sub> = 1737.1 km, but aim for deorbit perigee of 1700 km.

Thus,

$$a_{\text{required}} = (1700 + r_a)/2 = 1974.9$$

$$v_{a,\text{required}} = (\mu_{moon}(2/r_a - 1/a_{\text{required}}))^{1/2} = 1369.3 \text{ m/s}$$

Finally,

$$EOL \Delta V = v_{a,\text{required}} - v_a = -30.7 \text{ m/s}$$

<sup>250</sup> "MR-501B." Retrieved from <http://www.astronautix.com/m/mr-501b.html>

<sup>251</sup> "1N Monopropellant Hydrazine Thruster." Retrieved from <http://www.space-propulsion.com/spacecraft-propulsion/hydrazine-thrusters/1n-hydrazine-thruster.html>

<sup>252</sup> Assad Anis (2012). Cold Gas Propulsion System - An Ideal Choice for Remote Sensing Small Satellites, Remote Sensing - Advanced Techniques and Platforms, Dr. Boris Escalante (Ed.), ISBN: 978-953-51-0652-4, InTech, Available from: <http://www.intechopen.com/books/remote-sensing-advanced-techniques-andplatforms/cold-gas-propulsion-system-an-ideal-choice-for-remote-sensing-small-satellites>

### *Propellant Mass Calculation*

Exhaust velocity from Ariane Group 1N hydrazine thruster is 2200 m/s.

Thus, based on the rocket equation and approximating the maneuver as impulsive, the propellant requirement for EOL  $\Delta V$  is given by

$$m_p = m_f(e^{\Delta V/U_{ex}} - 1) = 3.2 \text{ kg}$$

Total impulse requirement from ACS:  $I = 11040 \text{ Ns}$  (sizing of momentum dumps in appendix I).  
Total propellant mass after margin: 12.7 kg

### *Propellant Tank Sizing*

Molar concentration of hydrazine at 313 K (max temperature of orbiter):<sup>253</sup>

$$\rho = 30 \text{ M/L}$$

Molar mass of Hydrazine (N<sub>2</sub>H<sub>4</sub>):

$$2 * \text{Molar Mass } N + 4 * \text{Molar Mass } H = 32.04 \text{ g/mol}$$

Density of Hydrazine:

$$\rho = 961.2 \text{ g/L}$$

Volume of hydrazine tanks needed:

$$14.11 \text{ L}$$

---

<sup>253</sup> Elts, Ekaterina & Windmann, Thorsten & Staak, Daniel & Vrabec, Jadran. (2012). Fluid phase behavior from molecular simulation: Hydrazine, Monomethylhydrazine, Dimethylhydrazine and binary mixtures containing these compounds. *Fluid Phase Equilibria*. s 322–323. 79–91. 10.1016/j.fluid.2012.03.008.

## Appendix K: Power

Lander power calculations:

Total Power Requirement	546.25 W
Total Energy Requirement	9280.1 Wh
Bus Voltage	28 V
Nominal Cell Voltage	2.1 V
Cell capacity	15 Ah
Cell Specific Energy	410 Wh/kg
Cell Dimensions (L,W,H)	1.45 dm, 0.78 dm, 0.10 dm

$$Load Current, I = \frac{Total Power}{Bus Voltage} = \frac{546.25}{28} = 19.5 A$$

$$Total Capacity = \frac{Total Energy}{Bus Voltage} = \frac{9280.1}{28} = 331.4 Ah$$

Layout:

$$\# \text{ in series} = \frac{Bus Voltage}{Nominal Cell Voltage} = \frac{28}{2.1} = 13.3 \Rightarrow 14 \text{ series cells required}$$

$$\# \text{ in parallel} = \frac{Total Capacity}{Cell Capacity} = \frac{331.4}{15} = 22.1 \Rightarrow 23 \text{ parallel strings required}$$

$$Expected mass = \frac{Total Energy Requirement}{Cell Specific Energy} = \frac{9280.1}{410} = 22.6 kg$$

$$Total Volume = (14 * 23) * (1.45 * 0.78 * 0.10) = 36.4 L$$

### Orbiter Power Calculations

Orbit Time	2.4 hr
Sun Time	1.595 hr
Eclipse Time	0.805 hr
Load Power Requirement - Eclipse	620.3 W
Load Power Requirement - Sun	230.3 W
Nominal Cell Voltage	3.6 V

Nominal Cell Capacity	1.43 Ah
Solar Cell Operating Voltage	2.059 V
Solar Cell Operating Current	0.422 A
Solar Cell Operating Power	0.869 W
Solar Cell Area	27 cm <sup>2</sup>

## For Eclipse

### Battery Sizing

$$\text{Discharge Current, } I = \frac{\text{Load Power Requirement (Eclipse)} + \text{Harnessing Losses}}{\text{Bus Voltage}}$$

$$= \frac{620.3 * 1.02 * 1.005}{28} = 22.71 \text{ A}$$

$$\text{Total Capacity} = I * \text{Eclipse Time} = 22.71 * 0.805 = 18.28 \text{ Ah}$$

$$\# \text{ of battery cycles} = \frac{24}{2.4} * 365 * 10 = 36,500 \text{ cycles over a mission duration of 10 years}$$

Using 60% DoD and an estimated 24% fade over the 36,500 cycles gives:

$$\text{EOL Capacity} = \frac{18.28}{0.60} = 30.47 \text{ Ah}$$

$$\text{BOL Capacity} = 30.47 * 1.24 = 37.78 \text{ Ah}$$

$$\# \text{ in series} = \frac{\text{Bus Voltage}}{\text{Nominal Cell Voltage}} = \frac{28}{3.6} = 7.78 \Rightarrow 8 \text{ series cells required}$$

$$\# \text{ in parallel} = \frac{\text{BOL Capacity}}{\text{Cell Capacity}} = \frac{37.78}{1.43} = 26.42 \Rightarrow 27 \text{ parallel strings required}$$

Calculating a battery weight based on a 8S3P battery pack manufactured by Enersys containing the same Quallion 1.43 Ah cell and weighing 1.78 kg, gives:

$$\text{Expected mass} = 1.78 * \frac{27}{3} = 16.02 \text{ kg}$$

## For Sunlit

$$\text{Battery Recharge Current} = \frac{37.78 * 0.60}{1.595 + 0.08} = 13.53 \text{ A}$$

$$\text{Battery Recharge Power} = \text{Recharge Current} * \text{Bus Voltage} = 13.53 * 28 = 378.84 \text{ W}$$

$$\text{Total Array Power Requirement} = 230.3 * 1.02 * 1.02 + 378.84 * 1.005 * 1.02 = 628 \text{ W}$$

Over the mission duration of 10 year there is a cell voltage fade of 11% and a cell current fade of 1%, which gives an EOL Power of 0.766 W and an EOL Voltage of 1.833 V

Layout:

$$\# \text{ in series} = \frac{\text{Max. Bus Voltage}}{\text{EOL Cell Voltage}} = \frac{33.6}{1.833} = 18.33 \Rightarrow 19 \text{ series cells required}$$

$$\# \text{ in parallel} = \frac{\text{Total Array Power Requirement}}{\# \text{ in series} * \text{EOL Cell Power}} = \frac{628}{19 * 0.766} = 43.15$$

$\Rightarrow 44 \text{ parallel strings required}$

$$\text{Total Solar Array Area} = 27 * (19 * 44) = 22,572 \text{ cm}^2 = 2.26 \text{ m}^2$$

Using a power density for the solar array of 25 W/kg, we get an estimated mass for the solar panels of:

$$\text{Mass of Panels} = \frac{628}{25} = 25.12 \text{ kg}$$

# Appendix L: Thermal

## L.1 Lander Coating Trade Study

Coating	Supplier	Kapton 3mil (ITO/NDA/Kapton on)	Gold	Gold Plate on Aluminum 7075	Silver-Beryllium-Copper	GSFC Dark Mirror Coating SiO-Cr-Al	Polished Aluminum 6061, Beryllium, Steel, Titanium, Stainless	Blue Anodized Titanium Foil	Ti-Shop
V9360-3M Aluminized Mylar	Cryospares	Capling et al.	Many	Many	PR Mallory and Co, Inc.	Deposition Sciences, Inc.	Many	Many	Ti-Shop
<b>Cost per square meter</b>		\$66.91	Kapton: \$42.83; VDA: \$0.01; ITO: \$1.75	Prohibitively expensive	\$551.84	unknown	No additional non-structural cost	\$255,500	
Emissivity		0.02	0.02	0.025	0.03	0.04	0.05 to 0.13	0.13	
Absorptivity		0.23	0.09	0.299	0.3	0.19	0.86	variable	0.7
Calculated Worst-Case Q (W)		39.42	39.42	49.27	59.12	59.12	78.82	98.52 to 256.11	256.11
<b>Other Relevant Notes</b>		Tape, not coating; ITO protects against high surface charges		Low changeability in space environment	Assumed plate is 0.5 microns thick	Patented; may be changeable in space environment	Comparatively fragile	Anodization can cause high surface charges, leading to arcing	

## L.2 Walkthrough of Lander Thermal Code

```

x      = 1;                      %percentage of surface covered in coating 1
e1    = 0.02;                    %Kapton 3mil (ITO/VDA/Kapton)
e2    = 0.853;                   %other coating (here unused)

sigma = 5.6703e-8;              %[W/m^2K]
Tsurf = 40;                     %[K] lunar surface temperature
Tsc   = 273;                     %[K] desired internal lander temperature
Abottom = 0.8047;               %[m^2] area of the underside of the lander
Atop   = 0.8047;                 %[m^2] area of the top of the lander
Asides = 8*16.072*56/1550;       %[m^2] combined area of all the lander sides
rfeet  = 0.1;                     %[m] radius of the landing pads
m     = 213.6;                   %[kg] mass of the lander
g     = 1.62;                     %[m/s^2] lunar gravity
emiss = (x*e1)+((1-x)*e2);      %emissivity of coating combination
Afeet  = 4*pi*rfeet^2;           %[m^2] area of the landing pads

%p      = m*g/ (Afeet*10e6);      %[MPa] contact pressure (here unused)254
%R      = 0.574*p^-0.562;          %[kW/m^2*C] thermal contact resistance as a
                                    function of contact pressure (here unused
                                    because the function was not valid for the
                                    values of contact pressure our lander
                                    would experience)

R      = 1.25e3;                  %[W/m^2*C] thermal contact resistance of
                                    lunar surface255

q_rad  = sigma*emiss*(Abottom*(Tsc^4-Tsurf^4) + Tsc^4*(Atop+Asides))      %[W] radiated heat, which is a combination
                                    of the top and sides of the lander
                                    radiating to deep space (T=0K) and the
                                    bottom of the lander radiating to the
                                    lunar surface (T=40K)

q_cond = (Tsc-Tsurf)*Afeet/R      %[W] heat conducted through the landing
                                    pads to the lunar surface

q      = q_rad + q_cond          %[W] total heat loss; therefore total heat
                                    input necessary to maintain lander at
                                    desired temperature

```

<sup>254</sup> Fletcher, L. S. (1991) Conduction in solids: Imperfect metal-to-metal contacts: Thermal contact resistance, Section 502.5, *Heat Transfer and Fluid Mechanics Data Books*, Genium Publishing Company, Schenectady, New York

<sup>255</sup>Grott, M., Knollenberg, J. and Krause, C. *Apollo lunar heat flow experiment revisited: A critical reassessment of the in situ thermal conductivity determination*. Journal of Geophysical Research, Vol 115, November 2010, p. 4.

### L.3 Lander Thermal Requirements

Power	0 to 30 °C
Payload: NIR Spectrometer	-20 to 40 °C
GNC	-25 to 50 °C
Communications	-50 to 70 °C
Propulsion	Min -50 °C
Launch Vehicle	-54 to 128 °C
Mechanisms (Drill Actuator)	-20 to 75 °C

## L.4 Orbiter Coating Trade Study

Coating	Aeroglaze Z306 Black Paint	E-Glass Fabric 5276	Aeroglaze A971 Yellow Paint	AMJ-400-IG Green Paint	Combination Coating
Supplier	Socomore	possibly unavailable	Socomore	AZ Technology	96.4% Black Paint
Cost per square meter	unknown	unknown	\$7.62	unknown	3.6% Green Paint
Emissivity	0.91	0.91	0.89	0.9	0.9096
Absorptivity	0.96	0.74	0.43	0.56	0.9456
Absorptivity to Emissivity Ratio	1.054945055	0.8131868132	0.4831460674	0.6222222222	1.039577836

## L.5 Walkthrough of Orbiter Code

Commented MATLAB code is as follows:

```

sigma = 5.67e-8; %stefan-boltzmann constant
PAS1 = 0.8047; %[m3] area of top or bottom of orbiter
PAS2 = ((16.072*56)*(1+(2*(sqrt(2)/2))))/1550; %[m3], one side of prism
facing sun (unused here)
PAS3 = ((16.072*56)*((2*cosd(22.5))+(2*cosd(67.5))))/1550; %[m3], one
corner of prism facing sun
PAS4 = 16.072*56/1550; %area of one side panel of the spacecraft
Hsu = 1353; %[W/m2], solar constant
Qsu = PAS3*Hsu; %worst case for heating
Asc = (2*PAS1)+(8*16.072*56/1550); %[m2] total area of orbiter
Flt = 0.93; % horizontal viewfactor to the lunar
surface256
FltV = 0.32; % vertical view factor to lunar surface257
PASspace = (8*PAS4*(1-FltV))+(PAS1*(1-Flt))+ PAS1;
%surfaces with radiating view to deep space:
%includes vertical view factor for the portion
of the sides that radiate to deep space
PASmoon = (8*PAS4*(FltV))+(PAS1*Flt);
%surfaces with radiating view to lunar
surface: includes vertical view factor for
the portion of the sides that radiate to the
lunar surface
ePlanet = 0.95; %emissivity of the lunar surface258
Tplanet = 250; %lunar average planet temperature [K]259
Qlt = PASmoon*sigma*ePlanet*(Tplanet^4); %calculating lunar IR flux260
aL = 0.12; %lunar albedo261
Qlr = aL*PASmoon*Hsu; %calculating lunar albedo flux
% this indented section is to be altered in order to a) determine the
percentage of green/black paint needed to maintain the sunlit temperature
and b) determine the percentage of louvers necessary to maintain the
shaded temperature
e1 = 0.9096; %emissivity of first coating (here, the

```

---

<sup>256</sup> Karam, Robert D.. Satellite Thermal Control for Systems Engineers. United States: American Institute of Aeronautics & Astronautics, 1998. p. 76

<sup>257</sup> Ibid.

<sup>258</sup> Martínez, Isidoro. Properties of Planets and their Moons, 1995.

<sup>259</sup> Ibid.

<sup>260</sup> Martínez, Isidoro. Spacecraft Thermal Modelling and Testing, 1995.

<sup>261</sup> Martínez, Isidoro. Properties of Planets and their Moons, 1995.

```

chosen combination of black262 and green263
paint)
e2 = 0.02; %emissivity of second coating264 (here, the
alpha1 = 0.9456; louver coating: Kapton 3mil (ITO/VDA/Kapton)
alpha2 = 0.09; %absorptivity of first coating
x = 0.474; %absorptivity of second coating
%percentage of the surface that is the first
coating (here, the percentage not covered
with louvers)

eIr = (x*e1)+((1-x)*e2); %emissivity of coating combo
alphaSu = (x*alpha1)+((1-x)*alpha2); %solar absorptivity of coating combo
% calculating the temperature while in sunlight
Q2int = 390; %internal heat generated by other subsystems
Tsc = (((Q2int+(eIr*Qlt)+(alphaSu*Qsu)+(alphaSu*Qlr))/(sigma*eIr*Asc))
^(1/4))-273.15; %temperature of orbiter in sun [C]
% calculating the temperature while in umbra
Qint = 390+300; %internal heat plus added heat from heaters
T2sc = (((Qint+(eIr*Qlt))/(sigma*eIr*Asc))^(1/4))-273.15;
%temperature of orbiter in shade [C]

```

---

<sup>262</sup> Choueiri, Edgar. “Spacecraft Thermal Control.” *MAE 432 Lecture Notes*, 2020.

<sup>263</sup> Kauder, Lonny. “Spacecraft Thermal Control Coatings References.” NASA, December 2005.

<sup>264</sup> Ibid.

## L.6 Walkthrough of TLI Code

Commented MATLAB code for the thermal calculations during TLI.

```

x      = 1.0;                                %percentage of e1 (in this case it is the entirety of the OMV)
Q_omv = 250;                                 %how much heat is needed from the OMV

eG    = 0.9;                                 %emissivity of green paint used on the orbiter
eB    = 0.874;                               %emissivity of black paint used on the orbiter
eW    = 0.91;                                %emissivity of white enamel used on the OMV
aG    = 0.56;                                %absorptivity of green paint used on the orbiter
aB    = 0.975;                               %absorptivity of black paint used on the orbiter
aW    = 0.09;                                %absorptivity of white enamel used on the OMV

e1    = eW;                                  %emissivity of white enamel used on the OMV
a1    = aW;                                  %absorptivity of white enamel used on the OMV

eO    = 0.036*eG + 0.964*eB;                %averaged emissivity of the orbiter using green and black paint
aO    = 0.036*aG + 0.964*aB;                %averaged absorptivity of the orbiter using green and black paint

eK    = 0.02;                                %kapton emissivity (used on the landers)
aK    = 0.09;                                %kapton absorptivity (used on the landers)

Hsu   = 1353;                               %[W/m2], solar constant at about 1 AU from sun
sigma = 5.6703e-8;                          %[W/m2K] Stefan-Boltzmann Constant

unit  = 0.00064516;                         %unit conversion from in2 to m2

Amin  = (56*40*3 + 46*42 + pi*31^2)*unit;  %Area of the "top" of the epsa ring (minimum Area that could face the sun)

Amax  = (pi*87*40 + pi*31*20)*unit;        %Area of the "sides" of the epsa ring (maximum Area that could face the sun)

At_land = (56*40*4 + 40*40)*3*unit;        %Area of the lander
At_orb  = (46*42 + 2*46*38 + 42*38)*unit;  %Area of the orbiter
At_omv  = (pi*31^2*2 + 2*pi*31*20)*unit;  %Area of the OMV
Ads    = (56*40*3 + 46*42 + 40*40*3 + 42*38 + pi*31^2*2 + 2*pi*31*20)*unit;  %Area facing deep space

x_land = At_land/(At_orb+At_land+At_omv);  %Percentage of area that is the lander
x_orb  = At_orb/(At_orb+At_land+At_omv);    %Percentage of area that is the orbiter

```

```

emiss = ((x*e1)+((1-x)*e2))*(1-x_land-x_orb) + eK*x_land + x_orb*eO;
%averaged emissivity over lander, orbiter, and OMV

alpha = ((x*a1)+((1-x)*a2))*(1-x_land-x_orb) + aK*x_land + x_orb*aO;
%averaged absorptivity over lander, orbiter, and OMV

qmax = Amax*Hsu; %heat calculated with the Area of the "sides" of the epsa ring
qmin = Amin*Hsu; %heat calculated with the Area of the "top" of the epsa ring

qdark = Amax*0.16*Hsu*emiss + 0.36*Amax*Hsu*alpha + Q_omv;
%heat calculated with Earth IR and albedo, since sc still close to Earth with added heat from the OMV

Tmax = ((qmax*alpha)/(sigma*emiss*Ads))^.25
%temperature if the sides of the ring faces the sun
Tmin = ((qmin*alpha)/(sigma*emiss*Ads))^.25
%temperature if the top of the ring faces the sun

Tdarks = (qdarks/(sigma*emiss*Ads))^.25 %temperature during the eclipse

```

## L.7 Orbiter Thermal Requirements

Power	0 to 40 °C
Gimbal	-45 to 95 °C
GNC	-20 to 50 °C
Communications	-50 to 70 °C
Propulsion	Min 2 °C
Launch Vehicle	-54 to 128 °C

## Appendix M: Command & Data Handling

Model	Mass (g)	Dimensions (cm)	Hardness, Total Dose (Krad)	Temperature Range (C)	Max Power (W)	Voltage (V)	Processor Speed (MIPS)	RAM (MB)	ROM (KB)	Release Date
RAD750 (3U)	549	10.0 x 16.0	100	-55 - 70	10.8	3.3	260	128	256	2005
RAD5545 (6U)	-	23.3 x 22.0	100	-55 - 125	35	5	5600	4000	4000000	2012
RAD6000 (6U)	900	23.3 x 22.0	1000	-25 - 105	7.5	5	26	16	4	1997
RAD750 (6U)	2000	23.3 x 22.0	100	-20 - 100	25	5	260	44	4500	2010
Centaur SBC	-	-	-	-	-	-	200	128	4000	<2011

### Processor Trade Study

Note that all boards but the Centaur SCB are produced by BAE Space: they were one of the only processor manufacturers with complete datasets available online. Their products are also among the most competitive on the market. The RAD750 or its predecessor, the RAD6000, have been used on all NASA Mars missions and the majority of all interplanetary missions since 2000. Though the RAD5545 is the newest model in the RAD series, the RAD750 meets Erebus system requirements at lower cost, mass, volume, and power consumption, as the RAD5545 is available only in 6U form factor. Because the orbiter is meant to interface with a variety of missions for a decade to come, however, it might require the greater performance of the RAD5545. This decision requires further research.

# Appendix N: Communications

## N.1 State Data

Table N.1: Breakdown of position and health data

Type of Data	State Data	Temperature/Pressure Data	Raw IMU Data	GN&C Hardware Data
Number of Bits (per reading)	832	800	192	192

## N.2 Antenna Sizing

The size of the patch antennas on the lander and the orbiter was determined through a link budget analysis using the following equation (variables defined in Table N.2):

$$P_R = P_T G_T G_R L_D = P_T \frac{16\pi^2 \epsilon_T \epsilon_R A_T A_R \lambda^2}{16\lambda^4 \pi^2 D^2} = P_T \frac{\epsilon_T \epsilon_R A_T A_R}{\lambda^2 D^2}$$

Assuming the antennas are the same size, the antenna area is found to be  $0.011m^2$ . This is used below in further link calculations.

## N.3 Link Budget Calculations

Link calculations were made using the following MATLAB script. Results are summarized Table N.2. Note that because the antenna sizes for the lander to orbiter connection are the same for the transmitting and receiving antenna, this calculation is the same for uplink and downlink.

```

% Runs the lander to orbiter link budget analysis. Alternate values used for the
orbiter to Earth analysis are provided in comments and in Table N.2%

% constants for the calculation
C_over_B = 1.5; % 2.5 for Ka-band
bitrate = 70000; % 40000000 for Ka-band
boltzmann = 1.38*10^-23;
noise_temp = 270;
lambda = 0.08; % 0.1 for Ka-band
distance = 4000000; % 406004670 for Ka-band
AT = 0.011; % 262.68 for Ka-band uplink, 0.0707 for downlink
AR = 0.011; % 0.0707 for Ka-band uplink, 262.68 for downlink
efficiency = 0.6;
illumination = 70;
PT = 2; % 6000 for Ka-band uplink
diameterT = 2* sqrt((AT/pi))

% find link budget
bandwidth = bitrate/C_over_B
S_over_N = 2*(C_over_B^2) - 1
PN = boltzmann*noise_temp*bandwidth
PR1 = S_over_N * boltzmann * noise_temp * bandwidth
LD = (lambda/(4*pi*distance))^2
LD_decible = 10*log10(LD)
GR = (4*pi*efficiency*AR)/(lambda^2);
GR_decible = 10*log10(GR)
GT = (4*pi*efficiency*AT)/(lambda^2);
GT_decible = 10*log10(GT)
PR2 = PT*GT*GR*LD;
link = PR2 - PR1
link_decible = 10*log10(link)
AreaTransmit = PR1/PT * (lambda^2)*(distance^2)/((0.6^2)*AR);

theta3db = illumination*lambda/diameterT      % find theta3dB value

```

Table N.2: Summary of known and calculated values used in the link budget (shaded indicated the value is calculated in the above script)

Symbol	Meaning	Known Values (lander to orbiter)	Known Values (orbiter to Earth)	Known Values (Earth to orbiter)
$\frac{C}{B}$	Spectral Efficiency	1.5	2.5	2.5
$\frac{S}{N}$	Signal to Noise Ratio	3.5	11.5	11.5
$P_R$	Receive power	6.09 E-16 W	6.86 E-13 W	1.71 E-12 W
$P_T$	Transmit power	2 W	40 W	6 kW
$G_T$	Transmit antenna gain	11.13 dB	37.27 dB	72.97 dB
$G_R$	Receive antenna gain	11.13 dB	72.97 dB	37.27 dB
$L_D$	Loss from free space transmission	-175.96 dB	-234.15 dB	-234.15 dB
$B$	Required bandwidth	0.047 MHz	16.00 MHz	40.00 MHz
$b$	Required bits/sec	0.07 Mbps	40 Mbps	40 Mbps
$k_B$	Boltzmann Constant	1.38	1.38	1.38
$P_N$	Noise power	1.74 E-16 W	5.96 E-14W	1.49 E-13W
$T$	Noise temperature	290 K (standard)	290 K (standard)	290 K (standard)
$D$	Distance between antennae	4,000,000 m	406,004,670 m	406,004,670 m
$A_T$	Transmitting antenna area	0.011	0.0707	262.68
$A_R$	Receiving antenna area	0.011	262.68	0.0707

$\epsilon$	Efficiency	0.6 for S-band	0.6 for Ka-band	0.6 for Ka-band
$\lambda$	Wavelength	0.08 m	0.01 m	0.01 m
	Link Budget	-156 dB	-129 dB	-86 dB

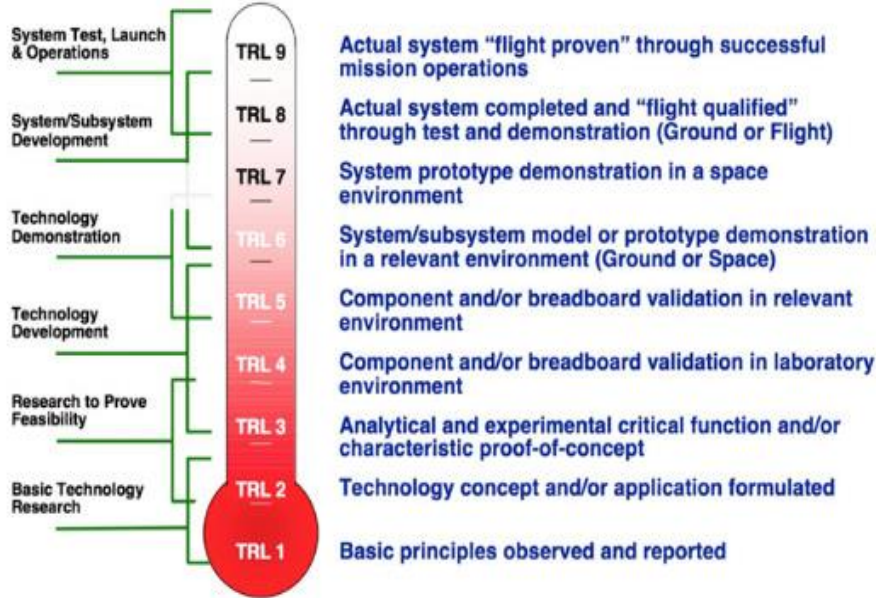
## Appendix O: Cost Estimation

Variable	Lander	Orbiter
Dry mass (in kg)	213.6	230.5
Beginning of Life Power (in Watts)	546.25	628
Data rate fraction (0.5 for median data rates, <0.5 for lower and >0.5 for higher data rates)	0.1	0.3
Advertized design life in (in months)	0.2	120
Percentage new (0.2-0.3: simple mod, 0.3-0.7 extensive mod, 0.7-1.0: new, >1.0: new technology)	0.5	0.3
Planetary? (0 for earth orbital, 1 for planetary)	1	1
Year (ATP date in 4 digit calendar year minus 1960)	61	61
InstrComp% (Instrument complexity percentile, 0.5 for median complexity, <0.5 for lower and >0.5 for higher complexity)	0.5	0.2
Team Experience (1=unfamiliar, 2=mixed, 3=normal, 4=extensive)	2	2
<b>Total Development Cost Estimate (41% error)</b>	<b>\$69M</b>	<b>\$61M</b>

Table O.1. Erebus lander and orbiter cost estimation using SMAD. Justifications for percentage new technology and instrument complexity can be found in section 7.6.1. The other variables are relatively obvious and require no further justification beyond the information already present in the report.

## Appendix P: Technology Readiness Levels

Throughout the report, the following graphic has been used to determine individual components' TRLs.



Source: NASA, 2015